UNIMORE
UNIVERSITÀ DEGLI STUDI DI
MODENA E REGGIO EMILIA

UNIVERSITÀ DEGLI STUDI
DI MODENA E REGGIO EMILIA

Dottorato di ricerca in Ingegneria industriale e del territorio

Ciclo XXXVIII

Bioactive Glasses as next-generation materials for biomedical devices: overcoming processing and delivery challenges.

Candidato: **Francesco Gerardo Mecca**

Relatore (Tutor): Prof.ssa Valeria Cannillo

Eventuale Correlatore (Co-Tutor): Prof. Devis Bellucci

Coordinatore del Corso di Dottorato: Prof. Alberto Muscio

ἓν μόνον ἀγαθὸν εἶναι, τὴν ἐπιστήμην

καὶ ἓν μόνον κακόν, ἀμαθίαν

Esiste un solo bene, la conoscenza,

e un solo male, l'ignoranza

Socrate, così citato da Diogene Laerzio, "Vite e dottrine dei filosofi illustri", c.ca III d.C

Abstract (English version)

Modern medicine is in constant need of innovation in the ideation of devices optimized for tissue engineering. The challenge in designing such devices is often found in the need for balancing overcoming obstacles in the manufacturing process and eliciting a positive reaction from the host body. In this context, bioactive glasses (BGs) stand out among other materials for tissue engineering. Since its development in the late '60s, BGs have proven to be materials of pivotal importance, thanks to their properties, such as osteoinductivity, osteoconductivity, bioactivity, resorbability, angiogenesis, wound healing capabilities, antibacterial properties and more.

However, BGs also come with their limitations, most notably the poor thermal properties of some widely studied composition, already available on the market, namely 45S5 Bioglass® and S53P4. In fact, exposure to high temperatures, required, for example, during the processing of BGs into devices for bone tissue engineering applications, causes crystallization of their originally amorphous structure. This phenomenon has several negative effects, such as slower bioactivity and dissolution kinetics, and worse mechanical properties. Several solutions to this phenomenon have been proposed in the literature: among them, the inclusion of dopant ions in the composition, capable of widening the processing window of BGs. Moreover, BGs are capable of expressing antibacterial properties against a wide range of bacteria strains. An investigation in the literature has shown that, besides the antibacterial efficacy of marketed compositions such as the above-mentioned S53P4, a common strategy for expanding the antibacterial properties of BG is doping with therapeutic or antibacterial ions, drug loading, or even a combination of these strategies.

In light of these considerations, this work presents two novel BG compositions, namely 45S5_MS and S53P4_MS, developed via the modification of 45S5 and S53P4 by incorporating magnesium (Mg) and strontium (Sr). Moreover, Bio_MS, an additional experimental BG with high crystallization temperature and optimal biological performance, was tested alongside the other formulations. A thorough investigation of the effect of Mg and Sr on thermal, mechanical, and biological properties was conducted, revealing enhanced overall properties in the magnesium–strontium-doped BGs. Moreover, 45S5_MS and S53P4_MS were employed in the development and optimization of electrospun composite scaffolds for tissue engineering composed of polycaprolactone (PCL) and BG, testing designing strategies, and addressing critical limitations commonly associated with this typology of biomedical devices. Special attention was dedicated to overcoming the intrinsically hydrophobic nature of electrospun PCL, which may limit scaffold functionality. To this end, a chemical surface modification treatment based on immersion in a sodium hydroxide (NaOH) solution was integrated into the fabrication process, resulting in improved wettability and biological response.

This work proposes a comprehensive design framework for next-generation BG–based biomedical devices, combining ion substitution to improve thermal stability and biological performance with tailored processing and surface modification strategies for electrospun

mats. Together, these approaches aimed to advance the clinical translatability of BGs and electrospun polymer/glass composite scaffolds.

Abstract (in italiano)

Oggigiorno, la medicina ha un costante bisogno di innovazione nell'ideazione di dispositivi ottimizzati per l'ingegneria tissutale. La sfida nella progettazione di tali dispositivi risiede spesso nella necessità di bilanciare il superamento dei vari ostacoli del processo di produzione garantendo una reazione favorevole da parte del corpo umano. In questo contesto, il vetro bioattivo (BG) si distingue tra gli altri materiali per l'ingegneria tissutale. Fin dal loro sviluppo alla fine degli anni '60, i BG si sono dimostrati materiali di fondamentale importanza, grazie alle loro numerose proprietà, come l'osteoinduttività, l'osteoconduttività, la bioattività, la riassorbibilità, l'angiogenesi, il supporto alla guarigione di ferite, le proprietà antibatteriche e altro ancora.

Tuttavia, i BG presentano anche dei limiti, in particolare le scarse proprietà termiche di alcune composizioni ampiamente studiate e già disponibili sul mercato, ovvero il 45S5 Bioglass® e l'S53P4. Infatti, l'esposizione ad alte temperature, necessarie ad esempio per la produzione di dispositivi (scaffold) in vetro bioattivo utili per l'ingegneria tissutale ossea, causa la cristallizzazione della loro struttura tipicamente amorfa. Questo fenomeno ha diverse conseguenze, come una bioattività e una cinetica di dissoluzione più lente, insieme a possibili criticità da un punto di vista meccanico e della stabilità del prodotto una volta impiantato in vivo. In letteratura sono state proposte diverse soluzioni a questa problematica: tra queste, l'inclusione di ioni droganti nella composizione, in grado di ampliare la finestra di lavorazione dei BG. Inoltre, certi BG sono in grado di esprimere proprietà antibatteriche nei confronti di diverse specie di batteri. Un'indagine in letteratura ha dimostrato che, oltre all'efficacia antibatterica di composizioni commerciali come il S53P4, una strategia comune per espandere le proprietà antibatteriche dei BG è il drogaggio con ioni terapeutici o antibatterici, il caricamento con farmaci o la combinazione di entrambe le strategie.

Considerando queste problematiche, in questo lavoro di Tesi sono state innanzitutto sviluppate e testate due composizioni di BG innovative, denominate 45S5_MS e S53P4_MS, ottenute modificando il 45S5 e l'S53P4 con magnesio (Mg) e stronzio (Sr). La progettazione di questi vetri bioattivi si è anche basata sul Bio_MS, un vetro sperimentale con alta temperatura di cristallizzazione e ottime prestazioni biologiche, testato insieme alle altre composizioni. È stata condotta un'indagine approfondita sull'effetto di Mg e Sr su diverse proprietà dei vetri bioattivi, riscontrando un miglioramento del comportamento termico, meccanico e biologico dei BG drogati con magnesio e stronzio. Inoltre, 45S5_MS e S53P4_MS sono stati impiegati nello sviluppo e nell'ottimizzazione di scaffold compositi elettrofilati in policaprolattone (PCL) e BG per l'ingegneria tissutale, integrando strategie di progettazione e superando problematiche, comunemente associate a questa tipologia di dispositivi biomedicali. Particolare attenzione è stata ricolta alla natura intrinsecamente idrofobica del PCL elettrofilato, che potrebbe limitarne la performance in ambiente biologico. A tal fine, il processo di fabbricazione è stato perfezionato con un trattamento chimico di modifica superficiale, basato sull'immersione in una soluzione di idrossido di sodio (NaOH), migliorando bagnabilità e risposta biologica degli scaffold elettrofilati.

Il presente lavoro di Tesi si propone dunque di definire un quadro progettuale completo per lo sviluppo di dispositivi biomedicali compositi a base di vetro bioattivo. Tale obiettivo è

stato perseguito integrando la sostituzione ionica, finalizzata a migliorare la stabilità termica e la risposta biologica dei BG, con tecniche di processamento e di modifica superficiale di membrane elettrofilate. In conclusione, questi approcci mirano a promuovere l'avanzamento dell'applicabilità clinica dei BG e degli scaffold compositi basati su polimero e vetro.

.

Table of contents

1 Introduction

Tissue engineering (TE) is a rapidly developing branch of regenerative medicine that requires strong interdisciplinarity among research fields, including cellular and molecular biology, materials science and engineering, and medicine [1]. Due to an ever-growing request for surgical attendance, several fields of medical research try to engineer materials and devices employable for tissue healing and regeneration, commonly referred to as biomaterials [2].

Biomaterials are a relatively novel concept in medicine, dating back to the second half of the 20th century. To date, the most accepted definition for what a biomaterial is, was outlined during the "Consensus Conference" in Chester, UK, in 1987:

"Any substance or combination of substances, other than drugs, synthetic or natural in origin, which can be used for any period of time, which augments or replaces partially or totally any tissue, organ or function of the body, in order to maintain or improve the quality of life of the individual."

In fact, in earlier medicine, it was widely believed that the only materials suitable for use inside the human body were those that did not react with it. Consequently, past research efforts primarily focused on identifying materials that did not express any harmful or toxic effects when interacting with the host body. Such candidates were found mainly amongst metals and plastics, such as titanium and ultrahigh-molecular-weight polyethylene (UHMWPE) [3]. These materials are today categorized as first-generation biocompatible materials. However, these biomaterials tend to promote fibrous tissue formation, and long-term implantation may result in prosthesis failure [4], [5]. In contrast, second-generation biocompatible materials have the ability to induce a controlled action–reaction when in contact with living tissue. The key difference between first- and second-generation biomaterials is the ability of the second one to actively interact with the host body, for example by dissolving when in contact with physiological environments or even integrating into living tissue. This property is commonly referred to as bioresorbability [6]. Some materials can even be engineered to be third-generation biocompatible materials. The key difference between second- and third-generation BGs lies in the latter's ability to induce specific reactions in the host body at the molecular level, such as promoting the formation of new healthy tissue through the release of therapeutic ions, activating genes and enhancing regenerative processes [6], [7].

Thus, biomaterials have gradually evolved from readily available substances to be integrated into the host body, into carefully designed materials, engineered to suppress or elicit specific responses from the host environment [8]. For this reason, the "biocompatibility" of a material refers in general to how well a material performs while interacting with host tissue. Indeed, biocompatibility considers both how the body reacts to the material being grafted onto it and how the material behaves in contact with the body's environment [9]. The modern concept of what a biomaterial does, extends beyond the sole intention to prevent adverse reactions upon contact with the host body. Instead, it aims at fully utilizing the material's chemical

and physical response to tailor its behavior to a specific intended function [8]. Among the wide variety of biomaterials currently available, Bioactive Glass (BG) stands out as one of the most remarkable, owing to its unique properties and functionalities, which effectively pioneered the field of biomaterials research [2], [10].

1.1 Bioactive glasses and their properties

Since the early 1800s, glass has been studied in relation to its properties when in contact with biological environments, cells, and bacteria [11]. However, Dr. Larry L. Hench was the first who successfully synthesized a bioactive glass in 1969, today worldwide known as 45S5 Bioglass® [10]. According to his writings [10], he felt inspired by U.S. Army Medical Corps Colonel Klinker when he asked Hench:

"If you can make a material that will survive exposure to high-energy radiation, can you make a material that will survive exposure to the human body?"

Bioglass® was the result following a two-years-long research effort, through the analysis of the $Na_2O–CaO–SiO_2$ system, where 45S5 sits near a ternary eutectic [10], [12]. BGs were originally designed using the melt-quench technique, an efficient and reliable way to manufacture glass from oxides and carbonates [10]. However, an alternative technique emerged about three decades ago, enabling the production of high-purity BGs via sol–gel synthesis, typically starting from Tetraethyl Orthosilicate (TEOS – for silicate BGs) and nitrates [13]. This process allows for a more precise tuning of the composition and does not require high temperatures for melting the glass [13], [14].

A wide variety of BGs have been developed over the years. Most notably, S53P4 (marketed as Bonalive®, Novamin® and more) is among the most clinically relevant. S53P4 is a BG with formulation similar to that of 45S5, and with remarkable dissolution properties [15], demonstrating high bioactivity and a significant release of ions. Moreover, S53P4 shows strong inhibitory effects on bacterial proliferation: this is associated with a high ability to increase the pH of the solution in which the BG is immersed [16], [17], [18].

BGs can exhibit essential properties for bone tissue engineering (BTE) such as osseointegration, osteoconductivity, and osteoinductivity. These terms describe, respectively, the ability of a material to bond with bone without the formation of fibrous tissue, the surface's capacity to facilitate bone growth, and the capability to stimulate stem cells to differentiate into bone-forming cells [19]. However, BGs have been mainly studied for their bioactivity. A material is considered bioactive when it has the ability to elicit a specific response from living tissue. Specifically, BGs' bioactive properties are expressed via their ability to bond to bone tissue, precipitating hydroxyapatite (HA) when grafted into a body [20]. This property can be readily verified *in vitro*, thanks to Professor Kokubo et al. [21], who introduced a testing procedure that has since become the standard for the initial evaluation of the ability to bond with bone tissue of these materials. BGs are typically immersed into a solution called simulated body fluid (SBF), consisting of inorganic salts and compounds dissolved in demineralized water [21]. Even with its limitations, Kokubo's procedure is arguably an invaluable tool for testing the *in vitro* capability of a material to precipitate hydroxyapatite [22].

A major challenge in BTE is the fabrication of BG-based structures suitable for implantation. These materials can be shaped into complex three-dimensional architectures, commonly referred to as scaffolds. Scaffolds represent a key component in tissue regeneration strategies. Specifically, for bone tissue applications, the challenge is to create a design able to mimic the architecture of cancellous bone [23]. Thermal treatments are often employed to form these type of structures, inducing sintering of the powders, which ultimately results in the formation of a three-dimensional (3-D) structure [24]. Moreover, thermal treatments are required in several additional applications, such as implant coating via BG powders thermal spraying and manufacturing of glass–ceramic composites [25].

BG powders are frequently subjected to thermal treatments involving exposure to temperatures above 600 °C [25]. However, such high temperatures can structurally modify the glass, inducing crystallization. Crystallization is generally regarded as a detrimental phenomenon in BGs. It typically occurs when the material is exposed to temperatures above its crystallization onset temperature (i.e., the temperature at which the crystallization process starts, T_{C_ONSET}) and becomes most pronounced at the crystallization peak temperature (T_C) [26], [27]. In fact, crystallization interferes with the bioactivity and mechanical performance of sintered BG powders, while also impeding viscous flow, thereby potentially slowing down the sintering process in crystallized materials. It has also been reported that crystallization could hinder the stability of the implant after its placement, considering that the residual amorphous and the crystalline phases of the material exhibit different dissolution kinetics [28]. It is also worth noting that, due to the close correlation between sintering and crystallization, these phenomena are often considered as a single process, referred to as sinter-crystallization [29].

In order to tackle the crystallization issue in BGs, various metallic and alkali ions have been employed as dopants for their ability to widen the processability window of the compositions (i.e., the difference between the crystallization temperature T_{C_ONSET} and the glass transition temperature T_G). Moreover, extensive efforts have been employed in identifying BG compositions with broader processing windows, such as formulations like 13-93, Bio_MS, and BGMS10 [30], [31], [32]. For the last two BGs, the improvement of the thermal properties is attributed to the lower content of alkaline elements and the presence of magnesium (Mg) and strontium (Sr) in the BG composition, recognized for their positive biological effects and their ability to modify thermal and mechanical properties [9–12]. Specifically, Mg has been investigated as a BG dopant due to its biological properties, as it is naturally present in bone and enamel and plays multiple important functions in the organism [33], [34], [35]. Moreover, magnesium deficiency has been associated with reduced bone density and an increased risk of osteoporosis [34], [36]. Meanwhile, Sr is a known osteoblast and osteoclast activity regulator [34], [37], and in some cases has also shown antibacterial effects [38], [39].

In this context, the Network Connectivity (NC) model has proven as a valuable tool in elucidating the impact of different ions on the structural characteristics of glass. NC describes the average number of oxygen atoms, acting as a bridge in the network. NC is

equal to 4 for pure silica [40]. Hill and Brauer [41] developed an equation, today used as model, based on experimental data by Watts et al. [42], expressed as follows [42], [43], [44]:

$$NC = \frac{[4 \cdot (Ms) + 6 \cdot (Mp)] - 2 \cdot [M_2O + M'O]}{Ms}, \quad (1)$$

where Ms and Mp represent the molar percentages of SiO_2 and P_2O_5 oxides present in the glass composition, respectively, and M_2O and M'O denote the alkali and alkali-earth metal oxides, respectively. The NC of BGs typically falls within the range of 2 to 3. Higher values indicate a stronger network, thus better thermal stability, but worsened bioactivity due to reduced solubility. A lower value stands for a weaker network, generally leading to poorer thermal properties [45].

However, additional considerations regarding the crystallization of BGs should be taken into account. As previously discussed, increasing attention has shifted from preventing crystallization to actively controlling it through compositional design, specifically via the incorporation of selected metallic and alkali ions allowing for adjustable structural and biological properties [46]. In parallel, significant efforts have also been devoted to the optimization of silicate-based bioactive glass-ceramics, in which crystallization does not compromise bioactivity, proving instead as advantageous thanks to improved mechanical properties of the crystalline phases [47]. Within this context, glass-ceramics such as Biosilicate® (composition in mol.%: 53.73 SiO_2, 21.22 Na_2O, 23.49 CaO, 1.56 P_2O_5) have been successfully developed [48]. This material has demonstrated excellent biological performance both in *in vitro* and *in vivo* trials, exhibiting apatite formation and bone regeneration capabilities comparable to those of the well-established 45S5 [48], also in clinical trials, as short- and long-term Dentine Hypersensitivity treatment material [49]. These features make such glass-ceramics particularly attractive for scaffold fabrication strategies involving sintering-based thermal processing, where controlled crystallization can enhance both structural integrity and functional performance [50].

BGs are also investigated for the various properties that they exhibit upon implantation. Among these, antibacterial activity is recognized as a characteristic trait of third-generation biomaterials [51]. Some antibacterial capabilities have been recounted to both 45S5 and, in particular, S53P4, against several bacteria. This is primarily achieved via alkalinization of the environment caused by BG dissolution [16], [52]. However, this effect is more easily achievable through different strategies. Specifically, it was mentioned that the addition of metallic ions in the composition of bioactive glasses can elicit specific responses in the host tissue, such as tissue revascularization, hemostatic effects, and most notably, antibacterial effects [53], [54]. Some of the mechanisms through which metal ions are effectively antibacterial are: the induction of pH changes – as already noted for 45S5 and S53P4 – which increase osmotic pressure inside the bacterium, but also mechanical disruption of the cell membrane, reduction in membrane binding ability, oxidation of functional molecules and proteins, modification of enzymes and DNA, and generation of reactive oxygen species [55].

The effectiveness of this strategy also lies with a limited ability of bacteria to develop resistance to metallic ions [56].

1.2 Electrospun polymer-based fibrous composite scaffolds

In recent years, research into regenerative medicine has focused on identifying viable strategies for manufacturing scaffolds for tissue regeneration. Among the various scaffold fabrication techniques employed for both soft and bone tissue engineering, electrospinning has been gaining increasing attention [57], thanks to its numerous upsides, such as ease of setup, relatively low materials cost, cost-effectiveness, and a wide range of achievable morphologies and compatible materials [58]. Research into BTE and wound healing began exploring electrospinning for fabricating nano- to micro-fibrous structures. This fiber morphology is particularly useful in tissue engineering, as it mimics the architecture of the extracellular matrix [59]. Indeed, one of the main strengths of this scaffold manufacturing technology is the ability to produce fibers with a tunable morphology in the 10^{-9}–10^{-6} m size range [60]. These unique characteristics make electrospun fibers ideal candidates for tissue regeneration [61]. However, the high tunability of the mats' properties also requires an extensive optimization of the machine parameters. Even minimal changes in the polymeric solution, manufacturing process, or environmental conditions can lead to significantly different results in the final product [62].

One of the most widely studied polymers for electrospinning is poly(ε-caprolactone) (PCL) [63], [64], [65], a biocompatible semi-crystalline polyester known for its high mechanical properties and optimal biodegradability [66], [67]. PCL is often used either in its pure form or blended with other polymers or insoluble particles, such as hydroxyapatite [68], [69], [70], or notably with BGs [71], [72], [73]. PCL-based electrospun fibers have been widely employed in biomedical applications, including as cardiac patches, cranial implants, and bone substitutes [74], [75], [76], [77], [78]. Moreover, recent research demonstrated that PCL/BG composite scaffolds show advantages over other PCL/ceramic composites, (where β-tricalcium phosphate or hydroxyapatite commonly serve as the ceramic phase), due to their superior mechanical properties and faster degradation kinetics, making them optimal candidates for BTE scaffolds [79].

The employment of BGs in electrospun scaffolds has gained relevance in recent years. Researchers have explored both the use of sol–gel-derived BGs as precursor solutions for electrospinning [80], [81] and the incorporation of suspended melt-derived particles into polymeric solutions [82], [83]. When utilizing melt-derived BG particles in electrospinning, it is crucial to obtain finely powdered material to ensure efficient transport and uniform incorporation into the fibrous structure. Even considering their limitations, BGs still remain an attractive material for producing electrospun scaffolds capable of exhibiting multiple beneficial biological properties in both soft and bone tissue related applications [81], [84], [85].

Lastly, the intrinsic hydrophobicity of electrospun PCL mats represents a significant challenge in the fabrication of this type of scaffold. Indeed, electrospun PCL mats have a highly hydrophobic surface, resulting in reduced biological performance, limited cell adhesion, and decreased protein adsorption [86], [87]. This can negatively affect the

scaffold's functionality and limit its applicability in clinical contexts. More considerations on the hydrophilicity of the scaffolds will be discussed in chapter "6 Optimization of PCL/BG scaffolds".

1.3 Aim of the Thesis

This Thesis aims to describe the development of two novel BG compositions to overcome known issues commonly associated with these materials, while also considering potential applications in devices for BTE and wound healing.

Firstly, this work focuses on a state-of-the-art analysis of BGs subjected to thermal treatments, with particular emphasis on their effects on glass structure, sintering, and crystallization. Further investigation in this field addresses compositional modifications of BGs through the incorporation of selected ions into the glass network, with particular attention to how these substitutions influence sintering behavior and crystallization. Additionally, chapter "2 Thermal properties of BGs and ion substitution" briefly analyzes potential applications that involve subjecting BGs to high temperatures, such as scaffold manufacturing, thermally sprayed coatings, and BG/ceramic composites manufacturing. Due to the high thermal energy involved, the feasibility of these applications is closely associated with the thermal properties of BGs, making it crucial to examine their effects in detail.

Additional research on BGs led to an exploration of the state of the art regarding their antibacterial capabilities, considering both well-established compositions and specifically engineered formulations that rely on the release of antibacterial metallic ions to exert their effects. As these materials continue to show promise in different biomedical applications, particular attention should be paid to their ability to inhibit bacterial growth, as this capability could prove essential for fully understanding and exploiting the properties of BGs in almost all applications. Various BG compositions reported in the literature will be examined for their antimicrobial or antibacterial activities, highlighting the specific mechanisms through which they inhibit bacterial growth or neutralize microorganisms. A dedicated section will explore the role of antibacterial ions such as silver, zinc, copper, and strontium, focusing on how these ions interfere with bacterial functions at the cellular level. Finally, both current and potential applications of antibacterial BGs will be discussed, along with other crucial aspects for translating these systems from research topics to practical applications, such as ion resistance, the combined use of antibiotics and BGs, and their effectiveness against biofilms.

Moving to the experimental section of this thesis, the thermal mechanical, dissolution and biological properties of Mg- and Sr- doped modified BG composition will be investigated. Indeed, a significant gap in the literature remains regarding systematic studies on co-doping with Mg and Sr in silicate BG composition and corresponding thermal treatments. The chosen reference BGs for this part of the investigation include two widely known commercial variants, namely 45S5 and S53P4. Additionally, the study examines a patented BG, referred to as Bio_MS, characterized by its distinctive composition and notable thermal

and biological properties, including the incorporation of Mg and Sr among other elements [32], [88]. Furthermore, our study expands the investigation by introducing modified versions of 45S5 and S53P4. Specifically, Mg and Sr are introduced as substitutes for calcium and sodium. This substitution is intended to modulate the glass network connectivity, thereby influencing both thermal behavior and biological response. Within this framework, this research focuses on two interconnected objectives. The first is to investigate the impact of sintering and crystallization on BGs. The second is to evaluate how doping, specifically with ions such as Mg and Sr, influences the processes of sintering and crystallization, as well as the biological response of these materials.

Lastly, chapters 5 and 6 focus on the exploration of electrospinning technology in order to manufacture electrospun PCL/BG composites. The aim of this portion of the investigation was to investigate the feasibility of electrospinning a PCL/45S5_MS suspension containing melt-derived BG, taking into account the challenges of achieving a homogeneous dispersion of BG particles within the electrospun mat [80], [89], [90], [91]. Furthermore, the study examined whether incorporating BG powder into electrospun mats could affect their dissolution behavior and biological performance, particularly in terms of cell proliferation and differentiation, thereby testing previous evidence supporting the potential application of 45S5_MS in soft tissue engineering. Moreover, the processing parameters were optimized, trying to avoid common issues of composite PCL/BG scaffolds, known to the literature and from previous results. To this end, electrospun PCL/S53P4_MS scaffolds were investigated, building on previously established fabrication methods. Firstly, BG incorporation efficiency was considered a crucial aspect of the electrospinning process. Subsequently, the effects of chemical surface modification treatment in NaOH on scaffold wettability and mechanical behavior were evaluated by testing the mats both before and after treatment. This was done to address the key issues of PCL-based BG-loaded electrospun mats, i.e. their highly hydrophobic behavior, low BG incorporation efficiency, and limited mechanical performance. In addition, the biological properties of the electrospun mats were investigated before and after chemical surface modification in NaOH, through cell adhesion tests and the evaluation of cell morphology.

Ultimately, this work aims to advance current knowledge in tissue engineering and biomedical device development by investigating one of the most promising biomaterials: bioactive glass. This Thesis seeks to elucidate the interplay between composition, thermal processing, and crystallization inhibition, and how these factors govern the resulting mechanical performance and biological response of BGs. Despite the extensive literature on bioactive glasses, significant knowledge gaps remain regarding the optimization of ion-doped systems. In addition, particular emphasis is dedicated to the implementation of effective delivery strategies, via the incorporation of BG into electrospun composite scaffolds, with the ultimate aim of producing clinically relevant devices for tissue engineering and wound healing.

2 Thermal properties of BGs and ion substitution

(This section has been published in "F. G. Mecca, D. Bellucci, and V. Cannillo, "Effect of Thermal Treatments and Ion Substitution on Sintering and Crystallization of Bioactive Glasses: A Review," *Materials*, vol. 16, no. 13, p. 4651, Jun. 2023, doi: 10.3390/MA16134651.")

As previously discussed, bioactive glasses are multifunctional biomaterials widely investigated in bone regeneration thanks to their ability to stimulate osteogenesis and form a stable chemical bond with living bone tissue [45], [92]. However, the low thermal stability of BGs often limits their employability in clinical settings [26]. In particular, when BGs are subjected to thermal treatments for sintering or scaffold fabrication, crystallization may occur. This phenomenon is generally undesirable in tissue engineering applications, as it can compromise densification when shaping it into 3-D porous scaffolds [93]. Moreover, crystallization reduces the reactivity of the glass network, potentially limiting the bioactivity of the BG [45], and leading to slower dissolution kinetics and ion release of the glass [28]. Specifically, the behavior of 45S5 and S53P4 powders during thermal treatments has been thoroughly studied in the literature, and some insights on the sintering behavior and crystallization of these materials are also provided in this work, in chapter "4 Novel Mg- and Sr-doped BG compositions".

This section of the thesis provides a comprehensive overview of the influence of different ions on the sintering and crystallization of BGs. Particular emphasis is placed on the importance of thermal treatments, as they have major implications in the manufacturing of medical devices (especially for BTE), ranging from scaffold fabrication [94] to implant coating through various deposition techniques [25]. The crystallization behavior of 45S5 is critically examined through an analysis of the literature, as this material still serves as a benchmark composition for understanding this phenomenon in silicate BG systems [10], [45].

Moreover, we tackle the implementation of manufacturing strategies in the literature, aimed at reducing the occurring of crystallization, while applying thermal treatment to BGs, such as ion substitution to increase thermal stability. Notably, zinc, potassium, and strontium have been widely investigated and shown to influence crystallization behavior, improve mechanical properties, and, in some cases, enhance biological performance [32], [95], [96], [97], [98].

Nevertheless, it should be noted that that research on ion substitution to increase the thermal stability, widening the processing window of BGs, is still ongoing. Further investigation is

therefore required to elucidate how different dopants modulate sintering dynamics, crystallization mechanisms, and the resulting performance of BGs.

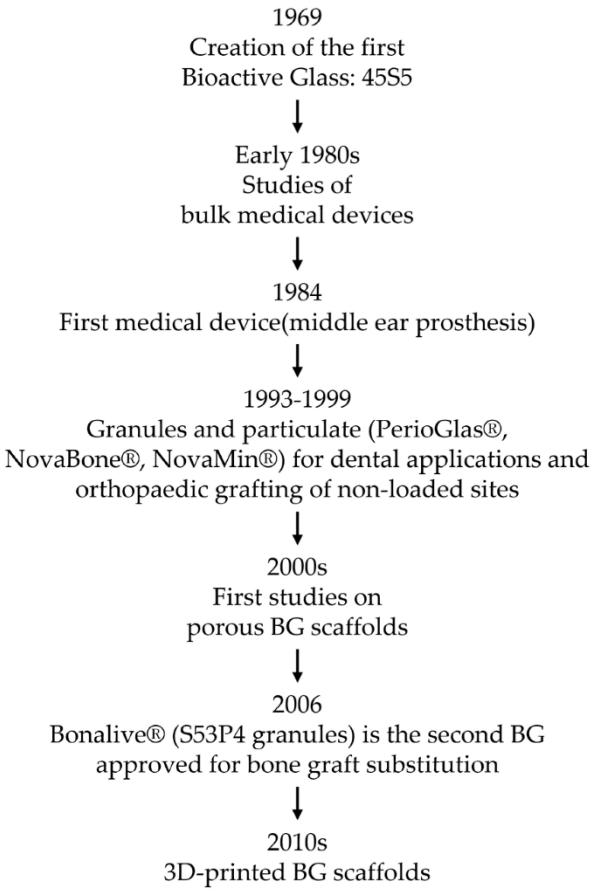

Figure 1: Flowchart of the timeline of the major breakthroughs in the bioactive glass field [45].

2.1 Why Thermal Treatments?

As previously mentioned, thermal processing is a necessary step for shaping bioactive glass powder into the desired form, depending on the application. Furthermore, the thermal treatment of BG powder triggers the formation of a liquid phase. Upon solidification, this liquid phase facilitates the sintering of the powder, thereby improving the mechanical properties of the BG material [99]. Many research papers have addressed the problem of thermally treating BG powders while minimizing the negative effects of crystallization, which can significantly impair BG's final properties. Thus, striking the right balance between promoting sintering and preserving the mechanical properties and bioactivity of BG necessitates meticulous control over thermal treatment processes, along with extensive research into different BG compositions. This equilibrium is of utmost importance in the development of bioactive glasses with optimal properties tailored for diverse biomedical applications.

Scaffolds are biodegradable porous 3D structures that can be made from various materials, including bioactive glass powders. Scaffolds serve as templates in large bone defects, to induce cell proliferation and vascularization of the damaged tissue [100]. Thus, using scaffolds may help replicate cancellous bone structure and permit cell proliferation [101],

[102], [103]. The development of an optimal scaffold for bone repair is a complex process that involves careful control of the properties of the materials and parameters used in their manufacturing. BG powders have shown great potential as a material for bioactive scaffold manufacturing due to their ability to enhance bone tissue regeneration. However, achieving the desired properties requires careful thermal treatment and compositional control. The desired properties of an ideal scaffold have been extensively discussed in the literature [104], [105]. Certain critical properties include the capacity to host cells, biocompatibility, and bioresorbability (i.e., the ability to dissolve in a biological environment without leaving behind harmful byproducts). Another crucial aspect is the high porosity of the scaffold, ideally surpassing 90%, coupled with a minimum pore size of 100 μm, to facilitate cell infiltration. Moreover, the scaffold must possess mechanical properties similar to that of bone [19].

Heat treatments are essential in the majority of manufacturing technologies for producing BG scaffolds for bone tissue engineering. The main techniques used today to produce scaffolds are foam replica, additive manufacturing, sol–gel, freeze-casting, and electrospinning [94]. Among these protocols, the foam replica and additive manufacturing techniques are the most frequently used ones to manufacture BG scaffolds. The foam replica technique and several additive manufacturing techniques produce a product known as a "green body". However, to achieve the final scaffold form with proper consolidation and improved mechanical properties, the raw "green body" must undergo a crucial heat treatment process [45], [94], [106], [107], [108].

Bioactive glass powders have also been used to coat bioinert metallic implants. This application has been studied to improve the mechanical performance of inorganic metallic grafts. Usually, the metallic materials used to manufacture these grafts (alloplastic implants), such as titanium and magnesium, promote the formation of fibrous tissue [25], [109]. Coating a metallic graft with a BG film may improve the chemical stability of the metallic substrate, providing a physical barrier to avoid in-body corrosion. This protective coating also reduces the risk of prosthesis rejection. The bioactivity of the BG can also improve the adhesion of the implant, as the BG coating is resorbed, and a superficial HA layer can form. Thus, the coating may help improving the general stability of the implant and attaining biological fixation [110].

Various techniques are utilized to deposit a surface coating of BG powder onto a metallic substrate. These techniques include enameling, sol–gel, electrophoretic deposition, plasma spraying (PS), and laser cladding. Enameling, PS, and laser cladding require exposing the powders to heat in order to sinter or melt the glass and create the superficial layer [25], [111]. Enameling is a widely recognized and traditional technique that involves the deposition on a substrate of a coating BG-containing slurry, which is subsequently dried and sintered. This process typically employs temperatures in the 800–900 °C range [112]. PS and thermal spraying techniques are both reliable methods for depositing BG coatings onto metallic inert substrates, in order to manufacture composite load-bearing grafts. The metallic substrate provides mechanical strength, while the bioactivity of BG ensures bone-bonding ability [25]. PS is an advanced technique that involves applying high voltages on inert gases to create a plasma, which can reach extremely high temperatures (thousands of degrees Celsius). This

intense heat melts the powders while rapidly accelerating the particles toward the surface, where the melt droplets quickly solidify. Nevertheless, the BG remains at high temperatures for an extended duration, which can result to the partial crystallization of the glass [113], [114].

Laser cladding, a more recent technique, operates at lower temperatures, typically ranging from 1000 °C to 1500 °C. A critical aspect of laser cladding technology is the risk of post-treatment cracking of the coating [115]. This occurs due to the significant difference in the coefficient of thermal expansion (CTE) between the BG and the substrate material. This may cause delamination of the coating layer. Solutions to mitigate this issue include (i) modifying the glass' composition to match its CTE with that of the substrate, (ii) depositing a "bond coat" with an intermediate CTE, (iii) implementing mechanical modifications to the substrate's surface, through roughening or patterning, and (iv) using chemical alterations to the substrate's surface [111]. Furthermore, Foppiano et al. successfully deposited a functionally graded BG coating, where silica content decreased while the coating thickness increased [116]. Currently, commercially available solutions for bioactive glass coatings on metallic implants are limited. Ongoing efforts are being made to improve the techniques and materials in order to optimize the results [25].

Over the past three decades, researchers have explored the potential of BG as a secondary phase in glass–ceramic composites, in combination with hydroxyapatite (HA) or β-tricalcium phosphate (β-TCP) as the primary phase [117], [118]. Hydroxyapatite ($Ca_{10}(PO_4)_6(OH)_2$) is a calcium-based mineral, chemically similar to biological apatite, which is the main mineral phase in bone tissue. Tricalcium phosphate ($Ca_3(PO_4)_2$) is a salt that can interact with living tissue and be resorbed. Both HA and TCP have been extensively studied and utilized in clinical settings due to their ability to promote bone growth in *in vivo* studies. This ability, commonly referred to as osteoconductivity, has made them candidates for the use in bone tissue engineering [119], [120]. Interestingly, HA and TCP exhibit distinct performance in terms of reactivity. For instance, HA is more stable in contact with living tissue, displaying lower dissolution rates. Conversely, TCP is more reactive, exhibiting rapid dissolution rates in contact with physiological pH [121]. This disparity in reactivity can be exploited to manufacture TCP/HA ceramic composites. In fact, by selecting specific TCP/HA ratios, it becomes possible to carefully tailor the composite's properties to meet specific requirements [122].

Bioactive glass–ceramic composites offer promising potential for bone tissue engineering. The primary motivation for using bioactive glass–ceramic composites is to enhance the mechanical properties of individual phases while concurrently tailoring the bioactivity of the composite by adjusting the content fraction of each phase. Studies indicate that an optimal fraction of ceramic particles, approximately 40 vol.%, results in the highest strength for the composite [123]. The inclusion of BG in the composite can offer advantages as it can improve the densification of the ceramic phase, acting as an effective sintering aid, which in turn leads to a final product with improved mechanical properties [124], [125]. For instance, the incorporation of as little as 2 wt.% bioactive glass into ceramic powders can substantially enhance the flexural bend strength of the composite [126].

The fraction of BG in the composite has a direct impact on the sintering rate of HA/BG composite. In fact, the presence of BG can influence the grain size of HA, leading to smaller grains, thereby enhancing the strength and sintering quality of the final material [126]. Furthermore, Baino et al. evinced that the presence of BG in TCP/BG composites may help improve the stability of β-TCP phase up to 1300 °C [127]. Without the stabilizing effect of the bioactive glass, the β phase would irreversibly convert to α phase around 1150 °C [127].

Additionally, the distinctive properties of BG, such as its ability to induce bone formation (in other words, the aforementioned osteoinductivity) and the presence of specific ions in the glass's composition, can be leveraged to further optimize the composite's performance [128], [129]. Thus, ongoing research on BG properties and applications has great potential for advancing biomaterials and regenerative medicine.

2.2 Effects of Crystallization of BGs

As we mentioned in chapter "1.1 Bioactive glasses and their properties", crystallization is considered to have a detrimental effect on bioactive glasses on several levels. Even though the crystallization peak temperature is higher than the glass transition temperature, in many cases, the crystallization of BGs takes place before significant densification can be achieved through sintering [99]. The main negative effects are (i) a modest change in volume (typically, the crystalline phase exhibits a distinct density in comparison to its amorphous counterpart), and (ii) loss of mechanical integrity in porous scaffolds, caused also by their brittleness [130]. Thus, the process of crystallization can have adverse effects, especially on the mechanical integrity of sintered products; for instance, the volume variation may create internal stresses, which, combined with the brittleness, severely hinder the mechanical performance of the samples.

From a strictly biological perspective, crystallization does not inhibit the bioactivity of bioactive glasses but rather slows it down. This delay in bioactivity also affects the conversion of the glass's outermost layer into hydroxyapatite once the material is implanted in the body and comes into contact with biological fluids. Peitl et al. found that crystallization slowed down the deposition onset of HA by three to four times in BGs containing phosphorus [131]. The slowing down of HA deposition onset is problematic since it could result in nonuniform dissolution of the scaffold, which, combined with the loss of mechanical performance, makes it unsuitable for human graft implantation. All the abovementioned effects are nevertheless linked to different parameters, such as heat treatment temperature and time; in fact, increasing the treatment time results in higher levels of densification, as well as higher crystallite and grain size. These effects do not appear to follow a linear trend over sintering time. In a study by Hashmi et al., it was observed that the crystallization rate of the BG (at a dwell temperature of 1000 °C) is higher in the 5–10 h range compared to the 0–5 or 10–15 h ranges [132]. However, as demonstrated by the wide range of applications mentioned above, the use of high temperatures is crucial in establishing the necessary sintering conditions for the manufacturing of BG delivery solutions.

One critical factor to consider is the narrow temperature range between the glass transition temperature (T_G) and the crystallization temperature (T_{C_ONSET}), i.e. the previously mentioned processing window. In fact, this process parameter plays a crucial role in

achieving successful sintering of the glass. In this regard, commercial bioactive glasses such as 45S5 and S53P4 have extremely narrow processing windows, which makes it difficult to subject these materials to thermal treatment without inducing crystallization. In order to expand the processing window, researchers have directed their efforts toward developing new BG compositions or modifying the existing ones. The objective is to achieve BGs with wider processing windows, thus allowing for successful sintering while limiting the crystallization process [133].

2.2.1 Crystallization of 45S5

Over the last few years, extensive research has been conducted on 45S5, with particular emphasis on its response to heat treatment. Previous studies have identified two distinct crystallization mechanisms for BGs, namely bulk and surface crystallization [134]. While the factors influencing the dominance of one mechanism over the other are not yet fully understood, it is evident that variations in granulometry and composition can have a significant influence on their respective prevalence. Different research papers highlighted a significant difference between the heat treatment of bulk and powdered 45S5 [99], [130], [134], [135]. This disparity is attributed to the size and granulometry of the sample, which play a crucial role in determining the outcome of the treatment. For instance, smaller granulometries (<300 μm) of 45S5 tend to undergo surface crystallization, whereas bulkier samples display bulk crystallization [130]. This disparity is evident when analyzing the differential thermal analysis (DTA) data for coarse and fine BG powders. In fact, Massera et al. reported a shift of the crystallization peak toward lower temperatures, coupled with a widening of the peak of 45S5 and S53P4 [136]. However, it should be noted that the crystallization mechanism of 45S5 is generally complex, involving a combination of different crystallization mechanisms [130].

Through analyzing DTA, differential scanning calorimetry (DSC), and X-ray diffraction (XRD) pattern data, it is possible to evaluate the characteristic temperatures and crystalline phases of a given bioactive glass. In past years, it was debated what the major crystalline phase was. While several authors agreed about identifying combeite ($Na_2Ca_2Si_3O_9$) as the main crystalline phase [131], [137], [138], more recent research by Li et al. [139] pointed out that, for lower temperatures in the 600–700 °C range, the main crystalline phase is actually $Na_2CaSi_2O_6$ [99], [139]. Today, it is widely accepted that, during the heating of 45S5 bioactive glass, two distinct crystallization processes occur. Silicorhenanite ($Na_2Ca_4(PO_4)_2SiO_4$) has been identified as the second phase, with a nucleation temperature of about 850 °C [99], [137]. The previous misinterpretation of combeite as the main crystalline phase may be attributed to the structural similarity between $Na_2Ca_2Si_3O_9$ and $Na_2CaSi_2O_6$, leading to ambiguous XRD patterns [137], [140].

Powdered 45S5 tends to have a slightly different behavior, with respect to bulkier forms (such as dense glass, granules > 300 μm, or fritted glass). This can be attributed to the presence of small-sized particles, which enable additional thermal phenomena, including sintering, to take place. As previously mentioned, sintering is a process of densification performed on powders, at temperatures below their melting point. It aims to consolidate the powders, leading to a more compact and durable material. There are three conditions that

must be met for powder sintering [141]: (i) the presence of a liquid phase that coexists with a solid phase. This occurs when the powder particles begin to melt on the surface; (ii) a decrease in the free enthalpy of the system, as this process becomes spontaneous at sufficiently high temperatures; (iii) the structural properties of the sintered product must be comparable to those of a compact material.

Without going into the details, the sintering behavior of a specific material can be evaluated through heating microscopy, which involves measuring the shrinkage of a compacted powder cylinder using the following equation [142]:

$$S_T = \frac{\Delta A}{A_0} \times 100\% \,, \tag{2}$$

where S_T is the total shrinkage, and ΔA is the difference between the area of the sample at room temperature (A_0) and the area of the sample at high temperature (A) [142]. Among the main studies dedicated to the crystallization of 45S5, we can mention Lefebvre et al. [27], [137]. In their research, the authors analyzed the five distinct stages observed in the crystallization process of this bioactive glass, utilizing DTA data. These stages include the initial glass transition occurring at 550 °C, a glass-in-glass phase separation at 580 °C, two crystallization phases at 610 °C and 800 °C, a secondary glass transition observed at 850 °C, and melting at 1200 °C [137]. According to the available data, the processing window of 45S5 is very narrow, covering a temperature range of only 60 °C. Consequently, it may not be the most suitable option for fabricating sintered bioactive glass manufacts. Furthermore, we would like to stress that the powder's chemistry, shape, and granulometry deeply affect the sintering and crystallization kinetics [143], [144]. This fact is of crucial relevance for the optimization of more complex structures, such as scaffolds that usually require a sintering process to consolidate.

2.3 Increasing the Thermal Stability of 45S5: The "Sol–Gel" Option?

To enhance the thermal stability of 45S5, researchers have undertaken investigations into the sol–gel method as a viable alternative to conventional melting technology. The sol–gel process involves the chemical synthesis of the glass using liquid and powdered precursors. This approach offers great flexibility in modifying the composition of the final glass by simply adjusting the precursor materials and incorporating various ions into the glass structure. However, it is important to note that the sol–gel process also requires a thermal treatment to trigger the chemical decomposition of the precursor reagents. In the case of 45S5, this thermal treatment may be conducted at a temperature lower than the glass's crystallization temperature [145]. Consequently, the end result of this process is a fully amorphous glass rather than a partially crystallized one.

In addition to crystallization, the elevated temperatures reached during the treatment can induce various phenomena in the bioactive glass. These include partial crystallization, sintering, shrinkage, and the evaporation of humidity and CO_2, resulting in significant mass loss [145], [146]. For example, Cacciotti et al. successfully synthesized 45S5 using the sol–gel method and reported a shift of the crystallization onset point to over 800 °C [145]. These

results were confirmed in subsequent research by Lombardi et al., where sol–gel-derived 45S5 showed crystallization of $Na_2Ca_2Si_3O_9$, with traces of $Na_2Ca_4(PO_4)_2SiO_4$ and SiO_2 after heat treatment at 900 °C [146]. Conversely to previous results, more recent research by Nawaz et al. reported the formation of combeite ($Na_2Ca_2Si_3O_9$) and rhenanite ($NaCaPO_4$) at 600 °C, and combeite and $Na_2Ca_2Si_2O_7$ at 700 °C [147]. This fact can be probably ascribed to the use of different treatment times or granulometry which is known to heavily influence the behavior of the glass.

2.4 The Effect of Thermal Treatments on Some Relevant Compositions

In the last 20 years, researchers focused on developing new BGs to achieve a widening of the processing window, which can enhance the properties and processability of BGs [45]. The properties of S53P4, a commercially available bioactive glass with a composition (in mol.%) of 53.8 SiO_2, 21.8 CaO, 22.7 Na_2O, and 1.7 P_2O_5, have been studied for almost three decades [148]. Lindfors et al. also highlighted its antibacterial properties in bone tissue infection therapy [18]. Massera et al. conducted extended analysis of the behavior of S53P4 bioactive glass, comparing it to the "gold" standard 45S5 [136]. The authors found that the behavior of S53P4 significantly deviates from that of 45S5. Although the processing window of the S53P4 glass is wider than that of 45S5, it is not wide enough to achieve sintering of the BG while preserving its amorphous nature.

To explore the sintering behavior of S53P4, researchers conducted a series of experiments and captured multiple micrographs of the powders at different sintering stages. These micrographs provided valuable insights into the progression of sintering, showcasing the distinct stages of sintering and the formation of necks between the particles [149]. After the heat treatment, the primary crystalline phase observed was $Na_2Ca_2Si_3O_9$. S53P4 exhibited surface crystallization of needle-like combeite crystals. This crystallization process occurred through a relatively straightforward nucleation and growth mechanism, in contrast to 45S5, where crystallization mechanisms tend to be more intricate. This finding implies that the properties of S53P4 may be less influenced by variations in grain size compared to other bioactive glasses, ultimately impacting the material's overall performance. Nevertheless, it is important to highlight that reducing the grain size still resulted in a lower crystallization temperature [136].

Brink and colleagues developed a novel bioactive glass, with the aim of improving the thermal properties of 45S5, called 13-93 (composition in wt.%: 53.0 SiO_2, 20.0 CaO, 6.0 Na_2O, 4.0 P_2O_5, 12.0 K_2O, and 5.0 MgO). Today, this composition is approved for *in vivo* use in Europe [150], [151]. Fu et al. conducted DTA on the 13-93 bioactive glass, revealing a glass transition temperature (T_G) of approximately 606 °C and a crystallization onset temperature (T_{C_ONSET}) around 714 °C. These findings indicate a processing window of approximately 108 °C [152]. The prevailing opinion suggests that 13-93 exhibits a significantly lower propensity for crystallization when compared to 45S5. However, there is a lack of consensus regarding the presence of a well-defined processing window for this particular bioactive glass. This discrepancy arises from the broad shape of the crystallization peak observed during DTA [133].

Fagerlund et al. [153] conducted a more in-depth analysis of 13-93 BG, comparing its performance to another newly developed BG, named 1-98 (composition in wt.%: 53.0 SiO_2, 1.0 B_2O_3, 22.0 CaO, 6.0 Na_2O, 2.0 P_2O_5, 11.0 K_2O, and 5.0 MgO). They utilized their data to generate a time–temperature–transformation (T–T–T) curve for both bioactive glasses, enabling a comparative analysis between them. The authors reported that 13-93 has a T_G of 612 ± 5 °C and 1-98 has a T_G of 608 ± 5 °C, in agreement with Fu [152], [153]. According to the DTA data, the crystallization peaks of 13-93 and 1-98 occur at 1038 ± 6 °C and 958 ± 6 °C respectively; on the other hand, the crystallization region is much wider than other glasses. In fact, T_{C_ONSET} is reported to be around 700 °C for both glasses, and the exothermic region is much wider than 45S5. According to the authors' findings, thermal treatment at temperatures exceeding 800 °C resulted in the predominant crystallization of wollastonite ($CaSiO_3$) in both glass compositions, as confirmed by X-ray diffraction analysis. The crystallites were observed to be needle-shaped, with dimensions ranging between 20 and 40 μm [153]. The presence of a wide crystallization region observed in the DTA data of the 13-93 and 1-98 BGs indicates their potential as promising candidates for biomedical applications. Thanks to their thermal behavior, these glasses could provide greater control over crystallization, which can be critical for tailoring their properties to suit specific biomedical needs.

More recent investigations include the development of a novel bioactive glass named BGMS10 (composition in mol.%: 47.2 SiO_2, 25.6 CaO, 2.3 Na_2O, 2.6 P_2O_5, 2.3 K_2O, 10.0 MgO, and 10.0 SrO), with an even wider processing window of about 210 °C [32]. The authors studied the thermal behavior of the BG and observed that the crystallization of $CaSiO_3$ takes place within the BG structure at temperatures exceeding 880 °C. This indicates a considerably broad processing window, as the T_G and T_{C_ONSET} were reported to be 670 and 880 °C, respectively. The research indicates that these favorable thermal properties are accompanied by equally promising biological properties [32], [154], [155]. Even though more work is needed in order to optimize this BG, biocompatibility tests have demonstrated that BGMS10 exhibits favorable interactions with living tissue, making it a viable solution for various applications [156].

A recent study led to another bioactive glass, named Bio_MS, with composition (in mol.%) 46.1 SiO_2, 31.3 CaO, 5.0 Na_2O, 2.6 P_2O_5, 5.0 MgO, and 10.0 SrO. Bio_MS has a T_G of about 638 °C, and the differential thermal analysis revealed a crystallization peak at 859 °C. This glass exhibits a reduced tendency to crystallize, coupled with promising sintering properties. Furthermore, extensive cytotoxicity assessments have been performed, demonstrating its biocompatibility. Most notably, Bio_MS displays excellent bioactivity and facilitates bone differentiation, making it highly suitable for biomedical applications [31].

ICIE16 is an enhanced biocompatible glass composition, produced using the sol–gel method, specifically formulated to enhance the workability of BGs. Its composition consists of 48.0 wt.% SiO_2, 6.6 wt.% Na_2O, 32.9 wt.% CaO, 2.5 wt.% P_2O_5, and 10.0 wt.% K_2O. Westhouser et al. conducted a study in which they successfully heat treated and sintered ICIE16 at 690 °C, resulting in the production of a sintered amorphous material. This is in contrast to the behavior of 45S5 glass composition [157]. Wu et al. studied the crystalline phases obtained from the heat treatment of ICIE16 BG scaffolds. They reported that the crystallization of

two main phases ($K_3Na(SO_4)_2$ and $Na_2CaSi_3O_8$) takes place at temperatures exceeding 700 °C [158]. In contrast, Nommeots-Nomm et al. identified $Ca_2Si_4Ca_3(PO_4)_2$ as the main crystalline phase [159]. This discrepancy is likely attributed to several factors, such as variations in heat treatment protocols and slight differences in the glass composition itself, which may induce significant reactions during the treatment process. However, ICIE16 is reported to be a potential candidate for use in sintered manufacts thanks to its relatively low T_G and high viscous flow. Given the complexity of the subject, further investigation is necessary to comprehensively identify all the factors contributing to the sinter-crystallization of bioactive glasses. Table 1 provides a summary of the glass transition and crystallization temperatures for the main BG compositions discussed above.

Table 1: Summary of glass transition (T_G) and crystallization peak (T_C) and onset (T_{C_ONSET}) temperatures of some relevant BGs.

BG	Glass Transition Temperature (T_G)	Crystallization temperatures: T_{C_ONSET}(Onset), T_C (Peak)	Ref.
45S5	550 °C	T_{C_ONSET} = 610 °C	[137]
S53P4	561 °C	T_C = 748 °C	[136]
13-93	612 °C	T_{C_ONSET} = 714 °C, T_C = 1038 °C	[152]
1-98	608 °C	T_{C_ONSET} = 700 °C, T_C = 958 °C	[153]
BGMS10	670 °C	T_{C_ONSET} = 880 °C, T_C = 932 °C	[32]
Bio_MS	638 °C	T_{C_ONSET} = 817 °C, T_C = 859 °C	[31]
ICIE16	575 °C	T_{C_ONSET} = 725 °C	[158]

2.5 Ion Substitution to Improve Thermal Properties of BGs

To tackle the various challenges typically associated with thermal treatments of BGs, scientists have delved into the incorporation of ions into the glass composition to customize the thermal properties of BGs according to specific requirements. In this section, the main effects of different ions on the thermal properties of BGs are discussed. The main objective is to examine the reported influence of ions on their respective BGs and explore the potential advantages of these modifications in enhancing the thermal properties of BGs for biomedical applications.

The mixed alkali effect (MAE) refers to the phenomenon where the inclusion of two or more alkali metal ions (such as Na, K, and Li) in a glass composition can lead to an enhancement of the properties of BGs, such as improved thermal stability, electrical conductivity, and mechanical strength [26]. The effect is believed to arise from changes in the glass structure, as a result of the presence of multiple alkali cations and the difference in the atomic sizes and bonding of the ions [160]. The MAE has been extensively studied in various BG systems and has shown to be promising for enhancing the properties of BGs for biomedical applications. Mixing different alkali ions in the glass structure has been shown to reduce the tendency of the glass to crystallize by introducing distortions in the structure of the glass. This facilitates the preservation of the material's amorphous structure. All these factors contribute to enhancing the viscous flow properties of the glass, thereby facilitating improved sintering of the BG [26], [161].

Specifically, Moghanian et al. conducted a study on the use of lithium as an additive ion in 58S BG, a bioactive sol–gel-derived glass. The authors found that lithium has a tendency to broaden the endothermic crystallization peak while lowering the crystallization peak temperature from 980 to 952 °C [162]. Maçon et al. studied the interaction between lithium and silica in a Si–Li sol–gel bioactive glass system. They discovered that lithium could act as nucleation site for Li_2SiO_2 phase [163]. This is probably due to the fact that the lithium ion is the smallest among the alkali metals, and its presence alone in the composition does not favor the broadening of the processing window. However, it does lower the T_G of the BG. Conversely, potassium, being larger than sodium and lithium, introduces distortions in the glass lattice, thereby impeding crystallization [96], [164].

Furthermore, the substitution of K ions in 45S5 for Na ions can slightly improve the mechanical properties of the material. This can be ascribed to the lattice distortion effect caused by potassium, resulting in improvements in microhardness, fracture toughness, and Young's modulus [96]. Moreover, the research has shown that increasing the total calcium content and substituting potassium for sodium may lead to improved thermal properties. However, it should be noted that this modification also results in a stronger glass network, which may have the unintended effect of slowing down the deposition of hydroxyapatite in simulated body fluid (SBF), as well as *in vivo* [165].

Strontium has been extensively studied as a substitute ion for calcium in various BG compositions. Generally, strontium acts as a network modifier, causing the expansion of the glass network. As strontium is a larger ion than calcium, this leads to a weakening of the lattice structure. Consequently, as strontium substitution increases, there is a linear decrease in the glass transition temperature. Furthermore, Sr substitution for Ca causes an increase in the density of the glass [97], [166]. Fujikura et al. reported that, with increasing strontium substitution in a 45S5-based glass, there was a decrease in crystallization temperature [97]. XRD analysis showed the crystallization of combeite phase during lower-temperature heat treatment. At temperatures exceeding 820 °C, the authors reported the crystallization of strontium-substituted combeite ($Na_2Sr_2Si_3O_9$) and a ring-structured silicate phase ($Sr_3(Si_3O_9)$) [97]. On the other hand, Massera et al. reported a different trend in a S53P4-based composition [166]. They found that the crystallization peak temperature decreases up to 5 mol.% SrO in the glass composition but then increases for higher concentrations. However, the authors specified that the combination of these two effects did not lead to a significant widening of the processing window [166].

Bellucci et al. investigated the presence of strontium and magnesium in BGMS10 and its "parent" glass BG_Ca_Mix [32]. They reported that magnesium has a similar effect on the bioactive glass as strontium, particularly concerning the thermal stability of the glass. However, the presence of Sr and Mg has extensively been reported to have positive effects on bone tissue formation [32], [167]. Moreover, magnesium has been shown to lower the glass transition temperature in BGs belonging to the $CaO–MgO–P_2O_5–SiO_2$ system. This is attributed to the weaker Si–O–Mg bond compared to Si–O–Si, resulting in a less robust network structure. This effect is paired with the ability of magnesium to inhibit crystallization of both the BG and the apatite layer deposited after SBF immersion [168]. Evidence suggests that magnesium is incorporated in the apatite-like crystals, decreasing the

number of calcium–phosphorus nucleation sites, and resulting in the stabilization of the amorphous structure [169], [170].

Zinc has been incorporated in both sol–gel and melt–quench (45S5) BG, resulting in a slight decrease in crystallization and nucleation temperatures. Similarly, substituting zinc for magnesium in BGMS10 also leads to a greater decrease in glass transition and crystallization temperatures [171]. For instance, the addition of 2 mol.% zinc to the glass composition in place of magnesium can result in a drop in T_G from 670 to 622 °C and in T_C from 932 to 881 °C [171]. XRD analysis performed by Srivastava et al. revealed that the presence of zinc ions did not affect the crystalline phases, which remained $Na_2Ca_2Si_3O_9$ and $Na_2CaSi_3O_8$ [95]. In contrast, Shruti et al. [172] observed the formation of a Zn_2SiO_4 phase after heat treatment at 700 °C. However, the difference in glass composition heavily influenced the crystallization process [95], [172]. Nevertheless, the use of zinc ions in glass compositions has some significant drawbacks due to its biological effects. Concentrations of zinc ions over 1 mol.% have been found to slow the formation of apatite, which is undesirable for biomedical applications [95], [172]. Additionally, there is a potential risk of cytotoxicity associated with higher concentrations of zinc ions in the glass [171]. Wetzel et al. conducted an investigation into the substitution of small amounts of magnesium or zinc for calcium in the 45S5 bioactive glass, ranging from 2.5 to 15 mol.% [173]. The results showed that the incorporation of these ions improved the processability of the glass. Due to the higher field strength of Mg^{2+} and Zn^{2+} compared to Ca^{2+}, their substitution led to an increase in crystallization temperature and a decrease in T_G. The researchers further noted that even a modest substitution of 2.5 mol.% was sufficient to induce this shift, while higher substitutions did not yield significant improvements in the outcomes [173], [174]. These seemingly contrasting results may be attributed to different interactions between ions within the glass structure, which give rise to complex and not easily predictable thermal behaviors.

Research has also focused on the incorporation of barium in bioactive glasses. In particular, researchers have investigated the impact of substituting barium oxide for both silicon and calcium. Arepalli et al. studied barium BaO substitution for SiO_2 in 45S5 [175]. They discovered that barium functions as a modifier of the glass network, leading to a decrease in both the crystallite nucleation temperature and the T_C of the glass. Specifically, the nucleation temperature dropped from 614 to 542 °C, while T_C decreased from 760 to 680 °C. The XRD analysis demonstrated that the primary crystalline phase was $Na_2Ca_2Si_3O_9$. Khoeini et al. opted to substitute barium for calcium in 45S5 [176]. Their findings are analogous to those of Arepalli et al. [175] and indicate that barium functions as a modifier, weakening the glass structure. Interestingly, Khoeini et al. [176] did not observe a reduction in the number of oxygen bonds in the glass structure as reported by Arepalli et al. [175]. Their research led to the conclusion that barium is inserted into the glass structure as an interstitial element [176]. This leads us to infer that, while barium may exhibit promising biological properties for specific applications, it does not seem to enhance the thermal performance of bioactive glass.

Cobalt has been the subject of investigation as a potential substitution ion in BGs in many research studies. Vyas et al. examined the effects of partially substituting cobalt for silicon in 45S5-based glass compositions, varying the cobalt content from 0 to 4 mol.% [177]. The

results showed a general improvement in the mechanical properties of the Co-containing glass. Specifically, the Young's modulus, shear modulus, bending strength, and density exhibited a linear increase with cobalt substitution, up to a maximum of 3 mol.%. It was observed that cobalt acts as an intermediate oxide up to 2 mol.%, after which it acts as a network modifier. This transition also affects the mechanical properties of the glass, which does not increase linearly over this limit [177]. Moreover, cobalt addition seems to lead to a weakening of the glass network, since Si–O–Co bonds are weaker than Si–O–Si. This influences the T_G of the material. DTA data showed that glass transition temperature decreases with increasing Co content [177], [178]. However, Co substitution also lowers the crystallization peak temperature from 718 °C to 616 °C. The formed crystalline phases were identified through XRD analysis of thermally treated samples, revealing the presence of two major cobalt-free phases: $Na_2Ca_2Si_3O_9$ and $Na_2CaSi_3O_8$ [107,109]. This observation further supports cobalt's role as an intermediate oxide in the glass composition.

Zirconium is another element that has recently been used for ion substitution in BGs. Kang et al. gradually replaced sodium with increasing fractions (up to 12%) of zirconium oxide in 45S5 [179]. Zirconium was found to act as a network modifier, increasing the number of bridging oxygen bonds and leading to a more rigid glass structure. This led to improved mechanical properties of the glass, including greater flexural and compression strength, as well as increased Vickers hardness [179], [180]. Furthermore, the presence of zirconium had an impact on the T_G of the BG, with an increase in zirconium content corresponding to a higher glass transition temperature. Unfortunately, zirconia is a well-known inert biomaterial, and the presence of zirconium in the glass structure can inhibit its bioactivity [180].

The field of BGs has gained unprecedented interest. The number of scientific papers regarding BGs is ever growing, as illustrated in Figure 2. The hope is that this active academic engagement will lead to other interesting discoveries about the effects of different ions on the thermal, mechanical, and biological properties of BGs. Table 2 reports a summary of the effects of ions on mechanical and thermal properties of BGs discussed in this section.

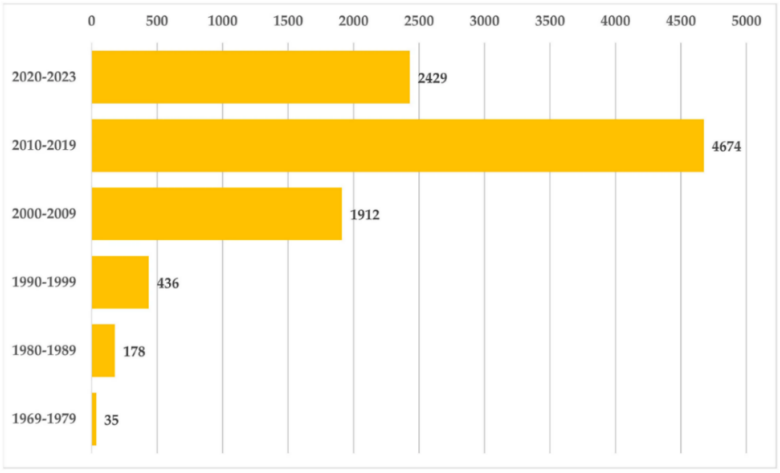

Figure 2: Number of scientific papers on BGs across different decades from the inception in 1969 to 2023. Notably, in the 2020–2023 interval, the publication count is already conspicuous. Data were retrieved via Scopus, with keywords "bioactive glass" or "bioglass".

Table 2: Summary of the effect of different ions on mechanical and thermal properties of BGs.

Ion	Parent BG	Substituted ion	Effect	Ref.
Mixed Alkali Metals	-	Na	Improved thermal stability Improved mechanical properties Hinders crystallization Broader processing window	[26], [161]
Li	58S	Addition	Broader crystallization peak Lower crystallization temperature New crystallized phase	[162]
K	45S5	Na	Improved mechanical properties	[96]
Sr	45S5	Ca	Increased density New crystallized phase	[166]
	S53P4	Ca	Lower crystallization temperature Lower crystallization temperature	[94]
Mg	-	Ca	Lower glass transition temperature Inhibit crystallization Less robust network	[97]
	-	Addition	More stable amorphous phase	[170]
Zn	45S5	Ca	Lower glass transition temperature Lower crystallization temperature Lower viscosity New crystallized phase (debated)	[95], [172]
	BGMS10	Mg	Lower glass transition temperature Lower crystallization temperature	[171]
Ba	45S5	Si	Lower glass transition temperature Lower crystallization temperature	[175]
	45S5	Ca	Lower glass transition temperature Lower crystallization temperature Reduced number of oxygen bonds	[176]
Co	45S5	Si	Improved mechanical properties Lower glass transition temperature Lower peak crystallization temperature	[177]
Zr	45S5	Na	Increased mechanical properties Increased number of bridging-oxygen	[179]

3 Antibacterial properties of BGs

(This section has been submitted for publication and is currently under revision in the *Journal of the American Ceramic Society.* Received: 16 Feb 2026)

As previously anticipated, BGs have evolved significantly over the years, and today they are considered third-generation biocompatible materials, capable of expressing specific functions and eliciting reactions when implanted [45]. In fact, BGs can release therapeutic ions contained in their composition when dissolving in physiological environments. Such ions can express their antibacterial activity at the implantation site. Specifically, BGs have been investigated for their antibacterial and antibiofilm properties [17], [181], [182]. For example, 45S5 Bioglass® has been reported to possess antimicrobial properties against Gram-negative bacteria; however, this effect is predominantly pH-related, which may be difficult to replicate in an *in vivo* biological environment [183]. Similarly, other commercially available compositions, such as S53P4, have demonstrated pronounced antibacterial responses when tested for their ability to inhibit bacterial growth and killing bacteria [52], [184]. In these early-generation compositions, antibacterial effects were primarily associated with pH alterations of the surrounding medium; meanwhile, more recent BG formulations have been engineered to incorporate specific antibacterial ions to achieve stronger and tunable effects. Metallic ions including silver, copper, zinc, strontium, iron, cerium, gallium, and boron can exert bactericidal activity, acting through multiple strategies, such as membrane disruption, enzyme interference, oxidative stress, or inhibition of DNA replication [185], [186].

In the context of antibacterial efficacy of BGs, the literature emphasizes the advantages of sol–gel derived BGs over the traditionally manufactured melt-quench BGs, as their antibacterial effects are enhanced due to specific features of sol–gel derived materials [187], [188]; for instance, their morphological properties (such as small nanoscale porosities), their high reactivity, their improved homogeneity, which can enhance specific effects of BG on the environment [14]. Sol–gel derived BGs are far more reactive than their melt-quench derived counterparts. These features allow sol–gel BGs to be valuable weapons against infectious bacteria [188], [189].

The most employed testing procedures for the antibacterial efficacy of BGs are ISO 22196:2011 [190] and JIS Z 2801 [191] which describe testing procedures for non-porous surfaces [192], and ASTM E2149-20, specific for dynamic conditions [193]. BG surfaces fall under two widely recognized types of antibacterial surfaces: “contact-kill” surfaces, which exert antibacterial effects through direct interaction with bacterial cells, and leachable surfaces, which rely on the release of antibacterial ions into the surrounding environment [194]. Nevertheless, several testing procedures are carried out to evaluate the antibacterial performance of BGs. Antibacterial testing procedures can be divided into several categories, including tests for materials with a high surface-to-volume ratio, inhibition zone on agar plates, eluate or solution tests, adhesion tests, and biofilm tests [195]. Among these, inhibition zone and eluate tests are the most commonly employed for BGs. For agar tests, inhibition halos with diameters exceeding 10–15 mm are typically considered indicative of antibacterial activity [192]. Nevertheless, this method presents notable limitations, including

restricted diffusion of certain ions in agar media, strain-dependent bacterial growth behavior, and its mainly qualitative nature [196]. Meanwhile, solution-based assays, while more appropriate for assessing ion-mediated antibacterial effects, also present limitations, as optical density measurements and colony–forming unit (CFU) counting do not discriminate between viable and non-viable bacteria [192].

This section analyzes and summarizes recent research on the antibacterial properties of BGs. Major attention is dedicated to their bacterial inhibition and killing ability, as this is crucial for understanding the full scope of capacities BGs possess. Starting from marketed and melt-quench derived compositions, numerous BGs are reviewed in this section with particular attention to doped BG compositions, containing therapeutic ions, such as silver, zinc, copper, and strontium, focusing on how these ions interfere with bacterial functions at the cellular level. Moreover, current and future applications for these materials were investigated, from scaffold manufacturing to implant coating, from substitutes for antibiotics to effective anti-biofilm agents.

3.1 Antibacterial properties of widely known melt-derived compositions

Several studies have demonstrated the antibacterial effects of 45S5. Hu et al. [197] showed that the antibacterial effect of 45S5 on *S. aureus*, *S. epidermidis* and *E. coli* is directly dependent on the concentration of BG in the medium. 50 mg/mL of 45S5 particles exhibited antibacterial effectiveness comparable to that of benzylpenicillin G against all bacteria tested. The authors attributed this activity primarily to the increase in pH of the solution; however, they also observed that BG powder debris could mechanically disrupt bacterial cell membranes [197]. Allan et al. [52] confirmed a direct correlation between the pH increase in an aqueous solution containing 45S5 Bioglass® and its antibacterial effect, comparing gingival bacterial death rates in the 45S5 eluate with those in a NaOH-diluted solution [52]. They also reported that S53P4 exhibited a stronger antibacterial effect compared to 45S5 [52]; however, more recent studies have yielded contrasting results, suggesting that 45S5 had can achieve comparable antibacterial performance when tested alongside S53P4 against various bacterial strains, including MRSA, an antibiotic-resistant staphylococcus [184]. These studies specifically highlighted the significant influence of particle size on BG antibacterial properties. In particular, 45S5 shows increased bacterial inhibition activity after 24 hours when used as fine particles, due to the higher surface to volume ratio and the resulting faster dissolution, especially against biofilm; on the contrary a coarser granulometry is associated with less effective antibacterial action [184]. Even if the impact of particle size appears less pronounced for S53P4, it remains a relevant parameter for this composition as well [184]. These differences in antibacterial effectiveness associated with granulometry likely contribute to the discrepancies reported in the literature regarding the relative antibacterial performance of 45S5 and S53P4 [52,184]

Further evidence of the antimicrobial properties of S53P4 has been reported in comparative studies. The effectiveness of powdered (particle size < 45 μm) S53P4 against a range of bacterial species was tested, together with five more powdered silicate and borosilicate melt-derived BGs, namely 13-93, H2-02, 18-04, 23-04 and 3-04 [17]. The compositions of these

bioactive glasses, together with those of the most relevant BGs cited further in this review, are reported in Table 3. Results showed that S53P4 performed better than all the other BG samples, both on average and in single experiments against bacteria lines, yielding the lowest bacterial growth rates. This enhanced activity was correlated with the rapid pH increase in the medium, favored by the fine granulometry of the BGs. Moreover, the strongest antibacterial effect for all BG samples occurred during the first 24 hours of immersion, coinciding with the greatest pH rise. In contrast, 23-04, H2-02, and 13-93 displayed the weakest antibacterial activity due to their limited ability to inhibit bacterial growth [17]. These findings confirmed earlier results by Zhang et al., who reported optimal bactericidal effects for S53P4 while only moderate effects were reported for 13-93 and 18-04 [16]. The researchers emphasized that BG antibacterial activity is largely pH-dependent and noted that under anaerobic conditions, the reduced pH increase may limit antibacterial efficacy [181]. The researchers emphasized that BG antibacterial activity is largely pH-dependent and noted that under anaerobic conditions, the reduced pH increase may limit antibacterial efficacy [198]. In recent years, S53P4 has gained attention as a potential candidate for bone tissue regeneration, demonstrating effectiveness against bone bacterial biofilms *in vitro* [181], [199].

Other melt-derived BG compositions have shown promising bactericidal properties. For instance, F18, a recently developed melt-quench derived silicate BG containing potassium and magnesium [200], was evaluated both *in vitro* and *in vivo*, showing encouraging results in fibroblast differentiation and apatite deposition [201]. Passos et al. tested F18 against *S. aureus*, both through direct contact with the powder after 6 hours and via eluates at different BG concentrations, against *S. aureus* biofilm [200].

Table 3: Compositions (mol.%) of the most relevant BGs mentioned in this review. When the exact molar percentage was not reported, ">0" indicates the presence of the corresponding oxide in the formulation.

composition	Ref.	SiO_2	Na_2O	CaO	P_2O_5	B_2O_3	K_2O	MgO	Al_2O_3	SrO
45S5	[10]	46.1	24.4	26.9	2.6					
S53P4	[17]	53.8	22.7	21.8	1.7					
3-04	[17]	51.3	4.9	24.5	0.5		9.7	9.1		
13-93	[17]	54.6	6.0	22.1	1.7		7.9	7.7		
13-93B3	[202]		8.8	20.5	1.6	43.7	12.5	12.8		
H2-02	[17]	53.7	5.9	23.9	1.2	1.1	7.1	6.8	0.3	
18-04	[17]	54.2	14.5	21.2	1.7	1.7		6.7		
23-04	[17]	57.1	4.9	21.7	0.4	1.8	7.3	6.8		
58S	[203]	60		36	4					
F18	[200]	>0	>0	>0	>0		>0	>0		
HX-BGC	[204]	>0	>0	>0	>0					>0

3.2 3. Antibacterial mechanisms in integrated bioactive glasses

As previously discussed, BGs such as 45S5 and S53P4, are able to exert antibacterial activity in the surrounding environment through various mechanisms that arise from their interaction with it. Firstly, a mechanical antimicrobial effect may arise from direct contact between BG

particles and bacterial cells, potentially leading to membrane disruption and loss of integrity, killing the microorganisms. Secondly, the pH increase derived from rapid ion exchange, plays a major role, especially during the early contact phase. This effect is strongly dependent on dissolution kinetics and is typically most pronounced within the first 24 h. However, based on their composition, BGs can also present a third antibacterial effect, more specifically related to their composition. Some BGs containing therapeutic ions (e.g., Ag^{+}, $Cu^{+/2+}$, Zn^{2+}) can induce ion-mediated antibacterial effects, regulated by the release of antibacterial ions from the BG into the environment. Notably, these processes do not act independently but are rather interconnected through the kinetics of glass dissolution.

Therapeutic ions incorporated within bioactive glasses are released into physiological fluids upon dissolution. These can exert specific effects on the bacterial population, which will be discussed in depth in the next sections. Briefly, these metallic and alkali ions can interfere with bacterial metabolism, membrane exchange, and intracellular processes inhibiting growth and proliferation while causing bacterial death. This links the antibacterial properties of BGs not only to their intrinsic biological effects but also to their release kinetics and composition, influencing the overall biological effect of the material. In the following sections, the antibacterial roles of specific ions incorporated in the glass compositions are discussed in detail to highlight their crucial role in the expression of antimicrobial properties in BGs.

3.2.1 Silver

Firstly, one of the most investigated metals for engineering BGs with antibacterial properties is silver (Ag). Although there is no unanimous consensus on the mechanisms by which Ag ions exert antibacterial activity, different theories have surfaced, such as inhibition of cellular respiration and nutrient absorption [186], [205]. These mechanisms are probably related to complex reactions between silver ions and macromolecules or proteins [206], as well as with the bacterial genetic material [207]. Furthermore, Ag nanoparticles added to biomaterials also result in the expression of antibacterial properties, likely related to cell membrane disruption and DNA damage [55]. Further research has demonstrated the ability of Ag nanoparticles embedded in mesoporous BG to reduce the CFU counts of both *S. aureus* and *P. aeruginosa* [208]. Nonetheless, research has also suggested that other metallic ions, primarily Copper (Cu) [186], as well as organic compounds containing thiol groups [209], could compete with Ag in antibacterial action, reducing its efficacy. However, a borate BG composition with Ag as a co-doped with cerium (Ce) showed excellent antibacterial efficacy against *E. coli* and *S. aureus* [210].

Sol–gel-derived BGs doped with variable concentrations of Ag (from 0.5 mol.% up to 3 mol.%) have been shown to express interesting bactericidal effects. Bellantone et al. produced Ag-doped sol–gel derived silicate BGs [182], and Ahmed et al. produced phosphate-based, Ag-doped, melt-derived BGs [211], and both demonstrated a strong correlation between Ag content in the BG and the antibacterial efficacy of the BG. Furthermore, they showed that Ag exhibits greater antibacterial activity against *P. aeruginosa* than against *S. aureus*, which in turn is more susceptible than *E. coli*. However, Ag-doped BGs exhibit greater antibacterial effects than undoped compositions; this was also

verified by testing sol–gel derived Ag-doped composition and 45S5 against *S. epidermidis* [212], *E. coli*, *S. aureus* and *P. aeruginosa* [182].

Another sol–gel derived BG composition containing 5 mol.% of Ag was tested against *E. coli*, where Ag adsorption by the bacteria was observed, indicating a direct interaction between the microbial cells and the glass dissolution products. This interaction was further supported by the inhibition of *E. coli* colony formation [213]. Similar encouraging results were found by substituting 2 to 4 mol.% of Ag in a 58S-based sol–gel composition [203].

Recent studies by Shendage et al., in which 1 mol.% to 5 mol.% of Ag was added as a dopant to a silicate sol–gel BG, not only confirmed the antibacterial activity against *S. aureus* and *E. coli*, but also suggested low cytotoxicity and angiogenic properties [214]. Still, the literature also suggests that Ag nanoparticles may express the opposite effect, potentially inhibiting vascularization [215]. The efficacy of Ag ion doping in sol–gel compositions was confirmed by Akhtach et al., who demonstrated that even low silver contents are sufficient to induce antibacterial activity against *E. coli* and *S. aureus* [216].

These findings support the potential of Ag-doped BGs as effective antibacterial materials for infection control.

3.2.2 Copper

Copper has also been shown to have a high potential for antibacterial activity. The antibacterial properties of Cu are well known in the literature and are retained even when Cu is present in alloys [217]. For this reason, metallic copper is currently widely used in applications with a high risk of contamination to prevent the spread of microorganisms [217], [218], both aerobic and anaerobic [218], [219]. In particular, researchers have shown that the ion Cu^{+} ion is more effective than Cu^{2+} in suppressing the activity of anaerobic bacteria [219]. The identified antibacterial mechanisms of copper ions include cell membrane disruption, oxidative damage, biochemical alteration and DNA damage [185], [220].

Numerous studies have demonstrated that the addition of up to 5 mol.% of copper in both sol–gel and melt-quench BG compositions has resulted in more pronounced antibacterial effects when compared to undoped compositions, both against aerobic and anaerobic bacterial strains (*E. coli* and *S. aureus*) [221], [222], [223], [224], [225], and against *S. epidermidis* [226]. Moreover, Cu has also been used as a dopant in borate- and phosphate-based BGs [227], [228]. Notably, results have shown that Cu-doped sol–gel BGs can exhibit stronger antibacterial properties than their Ag- and Fe-doped counterparts, probably due to the higher ion release of the former, which is correlated with lower network connectivity [223].

However, the antibacterial effects of Cu-doped BGs are strongly affected by dopant content in the composition, ion release kinetics, BG concentration in the eluate, the methodology used to assess the antibacterial properties, and the type of bacteria [221], [223], [229], [230], [231]. Specifically, Gram-positive bacteria (such as *S. aureus*) are less susceptible to copper-doped BGs than *E. coli* [223], [230]. Lastly, recent studies on Cu-doped 45S5 have shown a marked decrease in inhibition zone diameter for *E. coli*, *S. aureus* and *S. mutans* when Cu

concentration exceeded 0.5 mol.% [232]. Conversely, other studies have shown that low-Cu-doped sol–gel-derived BGs can exhibit strong bactericidal activity, mostly dependent on the BG concentration in the medium [233].

These findings highlight the need for more refined compositional optimization, as the antibacterial response of Cu in BGs does not necessarily scale linearly with ion content.

3.2.3 Zinc

Zinc (Zn) ions are essential for the metabolic activity of both prokaryotic and eukaryotic cells [234], [235]. Alongside its biological properties, the antibacterial properties of Zn have been documented for decades, also in combination with other agents [236]. These properties have also been more recently investigated by Phan et al. [237]. Notably, the authors associated the antibacterial effects of zinc with the inhibition of glycolytic enzymes and alkali production. However, its effectiveness was improved when combined with other antibacterial agents, as its activity was found to be lower than that of other ions, such as Cu^{2+} [237]. Anyways, excess of Zn ions in the environment can lead to a metal ion homeostasis imbalance, ultimately resulting in bacterial death [234], possibly via the inhibition of cellular respiration [238].

Sanchez-Salcedo et al. demonstrated that the amount of zinc in sol–gel-derived silicate BG was correlated with the antibacterial efficacy of the BG against *S. aureus*, both as a growth inhibitor and as a bactericide [239]. Moreover, Zn was shown to be an effective antimicrobial agent in a melt-derived BG composition when tested against *S. epidermidis*, *E. coli*, and *P. aeruginosa* [171].

In recent research, Zn is often introduced into BG compositions as a co-dopant ion. Fakher et al. demonstrated that Cu-Zn co-doped BGs exhibit optimal antibacterial properties against biofilms and planktonic forms of *S. epidermidis*, *E. coli*, and *P. aeruginosa* [240]. Similar results were found by modifying 58S, a sol–gel-derived BG, through the addition of Zn and Cu [241], by, and by introducing the same ions into 13-93B3, a melt-derived borate-based BG [202], and by adding Zn and Ag to a sol–gel based composition tested against *E. coli* [242].

However, co-doping with other elements, such as magnesium, has also resulted in enhanced antibacterial potential of mesoporous BG against both *E. coli* and *S. aureus* [243]. The authors attributed this effect primarily to the presence of Zn ions, whose higher concentrations were associated with increased antibacterial efficacy. Furthermore, the antibacterial effects of magnesium oxide and ions are still under debate in the literature, as contrasting results report both their ability and the lack of ability of Mg-based species to inhibit bacterial proliferation [244]. Lastly, it has also been reported that the inclusion of magnesium in borosilicate sol–gel-derived BGs resulted in high inhibition efficacy of *S. aureus* proliferation *in vitro*, with increasing MgO content in the composition [245].

3.2.4 Cerium

Rare earth elements such as cerium (Ce) have long been known to interact with living organisms, such as *E. coli*. It has been demonstrated that bacteria can absorb Ce ions,

resulting in the inhibition of oxygen uptake and cell membrane disruption at sufficient high concentrations [246]. While some studies report the efficacy of Ce as an antimicrobial agent when added as a dopant in BGs, while also retaining high bioactivity and apatite-forming ability, other studies report variable efficacy against different bacterial strains [247].

Youness et al. showed that the addition of at least 0.7 wt.% of Ce in a melt-derived phosphate-based BG is required in order to exhibit significant antibacterial effects against *S. aureus* and *E. coli*, with no bactericidal effects observed against *B. cereus*, *B. subtilis*, and *C. albicans* [248]. The toxicity of Ce against *E. coli* has been reported in several studies in the literature [242], [249], [250]; however, the relatively high concentrations needed may result in potential toxic effects on healthy tissue cells.

Similar results were reported by Morais et al. following the incorporation of Ce into a phosphate-based BG, which exhibited marked antimicrobial activity against *S. epidermidis* and *S. aureus*, but showed no significant efficacy against the Gram-negative bacterium *P. aeruginosa* [251]. However, some studies have successfully utilized co-doping of Ce and Ag to improve the antimicrobial properties of sol–gel BGs not only against *E. coli* but also against *S. aureus* and *P. aeruginosa* [252], [253].

3.2.5 Strontium

Strontium (Sr) is an ion often employed as a doping ion in BG compositions, thanks to its biological activity and its effects on the thermal stability of the BGs. This properties will be analyzed in depth in chapter "4 Novel Mg- and Sr-doped BG compositions" Dabsie et al. [254] showed that Sr ions do not exhibit strong antibacterial effects against eleven aerobic and anaerobic bacterial strains in direct culture antibacterial testing up to concentrations of 1.1 mol/L [254]. This result may also be related to the Sr ion concentration, as Subburam et al. [255] found a strong correlation between SrO nanoparticle concentration and the bactericidal activity of the suspension, with 25 μg/mL being the minimum concentration to express antibacterial properties [255].

A high content of Sr in BG compositions has been shown to induce growth inhibition in *P. gingivalis* and *A. actinomycetemcomitans* [256], and reducing the particle size of Sr-doped BG can improve its antimicrobial efficacy against *S. aureus* [257]. Nevertheless, the literature suggests that, in combination with other ions, Sr may produce positive results in antibacterial testing. Baheiraei et al. [39] tested Sr-containing sol–gel-derived silicate BGs and found strong antibacterial effects of the BGs in gel-cultured *E. coli* and *S. aureus*. This result was attributed both to the pH-altering effects of BGs and to the capacity of Sr ions to enhance the bactericidal effects of BG [39].

Similarly, 58S BG, doped with 5 and 10 mol.% Sr ions proved its bactericidal efficacy against *MRSA* [38]. The co-doping of BGs with Sr ions together with Zn, Cu, or Ag has also proved to be an efficient strategy to obtain a bioactive glass with positive biological properties that is also able to express bactericidal effects [224], [258], [259], even though Sr exhibits milder antibacterial action compared to Zn in similar ion-doped melt-derived BGs [260].

3.2.6 Iron

Iron (Fe) is not a commonly employed metal for bioactive glass doping. Gram-positive and Gram-negative bacteria are capable of adsorbing Fe^{3+} ions and reducing them to Fe^{2+}. The latter participates in redox reactions, leading to the generation of highly reactive hydroxyl radicals, inducing oxidative stress within bacterial cells, lipid peroxidation, protein oxidation, and DNA strand damage – phenomena that can lead to bacterial death [261].

The non-specific oxidative damage mechanism of the reactive species targets multiple cellular components simultaneously, reducing the likelihood of resistance development [262]. The presence of Fe ions in the BG compositions does not affect their cytocompatibility at concentrations below 50 µg/mL [223], [263]. A comprehensive outlook on the antibacterial properties of iron ions in BG compositions cannot yet be provided, as further research is required. Nonetheless, their strong bactericidal effects, comparable to those of Cu and Ag, has been observed against *E. Coli*, *S. aureus*, and *S. mutans*, as reported in the literature [223], [264].

3.2.7 Gallium

Gallium (Ga) ions have also been utilized as a dopant in BG compositions to exploit their multiple beneficial biological properties, such as antibacterial efficacy (possibly via disruption of metabolic activity and DNA damage) and the ability to enhance calcium absorption during bone formation [265], [266]. Various studies have explored the production of BGs doped with varying percentages of Ga in sol–gel compositions, ranging from 1 mol.% to 5 mol.%. Results indicate that increasing Ga concentrations are associated with enhanced antibacterial activity [54], [267], [268]. A focused study demonstrated the ability of Ga to inhibit the growth of the Gram-negative bacterium *P. aeruginosa* [269].

Nonetheless, despite these promising outcomes, the behavior of Ga ions – characterized by strong oxygen affinity and its relatively low mobility within BG matrices [270] – tends to slow their release from the glass [54], [266], [271]. The slow ion delivery may limit the attainment of bactericidal concentrations in the surrounding medium, thereby restricting the practical antibacterial efficacy of Ga-doped BGs [54], [271].

3.2.8 Boron

Among other elements, Boron (B) acts as a network former, analogous to Si or P ions, contributing to the amorphous network of BGs. B ions have also demonstrated potential antibacterial activity against bacteria present on human skin, which may cause wound infections [272]. The enhancing effect of B ions on the antibacterial properties of BG compositions has been explored in the literature [273], [274], [275]. Several strategies for boron incorporation into BGs have been reported, including the addition of hexagonal boron nitride to silicate melt-derived BGs, which has shown antibacterial activity against multiple bacterial strains [276].

Nonetheless, the mechanisms of action and the extent of antibacterial efficacy remain unclear, as few studies have systematically explored these properties in relation to B ion

content in the composition. This uncertainty may be related to the higher cytotoxicity observed for borate BGs in biocompatibility assays [277].

3.2.9 Co-doping strategies

As previously discussed, co-doping strategies are considered valuable tools for tailoring the functional behavior of BGs. Beyond antibacterial activity, the simultaneous incorporation of multiple ions can significantly influence glass dissolution, structural properties, and overall biological performance of bioactive glass. Consequently, increasing attention has been directed in the literature toward the development of multi-ion BG systems designed to combine complementary therapeutic effects [34]. Specifically, in the context of antibacterial applications, several studies have explored co-doping approaches to exploit potential synergistic interactions between ions. For example, the combined incorporation of Ag and Ce demonstrated their potential to enhance the antimicrobial activity of BGs against E. coli and S. aureus, suggesting that the interaction between the two ions may amplify bactericidal effects [210]. Similarly, other co-doped systems, including Cu-Sr [224], Ag-Zn-Sr [242], Zn-Mg [243], or Cu-Zn [240] doped BGs have been investigated to simultaneously improve antibacterial performance and additional biological properties such as osteogenic potential or angiogenic response. However, the optimization of multi-ion BG systems remains challenging, as the effects of co-doping are not necessarily additive and may lead to either synergistic or antagonistic behaviors.

3.2.10 Bacterial resistance to metallic ions

Despite being less subject to resistance development than conventional antibiotics, BGs containing antibacterial ions are not entirely exempt from bacterial adaptation mechanisms, especially over longer time frames [278]. Bacterial strains resistant to Ag, such as *E. coli*, *P. aeruginosa* and *K. pneumoniae* have been reported, mainly through plasmid-encoded efflux and transport mechanisms, although these occurrences are relatively rare and not yet fully elucidated [278], [279]. Cu resistance has been reported in literature. *P. aeruginosa* strains can develop periplasmic resistance to Cu^{2+} ions [278]. Cu resistance is relatively common and often intrinsic, primarily occurring via detoxification systems, frequently involving efflux, redox regulation, and sequestration mechanisms [278], [279].

Zn resistance is achieved through multiple strategies, including limiting its uptake, actively exporting excess ions, and, in some cases, converting it into less toxic forms [280]. Moreover, some bacterial strains can adapt to highly alkaline environments, which may attenuate pH-mediated antibacterial strategies of certain BGs [281]; this has also been highlighted when testing 45S5 and S53P4 against *S. gordoni* and *V. parvula*: where a strong antibacterial effect at 24 h was followed by partial bacterial recovery at 48 h, suggesting the development of adaptive tolerance mechanisms to high pH environments [184]. While these limitations should be considered, they do not negate the high potential of antibacterial BGs in combating bacterial infections.

Table 4: Summary of the antibacterial mechanisms associated with different ions incorporated into bioactive glass compositions, along with the bacterial strains against which they have been evaluated.

Dopant	Mechanisms of action	Efficacy	Tested against	Reference(s)
Ag	- Respiratory inhibition - nutrient adsorption - gene or protein modification	> 0.5 mol.% highly effective against most bacteria	*E. coli*	[182], [203], [210], [211], [213], [216], [222]
			S. aureus	[182], [208], [211], [216], [222]
			P. aeruginosa	[208]
			S. epidermidis	[208], [212]
Cu	- cell membrane disruption - oxidative damage - biochemical alteration - DNA damage	0.5 < x < 5 mol.% highly effective against most bacteria	*E. coli*	[216], [221], [222], [223], [224], [225], [230], [232]
			S. aureus	
			S. mutans	[232]
			S. epidermidis	[226]
Zn	- inhibition of enzymes and alkali production -metallic imbalance - Respiratory inhibition - improves antibacterial effect of other species	Effective at > 2 mol.% highly effective at > 4 mol.%	*E. coli*	[171], [227], [240], [241], [242], [243]
			S. aureus	[239], [243]
			P. aeruginosa	[171], [240]
			S. epidermidis	
Ce	- inhibition of oxygen adsorption - cell membrane disruption	Effective at > 0.7 mol.% Risk of cytotoxic effects. Low efficacy vs. Gram (–)	*E. coli*	[246], [247], [248], [249], [250], [282]
			S. aureus	[248], [251]
			S. epidermidis	[251]
			P. aeruginosa	[247], [251]
			B. cereus	[247], [248]
			B. subtilis	
			C. albicans	
Sr	Uncertain, probably correlated with pH increase or oxidative stress	Bactericidal at > 5 mol.% while also improving osteoblast activity	*E. coli*	[39], [224]
			S. aureus	[257]
			P. gingivalis	[256]
			A. actinomy-cetemcomitans	
			MRSA	[38]
			S. mutans	[259]

Fe	- Generation of highly reactive radicals - Inducing oxidative stress - Lipid and protein oxidation - DNA damage	Most effective in the 2-4 mol.% range, although still debated	*E. coli* *S. aureus* *S. mutans*	[223], [263], [264]
Ga	Uncertain, probably correlated with iron metabolism disruption and DNA damaging	Concentrations above 1 mol.% show increasing antibacterial activity	*E. coli* *S. aureus*	[54], [267], [268]
			P. aeruginosa	[269]
B	Uncertain, possibly correlated with pH alteration	Used as network former (> 40% mol.%) can be antibacterial but also cytotoxic	*E. coli*	[273], [274], [276]
			P. aeruginosa	[275], [276]
			S. aureus	[274], [275]
			B. subtilis *S. pyrogens*	[276]

3.3 From antibacterial mechanisms to biomedical applications

The well-documented antibacterial properties of BGs have enabled their transition from basic material testing to the development of clinically relevant biomedical applications, including medical devices [283], scaffolds for BTE [260], fillers for polymers, dental prostheses for caries care and prevention [284], and vehicles for antibiotic delivery [285]. In this section we will explore the more practical aspects of employing BGs for antibacterial purposes, creating a bridge between research findings and real-world applications.

3.3.1 Bioactive glasses versus antibiotics: building resistance

Evidence in the literature suggests that employing BGs for their antibacterial properties can offer advantages over conventional antibiotics. For example, as already mentioned, S53P4 has demonstrated antimicrobial activity against several antibiotic-resistant bacterial strains. Cunha et al. [286] showed that S53P4-loaded poly(methyl methacrylate) (PMMA) was able to neutralize several multidrug-resistant strains, with antibacterial kinetics comparable to those of antibiotic-loaded cements [286]. Similarly, Gergely et al. [287] reported that S53P4 exerted antibacterial efficacy similar to gentamicin-coated PMMA against *E. coli*, *S. aureus*, *P. aeruginosa*, and *K. pneumoniae* after 24 hours in a liquid suspension [287].

These capabilities extend to other BG compositions. Three sol–gel derived and multi-ion doped BGs were able to inhibit bacterial proliferation of *C. albicans* and *E. fecalis*, common cause of intracanal implants failure [288]. Additionally, hydrogels loaded with 10 mg/mL of 45S5 exhibited stronger antibacterial effects compared to 5 mg/mL double-antibiotic paste, commonly used in oral medicine [289].

These results suggest that BG-based antibacterial strategies may represent valuable aids or alternatives in scenarios where conventional antibiotics show reduced efficacy.

3.3.2 Antibiotic-loaded bioactive glass

The combined use of drug-loaded BGs has been explored in the literature. Antibiotics and other therapeutic agents can infiltrate into the porosities of BGs, enabling a localized, slow, and controlled release directly in situ [290]. For these reasons, sol–gel derived BGs and ceramics have been tested as drug carriers, showing encouraging results [291], [292]. In particular, mesoporous BGs exhibit exceptional drug-loading capability, while also allowing for prolonged release in *in vitro* tests [292].

Moreover, the use of melt-derived BG can be employed to regulate the porosity of drug-loaded polymeric scaffolds, increasing the tunability of the release profile of these devices [293]. Major efforts are being made to find effective strategies to manage osteomyelitis, and the use of antibiotic-loaded BG-containing scaffolds represents a viable option to inhibit bacterial development [294], [295].

Recent studies further confirmed the potential of sol–gel-derived BGs loaded with antibiotics, such as gentamicin and vancomycin, as well as other agents like ferulic acid, which have demonstrated strong bactericidal effects against *S. aureus* and *E. coli* [296], [297]. These findings support the further development and clinical translation of drug-loaded BG systems for the treatment of chronic and infection-related bone diseases.

3.3.3 Bone-related applications

Several medical fields consider antibacterial BGs to be promising materials for biomedical applications. Among them, BGs could be utilized for bone defect repair and treatment, exploiting their antibacterial properties to reduce the risk of infection, which could otherwise lead to graft failure and major complications for the patient. To address this, current research focuses on the production and optimization of antibacterial BG-based scaffolds for bone tissue engineering. Researchers have produced sol–gel-derived BG scaffolds doped with silver nanoparticles for BTE, showing strong antibacterial properties, with efficacy dependent on silver ion or nanoparticle content [298], [299].

Nevertheless, studies aimed at exploiting the antibacterial properties of BGs are still ongoing. Several research efforts are currently developing BG scaffolds suitable for BTE that provide antibacterial efficacy against common bacteria such as *E. coli* [260], also leveraging the antibacterial properties of Cu [300], [301], [302], [303]. Recently, an Ag-doped sol–gel-derived BG was tested for *in vivo* bone regeneration, resulting in optimal bone formation, cell proliferation, and osteoblast differentiation, and demonstrating strong antibacterial efficacy against the antibiotic-resistant staphylococcus *MRSA* [303]. Despite their great potential in bone tissue engineering application of BGs, several well-known limitations are associated with their use, such as poor mechanical integrity and brittleness [106], composition- and phase-dependent dissolution kinetics [28], or challenges related to crystallization and thermal processing during scaffold fabrication, already discussed in chapter “2 Thermal properties of BGs and ion substitution”. Furthermore, the incorporation of metallic ions, while beneficial for antibacterial activity, may also induce cytotoxic effects

at high concentrations [210]. Careful tuning of the BG composition can lead to the development of materials capable of exerting antimicrobial effects while preserving key biological and physicochemical properties, such as osteoblast proliferation and dissolution behavior.

Pastes and gels loaded with BGs are another effective delivery strategy for antibacterial BGs, particularly relevant in oral and dental applications. Early studies from the 1990s demonstrated that S53P4-loaded pastes effectively reduced CFU counts of several bacteria, including the cariogenic species *A. naeslundii* and *S. mutans* [304]. Later, Koller et al. showed that Bioglass®-loaded PMMA based bone cement exerts antimicrobial activity on *E. fecalis* (a common bacterium resistant to different antimicrobial agents), comparable to gentamicin-loaded formulations [305]. Similar inhibitory effects against *E. fecalis* were reported for a BG-containing paste with sol–gel-derived BG F18 [306], and a mel-derived silicate BG containing boron [307], highlighting the potential of BG-containing pastes as antibiotic-free antibacterial systems for safer oral implantation.

Moreover, BGs are also being designed for specific bone-related applications, such as HX-BGC, a recently developed melt-quench-derived patented BG for toothpaste [204]. This composition, compared to 45S5, exhibited stronger antibacterial effects against cariogenic bacteria, even at low concentrations [308].

Lastly, S53P4 has been recently used for the treatment of human Charcot foot [309], and chronic bone infections [18], [310]. The authors highlighted the antibacterial properties of S53P4 as a key advantage for BTE, and the clinical trial resulted in complete rehabilitation of the infected foot, paving the way for further clinical trials and optimization of this material [309].

3.3.4 Implant coatings

BGs possessing antibacterial properties have also been investigated as materials for implant coatings. Ye et al. studied the use of Cu-doped sol–gel-derived BG loaded with ofloxacin for implant coatings. The combined effect of the drug and the Cu^{2+} ions provided an effective inhibition of bacterial growth against *E. coli* and *S. aureus* [311]. The effectiveness of Cu doped BGs as implant coatings has been demonstrated on magnesium supports [312] and stainless-steel supports [313], proving antibacterial and antibiofilm activity against *E. coli*, *S. carnosus*, *S. aureus*, and *S. epidermidis* [312], [313]. The BG F18 was shown to reduce biofilm formation of *C. albicans*, *S. epidermidis*, and *P. aeruginosa* on titanium implants [314].

In a later study on sol–gel 58S-based BGs for dental titanium implants doped with cobalt, silver, and titanium, Ag-doped compositions showed clearly superior antibacterial efficacy [315]. However, an earlier study reported that titanium can reduce the antibacterial efficacy of melt-derived silicate and borate BGs used for metal coatings [316]. This evidence highlights multiple possibilities for employing BGs as coatings for metallic implants, also supported by the variability of procedures available to fabricate the coated implants, such as thermal spraying, sol–gel dip or spin coating, and more advanced hybrid techniques [25].

While BGs engineered for implant coatings must satisfy application-specific requirements regarding parameters such as porosity, surface roughness, thickness or morphology [171], the incorporation of antibacterial ions should not negatively influence the structural and dissolution properties of the BGs. In this context, Ag-doped BGs represent a promising strategy, as they can inhibit bacterial proliferation and biofilm formation which can easily occur on smooth-surfaced BG implant coatings.

3.3.5 Soft tissue and wound healing applications

While these findings offer a promising outlook for antibacterial BG-based devices for BTE, their relevance clearly extends beyond hard tissues. Antibacterial BGs have also been employed in electrospun wound healing and BTE scaffolds, showing high antimicrobial performance and accelerated healing after *in vivo* tests [283], [317], [318]. The intrinsic properties of BGs, combined with their ability to release therapeutic ions, have attracted increasing interest in soft tissue applications as well. Among the different challenges for these applications the restoration of vascularization in damaged tissues remains particularly critical. This limitation may be addressed through the use of Cu-containing BGs, which have repeatedly demonstrated the ability to promote a neovascularization response in injured tissues [300].

Early investigations explored antibacterial BG formulations using ex vivo porcine skin models [319], and more recent work has focused on electrospun BG or BG/polymer composites capable of delivering antibacterial activity directly within the wound environment [283], [311], [320], [321]. Collectively, these studies highlight the growing potential of BGs as multifunctional materials for soft-tissue repair and infection control.

3.3.6 Bioactive glasses versus biofilms

Bioactive glasses have demonstrated pronounced antibiofilm activity against a range of clinically relevant bacterial species. This is particularly interesting, as biofilms can exhibit much higher resistance to convention medications [322]. S53P4 has been reported to inhibit biofilm formation by up to 80% compared to control, with this effect appearing independent of particle size (granules versus powders) [181]. Although some studies have suggested a greater particle size dependence on antibiofilm properties, attributing higher efficacy to BG particles smaller than 45 μm, the potential of S53P4 is consistently supported in the literature. Coraça-Huber et al. also attributed marked inhibitory properties to S53P4 powder against *S. aureus* biofilms [199]. Similarly, 45S5 has also been shown to exert effective antibiofilm activity against multispecies biofilms [184].

Additional evidence further substantiates the antibiofilm capabilities of BGs. A Zn-loaded sol–gel derived BG composition was successfully employed to suppress biofilm formation of *P. gingivalis*, *A. actinomycetemcomitans*, and *P. intermedia* [323]. Moreover, the sol–gel derived F18 has been reported to inhibit biofilm development by *S. aureus* and *MRSA* biofilms [200].

Taken together, these findings indicate that bioactive glasses can effectively interfere with biofilm formation across multiple bacterial species and compositions, supporting their potential as non-pharmacological antibiofilm materials.

4 Novel Mg- and Sr-doped BG compositions

(This section has been published in "D. Bellucci, A Mazzilli, A. Martelli, F. G. Mecca, S Bonacorsi, F. D. Lofaro, F. Boraldi, D. Quaglino, and V. Cannillo, "Enrichment of strontium and magnesium improves the physical, mechanical and biological properties of bioactive glasses undergoing thermal treatments: New cues for biomedical applications," *Ceram. Int.*, vol. 50, no. 24, pp. 52819–52837, Dec. 2024, doi: 10.1016/J.CERAMINT.2024.10.135.")

The author of this thesis contributed to drafting the original manuscript, sample preparation, data analysis, and was primarily responsible for the sintering behavior assessment, density analyses and bioactivity evaluation.

As already discussed, BGs have excellent biological properties, nevertheless they exhibit certain limitations when exposed to high temperatures. This is because their tendency to crystallize leads to diminished bioactivity, reduced mechanical integrity, and altered dissolution kinetics. Specifically, 45S5 Bioglass® and S53P4 are of major importance as biomaterials, considering their remarkable propensity to elicit a positive response within the body, particularly in fostering bonding and/or interactions with host tissues [45]. However, their notable limitation is their poor thermal stability, which leads to sub-optimal results when being formed into amorphous bioactive glass scaffolds. This is mainly due to their resistance to being sintered without experiencing significant crystallization. This issue arises from their tendency to crystallize during sintering, mainly because of a limited processing window [45].

Some compositions have been developed and studied to exhibit a better perform under thermal stress. Among them Bio_MS (composition: 46.1 mol.% SiO_2, 31.3 mol.% CaO, 5 mol.% Na_2O, 2.6 mol.% P_2O_5, 5 mol.% MgO, 10 mol.% SrO) has exhibited an exceptionally high crystallization temperature (T_C) while also showcasing outstanding biological performance [31]. These distinct properties are attributed to the lower content of alkaline elements and the presence of magnesium (Mg) or strontium (Sr) in the BG composition, known for their positive biological effects and their ability to modify thermal and mechanical properties [167], [168], [324], [325]. Specifically, Mg is considered to be functioning as an intermediate oxide [326], [327]. Evidence in the literature suggests that Mg doping decreases the glass transition temperature (T_G) of BGs [42], [168] due to the lower strength of Si-O-Mg bond compared to Si-O-Si bond. Moreover, Mg doping can influence mechanical properties [328], [329], [330]. This effects is probably related to its higher ionic field strength [328]. Additionally, Mg-doped BG presents optimal biocompatibility, osteogenic and cell differentiation effects [331], [332], despite a possible reduction in hydroxyapatite precipitation *in vitro* on the material, compared to the case of undoped BG [333]. On the other hand, Sr is recognized for improving apatite formation [334], while still demonstrating optimal biological and cyto-differentiation properties [335]. The effects of Sr on mechanical and thermal properties remain, however, a subject of debate [97], [336], [337].

As previously stated, numerous studies have explored the individual role of Mg and Sr in BG behaviors, although their potential as co-dopants still needs to be explored. For this reason, we investigated their contributions to the thermal, mechanical, and biological

properties adding Mg and Sr as dopants in 45S5- and S53P4-based compositions (namely, 45S5_MS and S53P4_MS). This section reports the results of tests conducted on five melt-derived BGs, as produced and thermally treated. Their ideal sintering temperature was also estimated. The BGs were subjected to differential thermal analysis, heating microscopy, X-ray diffractometry, environmental scanning electron microscopy, measurement of the Young's modulus, simulated body fluid testing, cytotoxicity tests, cell viability, growth, adhesion and morphology. The results demonstrated improved thermal, mechanical and biological behaviors of the magnesium-strontium-doped BGs, thus paving the way for the development of BGs with enhanced biomedical perspectives.

4.1 Testing procedures

4.1.1 Preparation of the bioactive glass

This study aims to comprehensively investigate and characterize the effects of thermal treatment on the physical, chemical, and biological properties of BGs. The production of the glasses in this study utilized a well-established melt-quenching method, which has previously been employed for the production of other BGs [338]. High-quality raw materials in powder form (Carlo Erba Reagenti, Rodano-Milano, Italy) were accurately weighed and mixed for 2 hours in a laboratory rotary mixer. The mixture was melted in a platinum crucible following this thermal treatment: heated from room temperature to 1100 °C at 10 °C/min; decarbonated at 1100 °C for 1.5 hours; then heated from 1100 °C to 1450 °C at 10 °C/min and held for 1 hour at 1450 °C to obtain a homogeneous melt. The molten glass was subsequently quenched in water to achieve rapid cooling, resulting in the formation of a frit. The frit was then dried at 110 °C for 12 hours.

A portion of each frit was then ground in a porcelain jar and sieved to obtain powders with a particle size below 63 μm. Another portion was ground and sieved to produce granules with a grain size ranging between 250 and 500 μm. This specific grain size was chosen to optimize the *in vitro* biological response, based on insights from prior studies [45], [339].

The compositions of the BGs employed for the present study, expressed in mol.%, are detailed in Table 5. Please note that the MgO and SrO contents in 45S5_MS and S53P4_MS were chosen to be comparable to that of Bio_MS.

Table 5: Compositions (in mol.%) of the five BGs studied.

Sample	SiO_2	P_2O_5	Na_2O	CaO	MgO	SrO
45S5	46.1	2.6	24.4	26.9	-	-
S53P4	53.8	1.7	22.7	21.8	-	-
Bio_MS	46.1	2,6	5.0	31.3	5.0	10.0
45S5_MS	46.1	2.6	9.4	26.9	5.0	10.0
S53P4_MS	53.8	1.7	7.7	21.8	5.0	10.0

4.1.2 Thermal analysis

The thermal behavior of the produced BGs, in both powder and granule form, was investigated via Differential Thermal Analysis (DTA) using a Differential Thermal Analyzer

(STA 429 CD, Netzsch-Gerätebau GmbH, Selb, Germany). In this analysis, 30 mg of glass was placed in a platinum crucible and heated from room temperature to 1200 °C at a rate of 20 °C/min. The DTA curve obtained allowed for the determination of characteristic temperatures of the BGs, which are the glass transition temperature (T_G), onset crystallization temperature (T_{C_ONSET}), and peak crystallization temperature (T_C). Additionally, a heating microscope (HM) was employed to examine the behavior of the glass powders over a broader temperature range, from room temperature to 1600 °C, with a heating rate of 10 °C/min. This was conducted using a Misura 3.32 equipment (Expert System Solutions, Modena, Italy). The purpose of this analysis was to identify the sintering temperature (T_S) and the melting temperature (T_M) of the BGs.

4.1.3 Sintering behavior

To explore the impact of temperature on sintering, the glass powders were used to create disks that underwent heat treatment for three hours at five arbitrarily chosen temperatures: 650 °C, 750 °C, 850 °C, 950 °C, and 1050 °C. The evaluation of sintering quality was based on the observed degree of shrinkage. The process to create the green bodies involved subjecting the glass powders to uniaxial pressing at a pressure of 7 bar for 10 seconds. Subsequently, five green bodies of each BG were placed in a muffle furnace (AWF 13/12, Lenton - Laboratory Scientific Equipment, Randburg, South Africa) and subjected to heat treatment at the specified temperatures, employing a heating rate of 10 °C/min. Following the thermal treatment, the samples were air-cooled to reach room temperature. To assess the changes in size resulting from shrinkage, the diameters of the samples were measured using a digital caliper (LTF 327.09, LTF S.p.A., Antegnate, Italy). The temperature associated with the maximum observed shrinkage was considered the best sintering temperature (T_{BS}).

4.1.4 Phases analysis

To compare the impact of heat treatment on the five BG compositions, granules were subjected to heat treatment at two specific temperatures: T_C determined via DTA analysis, and T_{BS} determined as previously described. Both treatments lasted three hours. The phase composition of both untreated and treated granules, along with the potential formation of crystalline phases, was examined using X-Ray Diffractometry (XRD: X'Pert PRO; Panalytical, Almelo, the Netherlands). Data collection was obtained by a 2θ scan method in the range of 10–90° using Cu-kα X-ray line (step size: 0.017° 2θ).

4.1.5 Physical and mechanical properties

To determine the density of the samples treated at T_{BS}, cross-sectional analysis was conducted using image analysis techniques. The Environmental Scanning Electron Microscope (ESEM) (Quanta 2000, Fei Co., Eindhoven, The Netherlands) was employed to capture images of the samples, and ImageJ software was used to assess the porosity from the images. Following the density evaluation, the mechanical properties were examined using Open Platform equipment (CSM Instruments, Peseux, Switzerland) with a Vickers indenter tip. A load of 1000 mN was applied during indentation, with a loading/unloading rate of 2000 mN/min and a hold time of 15 s. Each sample was tested at least 15 times, and the load-

penetration depth curve was automatically recorded for each indentation. Young's modulus was automatically calculated using the method proposed by Oliver and Pharr [340].

4.1.6 SBF testing

The assessment of the bioactivity of the BG granules involved their immersion in Simulated Body Fluid (SBF), following the Kokubo protocol [21], [341]. Specifically, 1.5 g of BG granules were submerged in 50 ml of SBF and incubated at 37 °C for durations of 3, 7, and 14 days. The pH of the solution was monitored, and the SBF was replaced every 48 hours. The starting pH of the solution was 7.4 as specified by the Kokubo protocol [21], [22]. After each time interval, the granules were collected via filtration and washed with distilled water. At the end of the test the samples were air-dried at room temperature for 24 hours.

The apatite-forming ability of both heat treated and untreated glasses was assessed using XRD and micro-Raman spectroscopy (LabRAM, Horiba Jobin-Yvon, Villeneuve D'Aseq, France). The spectrometer was equipped with a diode laser operating at a wavelength of 632.8 nm and delivering 20 mW of power to the sample. The scattered photons were dispersed using a grating monochromator with a resolution of 1800 lines/mm and then captured by a CCD camera. An optic with a 100X Ultra Long Working Distance (ULWD) objective was utilized. The spectral data was collected through a series of 15 acquisitions, each lasting 20 seconds. Lastly, the microstructure of the samples was examined using ESEM equipped with X-ray energy dispersive spectroscopy (EDS) (Inca, Oxford Instruments, UK), conducted under low-vacuum conditions (~ 0.5 Torr).

4.1.7 Cytotoxicity according to ISO 10993

To prepare the eluates, BGs were incubated with Dulbecco Modified Eagle Medium (DMEM) (Thermo-Fisher Scientific, MA, USA) at 37 °C for 16 hours, as recommended by ISO 10993-12 procedures [342]. Eluates were sterilized using 0.22 µm filters (Merck-Life Science, Darmstadt, Germany).

Balb/3T3 embryonic mouse fibroblast cell line (American Type Culture Collection, ATCC) is widely used for testing cytotoxicity. Cells were seeded at a density of 103 cells/well in 96-well plates and cultured in DMEM supplemented with 10% fetal bovine serum, 1% penicillin-streptomycin and 1% non-essential amino acids (Thermo-Fisher Scientific). After 24 hours, the culture medium was replaced with eluates at different concentrations (i.e., 100%, 50%, 25% and 12.5%). Negative and positive controls were set using the culture medium only, or the culture medium plus 0.1% sodium dodecyl sulphate (SDS, Merck-Life Science), respectively. After additional 24 hours, cell morphology was evaluated under a phase-contrast microscope (DIAPHOT-TMD, Nikon, Japan) and cytotoxicity was assessed with the MTT assay as recommended by the ISO 10993-5 protocol (Biological Evaluation of Medical Devices - Part 5: Tests for *in vitro* cytotoxicity). Briefly, tetrazolium salts (1mg/mL in DMEM) were added to the cell culture and incubated at 37°C in humidified atmosphere (95% air and 5% CO_2) for 2 hours, then the medium was removed, and 200 µL of dimethyl sulphoxide were added to each well to dissolve formazan crystals. The optical density (O.D.) was measured at 540 nm using a multiplate reader (Multiskan FC, Thermo-Fisher Scientific). Data was expressed as percentage of O.D. values of metabolically active

living cells in cultures with the presence of eluates compared to cells incubated in the absence of eluates set at 100%. Blank absorbance was represented by the medium alone. MTT assay was performed in sextuplicate.

4.1.8 Cell viability and cell adhesion

Human dermal fibroblasts (HDFs) from adult donors (Cat #C-013-5C, Invitrogen, USA) were cultured and maintained according to Boraldi et al. [343]. BGs were sterilized by UV light and placed into 96-well ultra-low adhesion plates (Cat #3474, Corning, USA) without washing. HDFs were seeded onto BG (1.5 × 105 cells/50 mg of BG) and cultured in standard cell culture conditions for 7 days. The culture medium was changed every two days. At different times of culture (i.e., 1h, 4 and 7 days), cell viability and cell morphology were evaluated by MTT assay and by optical digital microscopy (VHX-7000, Keyence, Japan), respectively. For cell morphology, the cells were fixed with 20% cold methanol and stained with 0.5% crystal violet [344]. Area (total area of each cell), perimeter, aspect ratio (the ratio between the major and minor axis of a cell) were evaluated using the Image software (v.1.53t) on approximately 80 cells/sample.

4.1.9 Cell growth

For cell growth assessment, 12-well plates (Falcon) were prepared with a cell density of 6.0 × 104 cells/well in 1 mL of complete DMEM or in 1 mL of 100% eluate obtained from BG 45S5 T_{BS} (for the preparation of the eluate see paragraph 2.7). Cells were cultured for 7 days with changes of the medium (DMEM or eluate) on the fifth day of culture. Cell counts were performed at day 1, 4 and 7 after seeding using the Neubauer chamber.

4.1.10 Statistical analysis

One-way analysis of variance (ANOVA) was used for multiple comparisons and a Tukey post-hoc test was applied. Statistical analyses were performed using GraphPad Prism 8.0 software (San Diego, CA). Values are reported as mean ± standard deviation (SD). Differences were considered significant for $p < 0.05$.

4.2 Results and Discussion

4.2.1 Thermal analysis

Figure 1 (A-E) presents the DTA curves of the BGs, acquired while heating at a rate of 20 °C/min using fine powders (<63 μm). The observed glass transition temperatures TG for 45S5 and S53P4, measuring 520 °C and 530 °C, respectively, are consistent with data documented in existing literature [99], [134], [136], [142], [345]. Similarly, the data obtained for Bio_MS aligns with the analysis conducted in prior research [31], thereby establishing a foundational platform for comparing with other MS-doped BGs. However, it's important to note that while the findings concerning the crystallization temperature T_C of 45S5 and Bio_MS align with literature [31], [134], [136], [142], [345], [346], the data for S53P4 contradicts existing studies. Specifically, the recorded T_C is 648 °C, unlike the range found in other studies, which report a T_C between 730 °C and 805 °C [345], [347]. This discrepancy could potentially be attributed to the granulometry used for the DTA analysis or the heating

rate employed during evaluation. Further DTA analyses on BG granules confirmed the effect of granulometry size on thermal behavior.

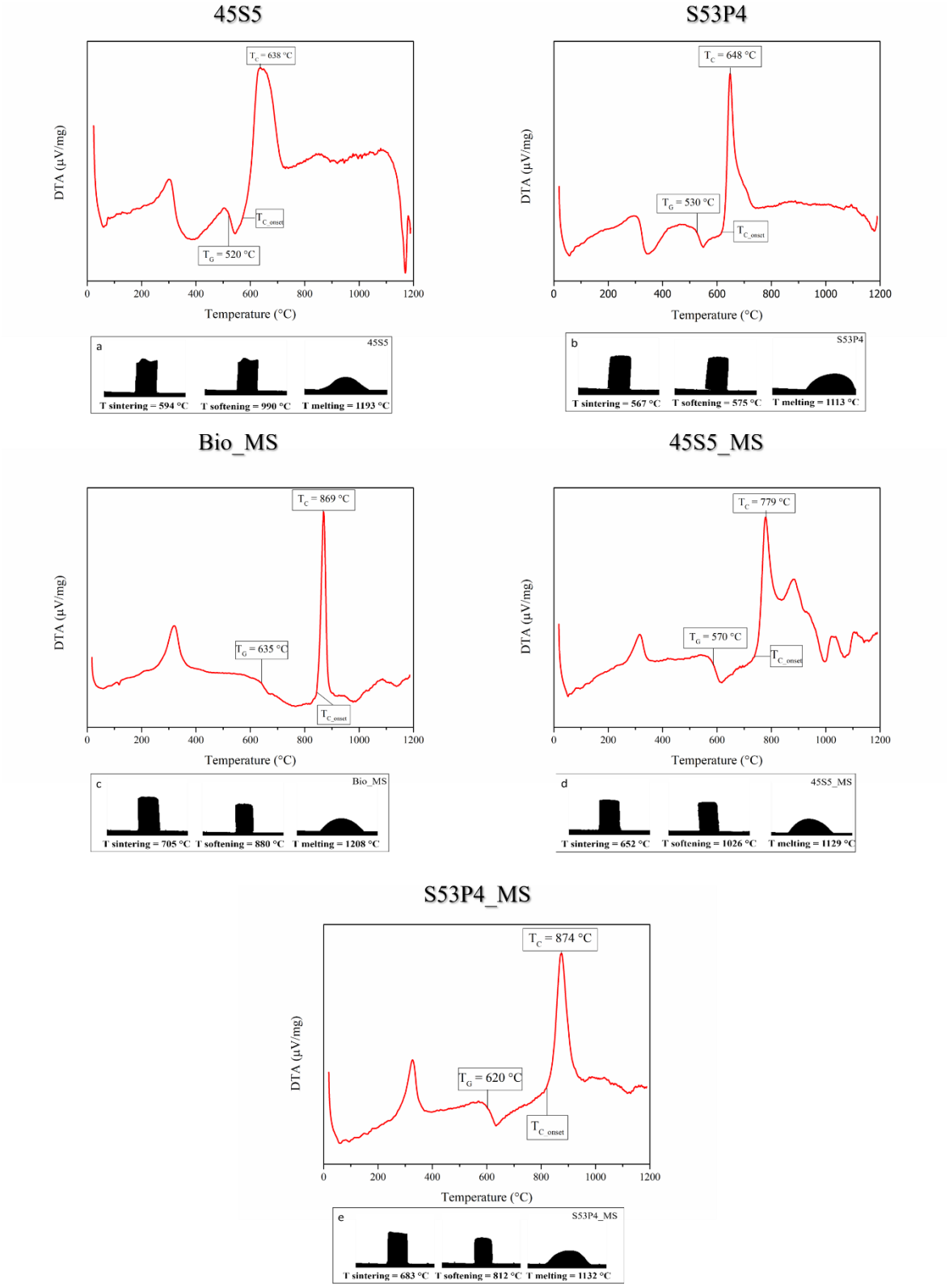

Figure 3: DTA and HM analyses of: (A) 45S5, (B) S53P4, (C) Bio_MS, (D) 45S5_MS and (E) S53P4_MS. Characteristic temperatures T_G, T_{C_ONSET} and T_C are highlighted on the DTA curves.

Figure 3 also illustrates the results of the HM analysis, delineating the sintering, softening (marking the initiation of BG collapse owing to viscous flow), and melting temperatures of the samples. The data highlighted that the "MS" samples exhibit higher sintering temperature compared to their parent glass, with Bio_MS showing to have the highest sintering temperature. However, this analysis alone does not comprehensively reveal the optimal sintering conditions for BGs but rather indicates the temperature at which the glass begins to contract. Therefore, additional studies were conducted to explore BGs behavior under various sintering conditions.

4.2.2 Sintering behavior

Table 6 showcases the results obtained from a shrinkage assessment conducted at different temperatures, with particular emphasis on the T_{BS} of the MS-doped compositions. For 45S5, as observed by Bretcanu et al. [142] and Lefebvre et al. [27], the sintering process reveals two distinct stages: an initial phase followed by a more prolonged and marked stage. Densification initiates at 650 °C during the first step, while the second densification phase starts at 950 °C, peaking at 1050 °C. The shrinkage associated with the first step measures approximately 2%, whereas a higher shrinkage rate of around 10% was recorded during the subsequent phase of densification. Remarkably, the T_{BS} identified in this study aligns with findings reported by Chen et al. [348]. In the case of the S53P4, the glass exhibited the highest level of shrinkage at 650 °C, suggesting this temperature as potentially ideal for the sintering process. However, this observation contradicts other studies that identified 720 °C as the optimal sintering temperature [345], [349]. It is worth noting that in these studies, the determination of the optimal sintering temperature relied on manually testing the fragility of BG-scaffolds produced at different temperatures. It is noteworthy to mention that the S53P4 samples encountered difficulty in being sintered at 1050 °C due to glass softening, thus making the measurement of shrinkage impossible in those conditions. Regarding Bio_MS, its identified T_{BS} aligns with the findings of a previous study [31]. Similarly, for other MS-doped bioactive glasses, the maximum densification occurred at 750 °C, diverging from the sintering temperatures suggested by the HM analysis, which were 50-100 °C lower. Notably, Bio_MS, 45S5_MS, and S53P4_MS also exhibit superior sinterability compared to commercial BGs.

Table 6: Values of shrinking (expressed as percentages) of the BG disks after heat treatment for 3 hours at different temperatures. The highlighted values represent the highest value of shrinkage measured for each BG.

	Shrinkage % at the respective temperatures				
Sample	650 °C	750 °C	850 °C	950 °C	1050 °C
45S5	2% (± 0.48)	2% (± 0.91)	3% (± 0.52)	7% (± 0.96)	10% (± 1.21)
S53P4	10% (± 0.68)	7% (± 1.81)	7% (± 0.96)	8% (± 1.51)	n.a.
Bio_MS	0% (± 0.40)	13% (± 0.55)	13% (± 1.24)	10% (± 0.62)	10% (± 1.30)
45S5_MS	13% (± 0.62)	14% (± 0.96)	13% (± 1.44)	9% (± 1.02)	9% (± 0.35)
S53P4_MS	8% (± 1.33)	14% (± 1.08)	11% (± 1.30)	7% (± 2.41)	14% (± 1.07)

Table 7 summarizes the characteristic temperatures found for the five glass compositions. The processing window, defined as the difference between the temperature of crystallization

onset and T_G, and the sinterability parameter ($S_C = T_{C\_ONSET} - T_{BS}$) are reported as well. The sinterability parameter S_C of a glass is an estimate of its sintering ability versus its crystallization trend. In particular, if T_{C_ONSET} is lower than the sintering temperature, then $S_C < 0$ and the glass is likely to crystallize before it can sinter; this usually results in non-optimal densification. On the other hand, if $S_C > 0$, the glass can sinter without crystallizing, and thus compaction is promoted.

It is crucial to highlight the beneficial effect of reducing the alkaline content and doping with Mg-Sr on the sintering behavior of BGs. This leads to increased sample shrinkage and widens the processing window of doped BGs. This observed trend likely results from various factors contributing to higher T_C: lower Na content in doped BGs, potentially reducing glass network mobility [135], enhanced stability of MgO-doped glasses due to the oxide's inhibitory effect on crystallization [324], higher entropy supporting the preservation of the BG network's amorphous structure, and the possible augmentation of flow viscosity owing to the presence of Sr^{2+} [350].

Table 7: Characteristic temperatures of the five BGs, obtained through various techniques: T_G glass transition temperature; T_{C_ONSET} onset crystallization temperature; T_C peak crystallization temperature; T_{BS} best sintering temperature; processing window (T_{C_ONSET} - T_G), and sinterability parameter ($S_C = T_{C\_ONSET} - T_{BS}$).

	T_G	T_{C_ONSET}	T_C	T_{BS}	Processing window	S_C
45S5	520 °C	560 °C	638 °C	1050 °C	40 °C	< 0
S53P4	530 °C	615 °C	648 °C	650 °C	85 °C	< 0
Bio_MS	635°C	830 °C	869 °C	750 °C	195 °C	80 °C
45S5_MS	570 °C	740 °C	779 °C	750 °C	170 °C	< 0
S53P4_MS	620 °C	810 °C	874 °C	750 °C	190 °C	60 °C

4.2.3 Phases analysis

Figure 4 presents XRD analysis results of 45S5 and 45S5_MS subjected to different heat treatments: untreated and heated at T_C and T_{BS} for 3 hours. Our analysis indicates that after post-thermal treatment, the primary crystalline phase identified is combeite ($Na_4Ca_4Si_6O_{18}$, JCPSD no. 01-079-1086). In addition, secondary phases such as $Na_2CaSi_3O_8$ (JCPSD no. 00-012-0671) were possibly identified, particularly in 45S5 samples treated at T_C. This aligns with previous studies on the crystallization of 45S5 [351], [352], although other crystalline phases have also been identified [138], [346].

Moreover, in agreement with previous observations by Boccaccini et al. [346] the peak splitting observed around $2\theta \approx 33°$ is more likely attributable to variations in lattice parameters rather than the presence of distinct crystalline phases. This interpretation is not limited to 45S5 but extends to other silica-based bioactive glasses that crystallize into similar sodium–calcium silicate structures [48]. Lastly, minor contributions from $Na_6Ca_3Si_6O_{18}$ (JCPSD no. 01-077-2189) cannot be excluded, as suggested by the analysis of 45S5_MS samples treated at T_C. The influence of Mg and Sr on crystallization behavior must be considered. Notably, the doped glass exhibits a lower degree of crystallization compared to pure 45S5. This finding suggests the potential for significant control over the crystallization

of doped BG, enabling regulation of the crystalline-to-amorphous BG ratio. Such control could potentially dictate the mechanical and bioactive properties of the BG [46]. It is important to note that the analyzed samples do not display any peak associated with crystalline phases of Mg and/or Sr, as confirmed in previous studies [98].

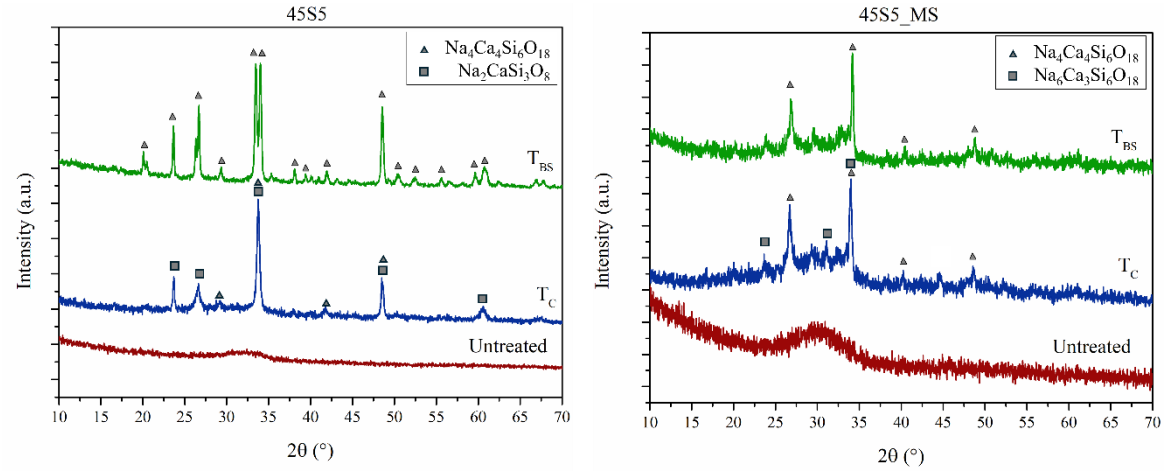

Figure 4: XRD spectra of 45S5 and 45S5_MS samples in different conditions: untreated (red curve), after heat treatment at T_C for 3 hours (blue curve), and after heat treatment at T_{BS} for 3 hours (green curve).

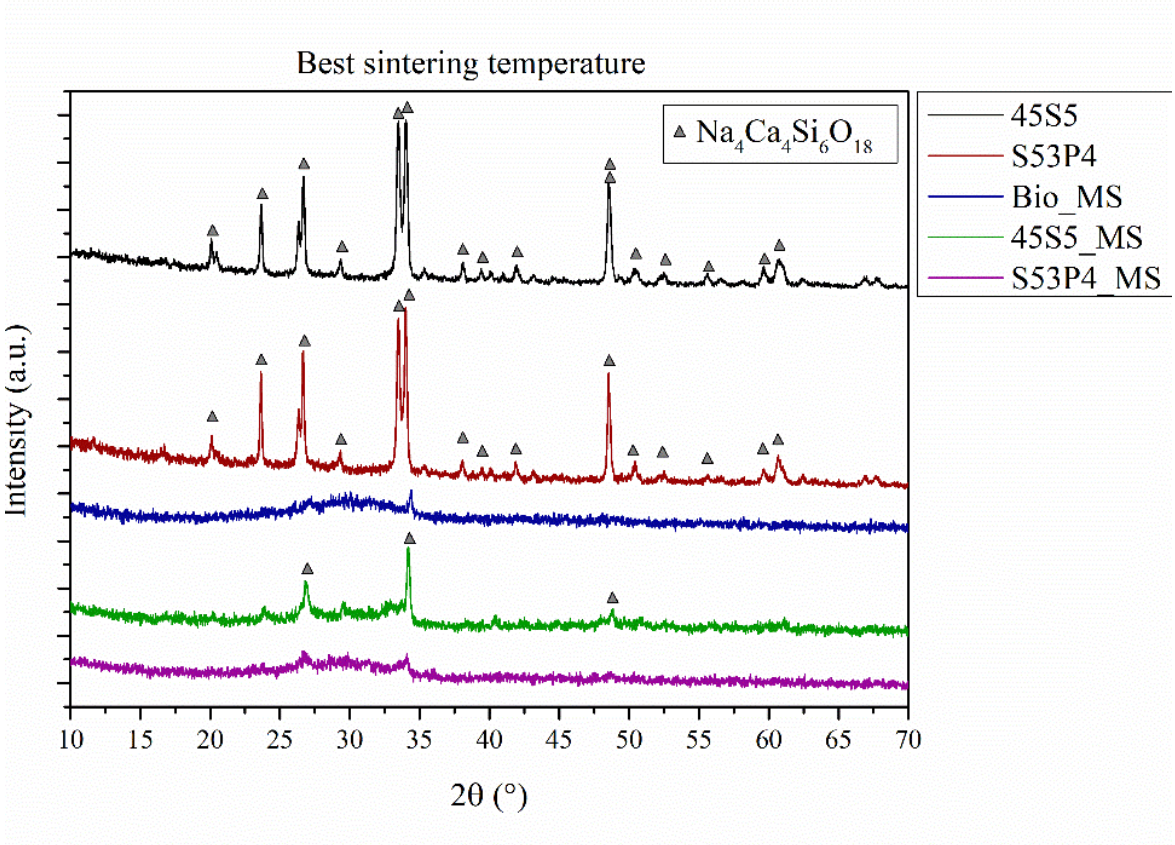

Figure 5: XRD spectra of the five BGs after heat treatment at T_{BS} for 3 hours.

Figure 5 displays the XRD analysis of the five BG compositions treated at T_{BS} for 3 hours. The analysis indicated the formation of combeite ($Na_4Ca_4Si_6O_{18}$, JCPSD no. 01-079-1086) in thermally treated S53P4, as reported elsewhere [353]. The impact of Mg-Sr doping and the concurrent reduction in the alkaline element content on crystallization is readily apparent,

as the doped BGs exhibit minimal to no crystallization. Specifically, a lower tendency to crystallize is observed in Bio_MS and S53P4_MS. This tendency could be attributed to their lower sodium content, resulting in reduced diffusion coefficients and slower rates of crystal growth [354].

4.2.4 Physical and mechanical properties

Figure 6 presents the cross-section images of BG samples heat treated at their respective T_{BS}. The diagram in Figure 7 illustrates the density obtained through image analysis. Notably, all examined BG compositions demonstrate exceptional density levels, surpassing 95%. While Bio_MS exhibits higher shrinkage compared to the commercial BGs, its density is slightly lower. This discrepancy in density may be attributed to larger pore dimensions observed in Bio_MS compared to those of other BG compositions. Regarding other MS-doped BG compositions, the higher shrinkage aligns with the increased density found by image analysis, confirming the superior sinterability of these BG compositions.

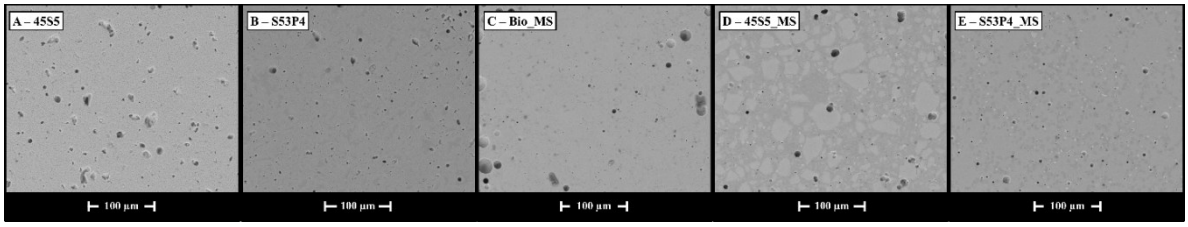

Figure 6: SEM micrographs of the cross-sections of the five BGs disks samples heat treated at their respective T_{BS}.

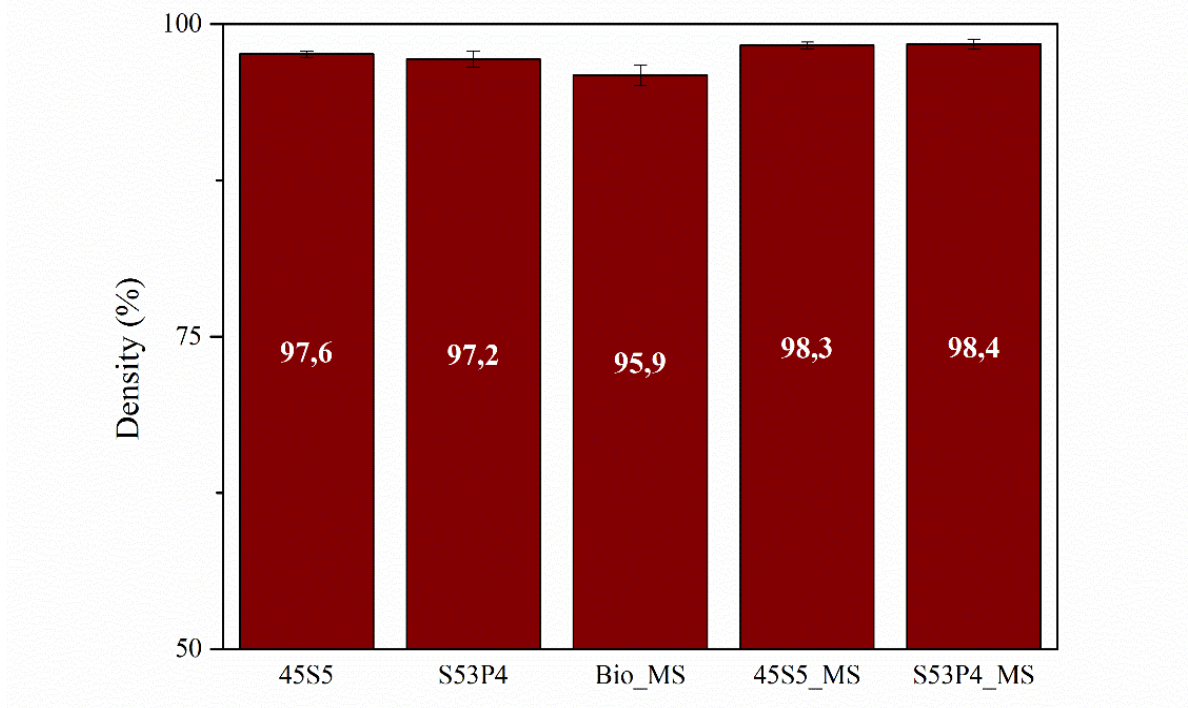

Figure 7: Calculated density of the BG disks after sintering at T_{BS}. Results were obtained analyzing the cross-section images.

The chart depicted in Figure 8 provides the results of the mechanical properties of the BGs analyzed in the present study. Consistently, the hardness values obtained for 45S5 and S53P4 align with established literature sources [355], [356]. However, there is a noticeable scarcity of studies specifically investigating the hardness of Bio_MS or the MS-doped compositions, although the results presented here indicate higher values compared to other Mg or Sr doped BGs [167], [357]. The impact of Mg and Sr on the hardness of 45S5_MS is clearly discernible from the data, as it results higher than the reference commercial BG. In contrast, data suggest a marginal reduction in hardness within the S53P4_MS sample. This distinct behavior might be linked to the different Mg-Sr/Si ratios. Notably, Mg exhibits dual characteristics as both a network modifier and a network former [34], potentially resulting in the formation of quite strong Mg-O-Si bond [357] or the weakening of the overall glass network [42]. In the case of Sr-doped BGs, the potential weakening of the glass structure is attributed to the small but significant expansion of the glass network as a consequence of the substitution of Ca by Sr [358]. This expansion occurs due to the larger size of the Sr^{2+} cation compared to Ca^{2+}. The impact of doping on the elastic modulus (E) appears to be minimal, aligning with findings similar to those reported by Sharifianjazi et al. [357]. Nonetheless, direct comparisons with existing literature present challenges due to the scarcity of studies specifically addressing the mechanical properties of bulk BG. It's important to note that the presence of residual pores and variations in powder granulometry might significantly impact the mechanical properties of sintered BGs [167], [359]. This aspect warrants further investigation and consideration in interpreting the presented results. Finally, it is important to note that BGs are intrinsically brittle materials and therefore, in load bearing applications, are used as coatings, e.g. on metallic prostheses. In this case, besides the fact that the BGs are thermally treated, it is important to pay attention to the mismatch of the coefficient of thermal expansion of the BG and the metallic substrate. In fact, due to such mismatch, thermal stresses may arise [360], [361].

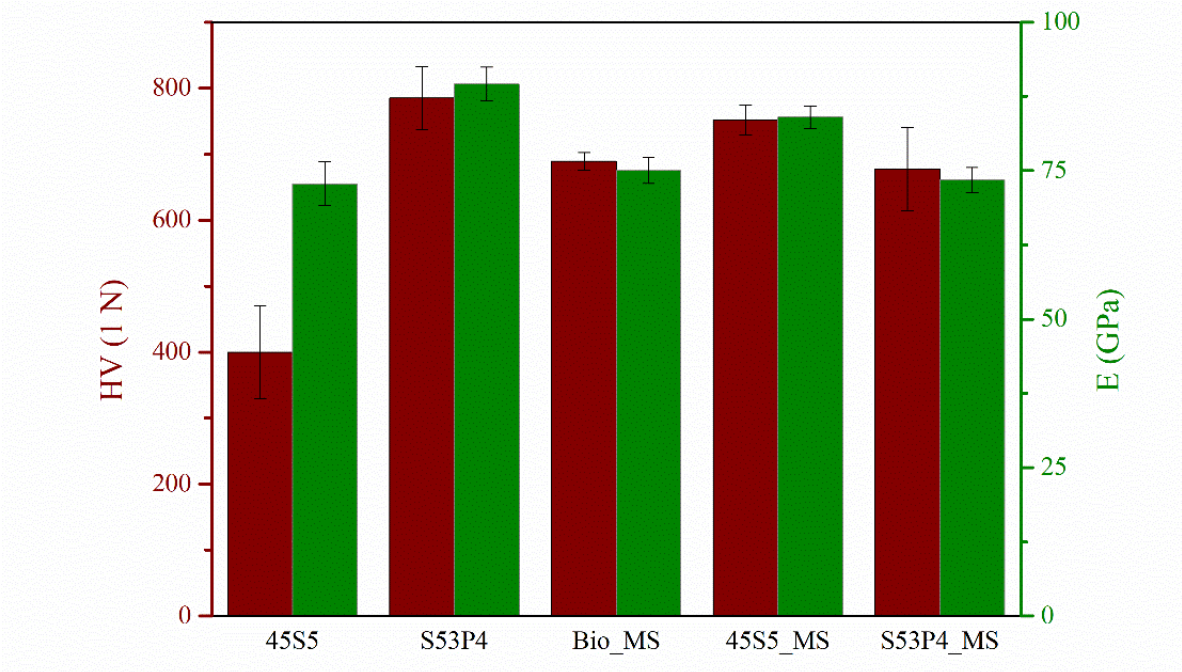

Figure 8: Mechanical properties (specifically, microhardness and elastic modulus) of the sintered BG disks.

4.2.5 SBF assessment

Figure 9 (A-C) compares the effects of different compositions on the pH of the SBF, to show the pH variation in the same heat treatment conditions. Results show that the heat treatment can influence the reactivity of BG compositions, as already discussed in chapter "2 Thermal properties of BGs and ion substitution". In the same figure, the optimal pH range for tissue regeneration has been added [362]. Indeed, it has been demonstrated that a weakly alkaline environment, up to pH 8, can enhance osteogenic activities and promote antibacterial effects without toxic effects on cells [17], [52], [363], [364]. Taking this into account, delayed and lower reactivity of BG can be seen positively, considering the need for a controlled, slower reaction while retaining bioactivity. This result was achieved with BGs doped with Mg and Sr and a lower alkali content. Moreover, these findings are consistent with the literature, which reports that Mg and Sr influence the reactivity of BG *in vitro* [168], [365]. Furthermore, it can be seen how the doped samples heat treated at T_{BS} are able to maintain a lower pH than the samples heat treated at T_C. This finding is promising for glasses containing Mg and Sr, since it may point to a greater propensity of these compositions for the application as sintered BGs, allowing a simpler and more successful development of sintered parts.

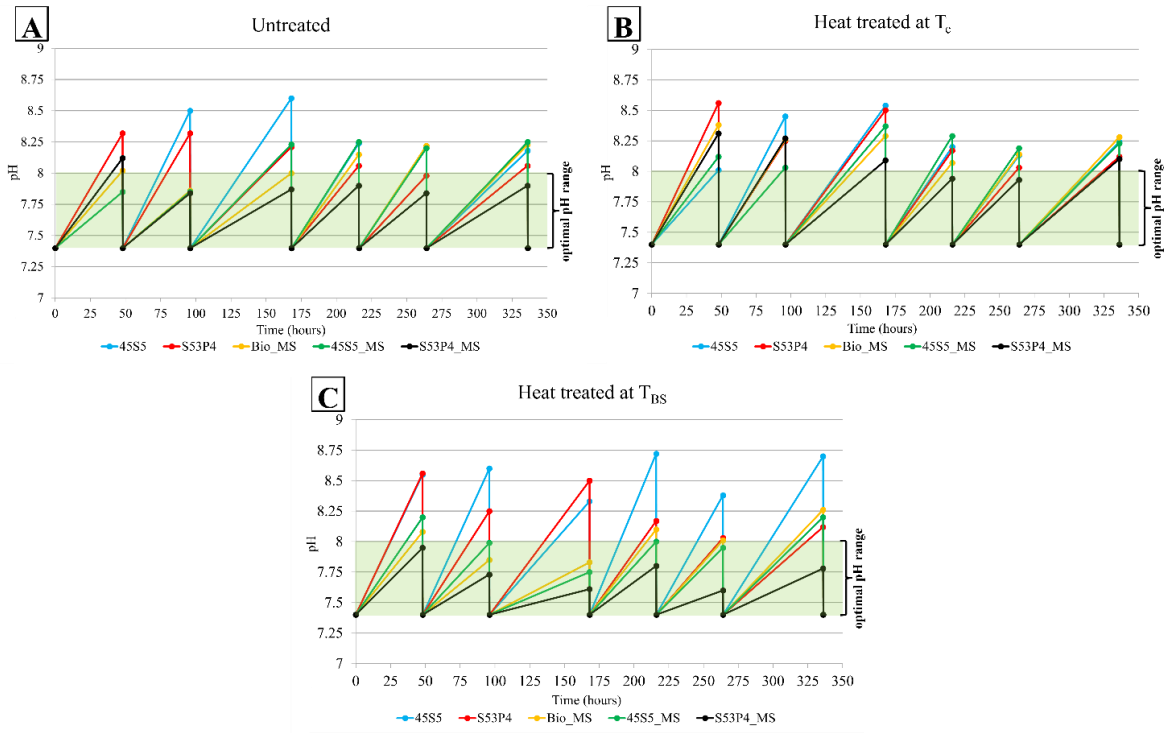

Figure 9: pH variation induced by the untreated samples (A), and by the heat-treated samples at T_C (B), and T_{BS} (C). The green area represents the optimal pH for osteoblast activity [366].

The *in vitro* bioactivity of a BG, specifically its ability to induce an HA precipitation, can be assessed using Raman spectroscopy. The results of the analysis are depicted in Figure 10, illustrating the Raman spectra of untreated granules of 45S5, S53P4, Bio_MS, 45S5_MS and S53P4_MS after soaking in SBF for 7 days. Analogous results were obtained from the analyses of crystals grown on the surfaces of heat-treated BG granules. Examination of the

spectra reveals the presence of typical peaks attributable to *in vitro* precipitated HA: one around 430 cm^{-1}, another at 590 cm^{-1}, and a prominent narrow peak at about 960 cm^{-1}. These peaks can be attributed to the bond stretching of the $(PO_4)^{3-}$ groups [367], [368]. Moreover, a peak at 1070 cm^{-1}, related to the stretching of the carbonate groups, confirms that the HA formed is carbonated, as reported in the literature [369]. These observations apply to all untreated samples following a 7-day immersion in SBF, thus confirming their bioactivity. However, the kinetics of HA deposition on the surface of the granules varies among the samples. The diminished reactivity of BGs containing Mg and Sr, which may ultimately lead to less HA precipitation, can be observed through the analysis of the Raman spectra. An example of this behavior is illustrated in Figure 11 (A-B), which shows the Raman spectra of untreated S53P4 and S53P4_MS granules, both as-fritted and after soaking in SBF for 3 and 7 days. Examination of the spectra of both samples before immersion in SBF reveals a broad peak at 625 cm^{-1}, corresponding to the vibration of the Si-O-Si silicate groups [370]. Additionally, a broad peak around 940 cm^{-1} is due to the vibration of the $(PO_4)^{3-}$ groups present in the BG structure [371]. After 3 days S53P4_MS exhibits result similar to those at time 0 day (Figure 11 B), whereas the spectrum of S53P4 showed peaks at 430 cm^{-1}, 590 cm^{-1}, 960 cm^{-1} and at 1070 cm^{-1} (Figure 11 A). Similar results were obtained for untreated 45S5 and 45S5_MS granules soaked in SBF; the Raman spectra observed for Bio_MS granules closely resemble those seen in glasses that contain strontium and magnesium (data not shown).

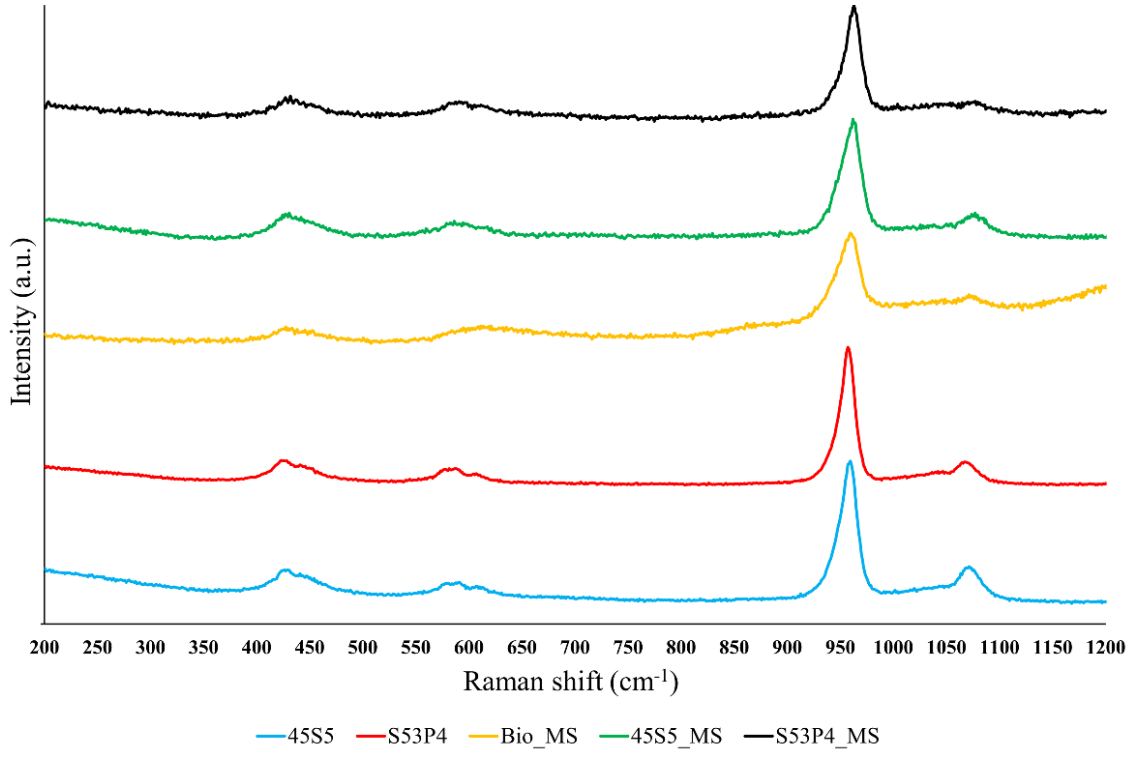

Figure 10: Raman spectra acquired on untreated BG granules after immersion for 7 days in SBF

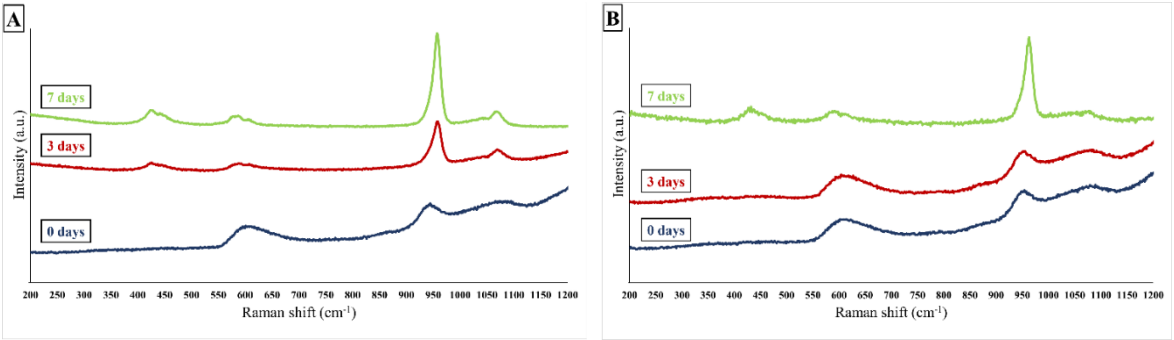

Figure 11: Raman spectra acquired on S53P4 (A) and S53P4_MS (B) untreated granules after immersion for different times in Simulated Body Fluid.

The surfaces of the samples after immersion in SBF were observed using SEM. A qualitative chemical analysis was conducted by means of EDS. Figure 12 and Figure 13 present the results of the SEM/EDS analysis of the surfaces of some representative BGs after soaking in SBF. Specifically, Figure 12 (A-D) shows the SEM/EDS of the S53P4 (A-B) and S53P4_MS (C-D) samples after 3 days of soaking in SBF solution, respectively. Results show that the surface of S53P4 is covered by spherical particles with a cauliflower-like structure, which is typical of the HA formed *in vitro*. However, these kinds of deposits cannot be detected on the surface of the S53P4_MS samples, apart from local formations, supporting the previous hypothesis of the slower reactivity of this composition compared to its counterpart that does not contain strontium and magnesium. Additional considerations can be made based on the EDS analysis. In fact, in the EDS spectrum of S53P4_MS, a pronounced presence of silicon is observed, indicative of the formation of a superficial silica gel layer. Gel formation is an essential part of the reactions leading to the precipitation of HA and dehydrates after extraction from SBF, resulting in the typical cracked surface visible in in Figure 12 (C) [371], [372]. Furthermore, the EDS analysis shows an increase in the phosphorus peak, attributable to the formation of localized precipitates rich in phosphorus and calcium, precursors of HA [373]. It can therefore be concluded that the HA formation process on S53P4_MS is at a less advanced stage. The presence of small amounts of magnesium and chlorine on the S53P4 sample (Figure 12 (A)) is likely due to the deposition of salts precipitating from the SBF, as reported by the literature [374]. Similar observations can be made for the 45S5 and 45S5_MS samples. Regarding Bio_MS, after 3 days, it tends to behave *in vitro* like the other glasses containing magnesium and strontium (data not shown).

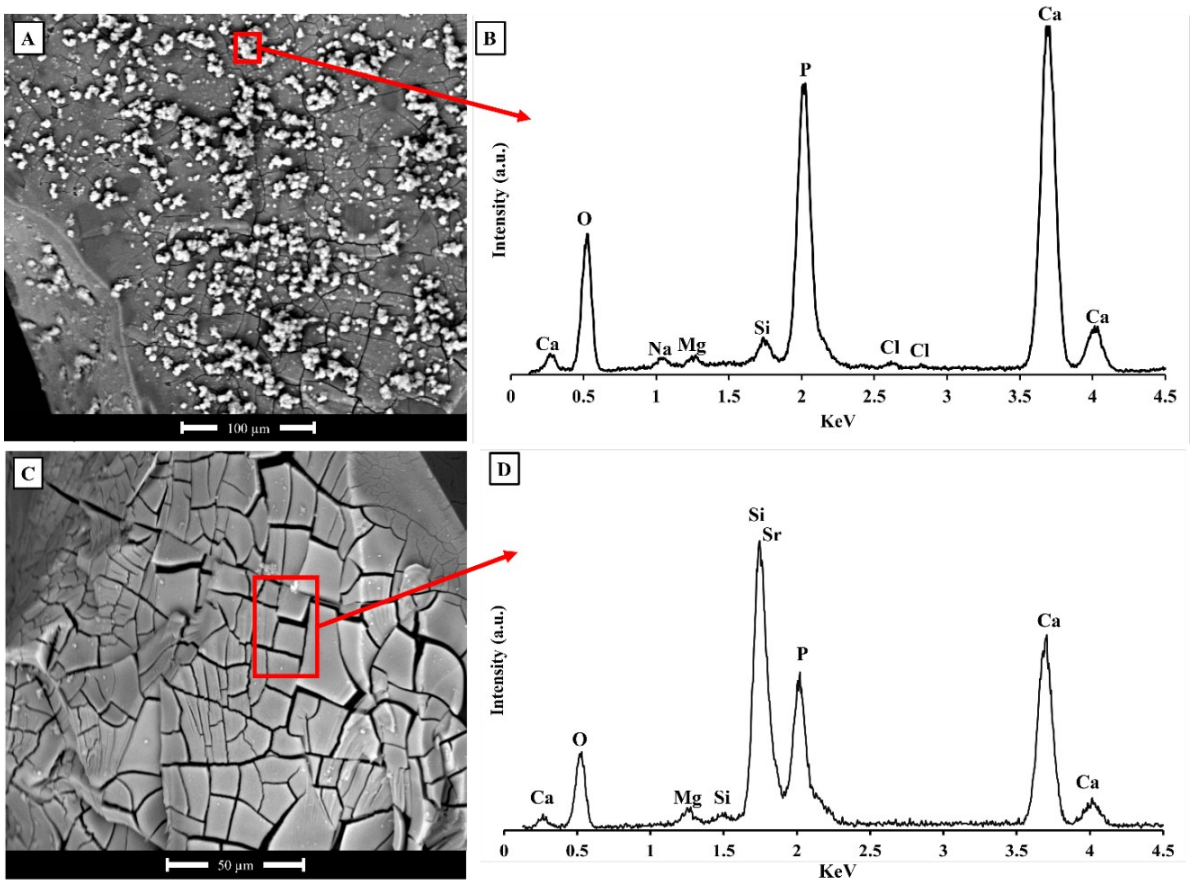

Figure 12: (A) SEM micrograph of S53P4 sample after 3 days of soaking in SBF, and (B) EDS analysis of the highlighter (red) area in micrograph (A). (C) SEM micrograph of S53P4_MS sample after 3 days of soaking in SBF, and (D) EDS analysis of the highlighter (red) area in micrograph (C).

Figure 13 (A-D) shows the EDS analysis for the 45S5_MS (A-B) and S53P4_MS (C-D) samples after heat treatment at T_C and 7 days of immersion in SBF. This analysis aims to highlight the different effects of Mg and Sr, as well as a lower alkali content, on two different BG compositions. On the surface of the 45S5_MS (Figure 13 (A)) some globular precipitates are clearly visible. EDS analysis confirms that these precipitates have high concentrations of Ca and P, supporting the hypothesis of HA formation on the surface (further confirmed by Raman investigation – data not shown). Figure 13 (C-D) shows the results of S53P4_MS after heat treatment at T_C. Some HA precipitates are visible, but the surface is less covered compared to the 45S5_MS samples, indicating lower bioactivity of the S53P4_MS sample, even after 7 days of exposure to SBF. Nevertheless, both experimental compositions are bioactive after heat treatment at T_C.

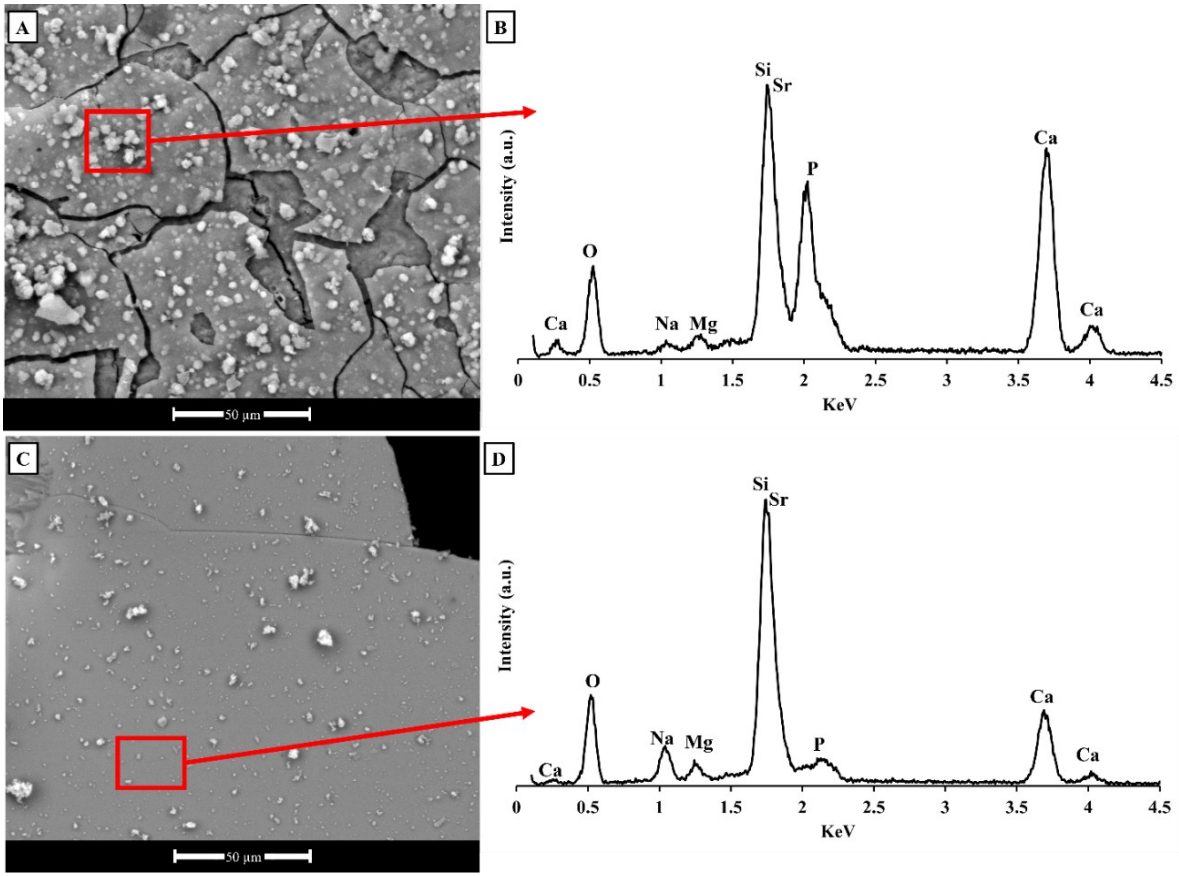

Figure 13: (A) SEM micrograph of 45S5_MS sample, heat treated at T_C after 7 days of soaking in SBF, and (B) EDS analysis of the highlighter (red) area in micrograph (A). (C) SEM micrograph of S53P4_MS sample, heat treated at T_C after 7 days of soaking in SBF, and (D) EDS analysis of the highlighter (red) area in micrograph (C).

These results are further supported by Figure 14, which illustrates SEM images comparing the temporal evolution of the surfaces of untreated BG samples containing Mg and Sr after 3, 7, and 14 days of soaking in SBF. It is evident that, after 3 days, the samples containing Mg and Sr present few-to-no deposits with the typical morphology of HA, thus confirming, as previously discussed, that the Mg/Sr doped compositions are less reactive than the undoped counterparts [365]. However, after 14 days of immersion, all surfaces are covered with a layer of HA, confirming the bioactivity of all BGs and the abundant deposition of HA on their surfaces after 14 days of immersion.

Finally, Figure 15 (A-J) presents SEM images of BGs, both non-heat-treated and heat-treated at T_C, after 14 days of soaking in SBF. These images demonstrate that all the samples are highly bioactive after 14 days in SBF, as they exhibit HA globular precipitates on their surfaces. This further supports the high reactivity of these BGs, even after thermal treatment.

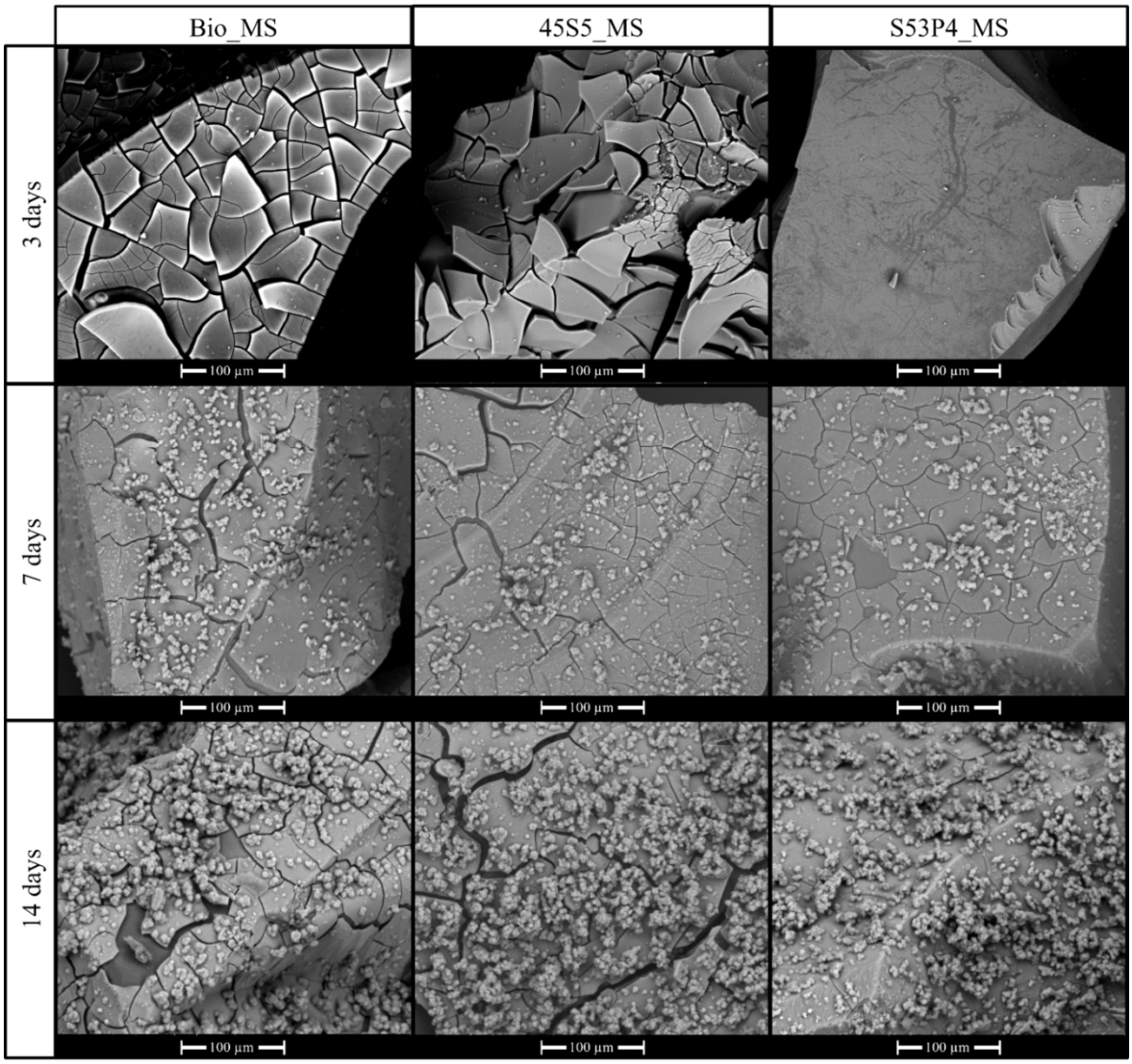

Figure 14: Grid of SEM micrograph of Bio_MS, 45S5_MS and S53P4_MS untreated samples after 3, 7 and 14 days of soaking in SBF.

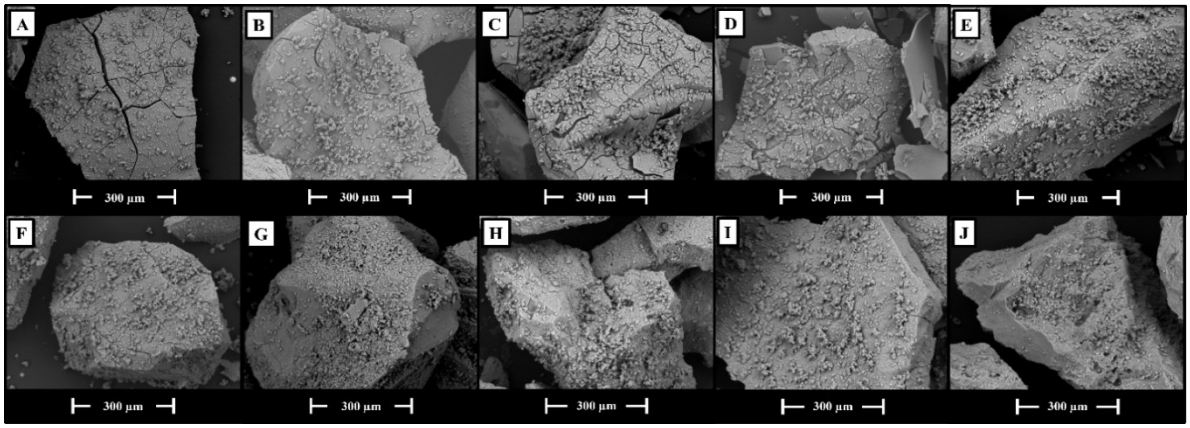

Figure 15: SEM micrographs of: 45S5 (A), S53P4 (B), Bio_MS (C), 45S5_MS (D), and S53P4_MS (E) untreated granules after 14 days of soaking in SBF, and 45S5 (F), S53P4 (G), Bio_MS (H), 45S5_MS (I), and S53P4_MS (J) granules heat treated at Tc after 14 days of soaking in SBF.

4.2.6 Biological assessment

A - Cytotoxicity test

MTT test is routinely used to evaluate the possible cytotoxicity of biomaterials and other medical devices, before conducting more detailed analyses on more complex experimental models [375]. MTT is a yellow tetrazolium salt that is metabolized by mitochondrial dehydrogenases leading to the formation of purple formazan crystals [376]. The intensity of the purple color is representative of the number of metabolically active cells capable of converting MTT, as an indicator of cell proliferation, viability and cytotoxicity. According to ISO 10993-5, samples are considered noncytotoxic when the cell viability is never below the threshold value of 70% compared to cells cultured in the absence of eluates (set at 100%) (Figure 16) Balb 3T3 fibroblasts were incubated with different concentrations (i.e., 100%, 50%, 25% and 12.5%) of eluates from the different BGs untreated and treated at different temperatures (Figure 16). Only the positive control (i.e., cells in DMEM+SDS) shows cytotoxicity, while all tested BGs, regardless of their different composition, heat treatment and eluates' concentration, do not exhibit any cytotoxic effect.

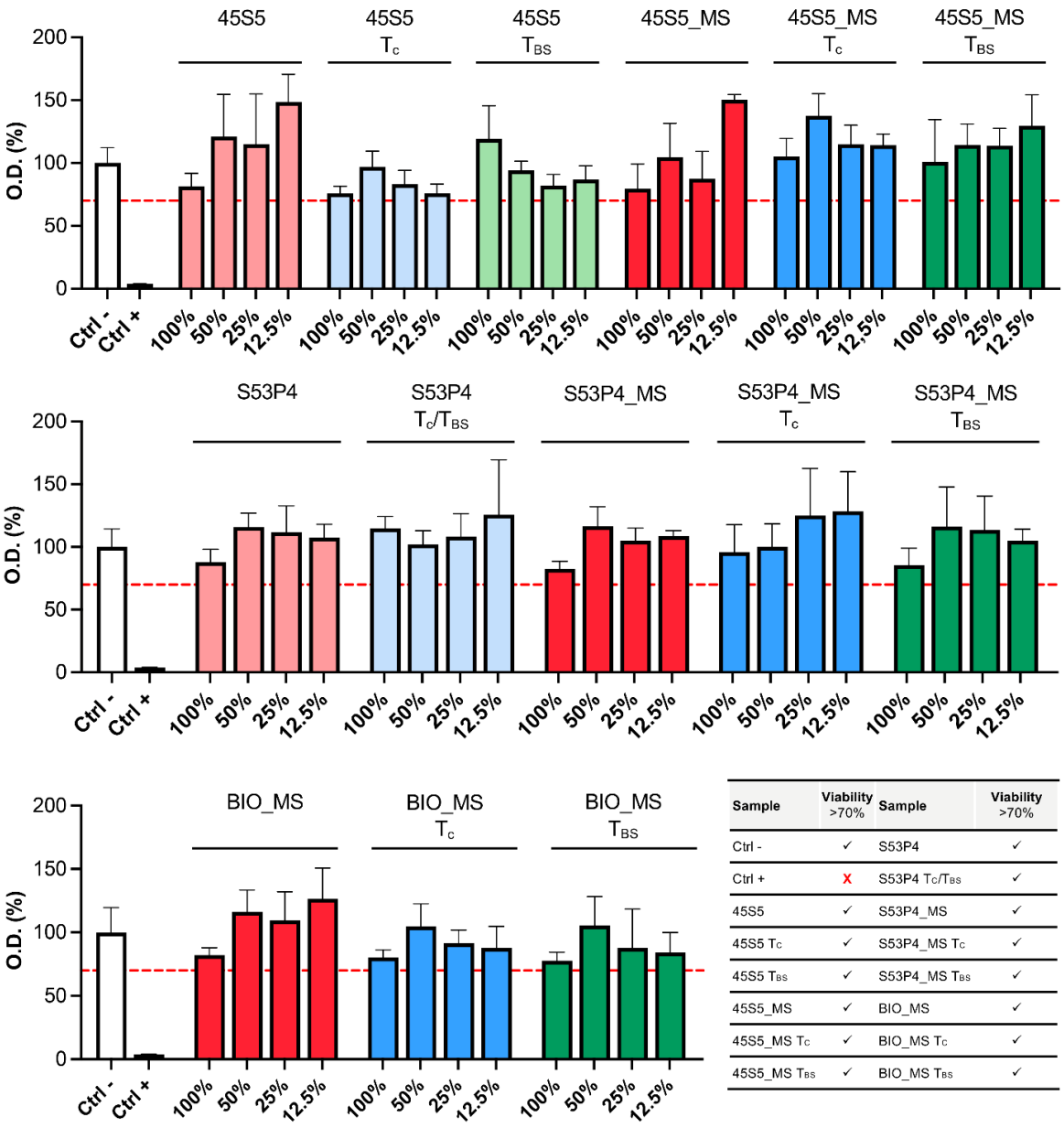

Sample	Viability >70%	Sample	Viability >70%
Ctrl -	✓	S53P4	✓
Ctrl +	X	S53P4 Tc/TBS	✓
45S5	✓	S53P4_MS	✓
45S5 Tc	✓	S53P4_MS Tc	✓
45S5 TBS	✓	S53P4_MS TBS	✓
45S5_MS	✓	BIO_MS	✓
45S5_MS Tc	✓	BIO_MS Tc	✓
45S5_MS TBS	✓	BIO_MS TBS	✓

Figure 16: ISO 10993-5 cytotoxicity test. The viability of the Balb 3T3 cell line was evaluated by the MTT test after 24 hours in the absence (DMEM, Ctrl-) or in the presence of different concentrations (100%, 50%, 25% and 12.5%) of eluates from the BGs. The positive control was represented by cells treated for 24 hours with DMEM plus 0.1% SDS (Ctrl +). Optical density (O.D.) from cells cultured in DMEM was set at 100%. The dotted line represents the threshold value of 70%, compared to Ctrl-, that, according to the ISO 10993-5 guidelines, is required to demonstrate the absence of cytotoxicity. Values represent the mean ± SD of two independent experiments.

B - Viability and adhesion of human dermal fibroblasts grown onto BGs

BGs have several well-known clinical applications in dental or orthopedic areas as scaffolds promoting bone regeneration [377], [378]. Data reported in previous sections have already highlighted the ability of BGs to favor the deposition of hydroxyapatite due to ion exchange on the BGs' surface, even in the absence of cells.

Therefore, we aimed at widening the spectrum of possible applications of BGs also in the field of soft connective tissue repair, given the clinical impact of defective wound healing [379]. In this study we have evaluated cell viability and the interactions between BGs and

human dermal fibroblasts (HDFs) in primary culture as a prototype of soft connective tissue mesenchymal cells producing the different components of the extracellular matrix [380], [381].

Since, we have previously demonstrated that a novel patented BG, Bio_MS [382], due to the integration of Mg and Sr (MS) in its composition, has promising applicative perspectives and improved thermal properties, we included in our biological evaluations also two commercially available BGs (i.e., 45S5 and S53P4) modified with the addition of MS.

Furthermore, to better investigate the behavior of cells directly interacting with BGs, HDFs were seeded on the surface of BGs and cell viability, adhesion properties and morphology of cells at different time points, up to 7 days, were evaluated.

Data reported in Figure 17 for Bio_MS indicates that cell viability is affected by the treatment at T_C but not at T_{BS}. To be noted, however, that reduction of cell viability at 4 and 7 days, compared to 1h, was always less than 20%.

Time	BIO_MS	BIO_MS T_C	BIO_MS T_{BS}
1 h	**100±5**	80±4	94±5
4 d	82±10§	69±11	83±13
7 d	85±7§	67±8	95±14

1 h	BIO_MS	BIO_MS T_C	BIO_MS T_{BS}
BIO_MS		**	
BIO_MS T_C			
BIO_MS T_{BS}			

4 d	BIO_MS	BIO_MS T_C	BIO_MS T_{BS}
BIO_MS			
BIO_MS T_C			
BIO_MS T_{BS}			

7 d	BIO_MS	BIO_MS T_C	BIO_MS T_{BS}
BIO_MS		*	
BIO_MS T_C			***
BIO_MS T_{BS}			

*Figure 17: Cell viability of human dermal fibroblasts grown for 1 hour (1h), 4 and 7 days (4d and 7d) on Bio_MS untreated or treated at different temperatures. Data are expressed as mean values ± SD. Values obtained with Bio_MS at 1h without any treatment were set at 100%. § p value < 0.05 of 4 or 7 days vs 1h in the same experimental condition; * p value < 0.05, ** p value < 0.01, *** p value < 0.001 between BGs untreated or treated at different temperatures at the same time point.*

Morphological observations and morphometrical analyses performed on HDFs grown on Bio_MS at different temperatures of treatment demonstrated good adhesion properties. A consistent number of cells adhered to the surface of BGs independently of treatments (see Figure 18). As expected, cells were round after 1 hour but appeared well spread and elongated after 4 and 7 days from seeding. After 7 days, fibroblasts on Bio_MS T_C appeared slightly, but significantly smaller compared to Bio_MS, suggesting that changes in the

characteristics of the BG's surface may influence the way cells interact with the BG. In this case, the bioactivity of Bio_MS treated at T_{BS} is not influenced by the sintering temperature. Indeed, as demonstrated in previous studies, one of the advantages of the Bio_MS formulation is the wide processing window with regards to heat treatment. Developing formulations that can be sintered without forming crystals and that are able to maintain good cell viability is an essential requirement for biomedical perspectives [156]. Since thermal treatments are necessary for the manufacturing of composite materials, porous scaffolds or coatings [156], Bio_MS treated at T_{BS} emerges as a possible candidate capable of maintaining high biocompatibility even after treatment at high temperatures.

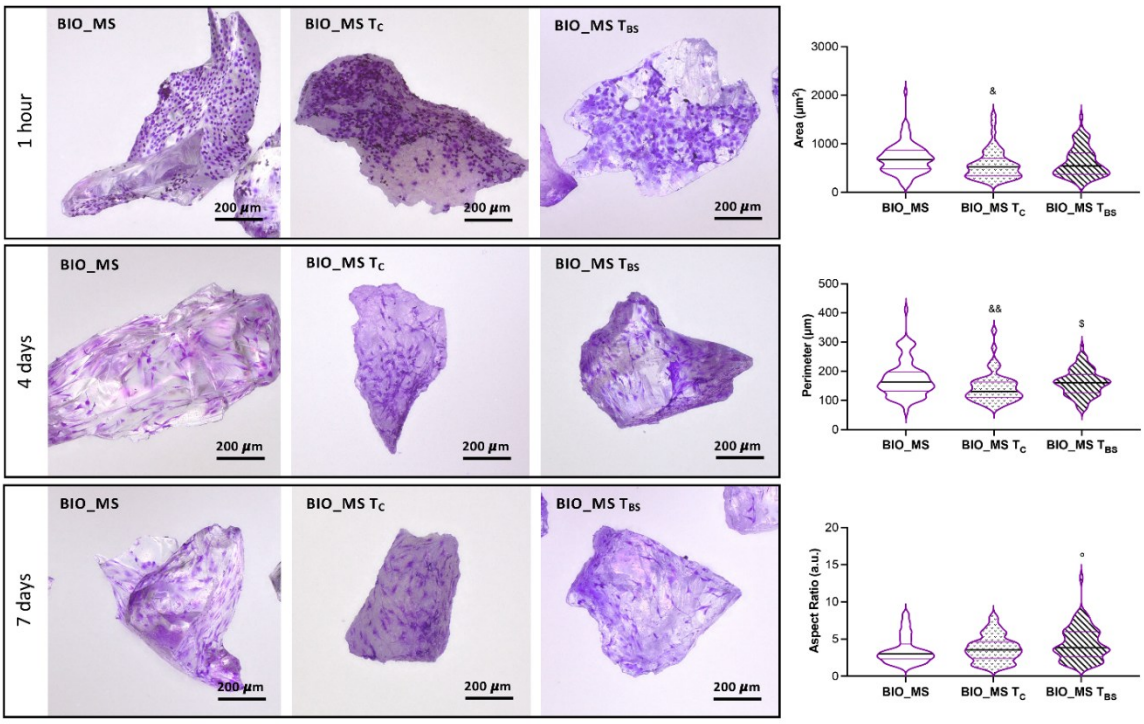

Figure 18: Representative images of HDFs seeded for 1 hour, 4 and 7 days on Bio_MS untreated and treated at different temperatures. Violin plot representing area, perimeter and aspect ratio evaluated after 7 days of culture. & $p<0.05$, && $p<0.01$ MS T_C vs MS; $ $p<0.05$ MS T_{BS} vs MS T_C; ° $p<0.05$ MS T_{BS} vs MS.

The same type of analyses described for Bio-MS, were performed on BGs used as reference standards and on the same commercial BGs also supplemented with MS. Figure 19 indicates that cell viability is progressively reduced on 45S5 without addition of MS and that these effects are particularly evident after treatment at T_{BS}. Data seems in contrast with the well-known properties of this BG, that represents the gold standard for implants, for supporting structures to be used in bone tissue regeneration [383] or for the re-mineralization of tooth enamel [384], [385]. However, its applicability and usability in the regeneration of loose connective tissues or in wound repair have been poorly investigated [386], [387], [388]. Within this context, it is worth mentioning that most of the data in the literature concerns the use of bone-related cells. For instance, 45S5 does not interfere with osteoblast viability, since these cells are well adapted to the extra- and intracellular alkalinization exerted by the BG [389]. Interestingly, a previous study by Day et al. [390], using a fibroblast cell line (208F) cultured on surfaces coated with 45S5, demonstrated a reduced cell proliferation depending on the time of culture (48 and 72 h) and/or on the concentration (0.01-0.2 wt./vol.%) of 45S5.

In the light of these data we can suggest that HDFs in primary culture, compared to other cells, may have different interactions with the BG and that even local changes in the pH, without any pre-treatment of the BG (e.g., with serum components, simulated body fluid - SBF, or with adhesive glycoproteins) [391], can influence cell adhesion [392] and cell proliferation, possibly mimicking *in vitro* what can happen *in vivo*, i.e. when the BGs are implanted.

It is well known that the adsorption of proteins on the BG is influenced by numerous factors, both external (e.g., pH and temperature) and internal (e.g., surface charges and topography of the BG surface) [393]. Interestingly, MS-doped BG showed a significantly improved cell viability, effects being also independent of temperatures. At 7 days of culture, the viability of cells grown on doped BGs was 1greater than on BGs. Noteworthy data obtained with the 45S5_MS T_{BS} vs 45S5 T_{BS} since addition of MS completely abolished the cytotoxic effect of the thermal treatment. In doped-BGs cell viability showed a general decrease at day 4 and an increase at day 7. These data suggest that 45S5_MS, regardless of treatment, induces an initial selection within the cell population in favor of a subpopulation capable of better adapting to the microenvironment, as already observed in the literature [394].

Time	45S5	45S5 T_C	45S5 T_{BS}	45S5_MS	45S5_MS T_C	45S5_MS T_{BS}
1 h	**100±11**	93±1	91±2	112±14	114±8	98±8
4 d	56±10§§§§	93±20	9±1§§§§	83±15§§§	75±5§§§§	93±9
7 d	67±10§§§	69±13$^{§§\#}$	8±2§§§§	96±10§	104±20$^{\#\#}$	113±12$^{§\#\#}$

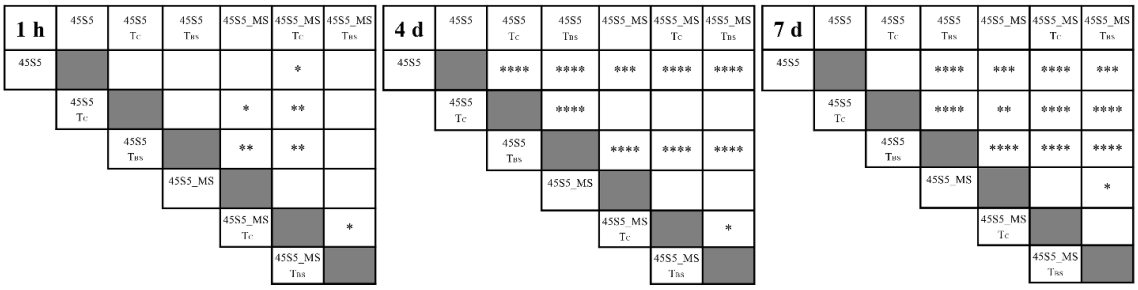

*Figure 19: Cell viability of human dermal fibroblasts grown for 1 hour (1h), 4 and 7 days (4d and 7d) on 45S5 and 45S5_MS untreated or treated at different temperatures. Data are expressed as mean values ± SD. Values obtained with 45S5 without any treatment at 1 h were set at 100%. § p value < 0.05, §§ p value < 0.01, §§§ p value < 0.001, §§§§ p value < 0.0001 of 4 or 7 days vs 1h in the experimental condition; # p value < 0.05, ## p value < 0.01 of 7 vs 4 days; *p value < 0.05, ** p value < 0.01, *** p value < 0.001, ****p value < 0.0001 between BGs untreated or treated at different temperatures at the same time point.*

The better performance observed for the doped 45S5 is associated with the addition of MS. This result is not surprising, as it has been already demonstrated that the addition of Mg to BGs promotes the adhesion of bone-derived cells [395]. Indeed, previous studies demonstrated that Mg promotes cell adhesion favoring the synthesis of collagen type I, vitronectin, fibronectin and the activation of kinases associated with focal adhesions in osteoblasts [35], [396] as well as in human fibroblasts [397]. Furthermore, also Sr can act as an inducer of cell adhesion and proliferation, as shown on BGs subjected to treatments at temperatures that can compromise the bioactivity of the biomaterial [337], and can promote

both osteogenesis and angiogenesis when added to BG nanoparticles [325]. Furthermore, Sr can maintain an optimal pH in the surrounding environment, thus ensuring good cell viability [398].

The interactions between cells and BGs were also assessed by evaluating the morphology of HDFs grown up to 7 days on 45S5 and 45S5_MS at different temperatures. Morphometric analyses were also performed at 7 days to quantitate differences in the spreading of the cells.

HDFs adhered well on all BGs at 1h, although, as expected, they are still round. Over time in culture, cells acquired a more elongated shape except for 45S5 T_{BS}. Due to the low number of cells on 45S5 T_{BS}, morphometric analyses on these samples were not performed.

MS-doped BG allowed to maintain the number of adhered cells that exhibited a more spread morphology compared to cells on 45S5 (Figure 20) confirming the beneficial role of MS addition.

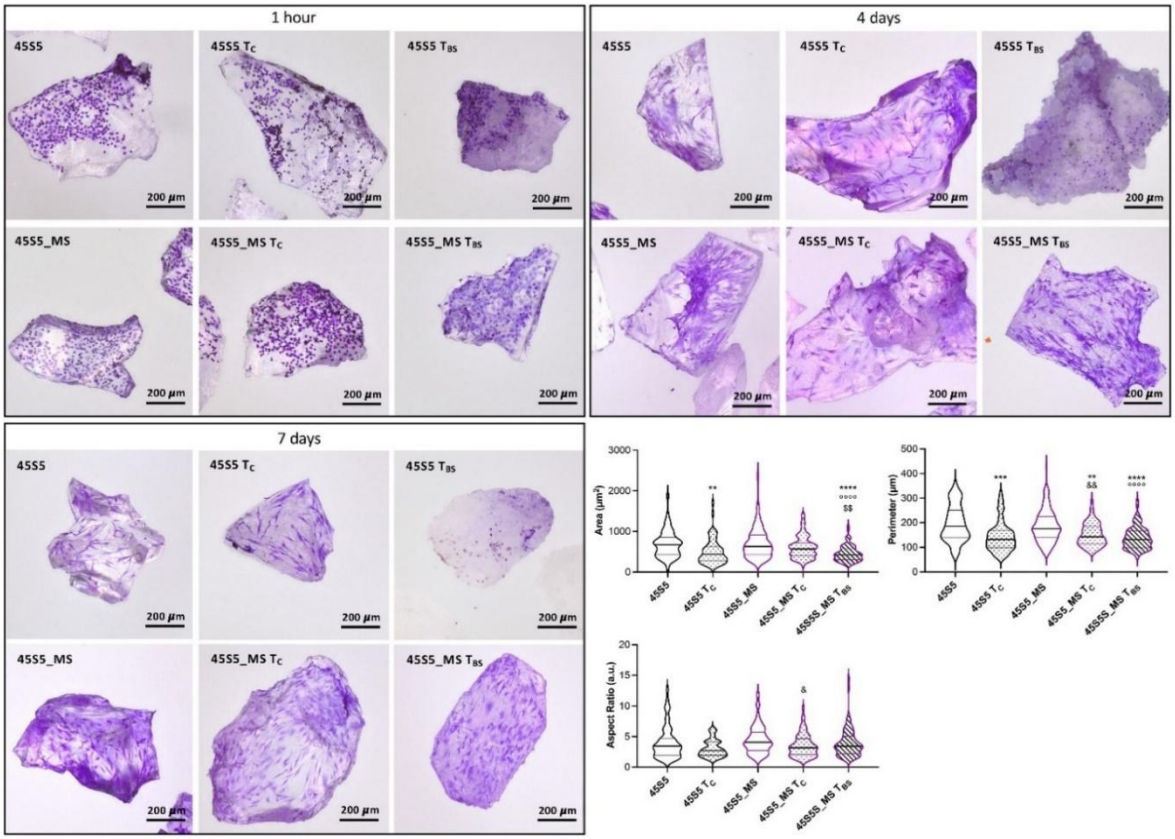

*Figure 20: Representative images of HDFs seeded for 1 hour, 4 and 7 days on 45S5 and 45S5_MS untreated and treated at different temperatures. Violin plot representing area, perimeter and aspect ratio evaluated after 7 days of culture. **p<0.01, ***p<0.001, ****p<0.0001 all conditions vs 45S5; &p<0.05, &&p<0.01 MS T_C vs MS; °°°°p<0.0001 MS T_{BS} vs MS; $$p<0.01 MS T_{BS} vs MS T_C.*

Since cell viability and adhesion were severely affected on 45S5 treated at T_{BS}, we wanted to test if the observed effects were due to the release of specific components affecting cell behavior or if the cells negatively responded to changes of the surface of the BGs. Therefore, HDFs were cultured on standard multi-well plates in the presence of DMEM or of 100%

eluates from 45S5 treated at T_{BS}. Fibroblasts, in the presence of 100% 45S5 T_{BS} eluates, exhibited good proliferation capabilities (see Figure 21).

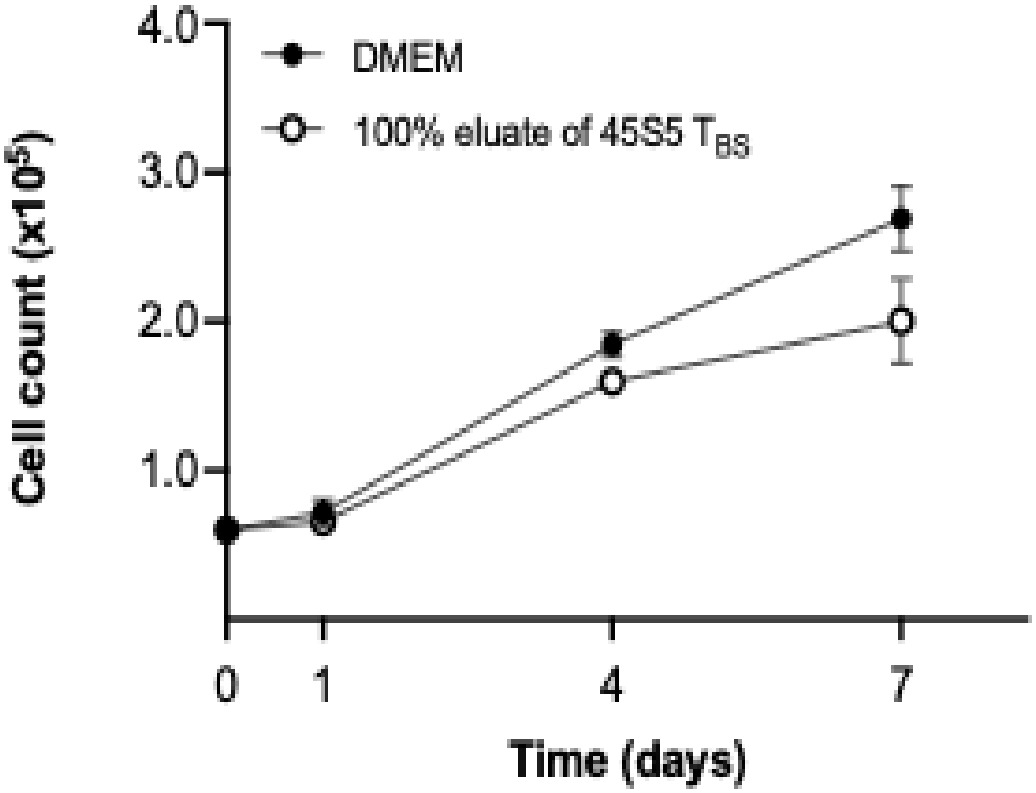

Figure 21: Cell proliferation. HDF were cultivated in DMEM or in DMEM+ 100% eluate from 45S5 T_{BS} and cell number evaluated at different time points after seeding. There are no significant differences between the two experimental conditions. Data are expressed as mean values ± SD.

Data demonstrates that the reduced cell viability observed with 45S5 treated at T_{BS} is not due to cytotoxic components released by the BG but could be linked to modifications of the microstructure of the BG following heat treatment, as suggested by previous studies [137]. The operating conditions adopted during the sintering process for the consolidation of the powders, can modify the compositional and structural characteristics of the BG, which in turn influence mechanical and biological properties. Indeed, it has been observed that, as the temperature increases, the surface of 45S5 goes from smooth to wrinkled with consequences on the bioactivity of the BG [137]. Therefore, cell viability is not influenced by ions and/or toxic components released by BG, but more likely by changes occurring on the surface of the BG after treatment at sintering temperature.

In Figure 22 data shows the viability of cells grown on the S53P4, that was developed and mainly used in clinical applications related to bone healing, vascularization, and cartilage repair [399], [400]. Although there are several data in the literature related to the effect of BG S53P4 on bone-derived cells (osteoblasts and osteoclasts) [401], [402], [403], to our knowledge, there are no studies on the use of dermal fibroblasts.

Time	S53P4	S53P4 T_C/T_{BS}	S53P4_MS	S53P4_MS T_C	S53P4_MS T_{BS}
1 h	**100±11**	86±8	127±11	110±5	125±9
4 d	82±6§§	79±14	104±11§	82±10§§	107±11
7 d	67±14§§§§	55±5§§§##	79±10§§§§#	97±10	120±19

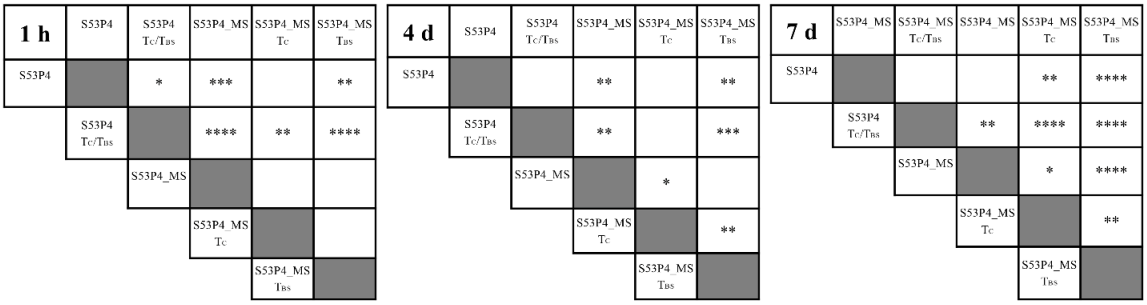

*Figure 22: Cell viability of human dermal fibroblasts grown for 1 hour (1h), 4 and 7 days (4d and 7d) on S53P4 and S53P4_MS untreated or treated at different. Data are expressed as mean values ± SD. Values obtained with S53P4 were set at 100%. § p value < 0.05, §§ p value < 0.01, §§§ p value < 0.001, §§§§ p value < 0.0001 of 4 or 7 days vs 1h in the same experimental condition; # p value < 0.05, ## p value < 0.01 of 7 vs 4 days; * p value < 0.05, ** p value < 0.01, *** p value < 0.001, ****p value < 0.0001 between BGs untreated or treated at different temperatures at the same time point.*

In the present study, cell viability is progressively reduced on the BG both without any heat treatment or at temperatures T_C/T_{BS}. Similarly, to 45S5_MS, also S53P4_MS showed significantly improved cell viability, effects being independent on temperatures. The interactions between cells and S53P4 BGs were assessed by evaluating the morphology of HDFs grown up to 7 days on the BGs. Morphometric analyses were also performed for 7 days to quantitate differences in the spreading of cells.

When HDFs were grown on S53P4, after 1h, cell behavior was similar to that on 45S5. By contrast after 4 and 7 days, the number of adhered cells was reduced on BG treated at T_C/T_{BS}, thus underlining the effect of treatment on adhesion and cell viability of cells in contact with BGs. On the contrary, S53P4_MS exhibited nicely spread and typically elongated HDFs. Data, once more, clearly demonstrated the positive effect of the addition of Mg and Sr to the BG (Figure 23).

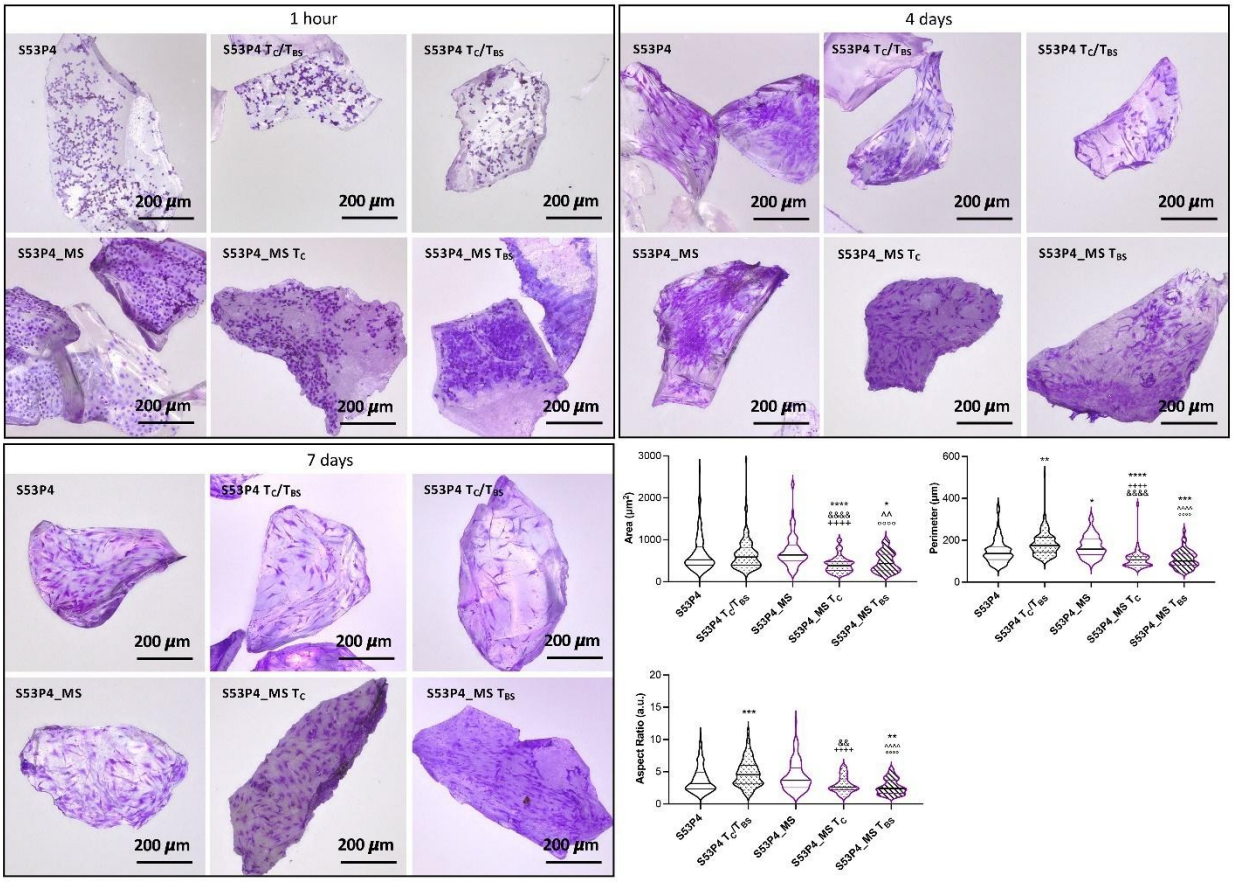

*Figure 23: Representative images of HDFs seeded for 1 hour, 4 and 7 days on S53P4 and S53P4_MS untreated and treated at different temperatures. Violin plot representing area, perimeter and aspect ratio evaluated after 7 days of culture. * p< 0.05, ** p< 0.01, *** p< 0.001, **** p< 0.0001 all conditions vs S53P4; && p< 0.01, &&&& p< 0.0001 MS T_C vs MS; °°°° p< 0.0001 MS T_{BS} vs MS; ++++ p< 0.0001 T_C/T_{BS} vs MS T_C; ^^ p< 0.01, ^^^^ p< 0.0001 T_C/T_{BS} vs MS T_{BS}.*

Finally, to better evaluate cell viability of HDFs in the different experimental conditions, BGs were compared to each other based on their formulation, regardless of the heat treatment. In particular, cell viability was evaluated on BGs without heat treatment (NHT), on BGs treated at crystallization temperatures (T_C) and on BGs treated at best sintering temperatures (T_{BS}). The cell viability data were compared with results of the non-thermally treated 45S5, considered the gold standard of BGs currently on the market [383].

In group NHT, cell viability on 45S5_MS and Bio_MS was higher than on standard BG (45S5) (Figure 24). In group T_C, cell viability was significantly higher for all BGs with MS compared to the same BGs without MS (Figure 22). In group T_{BS} it clearly emerges that the addition of MS to the BGs significantly increased the cell viability of HDFs compared to formulations without MS. Furthermore, cell viability was similar among the three MS-containing BGs (Figure 24).

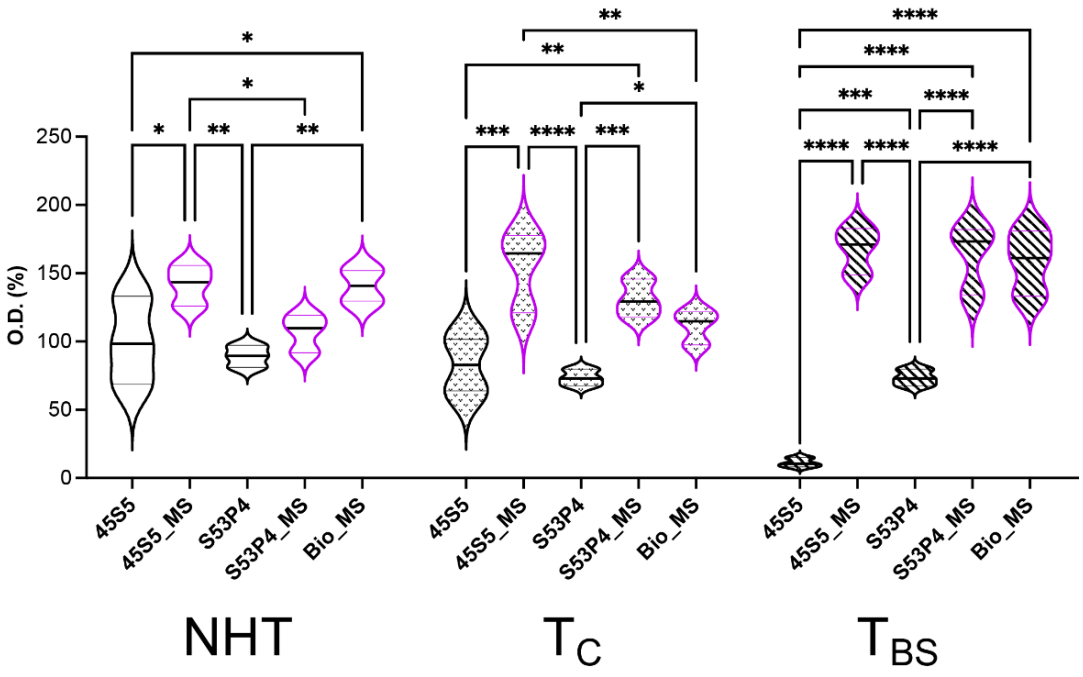

*Figure 24: Violin plot representation of the cell viability of HDFs grown on non-heat-treated (NHT) or heat-treated bioglasses (BGs) for 7 days. T_C = crystallization temperature; TBS= best sintering temperature. Values of optical density (O.D.) obtained with 45S5 in 7 days were set to 100%. * p value < 0.05; ** p value < 0.01; *** p value < 0.001; **** p value < 0.0001.*

5 Feasibility of electrospun PCL/BG composite scaffolds

(This section has been published in "F. G. Mecca, N. O. Muniz, D. Bellucci, C. Legallais, T. Baudequin, and V. Cannillo, "Inclusion of Magnesium- and Strontium-Enriched Bioactive Glass into Electrospun PCL Scaffolds for Tissue Regeneration," *Polymers 2025, Vol. 17,* vol. 17, no. 11, Jun. 2025, doi: 10.3390/POLYM17111555.")

As previously anticipated, electrospinning is a scaffold manufacturing technique that enables the fabrication of nano- to micro-fibrous, porous, unwoven flat scaffolds (or mats). The fibers are drawn out from a polymer-containing solution by applying a high electrical potential difference between a needle and a collector [404]. The incorporation of bioactive glass particles (specifically in the nano- to micro-size range) into the fiber structure may expand the range of applications of both BG and electrospun mats. The interest in the production of electrospun polymer/BG composites is due to their potential as functionalized scaffolds [61], [318], [405], [406]. However, the use of powdered melt-derived BGs suspended in the polymeric solution presents some limitations for electrospinning. In fact, achieving a homogeneous dispersion of BG particles can be challenging, as an agglomeration and physical alterations of the fiber morphology may occur.

In this section of the work, two BGs 45S5, and 45S5_MS have been employed as particulate load in electrospun PCL/BG composite scaffolds. As already described in chapter "4 Novel Mg- and Sr-doped BG compositions", 45S5_MS is a composition derived from 45S5, in which strontium and magnesium were introduced to partially substitute for calcium as a modifier. The addition of these ions into the BG composition is motivated by their positive biological effects, which are widely reported in the literature [98], [407], [408]. PCL is an FDA-approved semicrystalline polymer that has been extensively studied in biomedical applications due to its excellent mechanical properties and adjustable biodegradability [409], [410].

In vitro tests in SBF were conducted on the scaffolds. The employment of SBF can give insights into the dissolution behavior of these scaffolds [411], [412]. Typical effect of the immersion of BG particles in SBF is a marked increase in pH, as rapid dissolution leads to alkali ion release in the environment [392]. However, the interaction between PCL and SBF has been reported to induce non-trivial effects both on the polymer - swelling, weight loss - and to the SBF solution, which is acidified [413], [414], [415]. This phenomenon contrasts with the typical alkalizing behavior of BGs related to ion leaching [392].

For these reasons, considering the potential alkalinization of the solution [197] and ion release from the glass (specifically of magnesium from 45S5_MS), *in vitro* biological investigations can provide valuable complementary information on the overall performance of the scaffolds, offering insights into their potential for *in vivo* studies [22].

5.1 Testing procedures

5.1.1 Bioactive Glass Preparation

A detailed description of the preparation of the BGs 45S5 and 45S5_MS is reported in section "4.1.1 Preparation of the bioactive glass". Table 8 reports the compositions of the BGs employed in the current portion of the study.

Table 8: Compositions of 45S5 and 45S5_MS (also reported in chapter "4 Novel Mg- and Sr-doped BG compositions").

Oxide	45S5 Composition (mol.%)	45S5_MS Composition (mol.%)
SiO_2	46.1	46.1
CaO	26.9	26.9
Na_2O	24.4	9.4
P_2O_5	2.6	2.6
MgO	-	5
SrO	-	10

To obtain a powder suitable for electrospinning, the glass frit was milled into a fine BG powder. To obtain micro- to submicrometric particle sizes, a two-step milling process was used. First, the glass frit was ground using alumina milling balls and a jar inside a laboratory mill MGS1800/2 (MGS S.r.L, Fiorano Modenese, Italy) for 20 min. The ground BG was then sieved using a 63 μm sieve.

A second, more thorough, grinding step was performed using a PM100 (Retsch Gmbh, Haan, Germany) to obtain a finer powder. Ten grams of BG powder were placed inside a steel-reinforced zirconia jar with 5 mm-diameter zirconia milling balls. The jar was spun at 600 rpm for 20 min. This operation was repeated 3 times, for a total duration of 1 h. This milling process was carried out in three steps to maximize efficiency while allowing heat dissipation.

Both BGs underwent this procedure to obtain two final powders. Finally, to ensure that the BGs were thoroughly milled, a scanning electron microscope (Quanta FEG 250, FEI, Hillsboro, OR, USA) was used to qualitatively analyze their morphology.

5.1.2 Electrospinning of PCL/BG Scaffolds

PCL beads (MW = 80 kDa), dichloromethane (DCM), and dimethylformamide (DMF) were purchased from Sigma Aldrich Chimie S.a.r.l. (Saint-Quentin-Fallavier, France). Electrospun mats were obtained from a 12 wt.% precursor solution of PCL and BG powder. First, the BG powder was dispersed in 60 vol.% DCM and 40 vol.% DMF. DCM acts as the solvent for PCL, while DMF is usually added as a stabilizer of the electrospinning jet, because of its higher dielectric constant and lower vapor pressure [416]. The ratio 3:2 DCM/DMF was chosen based on previous experiments. Subsequently, the appropriate amount of PCL beads was added to the BG/solvent mixture. The resulting suspension was

stirred for 4 h. Four different suspensions were produced: (1) 90% of PCL and 10% of BG, (2) 80% of PCL and 20% of BG, each prepared using either 45S5 or 45S5_MS glass. Table 9 presents a summary of the compositions of each sample.

Table 9: Compositions of the precursor suspensions (expressed in percentages), with the relative BG and PCL content used before electrospinning

BG	Sample	PCL Beads (%)	BG Powder (%)
45S5	45_9010	90	10
	45_8020	80	20
45S5_MS	45_MS_9010	90	10
	45_MS_8020	80	20

The electrospinning parameters needed extensive optimization to achieve stable and efficient spinning of the suspension. A comprehensive overview of these parameters is presented in Table 3. Previous work by Baudequin et al. [78] was used as a reference for the manufacturing of these scaffolds. Briefly, the voltage was maintained between 17.8 kV and 20.0 kV to balance the quantity of suspension drawn out of the needle [417]. The working distance was fixed at 15 cm, and the flow rate was set to 1.5 mL/min. The suspension was fed through a 19-gauge, 8 cm long needle, chosen specifically to prevent clogging caused by BG agglomerates. A rotating cylinder collector was used at a speed of 300 rpm.

Table 10: Electrospinning parameters used for spinning samples in this study. The table includes the environmental parameters, which were measured at the beginning of the electrospinning process.

Sample	Voltage (kV)	Flow Rate (mL/h)	Working Distance (cm)	Total Spun (mL)	Ambient Parameters [1]	
					Ambient Temp. (°C)	Relative Humidity (%)
45_9010	18	1.5	15	3.3	22.1	68.3
45_8020	18	1.5	15	3.3	22.0	68.3
45_MS_9010	17.8	1.5	15	3.3	21.7	70.2
45_MS_8020	20	1.5	15	3.3	21.8	71.2

[1]Ambient parameters were measured in the laboratory at the start of the electrospinning process and are dependent on weather conditions.

The surfaces of the electrospun mats were studied using a field-emission scanning electron microscope (FE-SEM—Fei Nova NanoSEM 450, ThermoFisher Scientific, Eindhoven, The Netherlands) and an EDS detector QUANTAX-200 (Bruker Corp., Billerica, MA, USA), used for mapping the presence of silicon in the scaffolds, which is an indicator of the presence of BG in the electrospun mats. Small sections of the samples were cut and sputter-coated with a 10 nm gold layer. ImageJ (an open-source image analysis software—version 1.54j, NIH, Bethesda, MD, USA) was used to determine the mean fiber diameter. To achieve

this, at least 50 measurements were taken. A one-way ANOVA statistical analysis was performed to detect the statistical variance between the results. Moreover, a qualitative analysis based on visual observation to detect the BG particles was conducted to confirm their presence in the electrospun scaffolds.

The electrospun mats underwent a thermal gravimetric analysis (TGA) using an STA 429 CD (Netzsch GmbH, Selb, Germany) to quantitatively analyze the presence of BG powder in the electrospun mats as residue after thermal degradation of the PCL. Samples weighing 10 to 20 mg were heated at a rate of 20 °C/min to 600 °C. This temperature was chosen to avoid any possible crystallization occurring in the BG structure, following the results reported in chapter "4 Novel Mg- and Sr-doped BG compositions"

5.1.3 Mechanical Characterization

The mechanical properties of the electrospun mats were evaluated through uniaxial tensile testing using a traction test machine, Synergie 400 (MTS System Corp., Eden Prairie, MN, USA), equipped with a 100 N load cell and clamps for direct measurement. A tensile speed of 1 mm/min at room temperature was used to measure the samples' properties. The partial alignment of the fibers was considered a potential factor influencing the results. For this reason, two types of samples were cut from each mat: one along the longitudinal (L) direction, and one along the transversal (T) direction. The L-direction is parallel to the radial component of the cylinder's velocity, while the T-direction is parallel to the rotation axis of the collector cylinder. Five 5 × 20 mm strips were cut for each type of sample. The clamps of the traction test machine were set at a starting distance of 5 mm. The thickness of the samples was measured using a digital feeler gauge. Finally, the Young's modulus (E) and ultimate tensile strength (σ_{MAX}) were calculated from the obtained tensile stress–strain curve. A two-way ANOVA statistical analysis was conducted to evaluate the variance of the results.

5.1.4 Surface Wettability

The hydrophilicity of the samples, a key parameter for understanding their ability to support cell adhesion on their surfaces, was measured [418]. The water contact angles of the mats were assessed at room temperature using an automatic optical contact angle system (OCA 15EC, Dataphysics Instruments GmbH, Stuttgart, Germany) equipped with a 6.5× zoom lens. A 20× magnification was used to capture the measurements. Distilled water was dropped onto the surface of each sample and immediately photographed (t = 0) to measure the water contact angle. Each sample was measured at least 10 times at different locations to obtain an average value. A one-way ANOVA test was performed to assess the differences in the contact angles among the scaffolds. A significance level of $\alpha = 0.05$ was considered for all statistical evaluations.

5.1.5 Methods for tests in Simulated Body Fluid

Bioactivity tests were carried out according to Kokubo's method. The SBF solution was prepared in the lab by slowly and carefully mixing the salts under constant stirring. HCl was used to buffer the solution and adjust its pH to 7.4. The required quantity of SBF was calculated using the formula provided by Kokubo et al. [22]:

$$V_{SBF} = \frac{S_A}{10}, \tag{3}$$

where V_{SBF} is the volume of SBF in which the samples are soaked, and S_A is the total surface area of the sample.

The electrospun mats were cut into 45 × 5 mm strips and weighed using an analytical balance. The strips were then secured in Petri dishes, submerged in SBF, and incubated at a constant temperature of 37 °C. Every 48 h, the pH of the solution was measured before replacing it with fresh, unreacted SBF. The samples were extracted at three predetermined time points: 3, 7, and 14 days. After the immersion period, the samples were removed from the SBF, washed with demineralized water, and dried at 40 °C for at least 3 days to remove the residual solution from the pores. The scaffolds were then analyzed using an environmental scanning electron microscope (Fei Quanta 200, ThermoFisher Scientific, Waltham, MA, USA) equipped with an EDS detector (Inca, Oxford Instruments, Oxford, Abingdon, UK).

5.1.6 Materials for Biological Studies

Mouse fibroblast-like cells (L929, ATCC), immortalized adipose-derived stem cells (ASC52telo, ATCC), mesenchymal stem cell basal medium (ATCC-PCS-500-030), mesenchymal stem cell growth kit-low serum for adipose, and umbilical cord-derived MSCs (ATCC-PCS-500-040) were purchased from LGC Standards (Teddington, UK). BCIP/NBT alkaline phosphatase (ALP) substrate solution, DAPI, dexamethasone (D8893), β-glycerophosphate disodium salt hydrate (G9422), and L-ascorbic acid (A4544) were purchased from Sigma Aldrich Chimie S.a.r.l (Saint-Quentin-Fallavier, France). Dulbecco's Modified Eagle's Medium—low glucose, Osteocalcin (OCN) polyclonal antibody, goat anti-Rabbit IgG (H+L) cross-adsorbed secondary antibody Alexa Fluor™ 488, penicillin and streptomycin (PenStrep), and L-glutamine were purchased from ThermoFisher Scientifics (Eindhoven, The Netherlands). Dulbecco's phosphate-buffered saline (DPBS) and bovine serum albumin (BSA) were obtained from Dominique Dutscher SAS (Bernolsheim, France). Fetal bovine serum (FBS) was provided by Cytiva (Marlborough, MA, USA).

5.1.7 Biological Evaluation

A - Indirect Cell Culture

The cytotoxicity of the scaffolds was assessed in accordance with ISO 10993-5 guidelines [419] to evaluate the presence of cytotoxic compounds released into the media. The viability of the mouse fibroblast-like cells (L929) in indirect contact with the scaffolds was evaluated.

The cells were cultured and maintained in flasks with complete DMEM, supplemented with 10% FBS, 1% penicillin–streptomycin, and 1% L-glutamine, at 37 °C in a humidified atmosphere containing 5% CO_2. For the test, 96-well plates containing 100 µL of complete DMEM were seeded with 10,000 cells/well and incubated for 24 h. In parallel, electrospun mats were cut into small pieces, covered with complete DMEM, and incubated under agitation for 24 h at 37 °C and 5% CO_2. Before the test, the mats were disinfected by immersion in 70% EtOH for 30 min and then washed three times with DPBS under sterile

conditions. Latex was used as a negative control (CTRL (−)) and was disinfected using the same procedure.

After 24 h, the culture medium was replaced with 100 µL of the mat- or latex-extracted medium and incubated for another 24 h in the same conditions (n = 3). Complete DMEM served as the positive control (CTRL (+)).

Following incubation, 20 µL of the MTS solution were added to each well and incubated for 2 h at 37 °C and 5% CO2. The optical density (OD) was measured at 492 nm using a microplate reader (Tecan Spark 10, Männedorf, canton of Zürich, Switzerland). The absorbance values were normalized to positive control and expressed as relative cell viability (%).

B - Direct Cell Culture

In vitro cell tests were performed using human immortalized adipose-derived stem cells (ASC52telo). To assess the effect of BG presence, a pure PCL electrospun mat was used as a control.

Cells were cultured in complete mesenchymal stem cell basal medium, supplemented with 10% FBS, 1% penicillin–streptomycin, and 1% L-glutamine, at 37 °C and 5% CO_2. The electrospun mats were disinfected by immersion in 70% EtOH for 30 min and washed three times with DPBS under sterile conditions. They were then incubated overnight on a 24-well plate in complete medium at 37 °C and 5% CO_2. The mats were seeded with ASC52telo cells at a density of 10,000 cells per sample (Ø = 12 mm).

To evaluate the influence of the scaffolds on cell activity, two groups were established: one cultured in complete medium (proliferation group) and the other in osteogenic medium (complete medium supplemented with 1 M β-glycerophosphate, 50 mg/mL L-ascorbic acid, and 100 µM dexamethasone). The culture was maintained for 28 days, with medium changes every two days.

C - Qualitative Staining of Alkaline Phosphatase

After 28 days of culture, the medium from both groups was removed, and 500 µL of BCIP/NBT alkaline phosphatase substrate were added to each well. The samples were incubated in the dark at room temperature for 30 min. The substrate solution was then removed to stop the reaction, and the samples were washed with DPBS.

D - Immunofluorescence (IF) Staining of Osteogenic Bone Marker

The presence of osteogenic markers in the *in vitro* cultured samples was analyzed by IF-OCN staining. Samples cultured with ASC52telo for 14 and 28 days were collected, washed with phosphate-buffered saline (PBS), and fixed in 4% paraformaldehyde for 30 min. They were then permeabilized with 0.5% Triton X-100 for 20 min, washed three times with PBS, and saturated with 2% BSA for 2 h. The samples were incubated overnight at 4 °C with the primary OCN antibody. After washing with PBS and 0.1% BSA, the samples were incubated for 1 h at room temperature with the goat anti-rabbit IgG (H+L) cross-adsorbed secondary antibody Alexa Fluor™ 488 and DAPI, in a humid chamber. The samples were visualized using a confocal laser scanning microscope (LSM 980 Airy-Scan II, Carl Zeiss France

S.A.S., Rueil-Malmaison, France), with excitation/emission wavelengths of 405 nm for DAPI (blue) and 488 nm for OCN (green).

5.2 Results and Discussion

5.2.1 Characterization of the Electrospun Scaffolds

As previously described, the BG powders underwent an extensive milling process to ensure optimal results during suspension spinning. To evaluate the morphology of the powders after milling, SEM imaging was performed. The results are shown in Figure 25. The BG appears to have been successfully ground into a powder with dense particles and variable geometry. However, a significant agglomeration of the powder was observed, with smaller BG particles adhering to one another. This phenomenon, typical of nano-sized BG particles, has been previously reported in the literature and is attributed to residual surface charges [420], [421], [422]. The use of cyto-compatible deflocculants may mitigate this effect by improving particle dispersion within the suspension [422].

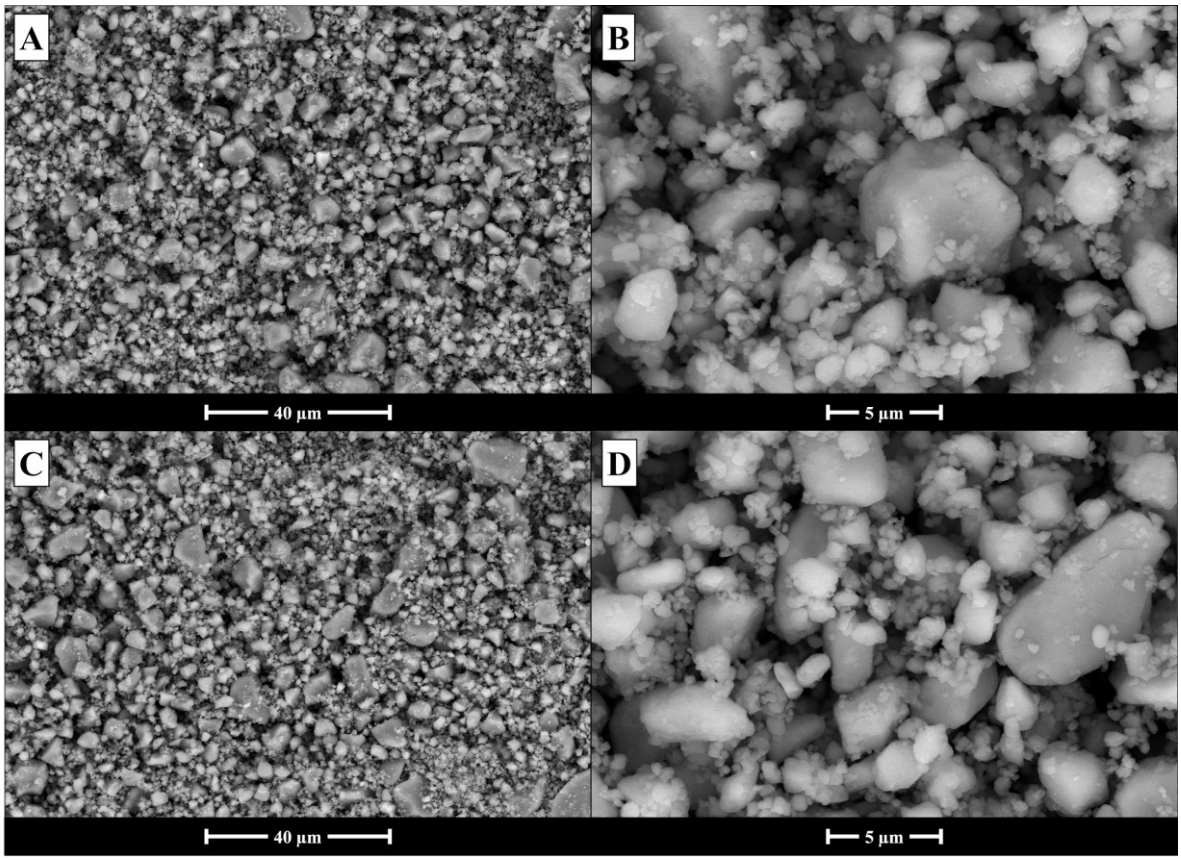

Figure 25: SEM analysis of the morphology of the powdered BG: (A, B) 45S5; (C, D) 45S5_MS samples, after milling with the PM100 rotary mill.

The structure of the as-spun mats was examined using SEM, and the results are re-ported in Figure 26. The images revealed the presence of BG particles embedded within the electrospun mats. In all four samples, BG particles were either adhered to the surface of the fibers or completely embedded within them. However, the micrographs in Figure 26 indicate that the BG particles are predominantly incorporated into the fiber structure rather than merely adhered to the surface. Furthermore, the EDS map in Figure 26 (E), showing the

presence of silicon atoms, confirms the widespread distribution of BG within the electrospun mat, further supporting the predominant incorporation of the BG particles into the fiber structure. Although this analysis was performed on all four samples, only the result for sample 45_MS_8020 is shown in Figure 26 (E) for the sake of conciseness. The inclusion of BG particles may have influenced the final morphology of the fibers, as reported in previous studies [70]. Embedded particles occasionally caused bulging along the fibers, which could compromise mechanical performance, as bead-on-string defects are known to introduce weak points in the fiber structure [423], [424].

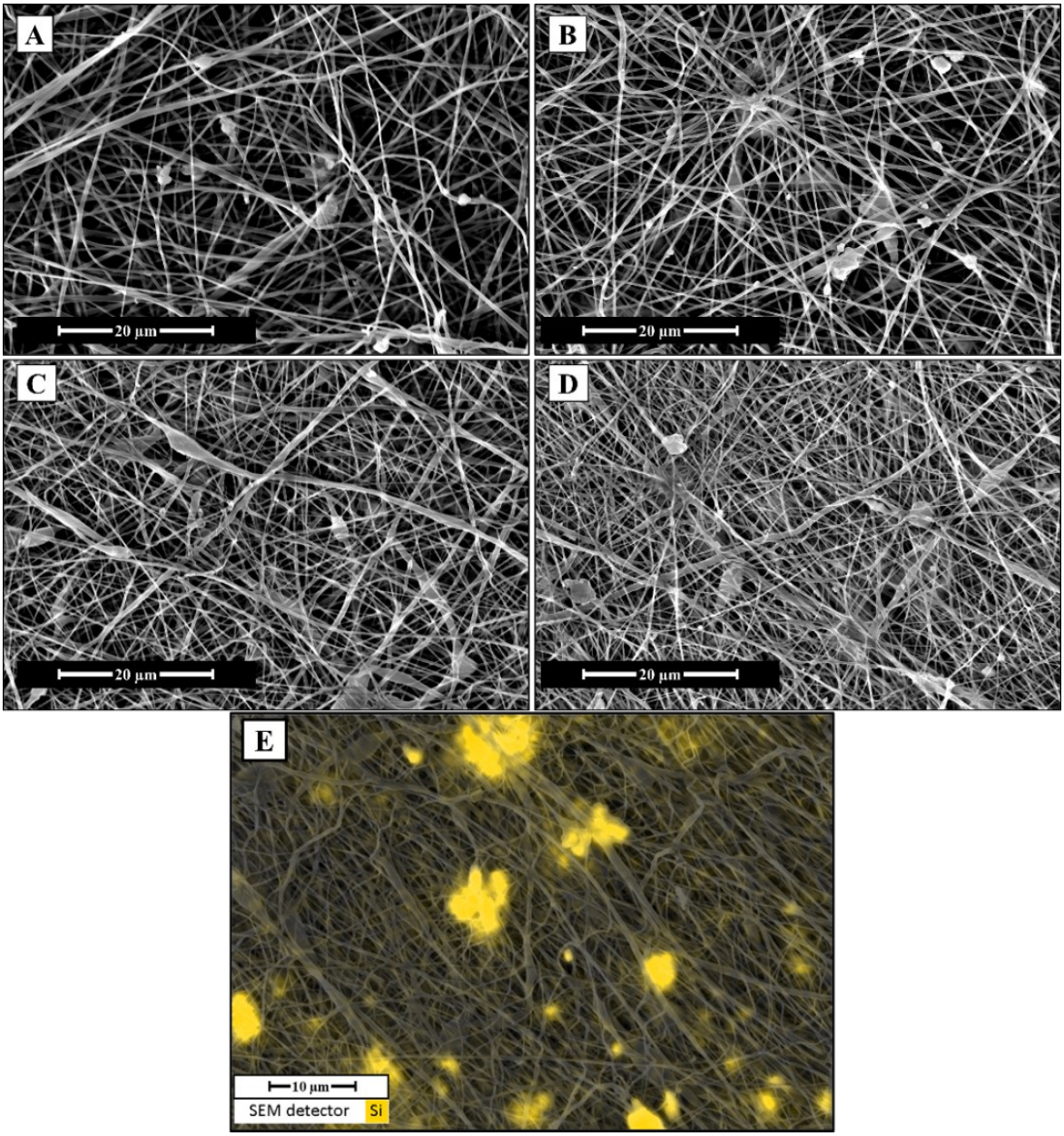

Figure 26: FE-SEM micrographs at 6000× magnification of the as-spun scaffolds: (A) 45_9010; (B) 45_8020; (C) 45_MS_9010; (D) 45_MS_8020. (E) EDS map of silicon superimposed on a 6000× magnification FE-SEM micrograph of sample 45_MS_8020.

To further evaluate the fiber morphology, an image analysis was carried out using ImageJ software (version 1.54j). The results for the four types of electrospun scaffolds are reported in Table 11. The measured fiber diameters are consistent with previous findings [425], [426].

However, a statistical analysis using one-way ANOVA revealed significant differences between the samples ($p < 0.05$). Tukey's HSD test confirmed that the greatest difference in fiber diameter was observed between 45_MS_9010 and 45_MS_8020. Considering the process parameters listed in Table 10, this difference may be attributed to the variation in applied voltage. The voltage between the needle and the collector has been shown to strongly influence the fiber diameter, with higher voltages generally resulting in thicker fibers compared to lower voltages [417], [427]. This effect is likely due to increased Coulombic forces that counteract the viscoelastic resistance of the polymer solution [427]. Nevertheless, the variables affecting fiber diameter are numerous and often difficult to control, including not only setup parameters but also environmental factors such as temperature and humidity [425].

Table 11: Results of the image analysis: mean fiber diameter, mean BG particle size, and the percentage of the area occupied by particles in the images.

Sample	Mean Fiber Diameter (µm)	Mean BG Particle Size (µm²)	Area Occupied by Particles (%)
45_9010	1.58 ± 0.32	2.57	1.16
45_8020	1.03 ± 0.23	2.44	1.85
45_MS_9010	0.53 ± 0.16	1.41	1.09
45_MS_8020	1.62 ± 0.46	1.73	1.99
PCL [1]	0.5–1	-	-

[1] Data for PCL, added as reference, was obtained from Baudequin et al. [78].

Further evaluation of the BG content in the electrospun mats was performed via TGA, which can provide insights into the thermal stability of the scaffolds, as well as the relative proportions of organic and inorganic components. The TGA plots, reported in Figure 27, show that the degradation of 45S5-loaded PCL began around 300–330 °C. A lower onset temperature of degradation is consistent with the literature findings for electrospun mats incorporating BG, as interactions between the BG particles and the polymer matrix can lead to partial chain scission and decreased thermal stability [428]. Interestingly, the degradation onset for 45S5_MS-based mats occurred at higher temperatures, suggesting a less pronounced interaction with PCL.

As expected, the samples prepared with a PCL-to-BG ratio of 90/10 exhibited a lower BG content, ranging from 3 wt.% to 5 wt.%, while the samples with an 80/20 ratio showed higher BG contents of 8 wt.% to 10 wt.%. Considering the thermal stability of BGs at the temperatures used in TGA (up to 600 °C), the discrepancy between the theoretical BG content and the actual values obtained via TGA may, in the first instance, be attributed to some critical issues in the electrospinning process. In particular, it is likely that solvent–powder interactions and suboptimal jet parameters hinder effective BG transport to the collector, while particle sedimentation— exacerbated by agglomeration— further reduces the incorporation efficiency. The combination of these effects could lead to a theoretical-to-nominal BG incorporation ratio lower than 50%, as observed in this study and re-ported

elsewhere in the literature. For example, recent works have already highlighted similar efficiency issues in the fabrication of BG-loaded electrospun mats [429], [430]. In this regard, the suboptimal nominal BG/PCL ratios, compared to the theoretical values of 10 wt.% and 20 wt.%, indicate room for improvement both in the preparation of the suspension for electrospinning and in the optimization of the process parameters. Despite the TGA results, we have chosen to retain the sample labels "9010" and "8020", referring to the weight ratios used in preparing the electrospinning suspensions. Obviously, these labels were selected for the sake of clarity and consistency but are not intended to imply direct correspondence to the final BG content in the electrospun scaffolds.

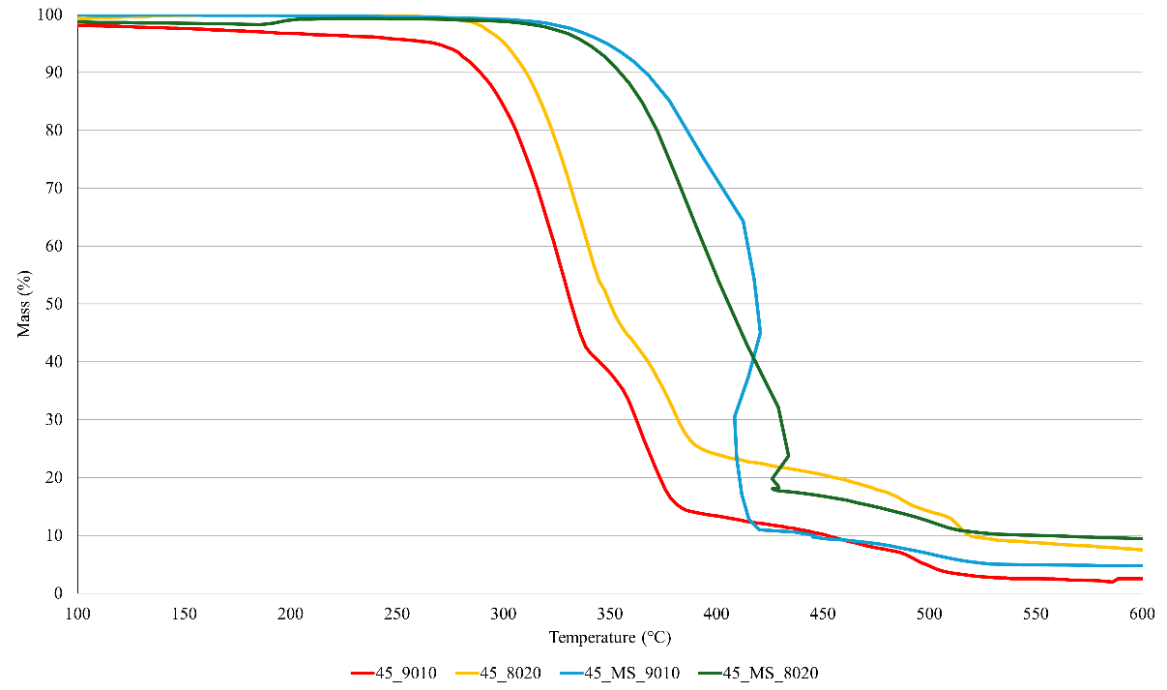

Figure 27: TGA plots showing thermal degradation of PCL and residual BG content in the electrospun mats.

5.2.2 Mechanical Characterization and Surface Wettability

In order to test the physical properties of the electrospun scaffolds, both tensile testing and water contact angle measurements were performed on the samples. Table 12 presents the results of the tensile testing. The results include σ_{MAX} and E in both the L and T directions, expressed in MPa. Five replicates were tested for each direction of each sample and then averaged. Additionally, the results include the mean value of all the measurements taken for each sample, regardless of orientation.

Table 12: Ultimate tensile strength and Young's Modulus of the samples measured via tensile testing. Two-way ANOVA showed significant statistical differences among samples and directions ($p < 0.05$) for both mechanical properties.

Sample	Orientation	σ_{MAX} (MPa)	Young's Modulus (MPa)
45_9010	L	2.21 ± 0.37	4.84 ± 0.62
	T	1.94 ± 0.33	4.43 ± 0.92
45_8020	L	4.32 ± 0.52	6.37 ± 1.64
	T	3.14 ± 0.57	5.58 ± 1.02
45_MS_9010	L	7.48 ± 0.48	14.68 ± 1.61
	T	4.79 ± 0.52	8.74 ± 0.68
45_MS_8020	L	2.16 ± 0.24	5.37 ± 0.43
	T	1.37 ± 0.14	4.49 ± 1.15
PCL [1]	L	-	14.89

[1] Data for PCL, added as reference, was obtained from Baudequin et al. [78].

All values of tensile strength in the L direction exceeded 2 MPa, and the Young's modulus values were all above 4.8 MPa. However, sample 45_MS_9010 showed the highest values, reaching 7.5 MPa and 14.68 MPa, respectively. A two-way ANOVA revealed that, both for the tensile strength and Young's Modulus, there was low variability within each direction of each sample. However, a statistically significant difference was found between the L and T directions, suggesting anisotropy in the samples. In addition, 45_MS_9010 exhibited significantly higher tensile strength and Young's modulus in both directions compared to the other samples. The higher mechanical properties of sample 45_MS_9010 could be linked to the lower fiber diameter, which has been reported to heavily influence both the tensile strength and Young's modulus [431]. Nonetheless, these results appear consistent with the previous literature on the topic [432]. However, the mechanical properties could be further improved, reaching higher tensile strength and Young's modulus values, as reported for pure PCL electrospun scaffolds by Baudequin et al. [78], even though the presence of embedded glass–ceramic particles may worsen the mechanical properties compared to pure electrospun scaffolds [431]. Further evidence of this behavior can be found when cross-referencing the mechanical properties of the other samples with their respective fiber diameter value. This makes it unlikely that the mechanical properties of the electrospun PCL/BG samples were influenced by the composition of the BG in this work.

Measuring the tensile strength in both the longitudinal and transversal directions revealed the anisotropic nature of the samples. The results show that both the ultimate tensile strength and Young's modulus are higher in the L-direction compared to the T-direction, indicating an uneven distribution of mechanical properties, likely due to a predominant fiber orientation within the scaffolds. The factors contributing to these phenomena include the type of collector (rotational or stationary), solution composition, voltage, working distance, and

flow rate [60], [433], all of which can induce anisotropy in mechanical properties. As mentioned in the Materials and Methods section, a rotational collector operating at 300 rpm was employed (which is a relatively low speed compared to other studies aiming to obtain aligned fibers [434], [435]). This approach aimed to achieve homogeneous fiber distribution while minimizing fiber alignment.

To evaluate the surface wettability of the PLC/BG scaffolds, water contact angle measurements were conducted on the samples using double-distilled water. Table 13 summarizes the results along with standard deviations (expressed in degrees °). Each value represents the average of ten measurements taken per sample surface.

Table 13: Contact angle values of the five electrospun mats with standard deviation. One-way ANOVA showed no significant differences among the samples (F = 0.565, p = 0.6416).

Sample	Angle Mean Value (°)
45_9010	119.68 ± 2.52
45_8020	119.82 ± 1.63
45_MS_9010	120.04 ± 2.80
45_MS_8020	120.94 ± 2.40
PCL [1]	122.8 ± 5

[1] Data for PCL, added as reference, was obtained from Baudequin et al. [78].

The results show that all samples exhibited contact angles above 119°, indicating a hydrophobic surface. Slight differences in contact angle values were observed across the samples, with sample 45_MS_8020 displaying the highest average contact angle. However, a statistical analysis indicated no significant differences in contact angle among the samples ($F = 0.565$ and $p = 0.642$), suggesting that the wettability of the samples is comparable and that variation in BG composition did not affect surface wettability. This could be related to previous results presented in the micrographs in Figure 26, which revealed that the BG particles are predominantly embedded within the fiber structure. These values fall within the range reported in other studies on similar electrospun scaffolds, which often describe hydrophobicity as a typical feature of electrospun PCL scaffolds [436], [437]. To reduce hydrophobicity, surface modification techniques such as plasma treatment or chemical functionalization could be applied to enhance scaffold hydrophilicity, promoting better cell attachment and facilitating tissue integration [438].

5.2.3 Tests in Simulated Body Fluid

To evaluate the bioactivity of the electrospun PLC/BG scaffolds, SBF testing was conducted according to Kokubo's protocol. pH changes were monitored in the SBF solution over a 14-day period, with measurements recorded every 48 h. The results are presented in Figure 28. After each measurement, the solution was refreshed to ensure consistent testing conditions and to better mimic the dynamic environment of physiological fluids.

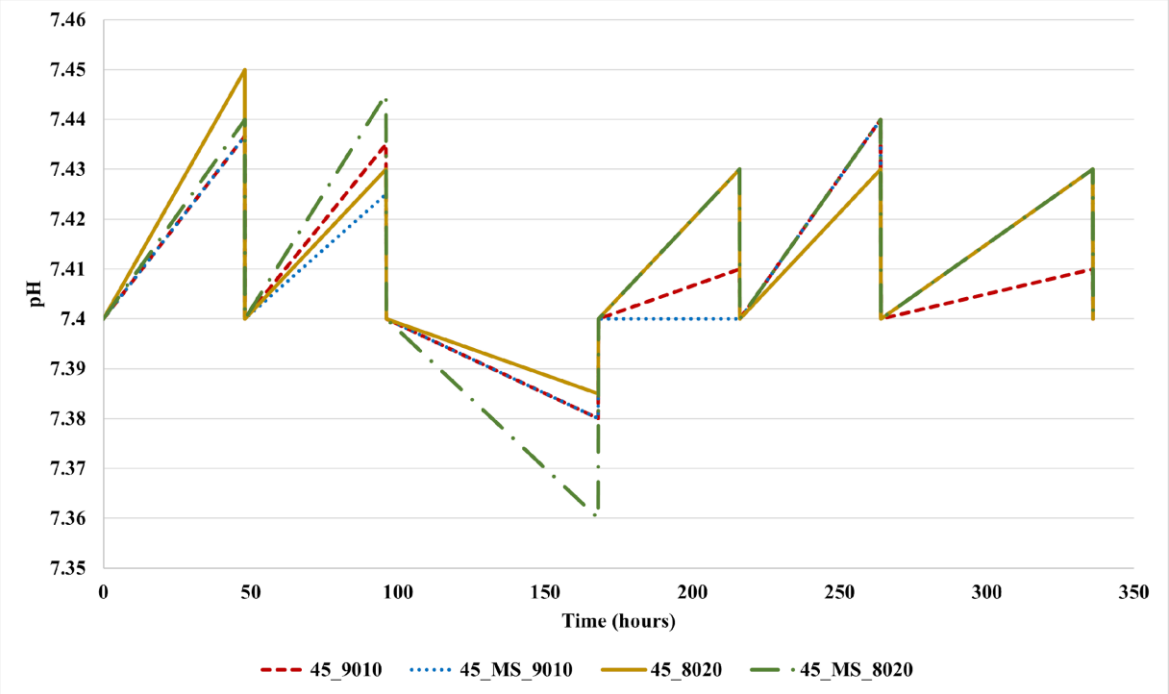

Figure 28: pH variation plot of the 4 electrospun scaffolds, submerged in SBF for 7 days. pH values were recorded every 48 h.

The electrospun samples induced minimal fluctuations in the pH of the solutions, which did not exceed 7.45. This may indicate limited ion exchange and PCL degradation in the solution. The latter hypothesis could be supported by the sudden acidification of the solution measured after the 7th day of immersion. Previous studies have also reported this drop in the pH of the SBF, which could be associated with PCL degradation [439].

In chapter "4 Novel Mg- and Sr-doped BG compositions" has already established that both 45S5 and 45S5_MS are bioactive, as they precipitated HA after 7 days of immersion in SBF [21], [22]. Additionally, 45S5_MS has demonstrated good biological behavior, exhibiting optimal cell viability and adhesion when tested with human dermal fibroblasts. For these reasons, our investigation focused on EDS analysis of the SBF-treated samples to determine whether calcium- and phosphorus-rich compounds were deposited on the surfaces of the BG particles embedded within the electrospun scaffolds. Figure 29 presents the results of the EDS analysis conducted on sample 45_MS_8020, taken as an example, along with SEM imaging of the sample surface. The analysis revealed a significant concentration of calcium and phosphorus on a white globule, along with the absence of silicon. This could be a potential indicator of HA deposition on the surface of the BG granule in the scaffold structure [373].

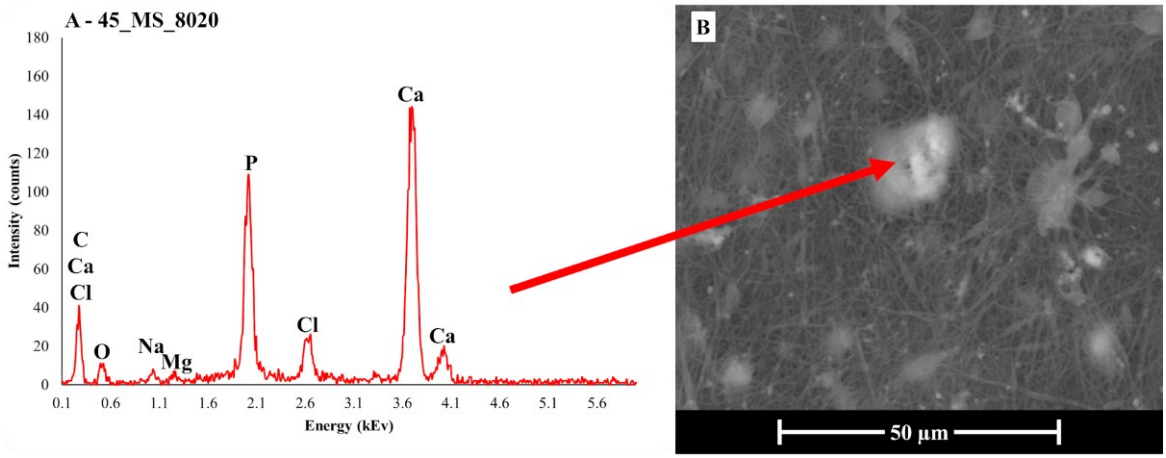

Figure 29: (A) EDS analysis of the surface of the 45_MS_8020 electrospun PCL/BG sample and (B) SEM image of the analyzed area. The red arrow points to the spot where the analysis was conducted.

Furthermore, the presence of Na and Cl, as detected by the EDS, could be attributed to salt precipitation from the solution [62,63]. Lastly, the SEM image in Figure 5B shows a damaged fiber structure, as the PCL began to degrade upon contact with SBF, as suggested by the acidification phenomenon previously mentioned.

5.2.4 Biological Assessment

A - In vitro Evaluation of Cytotoxicity

In tissue engineering, 45S5 and PCL are biomaterials that are widely employed. However, the addition of Mg and Sr to the BG composition could lead to an undesirable response in biocompatibility, inducing a decrease in cell viability. To evaluate the cytotoxicity of the mats, an indirect test was conducted according to ISO 10993-5 guidelines. Figure 30 shows the proliferation of the L929 cells that were cultured for 24 h in the extract of electrospun mats and latex and then normalized against the CTRL (+). It is possible to notice that the mats did not demonstrate a significant adverse effect on the cells after culture. For CTRL (−), the proliferation decreased to 70%, which could be related to the cytotoxicity of the latex.

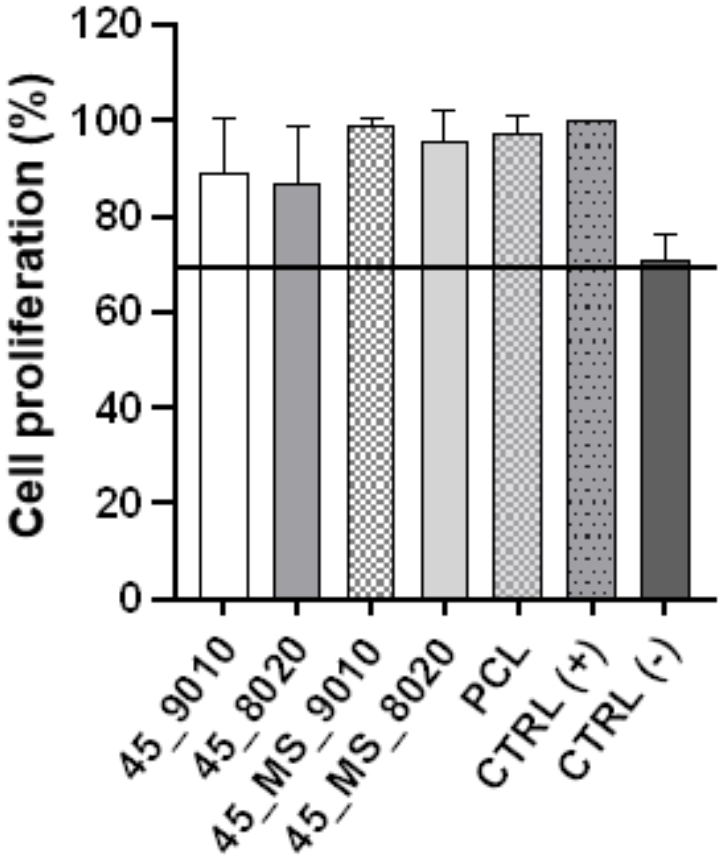

Figure 30: Indirect cytotoxicity test: Proliferation of L929 fibroblasts cultured in electrospun mats extracts, latex extracts, or complete DMEM medium for 24 h. CTRL (+) is the complete DMEM medium, and CTRL (−) is the latex-extract medium. The black line corresponds to 70% proliferation. Statistical analysis was performed using one-way ANOVA with Tukey post-test, with $p < 0.05$ ($n = 3$).

B - In vitro Evaluation of Osteogenic Induction Performance

To evaluate whether 45S5 and 45S5_MS play a role in osteogenesis, ALP, an earlier phenotype marker of osteoblast differentiation, and OCN, the most abundant non-collagenous bone protein produced exclusively by osteoblasts, were investigated. In this study, PCL electrospun scaffolds (fiber diameter around 480 nm) served as a control to compare the results obtained with the scaffolds containing BG and additives.

Briefly, bone formation by osteoblasts is divided into two steps: organic matrix formation/deposition and mineralization. Collagen proteins, including type I collagen, are secreted during organic matrix formation, followed by the production of several distinctive non-collagenous proteins, such as ALP, OCN, and osteopontin (OPN). Finally, the calcification process of the extracellular matrix is induced [440]. During matrix mineralization, the secretion of osteocalcin by osteoblasts is associated with the late phase of cell differentiation [441].

After 28 days of culture, the ALP staining (Figure 31) for samples in the osteogenic medium was more intense than in the proliferation medium, as expected, since the presence of osteogenic factors stimulates cell differentiation.

Stiffness and high surface area are crucial factors to consider when developing an ideal scaffold. Scaffolds designed with biophysical properties that mimic either cancellous or cortical bone provide a proper environment for cells to attach, proliferate, and migrate. Moreover, the interaction between mechanical properties and cell signaling can drive cells to differentiate into a tissue with mechanical properties comparable to the scaffold by influencing cell focal adhesion and the cytoskeleton [442], [443]. Furthermore, studies have demonstrated that the osteogenic potential of several stem cells, such as adipose stem cells, is significantly increased by a microfibrous environment [444].

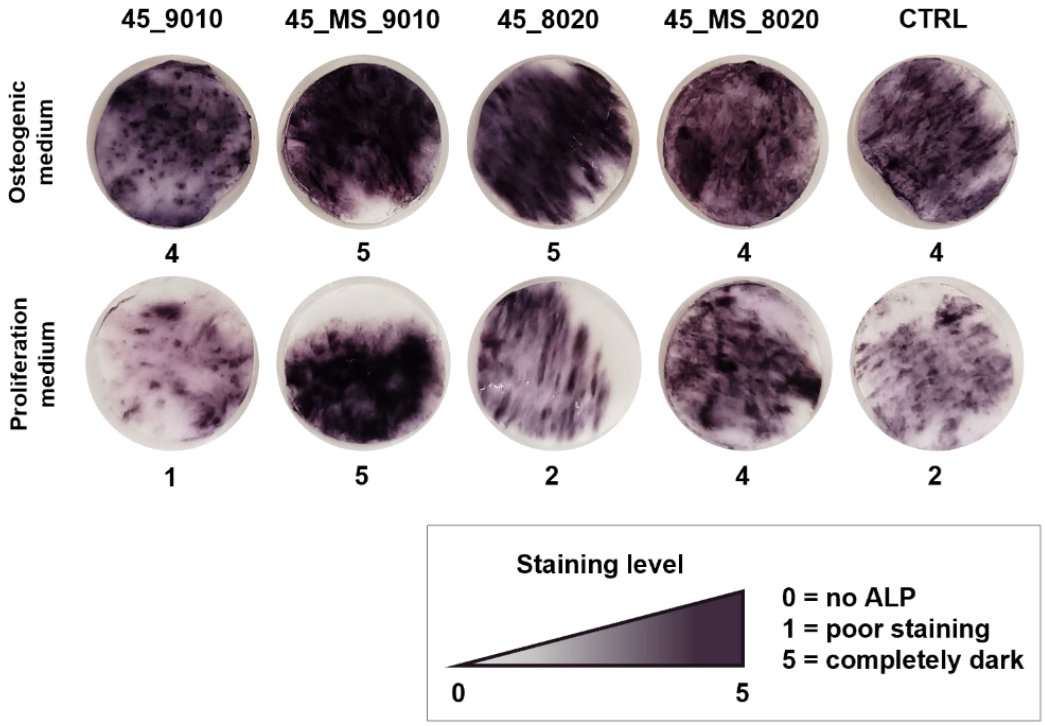

Figure 31: ALP staining of ASC52telo cultured on electrospun scaffolds in proliferation and osteogenic medium after a period of 28 days. A semi-quantitative score was attributed to each sample, from 0 = no ALP presence to 5 = completely dark.

By analyzing the results obtained by the scaffolds in a proliferation medium without osteogenic supplements, it can be inferred that the scaffolds with the highest level of ALP staining were those loaded with 45S5_MS, as well as the reference scaffold made of pure PCL. Specifically, PCL and 45_MS_9010 showed the highest E and the lowest fiber diameter, which are favorable properties for cell differentiation. Interestingly, in the case of sample 45_MS_8020, which had a lower Young's Modulus value (5.37 MPa) and a larger fiber diameter (1.62 μm), it also showed a high level of ALP staining. A previous study demonstrated that pure PCL and composite PCL electrospun scaffolds could induce bone differentiation without an osteogenic medium, and this differentiation could be more related to the morphology (alignment, multiple layers) and composition of the material than to the relationship between fiber diameter and stiffness [78]. It could be hypothesized that, in this study, the increase in ALP staining may be linked more closely to the presence of the doping ions in the BG (i.e., magnesium and strontium) than to the size and/or mechanical properties of the fibers.

The fluorescence images in Figure 32 and Figure 33 shows stained nuclei (blue) and osteocalcin (green) in the ASC52telo after 14 and 28 days of cell culture. On day 14, it was possible to observe the presence of OCN expression in all samples in both the proliferation and differentiation media, with enhanced OCN presence in the osteogenic medium. From day 14 to 28, an increase in OCN expression was observed for all samples, highlighting that the cells continued their growth process and suggesting differentiation towards osteo-blasts.

Despite the slightly hydrophobic characteristics of the electrospun samples, which could compromise cell adhesion, these results demonstrate that ASC52telo can adhere, spread, and proliferate on the scaffolds, indicating that the inclusion of 45S5 and 45S5_MS can provide a favorable microenvironment for cell growth.

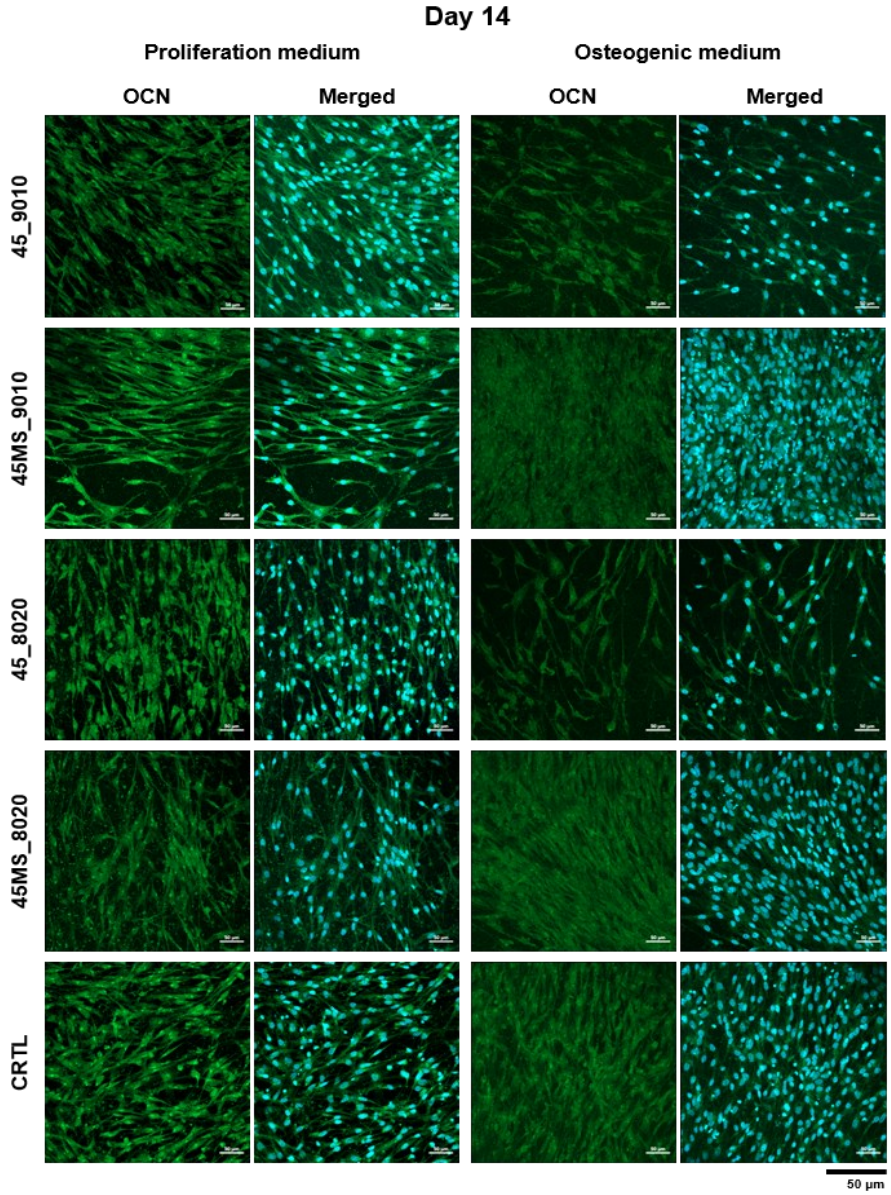

Figure 32: Immunofluorescence staining of osteocalcin (green) and cell nuclei (blue) in ASC52telo cultured on electrospun scaffolds in two media (proliferation and osteogenic) on day 14. Scale bars represent 50 µm (magnification 20×).

Furthermore, following the ALP staining results, on day 14, a higher cell density was observed in the mats containing Mg and Sr. Several studies have indicated the advantages

of bio-ceramics doped with magnesium and strontium, which can promote bone formation [408], [445], [446], [447]. The presence of Mg can stimulate the proliferation of osteoblasts [448], whereas Sr possesses therapeutic effects on osteoporosis by enhancing pre-osteoblastic differentiation [449]. *In vivo* studies have shown that BG doped with strontium and BG doped with magnesium increase new bone regeneration by stimulating osteoblast metabolic activity and proliferation [450], [451]. Another study revealed that the presence of Mg in tricalcium phosphate ceramic stabilized the cell–material interface and promoted higher cell attachment and growth [445], [448], [450].

These results demonstrate that the inclusion of enriched BG into PCL electrospun scaffolds might provide a favorable environment for cells and represent an alternative for tissue engineering.

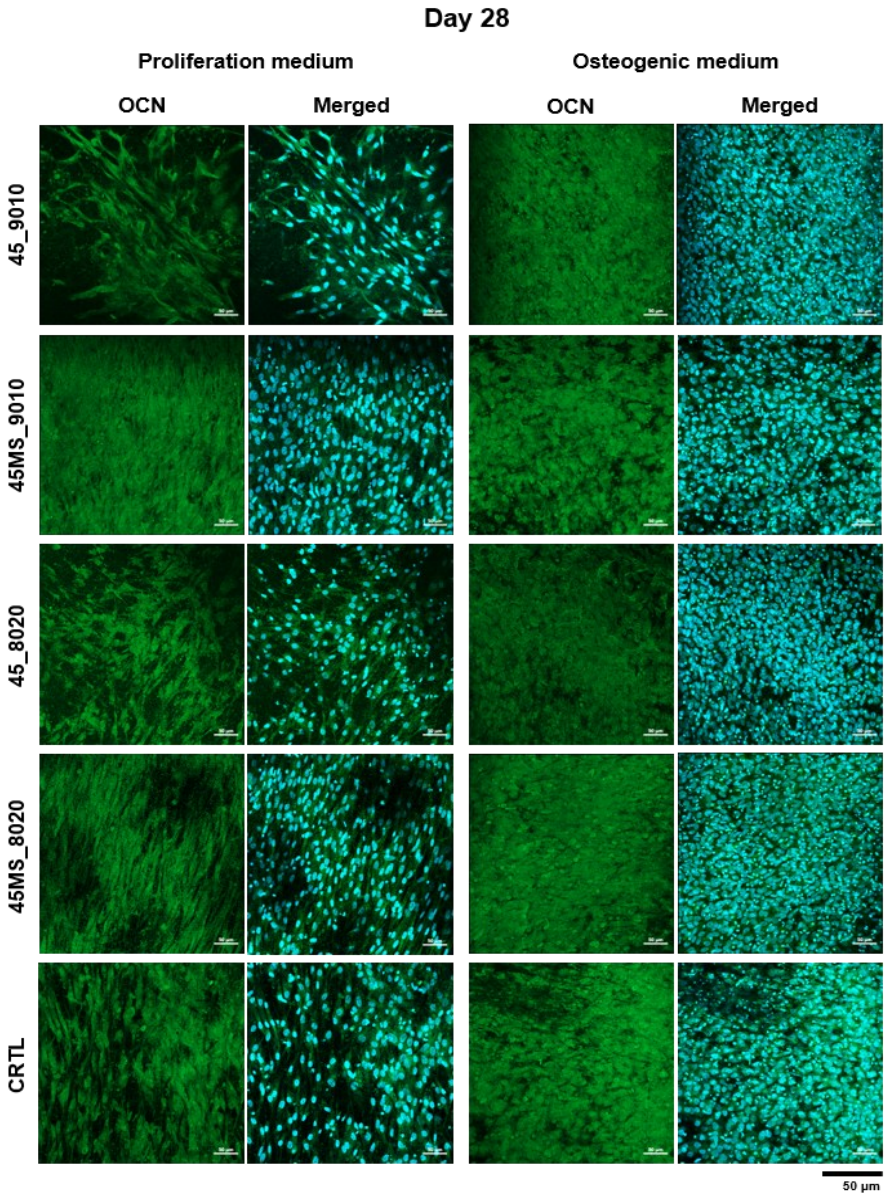

Figure 33: Immunofluorescence staining of osteocalcin (green) and cell nuclei (blue) in ASC52telo cultured on electrospun scaffolds in two media (proliferation and osteogenic) on day 28. Scale bars represent 50 µm (magnification 20×).

6 Optimization of PCL/BG scaffolds

(This section has been submitted to *Polymers* and is currently under revision. Received: 12 Feb 2026)

Further efforts were dedicated to the optimization of the PCL/BG composite scaffolds discussed in the previous chapter. While previous results showed the feasibility of producing electrospun scaffolds incorporating melt-derived BG powder, several limitations emerged. A low efficiency of BG electrospinning, such as agglomeration and an uneven particle size distribution led to reduced BG presence in the final products in the previously described scaffolds. Moreover, the highly hydrophobic behavior of the scaffolds was tackled, considering that low wettability of the mats is a major hinderance for electrospun PCL, as discussed in section "1.2 Electrospun polymer-based fibrous composite scaffolds" [418].

To address these issues, several precautions were implemented into the production process. Specifically, an upgraded electrospinning system, equipped with a scanning emitter, enabling improved fiber distribution, a negative voltage generator (useful for improving deposition quality and reducing waste), and wider needles, which could also ease the employment of higher flow rates [452]. Tuning the composition of the electrospinning solution is also a major concern when producing electrospun scaffolds. Higher PCL content in the polymeric solution is usually associated with thicker fiber formation during the production process [453]. This can also result in worse mechanical performance as fiber thickness has been shown to be inversely correlated with ultimate strength of the electrospun mats [454].

Besides compositional optimization, surface properties are a critical limitation of electrospun PCL-based scaffolds. As discussed in section "1.2 Electrospun polymer-based fibrous composite scaffolds" a low wettability of the mats is a limitation for electrospun PCL scaffolds, as it can lead to lower protein adsorption and cell adhesion [86], [87]. While the incorporation of BG particles did not result in improved wettability of the scaffolds, different strategies have been explored to address this issue, such as plasma treatment or functionalization by immersion in a sodium hydroxide (NaOH) solution [455]. Among these approaches, chemical treatment in NaOH is an accessible and practical solution for several reasons, including the high availability of reagents, low cost, and ease of implementation, especially when compared to plasma treatment. Increasing the hydrophilicity of these devices could significantly enhance their biological performance, providing a valuable tool for various applications in tissue engineering, including skin tissue healing, infection control, and BG delivery for bone regeneration. Meanwhile, employing cost-effective production strategies could more easily bring this technology into industrial production.

6.1 Testing procedures

6.1.1 Production of PCL/BG electrospun scaffolds and chemical treatment

The BG S53P4_MS was manufactured using the traditional melt-quench technique, already described in chapter "4 Novel Mg- and Sr-doped BG compositions". The frit obtained after melting and cooling the BG, was ground into a powder via dry milling for 20 min, using an

alumina jar and a laboratory mill MGS1800/2 (MGS S.r.L., Fiorano Modenese, Italy), then sieved to a powder with granulometry <63 μm. The BG powder underwent a second, wet milling in ethanol (EtOH) for 1 hour, using a BG:EtOH:balls weight ratio of 1:20:20. The BG/EtOH suspension was allowed to decant, the supernatant was removed, and the remaining wet slurry was dried in a ventilated oven at 50 °C for 48 hours.

Electrospun scaffolds were manufactured using an electrospinning machine Spinbox® (Bionicia, Valencia, Spain), equipped with a rotating collector, syringe pump, negative voltage generator, and scanning emitter. The mats were prepared starting from a BG suspension in a PCL solution. The appropriate amount of S53P4_MS was weighed and placed into a glass vial. 3.5 mL of DMF were added into the vial, which was then sonicated for 10 minutes. The appropriate amount of PCL (MW~80.000 – acquired from VWR International S.r.L., Milano, Italy) was weighed and added to the vial together with 6.5 mL of DCM. These solvents were chosen accordingly to experimental procedures previously determined and described in chapter "5 Feasibility of electrospun PCL/BG composite scaffolds". The solvent ratio was chosen based on previous experimentation with different solutions. The suspension was then stirred overnight. The detailed compositions of the suspensions for each are reported in Table 14. Three formulations were prepared in order to investigate the effect of BG loading on the electrospun scaffolds. The sample SP_H represents an intermediate composition, with a nominal BG content of 23.08 wt.% relative to the total solid phase. The formulation SP_L was prepared with a lower BG content (13.04 wt.%), while SP_X contained higher amounts of both PCL and BG compared to SP_H, maintaining the same nominal BG fraction (23.08 wt.%). The selected BG contents are consistent with values commonly reported in the literature for electrospun polymer/BG composites, as excessively high ceramic loading may alter electrospinnabilty and compromise fiber formation [456], [457], [458]. Moreover, these BG concentrations sit in the 5-40 wt.% range, ideal for osteoblast growth and Ca–P formation in composites [106]. Prior to electrospinning, the suspensions were sonicated for an additional 5 minutes, then poured into a syringe and electrospun through a 17 G needle (internal diameter Φ_i=0.1067 mm). The electrospinning parameters for each sample are reported in Table 15. In brief, the total voltages employed were between 17 and 18.5 kV, while flow rate and needle-collector distance were constant at 2.4 mL/h and 15 cm, respectively.

Table 14: Compositions of the suspensions used to manufacture electrospun samples.

	SP_H	**SP_L**	**SP_X**
DCM	6.5 mL	6.5 mL	6.5 mL
DMF	3.5 mL	3.5 mL	3.5 mL
PCL	0.90 g	0.90 g	1.00 g
S53P4_MS	0.27 g	0.135 g	0.3 g
Nominal PCL/BG weight ratio	23.08%	13,04%	23,08%

Table 15: Electrospinning parameters employed in the production of samples.

	SP_H	SP_L	SP_X
Applied voltage	12 kV	11.5 kV	13.5 kV
Negative voltage	-5 kV	-5 kV	-5 kV
Flow rate	2.4 mL/h	2.4 mL/h	2.4 mL/h
Needle-collector distance	15 cm	15 cm	15 cm
Scanning emitter speed	25 mm/s	25 mm/s	25 mm/s
Rotating collector speed	250 rpm	250 rpm	250 rpm
Total electrospun volume	5 mL	5 mL	5 mL

In order to increase the wettability of the electrospun scaffold, aiming to improve its biological properties and better exploit the properties of BG, the samples were chemically treated in a NaOH 1M solution, following procedures reported in the literature [455] using Milli-Q bi-distilled water and NaOH pellets (Incofar S.r.L., Modena, Italy). Samples were secured onto a petri dish and submerged in the NaOH solution at room temperature for 4 hours. The samples were then extracted, washed with bi-distilled water, and dried at room temperature for 24 hours. The treated samples were named accordingly SP_HT, SP_LT, and SP_XT and characterized as follows.

6.1.2 Characterization

Various properties of S53P4_MS, including its biological properties, have already been investigated in chapter "4 Novel Mg- and Sr-doped BG compositions". To increase the stability of the suspension during the electrospinning process, and improve the quality of the fibers, BG particles should have a fine particle size [85]. The granulometry of the powders, both sieved after the first milling step and after re-milled, was verified using a laser-diffraction particle size distribution analyzer (Malvern Panalytical, Malvern, UK). Moreover, the powders were observed under FE-SEM (Fei Quanta 200, ThermoFisher Scientific, Waltham, MA, USA) equipped with both a secondary electron detector and a backscattered electron detector working simultaneously. The micrographies were acquired at 1600× magnification. The characteristic diameters $D_{0.1}$, $D_{0.5}$, and $D_{0.9}$, corresponding to the particle diameters below which 10%, 50%, and 90% of the particle population are found, respectively, are reported along with the particle size reduction (PSR), calculated as:

$$PSR = \frac{(D_s - D_d)}{D_s} \times 100\%\,, \tag{4}$$

where D_s is the mean diameter after single milling, and D_d is the mean diameter after the second milling.

TGA was conducted on the electrospun samples to quantify the effective electrospinning yield of BG. The analysis was carried out by heating the samples to a temperature sufficient to ensure complete thermal degradation of the polymeric phase (PCL), while remaining below the temperature range at which thermal reactions of BG occur. Small samples were cut from the electrospun mat, weighed, and placed in a simultaneous thermal analyzer STA 429 CD (Netzsch GmbH, Selb, Germany). A heating rate of 20 °C/min was applied up to temperature of 600 °C, in air atmosphere; this temperature was selected considering the high thermal stability of S53P4_MS up to 700 °C.

The electrospun mats were characterized using a FE-SEM (Fei Quanta 200, ThermoFisher Scientific, Waltham, MA, USA), equipped with a secondary electron detector. Images of the sample surfaces were acquired at magnifications of 3000× and 5000×. Small patches were cut from the mats and sputter-coated with a 10 nm gold layer. Moreover, EDS (Quantax200, Bruker Corp., Billerica, MA, USA) was used to verify the presence and spatial distribution of S53P4_MS within the electrospun fibers via elemental mapping detecting silicon. SEM micrographies were subsequently used to determine the mean diameter of the fibers using the open-source image analysis software ImageJ (version 1.54d, NIH, Bethesda, MD, USA). The 5000× magnification micrographies were employed to measure the fiber diameter. At least 50 measurements were taken on each sample. Mean fiber diameter and standard deviation were thus calculated. A one-way ANOVA with Tukey's post-test was performed on the fiber diameter data. Statistical significance was set at $p < 0.05$.

Water contact angles of the electrospun samples were measured using an automatic optical contact angle system (OCA 15EC, Dataphysics Instruments GmbH, Stuttgart, Germany) equipped with a 6.5× zoom lens. The measurements were conducted on samples both as-spun and after treatment in NaOH in order to compare the wettability of treated and untreated samples. Small 5 × 2 cm strips were cut from the samples and secured to a flat dish. 2 µL drops were dispensed on the surfaces and, after waiting 5 seconds, both right and left angles were measured digitally (SCA 20, DataPhysics, Germany). At least 10 measurements were acquired for each sample. The collected data was then used to calculate the mean contact angle for the samples' surfaces. A two-way ANOVA analysis for unbalanced data (α=0.05, variable A: sample type, variable B: treatment condition) was conducted to evaluate the variance of the results, particularly with respect to chemical treatment. For sake of clarity, resulting data includes the contact angle reduction factor (RCA) calculated as:

$$R_{CA} = \frac{\theta_{ut} - \theta_t}{\theta_{ut}} \times 100\% , \quad (5)$$

where θ_{ut} is the mean contact angle of the as-spun samples and θ_t is the contact angle of the treated samples, employed to quantify the variability in contact angle measurement.

Before the tensile testing, the samples' thicknesses were measured. Optical imaging was used to determine the mean thickness of the electrospun mat, thanks to the improved thickness uniformity achieved via the scanning-emitter-assisted electrospinning process. Small patches of electrospun samples were cut from the mat, from zones adjacent to those used for tensile tests. These small patches were secured between two semi-rigid supports and embedded in cold-curing resin. After 24 hours of curing, the resin was sectioned and

polished; the cross-sections were examined under an optical microscope (Olympus Corp., Tokyo, Japan) at 500× magnification. The mean thickness of the samples was subsequently measured using ImageJ (version 1.54d).

The ultimate tensile strength (σ_{MAX}) and elongation at failure (ε_b) were measured using a universal testing machine (Z050, Zwick-Roell GmbH & Co. KG, Ulm, Germany) equipped with a 10 kN load cell (XForce HP, Zwick-Roell). Samples were cut into small strips and secured onto two polymeric grips. A preload of 0.2 N was applied to the samples, and the test was conducted at a speed of 5 mm/s, ultimately causing failure of the samples. At least 5 repetitions were conducted for each sample. The data collected were then used to calculate the mean value for the samples' σ_{MAX} and ε_b. One-Way analysis of variance was conducted on the samples to determine statistically significant differences among the scaffold formulation and treatments. Additionally representative stress–strain curves are shown to qualitatively illustrate the mechanical response of untreated and treated scaffolds.

6.1.3 Biological test: cell spreading

Prior to cell seeding, the PCL/BG scaffolds were sterilized by incubation in 70% ethanol for 30 minutes followed by three washes with DPBS, (Thermo-Fisher Scientific, MA, USA). HDF (Cat. #C-013-5C, ThermoFisher Scientific), at the concentration 1.0×10^4 cells were suspended in 1 mL of Dulbecco's Modified Eagle Medium (DMEM) supplemented with 10 % fetal bovine serum, 1% penicillin-streptomycin and 1% non-essential amino acids (acquired from Thermo Fisher Scientific). 1 mL of this suspension was placed onto each scaffold cut in order to have the same surface area (1 cm^2) for the same number of cells. Scaffolds were placed on non-treated cell-culture plates for 1 hour to let cells adhere to the scaffold. Then, each scaffold was transferred into 24-well cell culture plates (Corning, NY, USA) and incubated at 37 °C with 5% CO_2 in complete DMEM. After the transfer there were no cells left on the untreated culture plates. After 24 hours, all samples were fixed with 4% paraformaldehyde for 15 minutes.

Fluorescent markers were used to boost the visualization of cells and their morphology on the scaffolds. Briefly, cells were permeabilized with 0.5% Tween-20 in DPBS for 10 minutes and then incubated for 5 minutes with 300 nM DAPI (D1306, ThermoFisher Scientific) and for 45 minutes with iFluor-488-conjugated phalloidin (1:1000 dilution, ab176753, Abcam, UK), for staining the nuclei and the actin cytoskeleton, respectively. Samples were then washed with DPBS and observed with a 20× Olympus objective mounted on EVOS M5000 (Thermo-Fisher Scientific).

To quantify the number of fibroblasts attached and grown on the scaffolds, nuclei were counted using the ImageJ software (v.1.53t) on 10 images from each sample taken randomly on the whole surface of the scaffolds. Experiments were done in duplicate. One-way ANOVA was used for multiple comparisons and a Tukey post-hoc test was applied. Statistical analyses were performed using GraphPad Prism 8.0 software (San Diego, CA). Values are reported as mean and standard deviation. Differences were considered significant for $p<0.05$.

6.2 Results and discussion

6.2.1 Morphological and compositional characterization of electrospun PCL/BG scaffolds

S53P4_MS underwent a double milling process to ensure fine particle size of the powders. This approach was followed to minimize BG sedimentation during electrospinning, which can lead to reduced BG incorporation in the final product compared to the nominal weight ratio. Furthermore, reducing the maximum particle diameter also decreases the risk of clogging the tubing and needle.

Figure 34 (A-B) presents the SEM micrographs of the S53P4_MS powder after the initial milling and sieving process, and after the subsequent wet milling process. The cumulative and differential particle size distributions obtained from the granulometric analysis are presented in Figure 34 (C-D). Meanwhile, Table 16 reports the characteristic diameters D0.1, D0.5, and D0.9, and particle size reduction. Results show a sharp reduction in particle size following the wet milling step. The particle size reduction was approximately 70% across the characteristic diameters, confirming the effectiveness of wet milling in refining the BG powder. This creates conditions for more stable electrospinning, reducing the risk of sedimentation and clogging.

Table 16: Results of the granulometric analysis on S53P4_MS powders after a single and double milling process, expressed as $D_{0.1}$, $D_{0.5}$, and $D_{0.9}$ (in μm), and PSR values.

	$D_{0.1}$	$D_{0.5}$	$D_{0.9}$
Single milling	3.34	12.86	33.40
Double milling	1.00	3.57	11.22
PSR	70%	72%	66%

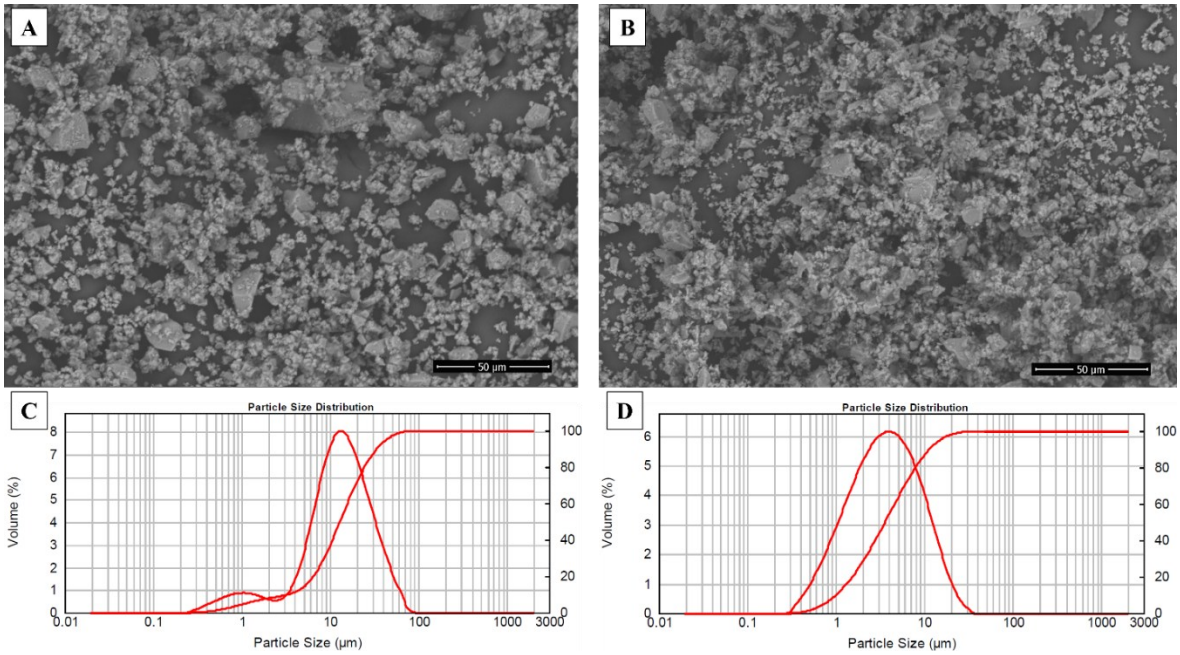

Figure 34: SEM micrographies of the S53P4_MS powders after the initial milling (A) and after the second milling (B), and their corresponding cumulative and differential distribution for the single- (C) and double-milled (D) powder.

The surface and fiber morphology of the electrospun PCL/BG scaffolds before and after chemical treatment were investigated by SEM imaging, and the results are reported in Figure 2. The micrographs show successful electrospinning of the suspensions, with BG particles predominantly embedded within the fibers. SEM analysis also revealed the presence of beads, a morphological defect of the mats consisting of localized fiber thickening [459], likely linked to flow fluctuations caused by the suspended BG powders [459]. Moreover, chemical treatment did not cause any visible morphological alterations to the fibers. SEM micrographs were further employed to measure the mean fiber diameter, and the results are reported in Table 17. Notably, the BG particles are in the micrometer size range, while the electrospun fibers exhibit diameters in the nanometric range. This dimensional mismatch suggests that BG particles are not fully encapsulated within the polymeric matrix; instead, they are likely to induce localized bulges along the fibers (unavoidable in these conditions) and may remain partially exposed at the fiber surface. However, this could prove useful as direct contact between BG particles and physiological fluids is required to promote ion release and fully exploit the dissolution-related properties of bioactive glasses.

One-way ANOVA revealed a statistically significant difference among the samples ($p=0.019$). Tukey's post-test identified a significant difference between samples SP_H and SP_X, while no significant difference was detected between SP_L and SP_H, or SP_L and SP_X. Notably, SP_L, characterized by a lower nominal BG content compared to the other samples, did not exhibit a markedly different mean fiber diameter, suggesting that variations in BG loading within the investigated range do not strongly affect fiber diameter [85]. Furthermore, EDS maps (Figure 36) were acquired on untreated samples to detect silicon atoms, indicative of the presence of BG. The results further confirmed the presence and homogeneous spatial distribution of BG within the electrospun fibrous mats.

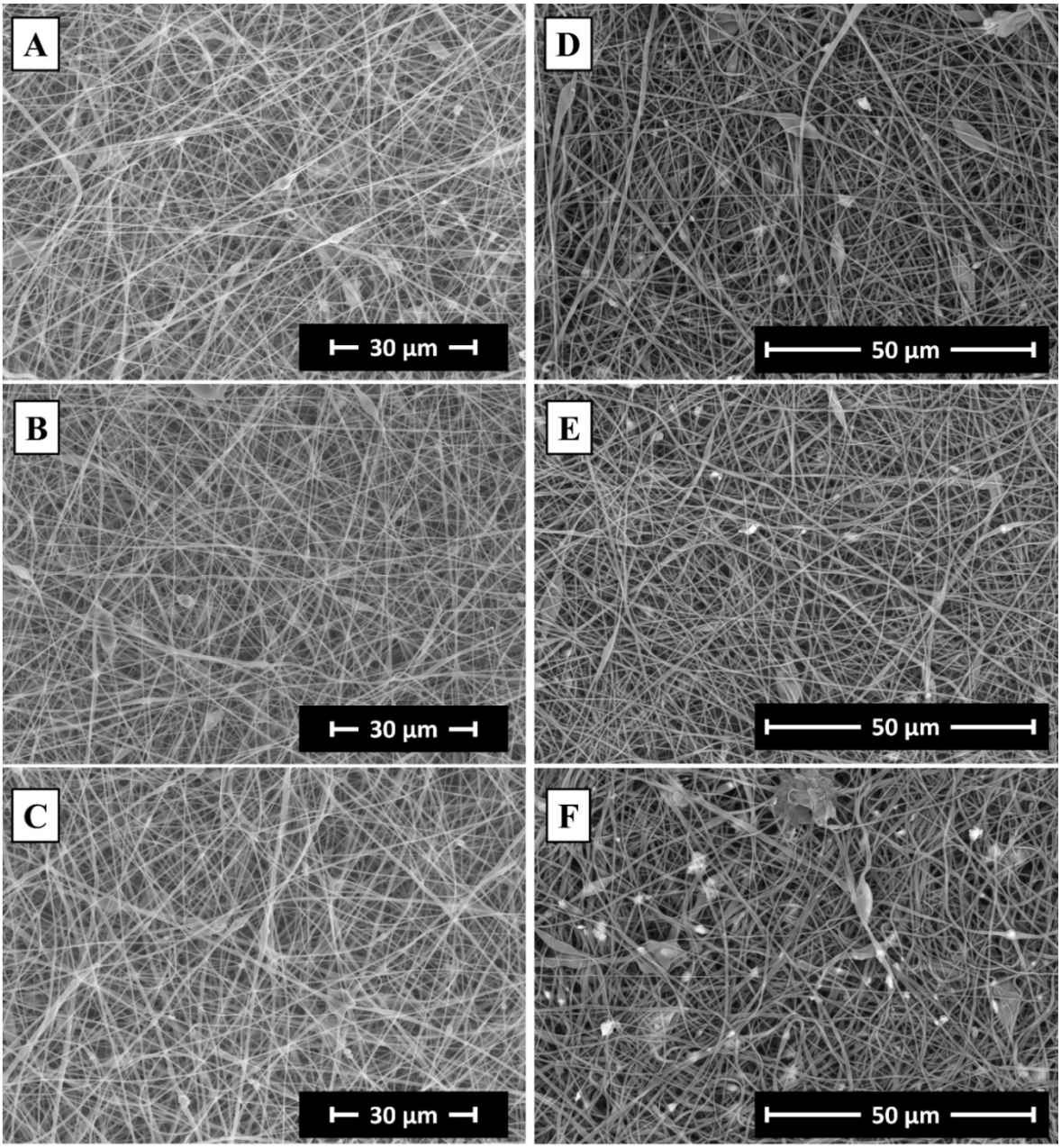

Figure 35: SEM micrographs of the as-spun SP_H (A), SP_L (B) and SP_X (C) samples; and chemically treated SP_H (D), SP_L (E) and SP_X (F) samples.

Table 17: Mean fiber diameter and standard deviation of the electrospun samples. One-way ANOVA and Tukey's post-test showed statistically significant differences between samples SP_H and SP_X ($p<0.05$).

	SP_H	SP_L	SP_X
Mean fiber diameter	0.376 ± 0.102 µm	0.390 ± 0.119 µm	0.423 ± 0.144 µm

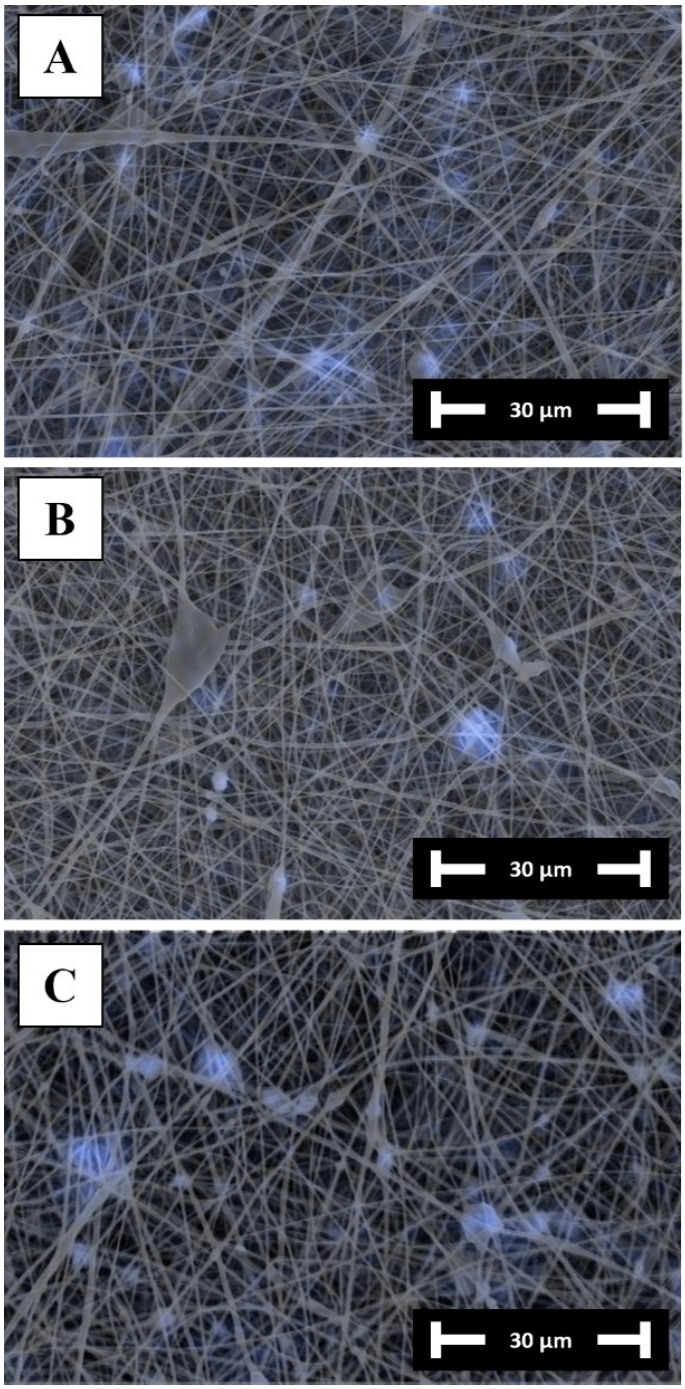

Figure 36: EDS maps of the untreated electrospun samples SP_H (A), SP_L (B), and SP_X (C). Blue highlighted areas indicate the presence of BG particles.

Thermal gravimetric analysis was employed to quantify the effective BG content in the electrospun mats, compared to the nominal values. Results are reported in Figure 37 and summarized in Table 18. TGA revealed that the actual BG content was lower than the nominal value. This was expected, as incorporating insoluble powders as a load during electrospinning is commonly associated with reduced loading efficiency in the final product [430], [460]. Across all electrospun samples, the retained BG content ranged between 65% and 71% of the nominal value. These values are consistent with previously reported results in the literature [460] and represent an improvement over previous efforts reported in chapter

"5 Feasibility of electrospun PCL/BG composite scaffolds". The enhanced efficiency observed in this work can reasonably be attributed to the modified procedures, including tuning of the electrospinning setup and parameters, as well as the optimized particle size achieved through wet milling. Future efforts could focus on further increasing BG electrospinning efficiency by refining particle dispersion and minimizing sedimentation during manufacturing.

Table 18: Nominal and measured BG/PCL weight ratios of the untreated electrospun scaffolds and relative electrospinning efficiency.

	Real BG mass %	Nominal BG mass %	Yield
SP_H	15.15	23,08	65.64%
SP_L	9.04	13,04	69.32%
SP_X	16.53	23,08	71.62%

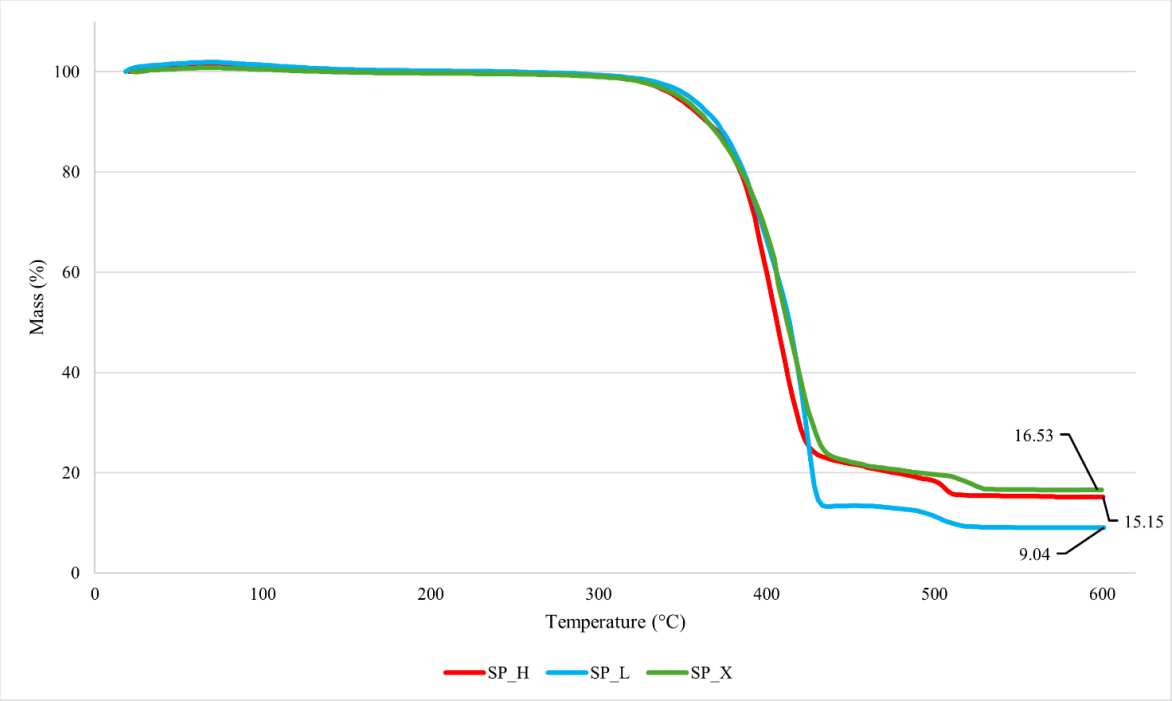

Figure 37: TGA curves of the electrospun PCL/BG scaffolds, showing polymer degradation and residual BG content.

6.2.2 Wettability and mechanical behavior of electrospun scaffolds

The effect of chemical treatment in 1M NaOH solution for 4 hours on the surface wettability of the PCL/BG scaffolds was evaluated by measuring and comparing the water contact angle of treated and untreated samples. Table 19 summarizes these results, indicating the mean contact angle and standard deviation of the treated and untreated samples, as well as the RCA. The as-spun electrospun mats showed mean contact angles ranging between 118° and 123°, confirming the hydrophobic nature of electrospun PCL. Meanwhile, the surface of the chemically treated mats exhibited a more hydrophilic behavior, with contact angles ranging from 85° to 94°. The substantial reduction in contact angle demonstrates that NaOH treatment effectively enhanced scaffold wettability.

Two-way ANOVA for unbalanced data revealed a highly significant main effect of the NaOH treatment on surface wettability ($p << 0.05$), independently of scaffold formulation ($p=0.629$), suggesting that the effect of NaOH treatment was consistent across all scaffold formulations. Notably, the treated samples showed higher dispersion of measurements compared to the as-spun samples. This could be attributed to the improved local absorption of water in specific regions of the fibrous structure, likely resulting from surface chemical modification. These results are in accordance with previous findings and further confirm the effectiveness of NaOH treatment on the surface wettability of hydrophobic electrospun PCL [455].

Table 19: Mean contact angle and standard deviation of the treated and untreated samples, and RCA expressed as percentage.

	mean contact angle (°)	**R_{CA}**
SP_H	118.88 ± 4.81	26.39 %
SP_HT	85.96 ± 9.92	
SP_L	122.74 ± 4.48	27.69 %
SP_LT	93.52 ± 5.11	
SP_X	121.45 ± 4.41	23.81 %
SP_XT	89.40 ± 11.21	

The mechanical properties of the electrospun PCL/BG scaffolds were evaluated via tensile testing. Figure 38 shows the results of the tests, expressed as mean values of ultimate tensile stress and elongation at break. In addition, Figure 39 presents exemplary engineering stress–strain curves of samples SP_H and its chemically treated counterpart, SP_HT, providing a qualitative comparison of their mechanical response.

Overall, the mechanical properties of these scaffolds were improved compared to previously reported results (refer to Table 12). This could be generally attributed to the finer fiber diameter achieved in the present work, which has been previously associated with improved mechanical performance in electrospun fibrous mats [431], [454]. Untreated scaffolds exhibited tensile strength values in the range of 3–6 MPa, while NaOH-treated samples showed higher tensile strength values between 6–9 MPa. A similar trend was observed for the ultimate strain, which ranged from 130–170% for untreated scaffolds and increased to 140–190% after surface treatment. The results for tensile strength fall within the range typically reported for electrospun PCL-based composite scaffolds, while maintaining relatively high elongation at break [456], [458], [461]. Moreover, samples SP_L and SP_LT clearly exhibited higher tensile resistance compared to other formulations, which could be ascribable to lower BG content, as higher ceramic loading is often associated with reduced mechanical integrity in composite electrospun scaffolds [456]. The influence of BG content on the mechanical response of electrospun scaffolds has been widely discussed in the literature. BG nanoparticles embedded into PCL-based fibrous scaffolds can initially increase tensile strength due to a reinforcing effect of the ceramic phase, although higher BG concentration may lead to a reduction in strength [458]. Several different studies point out that excessive inorganic filler in electrospun mats could lead to stress concentration and

promote brittle behavior [73], [456]. Additionally, previous works have highlighted that the mechanical performance of electrospun composites is strongly influenced by the dispersion of BG particles within the polymer matrix. Indeed, poor dispersion and particle clustering may result in localized stress concentration resulting in worsened mechanical properties [73].

Notably, the mechanical properties of the scaffolds treated in NaOH solution were higher than those of untreated samples, in both elongation at break and ultimate tensile strength. This could be related to the chemical treatment, although the underlying mechanisms governing this behavior are not fully elucidated. One-way Anova supports these observations, revealing statistically significant differences among the samples ($F = 15.32$, $p << 0.05$). Tukey's post-test revealed a significant increase of tensile strength between treated and untreated samples, except for SP_X compared with SP_XT ($p = 0.17$). Interestingly, statistical analysis revealed the influence of BG loading in the scaffolds, as SP_L shows significantly higher tensile strength compared to SP_H ($p < 0.05$), indicating that lower BG content leads to higher tensile strength in electrospun scaffolds. In contrast, statistical analysis performed on εb did not reveal significant differences among the investigated groups ($F = 2.148$, $p = 0.108$). Although variations in elongation at break were observed among the samples, these differences can be attributed to experimental variability rather than systematic effects related to scaffold composition or surface modification.

Nevertheless, these results suggest that NaOH treatment, when applied to randomly oriented electrospun fibers for up to 4 hours, does not compromise the mechanical performance of the fibrous scaffolds. Cues for this behavior have previously been presented by Bosworth et al., even though it is not fully discussed [455]. Based on the available evidence, the improvement in tensile strength after NaOH treatment could be attributed to a combination of factors. Firstly, the partial surface hydrolysis of PCL caused by NaOH could promote localized fiber fusion [462], potentially leading to a favorable balance between stiffness and ductility for this system. Secondly, NaOH treatment has been reported to induce fiber flattening [455], [462], resulting in thinner scaffolds compared to the untreated samples. This morphological change may have contributed to an apparent increase in tensile properties, as a smaller cross-sectional area influences stress calculations. However, further dedicated investigations would be required to fully elucidate this behavior.

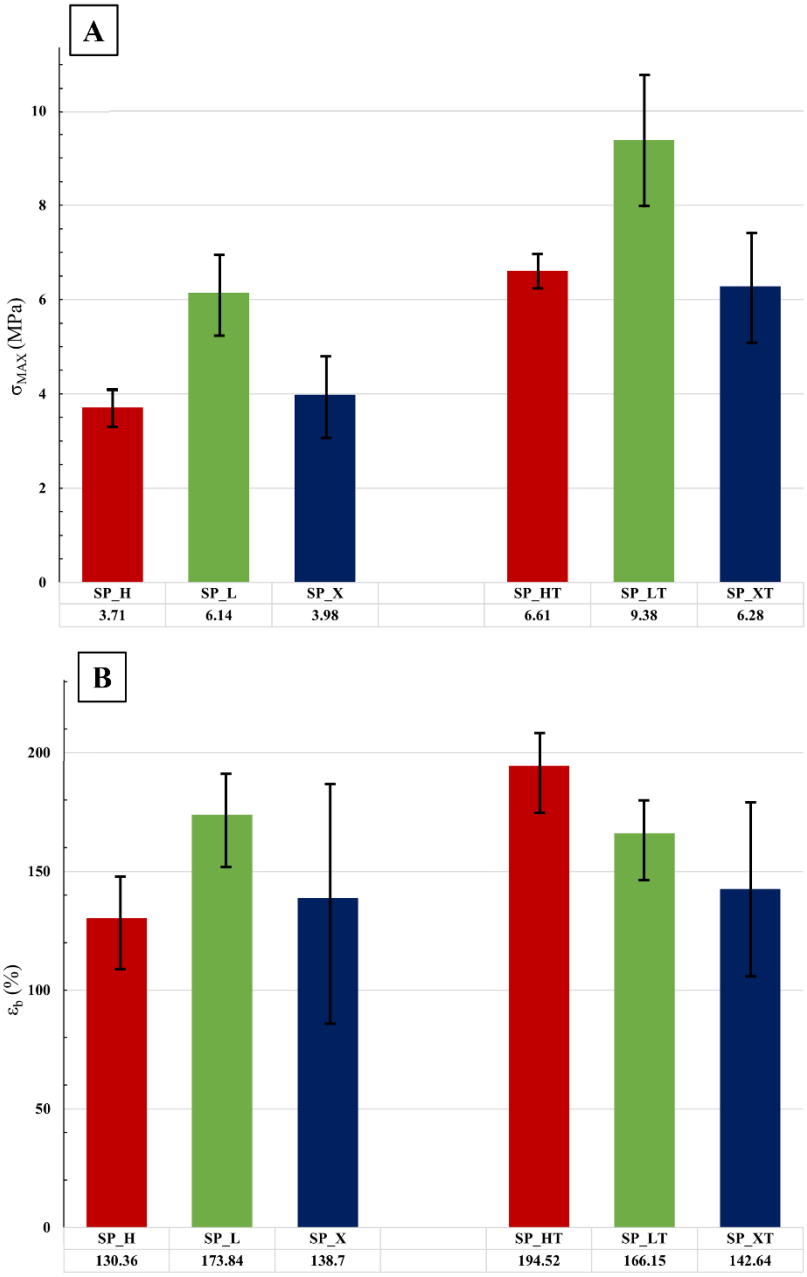

Figure 38: Traction test results reporting (A) σ_{MAX} (expressed in MPa) and (B) ε_b (%) of the treated and untreated electrospun PCL/BG samples.

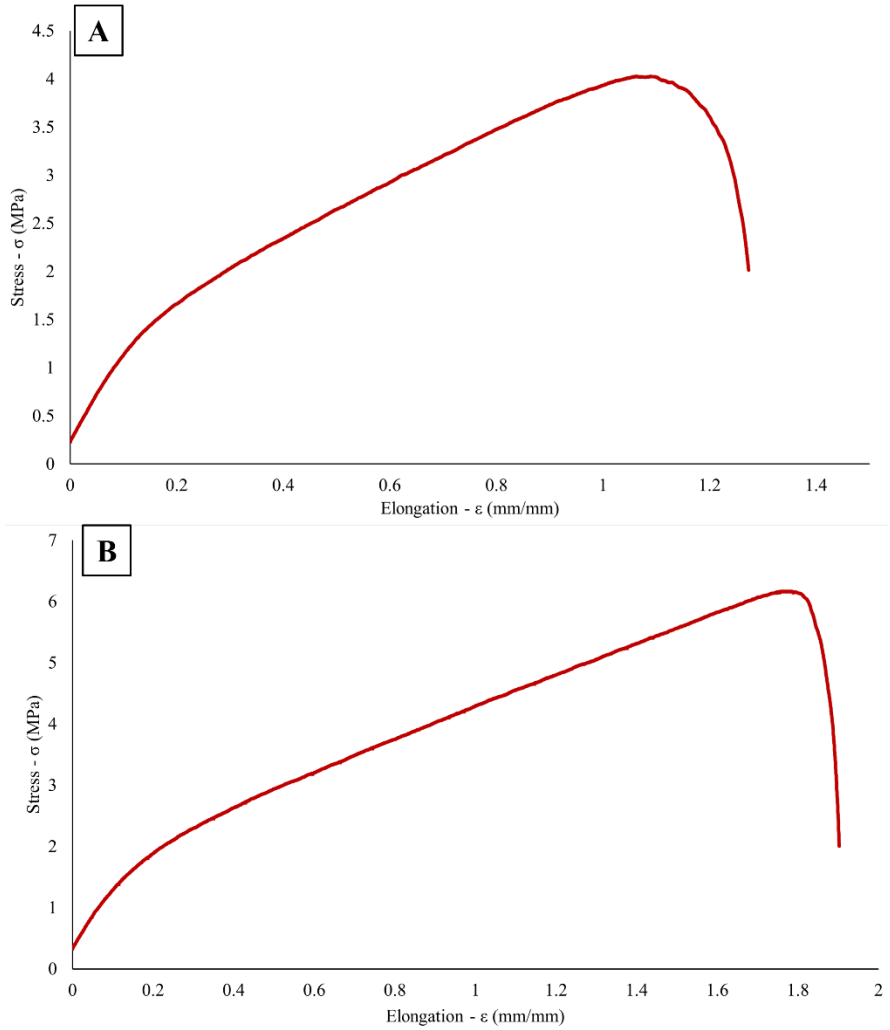

Figure 39: Representative engineering stress-strain curves of the samples SP_H (A) and the chemically treated SP_HT (B).

6.2.3 Cell spreading test

To test the affinity of cells to the different electrospun PCL/BG scaffolds, HDF were cultured for 24 hours on SP_H, SP_L, and SP_X untreated or treated with NaOH. The morphology of the cells appeared shriveled and stretched alongside rounder cells in the SP_X sample; by contrast, cells were elongated and more expanded on all other samples, and especially on those treated with NaOH, indicating higher affinity for these surfaces. In particular, fibroblasts seeded on the SP_L scaffolds were more numerous, and in several areas on the SP_LT, cells appeared already at subconfluence with well-marked cytoskeletal structures (Figure 40 (A)).

To better evaluate the number of cells on the different scaffolds, the DAPI-stained nuclei were counted. Adhesion of cells showed best results on SP_L > SP_H > SP_X. In all cases, treatment with NAOH increased the number of adherent cells compared to the corresponding untreated scaffold (Figure 40 (B)). Results highlight that alkaline treatment, by increasing the wettability of the scaffolds favors the attachment of the serum adhesive glycoproteins present the culture medium, thus promoting cell adhesion and spreading as already suggested [463]. The lower affinity for cells shown by the SP_X samples could be due to the larger

size of the fibers, which creates a structure that does not favor contact with fibroblasts and that can be overcome, at least partially, by NaOH treatment.

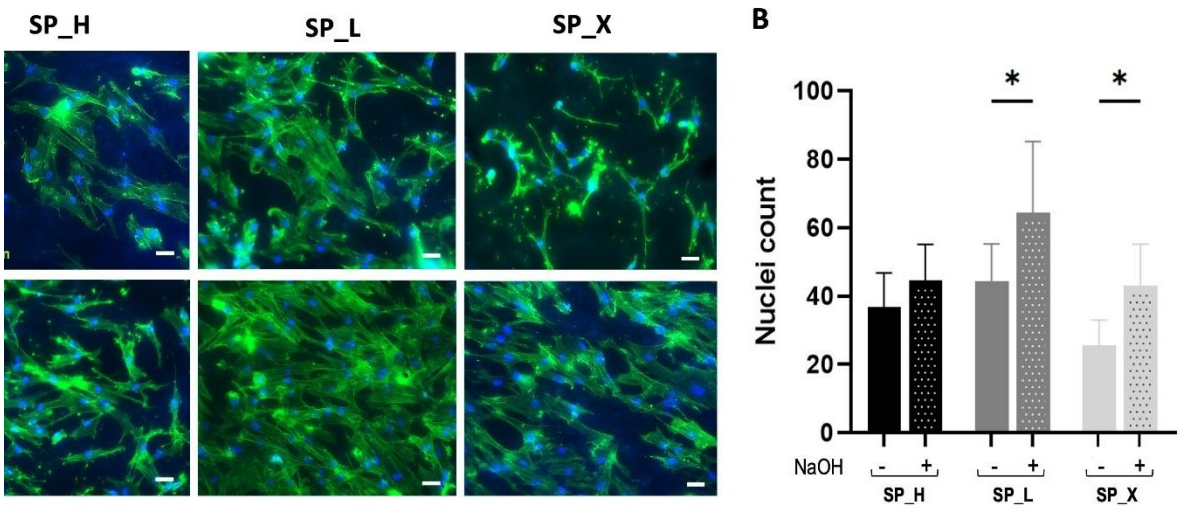

*Figure 40: Representative images of HDF seeded on SP_H, SP_L and SP_X scaffolds untreated or treated with NaOH. Nuclei and cytoskeleton are stained with DAPI (blue) and phalloidin (green), respectively. Scale bar= 100 µm. (B) Nuclei count of HDF seeded on the different scaffolds. Data are shown as mean, error bar represents standard deviation . *p value < 0.05.*

Conclusions

The ultimate goal of this study was to expand knowledge of biomaterials for tissue engineering, with a specific focus on the properties, applicability, and delivery strategies of bioactive glasses. This was achieved by investigating the properties and interactions of BGs, both through a review of the literature and through experimental work.

BGs show great promise and offer a wide range of potential applications. Some of these require heat treatments to enhance the mechanical properties of the glasses or to sinter the BGs powders. In this context, the crystallization behavior of the "gold" standard 45S5 BG during thermal treatments remains a subject of debate, particularly regarding the main crystalline phase formed after the first crystallization step, namely whether it is $Na_2Ca_2Si_3O_9$ or $Na_2CaSi_2O_6$.

Despite this challenge, significant progress has been made in improving the thermal properties of these materials through sol–gel synthesis (which allows for a lower concentration of network modifiers in the BG), new glass formulations, and ion substitution. These advancements have opened up new possibilities for the utilization of BGs in areas such as scaffolds, composites, and thermally sprayed coatings. Nonetheless, further research is necessary to fully unlock the potential of these remarkable materials. Continued investigation into the effects of different ions on sintering and crystallization is crucial for further advancements in the field of BGs. Lastly, it is important to investigate the impact of glass composition on thermal residual stresses arising from the mismatch between the coefficients of thermal expansion of BGs and other phases, such as in composites or BG coatings. This investigation could be conducted through numerical simulations [361] to better understand the role of glass composition in managing thermal stresses.

Among the many advantageous properties of BGs, such as osteoinductivity, bioresorbability, and the ability to promote biomineralization, one is their capacity to be engineered for antibacterial activity, a feature that has proven valuable in various applications. Since the early 2000s, studies have demonstrated that chemically diverse BG compositions can inhibit bacterial growth. Two main mechanisms drive this behavior: (i) alkalinization of the surrounding environment and (ii) the release of therapeutic metal ions with intrinsic antibacterial activity. The latter approach allows for a more precise and controlled modulation of the antibacterial response.

BGs exploiting these mechanisms could be employed not only for BTE, where reducing post-operative infection could significantly improve clinical outcomes, but also for soft-tissue repair, maxillofacial and dental applications, and implant coatings. The gradual transition of these materials into clinical use confirms their practical viability. As research progresses, BGs designed with tailored antibacterial functions are likely to become increasingly relevant in next-generation biomedical devices and regenerative therapies.

While investigating the effects of the substitution of Mg^{2+} and Sr^{2+} ion substitution MS-doped BGs compositions, several interesting results emerged. Firstly, both T_G and T_C show a significant increase in value in MS-doped BGs, while also exhibiting a wider processing window. This may allow for low temperature sintering of the BGs. Applying heat treatment

to the MS-doped BGs resulted in quasi-amorphous or low-crystallinity structures. Lower temperatures enabled the production of sintered BG samples while retaining a mostly amorphous structure. Densification was also higher for the MS-doped BGs. Specifically, 45S5_MS exhibited improved mechanical properties following sintering heat treatment compared with sintered 45S5. Meanwhile S53P4_MS showed mechanical properties similar to the other BGs in this study.

When immersed in SBF, the MS-doped BGs exhibited slower reaction kinetics compared to the undoped compositions. This behavior can also prove beneficial, as the pH of the solution increased less compared to the undoped BGs, an effect associated with improved cytocompatibility [366], [464].

Biological tests showed a good interaction between bioglasses and Human Dermal Fibroblast suggesting their potential use in soft connective tissues, in addition to their established use in bone and cartilage regeneration. Heat treatment can modify the surface of BGs with consequences on cellular adhesion, as highlighted in the case of 45S5 T_{BS}. Moreover, the positive effect of the dopants on the biological properties is particularly evident when BGs are treated at T_C and T_{BS}. The addition of Mg^{2+} and Sr^{2+} ions in 45S5 and S53P4 - already widely used for orthopedic and dental applications - further improved the biological performance and thermal stability of the BGs.

Electrospun composite mats were produced using PCL, incorporating melt-quenched BG powders into the scaffold structure. The mats underwent extensive testing, including mechanical characterization, surface wettability assessment, SBF testing, and biological evaluation. The BG powders were successfully incorporated into the electrospun mats.

The results from the tests conducted on these scaffolds can be summarized as follows. The mechanical characteristics of the mats were consistent with previous research on PCL and composite electrospun mats, indicating a minimal influence of BGs on the structural integrity of the scaffolds. The surface wettability was low, reflecting the high hydrophobicity of the scaffolds. This outcome is attributed to the hydrophobic nature of PCL, combined with the micro-fibrous morphology of the mats. The analysis of the samples after SBF testing suggests that the BG was exposed to the solution and was capable of forming apatite-like crystals. However, additional precipitates containing high concentrations of Na^+ and Cl^- ions were also observed, as confirmed by EDS analysis. Furthermore, the solution could induce degradation of PCL, which can lead to the acidification of the immersion medium. Indirect cytotoxicity tests with L929 mouse cells confirmed the non-cytotoxicity of the electrospun scaffolds, with viabilities in the range of 85% to 100%. ALP activity testing revealed that the presence of Mg and Sr was associated with higher ALP staining, which could be favorable for cell differentiation. Fluorescence imaging revealed that, from days 14 to 28, osteocalcin expression persisted, suggesting cell proliferation and differentiation, especially in the scaffolds with additives.

These results suggest that the inclusion of Mg- and Sr-enriched BG powders, produced via the traditional melt–quench technique, can serve as a viable alternative to unloaded PCL electrospun scaffolds. Not only do they enhance biological performance, but they also preserve the key characteristics of pure PCL. Further work should focus on optimizing the

processing parameters for scaffold fabrication and improving the surface wettability. This could enhance the scaffold's healing properties by promoting better cell adhesion to the fibers. Additional research could also explore specific properties of BGs, such as their angiogenic potential, which supports vascularization and wound healing, and their antibacterial activity, which helps reduce infection risk. These properties may significantly influence the treatment of soft tissue wounds and patient outcomes, potentially opening new applications for composite electrospun BG/PCL scaffolds.

The implementation of a wet-milling step allowed for high degree of refinement of BG powders prior to solution preparation, improving the electrospinning efficiency. Morphological analyses confirmed uniform fiber formation and adequate dispersion of the BG within the mats. Moreover, the chemical treatment did not visibly modify the fibers, although NaOH treatment significantly enhanced the wettability of the scaffolds.

The mechanical characterization of the PCL/S53P4_MS scaffolds suggested that ceramic loading can negatively influence the mechanical performance of the mats; however, the samples showed improved tensile strength compared to previous systems. This is likely associated with the lower fiber diameter, which had a major influence in this work. Furthermore, the chemical treatment did not compromise mechanical integrity; on the contrary, it was associated with improved tensile performance.

Cell seeding evaluation using HDFs revealed that NaOH-treated scaffolds had enhanced cell adhesion compared to the untreated surfaces, consistent with the improved wettability of the modified surfaces. This is probably associated with improved protein adsorption from the culture medium. Among the investigated formulations, SP_L exhibited the most favorable cellular response, indicating that both composition and fiber morphology influence interactions between cells and the material.

These results indicate that particle size refinement, electrospinning optimization, and surface modification can contribute to improvements in the properties of PCL/BG scaffolds. While further investigation is needed, these findings provide a basis for the continued development of electrospun composites for potential tissue engineering applications.

Acknowledgements

First and foremost, I would like to acknowledge the financial support of the EcosistER project, which made it possible to work on such a stimulating and relevant research topic. Nonetheless, this work would not have been possible without the support, guidance, and contributions of many people, to whom I am sincerely grateful.

I would like to express my deepest gratitude to my supervisors, Prof. Valeria Cannillo, and Prof. Devis Bellucci, for their continuous guidance, critical insight, and support throughout this research.

I would also like to thank all the members and colleagues of the Faculty of Engineering “Enzo Ferrari” in UniMoRe. Their support in experimental work and daily discussions created a stimulating and collaborative environment. I am equally thankful to my fellow Ph.D. candidates and lab colleagues, whose external viewpoint and expertise enriched both this experience and the quality of the work.

Finally, beyond the academic environment, I would like to thank my friends and family for their constant presence during this journey. Their support made the challenging moments manageable and the positive ones more meaningful.

Bibliography

[1] Y. Ding, M. T. Souza, W. Li, D. W. Schubert, A. R. Boccaccini, and J. A. Roether, "Bioactive Glass–Biopolymer Composites for Applications in Tissue Engineering," *Handbook of Bioceramics and Biocomposites*, pp. 1–26, 2015, doi: 10.1007/978-3-319-09230-0_17-3.

[2] E. Marin, F. Boschetto, and G. Pezzotti, "Biomaterials and biocompatibility: An historical overview," *J. Biomed. Mater. Res. A*, vol. 108, no. 8, pp. 1617–1633, Aug. 2020, doi: 10.1002/jbm.a.36930.

[3] L. L. Hench and J. Wilson, "Clinical Performance of Skeletal Prostheses", 1st ed., vol. 14. Springer Dordrecht, 1996.

[4] L. L. Hench and I. Thompson, "Twenty-first century challenges for biomaterials," *J. R. Soc. Interface*, vol. 7, no. Suppl 4, p. S379, Aug. 2010, doi: 10.1098/RSIF.2010.0151.FOCUS.

[5] X. Yu, X. Tang, S. V. Gohil, and C. T. Laurencin, "Biomaterials for Bone Regenerative Engineering," *Adv. Healthc. Mater.*, vol. 4, no. 9, p. 1268, Jun. 2015, doi: 10.1002/ADHM.201400760.

[6] L. L. Hench and J. M. Polak, "Third-generation biomedical materials," *Science (1979).*, vol. 295, no. 5557, pp. 1014–1017, Feb. 2002, doi: 10.1126/SCIENCE.1067404.

[7] J. R. Jones and L. L. Hench, "Regeneration of trabecular bone using porous ceramics," *Curr. Opin. Solid State Mater. Sci.*, vol. 7, no. 4–5, pp. 301–307, Aug. 2003, doi: 10.1016/J.COSSMS.2003.09.012.

[8] R. Barbucci, S. Lamponi, and A. Magnani, "Biological Performance of Materials," *Chemistry at the Beginning of the Third Millennium*, pp. 161–183, 2000, doi: 10.1007/978-3-662-04154-3_8.

[9] J. M. Anderson, "Biocompatibility," *Polymer Science: a Comprehensive Reference*, vol. 1–10, pp. 363–383, Jan. 2012, doi: 10.1016/B978-0-444-53349-4.00229-6.

[10] L. L. Hench, "The story of Bioglass," *J. Mater. Sci. Mater. Med.*, vol. 17, no. 11, pp. 967–978, Nov. 2006, doi: 10.1007/S10856-006-0432-Z.

[11] J. L. Weaver, P. T. DePriest, A. E. Plymale, C. I. Pearce, B. Arey, and R. J. Koestler, "Microbial interactions with silicate glasses," *Materials Degradation,* vol. 5, no. 1, pp. 1–18, Mar. 2021, doi: 10.1038/s41529-021-00153-w.

[12] A. Pedone, T. Charpentier, G. Malavasi, and M. C. Menziani, "New Insights into the Atomic Structure of 45S5 Bioglass by Means of Solid-State NMR Spectroscopy and Accurate First-Principles Simulations," *Chem. Mater*, vol. 22, pp. 5644–5652, 2010, doi: 10.1021/cm102089c.

[13] L. L. Hench and J. K. West, "The Sol-Gel Process," *Chem. Rev*, vol. 90, pp. 33–72, 1990, doi: 10.1021/cr00099a003.

[14] J. Zhong and D. C. Greenspan, “Processing and Properties of Sol-Gel Bioactive Glasses,” *Journal of Biomedical Materials Research*, vol. 53, no. 6, pp 694-701, 2000, doi: 10.1002/1097-4636(2000)53:6<694::aid-jbm12>3.0.co;2-6.

[15] Bonalive, “Our story - Bonalive.” Accessed: Jan. 29, 2026. [Online]. Available: https://www.bonalive.com/en/our-story/

[16] D. Zhang *et al.*, “Comparison of Antibacterial Effect of Three Bioactive Glasses,” *Key Eng. Mater.*, vol. 309–311, pp. 345–348, May 2006, doi: 10.4028/WWW.SCIENTIFIC.NET/KEM.309-311.345.

[17] D. Zhang *et al.*, “Antibacterial effects and dissolution behavior of six bioactive glasses,” *J. Biomed. Mater. Res. A*, vol. 93A, no. 2, pp. 475–483, May 2010, doi: 10.1002/JBM.A.32564.

[18] N. Lindfors *et al.*, “Antibacterial Bioactive Glass, S53P4, for Chronic Bone Infections – A Multinational Study,” *Adv. Exp. Med. Biol.*, vol. 971, pp. 81–92, 2016, doi: 10.1007/5584_2016_156.

[19] T. Albrektsson and C. Johansson, “Osteoinduction, osteoconduction and osseointegration,” *European Spine Journal*, vol. 10, no. Suppl 2, p. S96, 2001, doi: 10.1007/S005860100282.

[20] M. Bohner and J. Lemaitre, “Can bioactivity be tested in vitro with SBF solution?,” *Biomaterials*, vol. 30, no. 12, pp. 2175–2179, Apr. 2009, doi: 10.1016/J.BIOMATERIALS.2009.01.008.

[21] T. Kokubo, H. Kushitani, S. Sakka, T. Kitsugi, and T. Yamamuro, “Solutions able to reproduce in vivo surface-structure changes in bioactive glass-ceramic A-W3,” *J. Biomed. Mater. Res.*, vol. 24, no. 6, pp. 721–734, Jun. 1990, doi: 10.1002/JBM.820240607.

[22] T. Kokubo and H. Takadama, “How useful is SBF in predicting in vivo bone bioactivity?,” *Biomaterials*, vol. 27, no. 15, pp. 2907–2915, May 2006, doi: 10.1016/J.BIOMATERIALS.2006.01.017.

[23] N. Abbasi, S. Hamlet, R. M. Love, and N. T. Nguyen, “Porous scaffolds for bone regeneration,” *Journal of Science: Advanced Materials and Devices*, vol. 5, no. 1, pp. 1–9, Mar. 2020, doi: 10.1016/J.JSAMD.2020.01.007.

[24] A. N. Begum, V. Rajendran, and H. Ylänen, “Effect of thermal treatment on physical properties of bioactive glass,” *Mater. Chem. Phys.*, vol. 96, no. 2–3, pp. 409–417, Apr. 2006, doi: 10.1016/J.MATCHEMPHYS.2005.07.031.

[25] R. Sergi, D. Bellucci, and V. Cannillo, “A Comprehensive Review of Bioactive Glass Coatings: State of the Art, Challenges and Future Perspectives,” *Coatings 2020,* vol. 10, no. 8, Aug. 2020, doi: 10.3390/COATINGS10080757.

[26] D. Groh, F. Döhler, and D. S. Brauer, “Bioactive glasses with improved processing. Part 1. Thermal properties, ion release and apatite formation,” *Acta Biomater.*, vol. 10, no. 10, pp. 4465–4473, Oct. 2014, doi: 10.1016/J.ACTBIO.2014.05.019.

[27] L. Lefebvre, L. Gremillard, J. Chevalier, R. Zenati, and D. Bernache-Assolant, “Sintering behaviour of 45S5 bioactive glass,” *Acta Biomater.*, vol. 4, no. 6, pp. 1894–1903, 2008, doi: 10.1016/J.ACTBIO.2008.05.019.

[28] O. P. Filho, G. P. L. Torre, and L. Hench, “Effect of crystallization on apatite-layer formation of bioactive glass 45S5.,” *J. Biomed. Mater. Res.*, Apr. 1996, doi: 10.1002/(SICI)1097-4636(199604)30:4<509::AID-JBM9>3.0.CO;2-T.

[29] F. Baino and E. Fiume, “Mechanical characterization of 45S5 bioactive glass-derived scaffolds,” *Mater. Lett.*, vol. 245, pp. 14–17, Jun. 2019, doi: 10.1016/J.MATLET.2019.02.086.

[30] M. Brink, “The influence of alkali and alkaline earths on the working range for bioactive glasses.,” *J. Biomed. Mater. Res.*, Jul. 1997, doi: 10.1002/(SICI)1097-4636(199707)36:1<109::AID-JBM13>3.0.CO;2-D.

[31] D. Bellucci, E. Veronesi, M. Dominici, and V. Cannillo, “A new bioactive glass with extremely high crystallization temperature and outstanding biological performance,” *Materials Science and Engineering: C*, vol. 110, p. 110699, May 2020, doi: 10.1016/J.MSEC.2020.110699.

[32] D. Bellucci and V. Cannillo, “A novel bioactive glass containing strontium and magnesium with ultra-high crystallization temperature,” *Mater. Lett.*, vol. 213, pp. 67–70, Feb. 2018, doi: 10.1016/J.MATLET.2017.11.020.

[33] S. Kargozar *et al.*, “Osteogenic Potential of Magnesium (Mg)-Doped Multicomponent Bioactive Glass: In Vitro and In Vivo Animal Studies,” *Materials,* vol. 15, no. 1, Jan. 2022, doi: 10.3390/MA15010318.

[34] I. Cacciotti, “Bivalent cationic ions doped bioactive glasses: the influence of magnesium, zinc, strontium and copper on the physical and biological properties,” *Journal of Materials Science*, vol. 52, no. 15, pp. 8812–8831, Mar. 2017, doi: 10.1007/S10853-017-1010-0.

[35] H. Zreiqat *et al.*, “Mechanisms of magnesium-stimulated adhesion of osteoblastic cells to commonly used orthopaedic implants,” *J. Biomed. Mater. Res.*, vol. 62, no. 2, pp. 175–184, Nov. 2002, doi: 10.1002/JBM.10270

[36] M. Percival, “Bone Health & Osteoporosis,” Nov. 1999.

[37] E. Bonnelye, A. Chabadel, F. Saltel, P. J.- Bone, and undefined 2008, “Dual effect of strontium ranelate: stimulation of osteoblast differentiation and inhibition of osteoclast formation and resorption in vitro,” *Bone*, vol. 42, no. 1, pp. 129–138, 2008, doi: 10.1016/j.bone.2007.08.043.

[38] A. Moghanian, S. Firoozi, and M. Tahriri, “Characterization, in vitro bioactivity and biological studies of sol-gel synthesized SrO substituted 58S bioactive glass,” *Ceram. Int.*, vol. 43, no. 17, pp. 14880–14890, Dec. 2017, doi: 10.1016/J.CERAMINT.2017.08.004.

[39] N. Baheiraei, H. Eyni, B. Bakhshi, R. Najafloo, and N. Rabiee, “Effects of strontium ions with potential antibacterial activity on in vivo bone regeneration,” *Scientific Reports*, vol. 11, no. 1, pp. 1–9, Apr. 2021, doi: 10.1038/s41598-021-88058-1.

[40] D. S. Brauer, “Bioaktive Gläser: Struktur und Eigenschaften,” *Angewandte Chemie*, vol. 127, no. 14, pp. 4232–4254, 2015, doi: 10.1002/ange.201405310.

[41] R. G. Hill and D. S. Brauer, “Predicting the bioactivity of glasses using the network connectivity or split network models,” *J. Non. Cryst. Solids*, vol. 357, no. 24, pp. 3884–3887, 2011, doi: 10.1016/j.jnoncrysol.2011.07.025.

[42] S. J. Watts, R. G. Hill, M. D. O’Donnell, and R. V. Law, “Influence of magnesia on the structure and properties of bioactive glasses,” *J. Non. Cryst. Solids*, vol. 356, no. 9–10, pp. 517–524, Mar. 2010, doi: 10.1016/J.JNONCRYSOL.2009.04.074.

[43] R. G. Hill and D. S. Brauer, “Predicting the glass transition temperature of bioactive glasses from their molecular chemical composition,” *Acta Biomater.*, vol. 7, no. 10, pp. 3601–3605, 2011, doi: 10.1016/j.actbio.2011.06.023.

[44] M. D. O’Donnell, “Predicting bioactive glass properties from the molecular chemical composition: Glass transition temperature,” *Acta Biomater.*, vol. 7, no. 5, pp. 2264–2269, 2011, doi: 10.1016/j.actbio.2011.01.021.

[45] J. R. Jones, “Review of bioactive glass: From Hench to hybrids,” *Acta Biomater.*, vol. 9, no. 1, pp. 4457–4486, Jan. 2013, doi: 10.1016/J.ACTBIO.2012.08.023.

[46] M. Montazerian, A. Shearer, and J. C. Mauro, “Perspectives on the impact of crystallization in bioactive glasses and glass-ceramics,” *International Journal of Ceramic Engineering and Science*, vol. 6, no. 1, p. e10194, 2023, doi: 10.1002/ces2.10194.

[47] M. Montazerian and E. Dutra Zanotto, “History and trends of bioactive glass-ceramics,” *J. Biomed. Mater. Res. A*, vol. 104, no. 5, pp. 1231–1249, May 2016, doi: 10.1002/JBM.A.35639.

[48] M. C. Crovace, M. T. Souza, C. R. Chinaglia, O. Peitl, and E. D. Zanotto, “Biosilicate® — A multipurpose, highly bioactive glass-ceramic. In vitro, in vivo and clinical trials,” *J. Non. Cryst. Solids*, vol. 432, pp. 90–110, Jan. 2016, doi: 10.1016/J.JNONCRYSOL.2015.03.022.

[49] C. Tirapelli, H. Panzeri, E. H. G. Lara, R. G. Soares, O. Peitl, and E. D. Zanotto, “The effect of a novel crystallised bioactive glass-ceramic powder on dentine hypersensitivity: a long-term clinical study,” *J. Oral Rehabil.*, vol. 38, no. 4, pp. 253–262, Apr. 2011, doi: 10.1111/J.1365-2842.2010.02157.X.

[50] H. Elsayed, P. Colombo, M. C. Crovace, E. D. Zanotto, and E. Bernardo, “Suitability of Biosilicate® glass-ceramic powder for additive manufacturing of highly porous scaffolds,” *Ceram. Int.*, vol. 47, no. 6, pp. 8200–8207, 2021, doi: 10.1016/j.ceramint.2020.11.179.

[51] M. N. Helmus, D. F. Gibbons, and D. Cebon, “Biocompatibility: Meeting a Key Functional Requirement of Next-Generation Medical Devices,” *Toxicol. Pathol.*, vol. 36, no. 1, pp. 70–80, 2008, doi: 10.1177/0192623307310949.

[52] I. Allan, H. Newman, and M. Wilson, “Antibacterial activity of particulate Bioglass® against supra- and subgingival bacteria,” *Biomaterials*, vol. 22, no. 12, pp. 1683–1687, Jun. 2001, doi: 10.1016/S0142-9612(00)00330-6.

[53] M. Awais *et al.*, “A Review on the Recent Advancements on Therapeutic Effects of Ions in the Physiological Environments,” *Prosthesis 2022*, vol. 4, no. 2, pp. 263–316, Jun. 2022, doi: 10.3390/PROSTHESIS4020026.

[54] S. Pourshahrestani *et al.*, “Gallium-containing mesoporous bioactive glass with potent hemostatic activity and antibacterial efficacy,” *J. Mater. Chem. B*, vol. 4, no. 1, pp. 71–86, Dec. 2015, doi: 10.1039/C5TB02062J.

[55] M. Godoy-Gallardo *et al.*, “Antibacterial approaches in tissue engineering using metal ions and nanoparticles: From mechanisms to applications,” *Bioact. Mater.*, vol. 6, no. 12, pp. 4470–4490, Dec. 2021, doi: 10.1016/J.BIOACTMAT.2021.04.033.

[56] M. F. Salas Orozco, N. Niño-Martínez, G. A. Martínez-Castañón, F. T. Méndez, and F. Ruiz, “Molecular Mechanisms of Bacterial Resistance to Metal and Metal Oxide Nanoparticles,” *International Journal of Molecular Sciences*, vol. 20, no. 11, p. 2808, Jun. 2019, doi: 10.3390/IJMS20112808.

[57] I. Jun, H. S. Han, J. R. Edwards, and H. Jeon, “Electrospun Fibrous Scaffolds for Tissue Engineering: Viewpoints on Architecture and Fabrication,” *Int. J. Mol. Sci.*, vol. 19, no. 3, p. 745, Mar. 2018, doi: 10.3390/IJMS19030745.

[58] A. Keirouz *et al.*, “The History of Electrospinning: Past, Present, and Future Developments,” *Adv. Mater. Technol.*, vol. 8, no. 11, p. 2201723, Jun. 2023, doi: 10.1002/ADMT.202201723.

[59] H. Zhong, J. Huang, J. Wu, and J. Du, “Electrospinning nanofibers to 1D, 2D, and 3D scaffolds and their biomedical applications,” *Nano Research*, vol. 15, no. 2, pp. 787–804, Aug. 2021, doi: 10.1007/S12274-021-3593-7.

[60] Y. Li *et al.*, “Developments of Advanced Electrospinning Techniques: A Critical Review,” *Adv. Mater. Technol.*, vol. 6, no. 11, p. 2100410, Nov. 2021, doi: 10.1002/ADMT.202100410.

[61] N. Palani, P. Vijayakumar, P. Monisha, S. Ayyadurai, and S. Rajadesingu, “Electrospun nanofibers synthesized from polymers incorporated with bioactive compounds for wound healing,” *Journal of Nanobiotechnology*, vol. 22, no. 1, pp. 1–30, Apr. 2024, doi: 10.1186/S12951-024-02491-8.

[62] F. E. Ahmed, B. S. Lalia, and R. Hashaikeh, “A review on electrospinning for membrane fabrication: Challenges and applications,” *Desalination*, vol. 356, pp. 15–30, Jan. 2015, doi: 10.1016/J.DESAL.2014.09.033.

[63] B. Joseph, R. Augustine, N. Kalarikkal, S. Thomas, B. Seantier, and Y. Grohens, “Recent advances in electrospun polycaprolactone based scaffolds for wound healing and skin bioengineering applications,” *Mater. Today Commun.*, vol. 19, pp. 319–335, Jun. 2019, doi: 10.1016/J.MTCOMM.2019.02.009.

[64] M. Chen, H. Michaud, and S. Bhowmick, “Controlled vacuum seeding as a means of generating uniform cellular distribution in electrospun polycaprolactone (PCL) scaffolds,” *J. Biomech. Eng.*, vol. 131, no. 7, Jul. 2009, doi: 10.1115/1.3173283/400972.

[65] A. K. Ekaputra, Y. Zhou, S. M. K. Cool, and D. W. Hutmacher, “Composite electrospun scaffolds for engineering tubular bone grafts,” *Tissue Eng. Part A*, vol. 15, no. 12, pp. 3779–3788, Dec. 2009, doi: 10.1089/TEN.TEA.2009.0186.

[66] M. A. Woodruff and D. W. Hutmacher, “The return of a forgotten polymer—Polycaprolactone in the 21st century,” *Prog. Polym. Sci.*, vol. 35, no. 10, pp. 1217–1256, Oct. 2010, doi: 10.1016/J.PROGPOLYMSCI.2010.04.002.

[67] S. Wei *et al.*, “Vancomycin–impregnated electrospun polycaprolactone (PCL) membrane for the treatment of infected bone defects: An animal study,” *J. Biomater. Appl.*, vol. 32, no. 9, pp. 1187–1196, Apr. 2018, doi: 10.1177/0885328218754462.

[68] M. Sattary, M. Rafienia, M. T. Khorasani, and H. Salehi, “The effect of collector type on the physical, chemical, and biological properties of polycaprolactone/gelatin/nano-hydroxyapatite electrospun scaffold,” *J. Biomed. Mater. Res. B Appl. Biomater.*, vol. 107, no. 4, pp. 933–950, May 2019, doi: 10.1002/JBM.B.34188.

[69] A. K. Jaiswal, H. Chhabra, S. S. Kadam, K. Londhe, V. P. Soni, and J. R. Bellare, “Hardystonite improves biocompatibility and strength of electrospun polycaprolactone nanofibers over hydroxyapatite: A comparative study,” *Materials Science and Engineering: C*, vol. 33, no. 5, pp. 2926–2936, Jul. 2013, doi: 10.1016/J.MSEC.2013.03.020.

[70] R. Jirkovec, P. Holec, S. Hauzerova, A. Samkova, T. Kalous, and J. Chvojka, “Preparation of a Composite Scaffold from Polycaprolactone and Hydroxyapatite Particles by Means of Alternating Current Electrospinning,” *ACS Omega*, vol. 6, no. 13, pp. 9234–9242, Apr. 2021, doi: 10.1021/ACSOMEGA.1C00644.

[71] B. A. Allo, A. S. Rizkalla, and K. Mequanint, “Synthesis and Electrospinning of ε-Polycaprolactone-Bioactive Glass Hybrid Biomaterials via a Sol−Gel Process,” *Langmuir*, vol. 26, no. 23, pp. 18340–18348, Dec. 2010, doi: 10.1021/LA102845K.

[72] Z. Tabia, S. Akhtach, M. Bricha, and K. El Mabrouk, “Tailoring the biodegradability and bioactivity of green-electrospun polycaprolactone fibers by incorporation of bioactive glass nanoparticles for guided bone regeneration,” *Eur. Polym. J.*, vol. 161, p. 110841, Dec. 2021, doi: 10.1016/J.EURPOLYMJ.2021.110841.

[73] E. Piatti, M. Miola, L. Liverani, E. Verné, and A. R. Boccaccini, “Poly(ε-caprolactone)/bioactive glass composite electrospun fibers for tissue engineering applications,” *J. Biomed. Mater. Res. A*, vol. 111, no. 11, pp. 1692–1709, Nov. 2023, doi: 10.1002/JBM.A.37578.

[74] B. Banimohamad-Shotorbani, A. Rahmani Del Bakhshayesh, A. Mehdipour, S. Jarolmasjed, and H. Shafaei, “The efficiency of PCL/HAp electrospun nanofibers in bone regeneration: a review,” *J. Med. Eng. Technol.*, vol. 45, no. 7, pp. 511–531, 2021, doi: 10.1080/03091902.2021.1893396.

[75] D. Prakashan, A. Singh, A. D. Deshpande, V. Chandra, G. T. Sharma, and S. Gandhi, “Bone marrow derived mesenchymal stem cells enriched PCL-gelatin nanofiber scaffold for improved wound healing,” *Int. J. Biol. Macromol.*, vol. 274, p. 133447, Aug. 2024, doi: 10.1016/J.IJBIOMAC.2024.133447.

[76] C. Meng *et al.*, “Heterogeneous porous PLLA/PCL fibrous scaffold for bone tissue regeneration,” *Int. J. Biol. Macromol.*, vol. 235, p. 123781, Apr. 2023, doi: 10.1016/J.IJBIOMAC.2023.123781.

[77] N. Rivoallan *et al.*, “Comparison of hydroxyapatite and honeycomb micro-structure in bone tissue engineering using electrospun beads-on-string fibers,” *Int. J. Artif. Organs*, vol. 47, no. 8, pp. 642–649, Aug. 2024, doi: 10.1177/03913988241268033.

[78] T. Baudequin *et al.*, “The Osteogenic and Tenogenic Differentiation Potential of C3H10T1/2 (Mesenchymal Stem Cell Model) Cultured on PCL/PLA Electrospun Scaffolds in the Absence of Specific Differentiation Medium,” *Materials*, vol. 10, no. 12, p. 1387, Dec. 2017, doi: 10.3390/MA10121387.

[79] E. Daskalakis *et al.*, “Accelerated Degradation of Poly-ε-caprolactone Composite Scaffolds for Large Bone Defects,” *Polymers (Basel).*, vol. 15, no. 3, Feb. 2023, doi: 10.3390/POLYM15030670.

[80] M. Nagrath, A. Alhalawani, A. Rahimnejad Yazdi, and M. R. Towler, “Bioactive glass fiber fabrication via a combination of sol-gel process with electro-spinning technique,” *Materials Science and Engineering: C*, vol. 101, pp. 521–538, Aug. 2019, doi: 10.1016/J.MSEC.2019.04.003.

[81] H. Lu, T. Zhang, X. P. Wang, and Q. F. Fang, “Electrospun submicron bioactive glass fibers for bone tissue scaffold,” *Journal of Materials Science: Materials in Medicine*, vol. 20, no. 3, pp. 793–798, Nov. 2008, doi: 10.1007/S10856-008-3649-1.

[82] M. Shams, M. Karimi, M. Ghollasi, N. Nezafati, and A. Salimi, “Electrospun poly-l-lactic acid nanofibers decorated with melt-derived S53P4 bioactive glass nanoparticles: The effect of nanoparticles on proliferation and osteogenic differentiation of human bone marrow mesenchymal stem cells in vitro,” *Ceram. Int.*, vol. 44, no. 16, pp. 20211–20219, Nov. 2018, doi: 10.1016/J.CERAMINT.2018.08.005.

[83] G. Hochleitner, M. Kessler, M. Schmitz, A. R. Boccaccini, J. Teβmar, and J. Groll, “Melt electrospinning writing of defined scaffolds using polylactide-poly(ethylene glycol) blends with 45S5 bioactive glass particles,” *Mater. Lett.*, vol. 205, pp. 257–260, Oct. 2017, doi: 10.1016/J.MATLET.2017.06.096.

[84] D. Moura *et al.*, “Development of a bioactive glass-polymer composite for wound healing applications,” *Materials Science and Engineering: C*, vol. 76, pp. 224–232, Jul. 2017, doi: 10.1016/J.MSEC.2017.03.037.

[85] M. Luginina, K. Schuhladen, R. Orrú, G. Cao, A. R. Boccaccini, and L. Liverani, “Electrospun PCL/PGS Composite Fibers Incorporating Bioactive Glass Particles for Soft

Tissue Engineering Applications," *Nanomaterials*, vol. 10, no. 5, p. 978, May 2020, doi: 10.3390/NANO10050978.

[86] C. H. Kim, M. S. Khil, H. Y. Kim, H. U. Lee, and K. Y. Jahng, "An improved hydrophilicity via electrospinning for enhanced cell attachment and proliferation," *J. Biomed. Mater. Res. B Appl. Biomater.*, vol. 78B, no. 2, pp. 283–290, Aug. 2006, doi: 10.1002/JBM.B.30484.

[87] I. Tiyek, A. Gunduz, F. Yalcinkaya, and J. Chaloupek, "Influence of Electrospinning Parameters on the Hydrophilicity of Electrospun Polycaprolactone Nanofibres," *J. Nanosci. Nanotechnol.*, vol. 19, no. 11, pp. 7251–7260, May 2019, doi: 10.1166/JNN.2019.16605.

[88] R. Sergi, D. Bellucci, R. Salvatori, A. Anesi, and V. Cannillo, "A Novel Bioactive Glass Containing Therapeutic Ions with Enhanced Biocompatibility," *Materials,* vol. 13, no. 20, pp. 1–16, Oct. 2020, doi: 10.3390/MA13204600.

[89] M. N. Rahaman *et al.*, "Bioactive glass in tissue engineering," *Acta Biomater.*, vol. 7, no. 6, p. 2355, 2011, doi: 10.1016/J.ACTBIO.2011.03.016.

[90] A. R. Boccaccini, M. Erol, W. J. Stark, D. Mohn, Z. Hong, and J. F. Mano, "Polymer/bioactive glass nanocomposites for biomedical applications: A review," *Compos. Sci. Technol.*, vol. 70, no. 13, pp. 1764–1776, Nov. 2010, doi: 10.1016/J.COMPSCITECH.2010.06.002.

[91] E. Norris *et al.*, "Electrospinning 3D bioactive glasses for wound healing," *Biomedical Materials*, vol. 15, no. 1, p. 015014, Feb. 2020, doi: 10.1088/1748-605X/AB591D.

[92] P. V. Giannoudis, H. Dinopoulos, and E. Tsiridis, "Bone substitutes: An update," *Injury*, vol. 36, no. 3, pp. S20–S27, Nov. 2005, doi: 10.1016/J.INJURY.2005.07.029.

[93] O. Guillon, S. Cao, J. Chang, L. Wondraczek, and A. R. Boccaccini, "Effect of uniaxial load on the sintering behaviour of 45S5 Bioglass® powder compacts," *J. Eur. Ceram. Soc.*, vol. 31, no. 6, pp. 999–1007, Jun. 2011, doi: 10.1016/j.jeurceramsoc.2010.12.031.

[94] P. Deb, A. B. Deoghare, A. Borah, E. Barua, and S. Das Lala, "Scaffold Development Using Biomaterials: A Review," *Mater. Today Proc.*, vol. 5, no. 5, pp. 12909–12919, Jan. 2018, doi: 10.1016/J.MATPR.2018.02.276.

[95] A. Kumar Srivastava and R. Pyare, "Characterization of ZnO Substituted 45S5 Bioactive Glasses and Glass-Ceramics," *Journal of Materials Science Research*, vol. 1, no. 2, 2012, doi: 10.5539/jmsr.v1n2p207.

[96] V. Cannillo and A. Sola, "Potassium-based composition for a bioactive glass," *Ceram. Int.*, vol. 35, no. 8, pp. 3389–3393, Dec. 2009, doi: 10.1016/J.CERAMINT.2009.06.011.

[97] K. Fujikura, N. Karpukhina, T. Kasuga, D. S. Brauer, R. G. Hill, and R. V. Law, "Influence of strontium substitution on structure and crystallisation of Bioglass® 45S5," *J. Mater. Chem.*, vol. 22, no. 15, pp. 7395–7402, Mar. 2012, doi: 10.1039/C2JM14674F.

[98] S. R. Gavinho *et al.*, "Bioactive Glasses Containing Strontium or Magnesium Ions to Enhance the Biological Response in Bone Regeneration," *Nanomaterials*, vol. 13, no. 19, p. 2717, Oct. 2023, doi: 10.3390/NANO13192717/S1.

[99] A. R. Boccaccini, Q. Chen, L. Lefebvre, L. Gremillard, and J. Chevalier, “Sintering, crystallisation and biodegradation behaviour of Bioglass®-derived glass–ceramics,” *Faraday Discuss.*, vol. 136, no. 0, pp. 27–44, Aug. 2007, doi: 10.1039/B616539G.

[100] J. R. Jones, E. Gentleman, and J. Polak, “Bioactive glass scaffolds for bone regeneration,” *Elements*, vol. 3, no. 6, pp. 393–399, 2007, doi: 10.2113/GSELEMENTS.3.6.393.

[101] D. Bellucci, V. Cannillo, A. Sola, F. Chiellini, M. Gazzarri, and C. Migone, “Macroporous Bioglass®-derived scaffolds for bone tissue regeneration,” *Ceram. Int.*, vol. 37, no. 5, pp. 1575–1585, 2011, doi: 10.1016/j.ceramint.2011.01.023.

[102] Q. Chen, D. Mohn, and W. J. Stark, “Optimization of Bioglass® Scaffold Fabrication Process,” *Journal of the American Ceramic Society*, vol. 94, no. 12, pp. 4184–4190, Dec. 2011, doi: 10.1111/J.1551-2916.2011.04766.X.

[103] E. A. Aguilar-Reyes, C. A. León-Patiño, E. Villicaña-Molina, V. I. Macías-Andrés, and L. P. Lefebvre, “Processing and in vitro bioactivity of high-strength 45S5 glass-ceramic scaffolds for bone regeneration,” *Ceram. Int.*, vol. 43, no. 9, pp. 6868–6875, 2017, doi: 10.1016/j.ceramint.2017.02.107.

[104] Q. Z. Chen, I. D. Thompson, and A. R. Boccaccini, “45S5 Bioglass®-derived glass–ceramic scaffolds for bone tissue engineering,” *Biomaterials*, vol. 27, no. 11, pp. 2414–2425, Apr. 2006, doi: 10.1016/J.BIOMATERIALS.2005.11.025.

[105] S. Bose, M. Roy, and A. Bandyopadhyay, “Recent advances in bone tissue engineering scaffolds,” *Trends Biotechnol.*, vol. 30, no. 10, pp. 546–554, Oct. 2012, doi: 10.1016/J.TIBTECH.2012.07.005.

[106] L. C. Gerhardt and A. R. Boccaccini, “Bioactive Glass and Glass-Ceramic Scaffolds for Bone Tissue Engineering,” *Materials*, vol. 3, no. 7, pp. 3867–3910, Jul. 2010, doi: 10.3390/MA3073867.

[107] E. Fiume, S. Ciavattini, E. Verné, and F. Baino, “Foam Replica Method in the Manufacturing of Bioactive Glass Scaffolds: Out-of-Date Technology or Still Underexploited Potential?,” *Materials*, vol. 14, no. 11, 2021, doi: 10.3390/MA14112795.

[108] D. Bellucci, A. Sola, P. Gentile, G. Ciardelli, and V. Cannillo, “Biomimetic coating on bioactive glass-derived scaffolds mimicking bone tissue,” *J. Biomed. Mater. Res. A*, vol. 100 A, no. 12, pp. 3259–3266, 2018, doi: 10.1002/JBM.A.34271.

[109] H. Hornberger, S. Virtanen, and A. R. Boccaccini, “Biomedical coatings on magnesium alloys – A review,” *Acta Biomater.*, vol. 8, no. 7, pp. 2442–2455, Jul. 2012, doi: 10.1016/J.ACTBIO.2012.04.012.

[110] J. Henao, C. Poblano-Salas, M. Monsalve, J. Corona-Castuera, and O. Barceinas-Sanchez, “Bio-active glass coatings manufactured by thermal spray: a status report,” *Journal of Materials Research and Technology*, vol. 8, no. 5, pp. 4965–4984, Sep. 2019, doi: 10.1016/J.JMRT.2019.07.011.

[111] B. Garrido, S. Dosta, and I. G. Cano, “Bioactive glass coatings obtained by thermal spray: Current status and future challenges,” *Boletín de la Sociedad Española de Cerámica y Vidrio*, vol. 61, no. 5, pp. 516–530, Sep. 2022, doi: 10.1016/J.BSECV.2021.04.001.

[112] C. Y. Tang, C. P. Tsui, D. J. Janackovic, and P. S. Uskokovic, “Nanomechanical properties evaluation of bioactive glass coatings on titanium alloy substrate,” *Journal of Optoelectronics and Advanced Materials*, vol. 8, no. 3, pp. 1194–1199, 2006.

[113] L. Pawlowski, “The Science and Engineering of Thermal Spray Coatings: Second Edition,” *The Science and Engineering of Thermal Spray Coatings: Second Edition*, pp. 1–626, Mar. 2008, doi: 10.1002/9780470754085.

[114] C. Gabbi, A. Cacchioli, B. Locardi, and E. Guadagnino, “Bioactive glass coating: physicochemical aspects and biological findings,” *Biomaterials*, vol. 16, no. 7, pp. 515–520, May 1995, doi: 10.1016/0142-9612(95)91123-G.

[115] M. Krzyzanowski, S. Bajda, Y. Liu, A. Triantaphyllou, W. Mark Rainforth, and M. Glendenning, “3D analysis of thermal and stress evolution during laser cladding of bioactive glass coatings,” *J. Mech. Behav. Biomed. Mater.*, vol. 59, pp. 404–417, Jun. 2016, doi: 10.1016/J.JMBBM.2016.02.023.

[116] S. Foppiano, S. J. Marshall, E. Saiz, A. P. Tomsia, and G. W. Marshall, “Functionally graded bioactive coatings: Reproducibility and stability of the coating under cell culture conditions,” *Acta Biomater.*, vol. 2, no. 2, pp. 133–142, Mar. 2006, doi: 10.1016/J.ACTBIO.2005.12.003.

[117] R. G. T. Geesink, “Experimental and clinical experience with hydroxyapatitie-coated hip implants,” *Orthopedics*, vol. 12, no. 9, pp. 1239–1242, 1989, doi: 10.3928/0147-7447-19890901-13.

[118] L. Sun, C. C. Berndt, K. A. Gross, and A. Kucuk, “Material fundamentals and clinical performance of plasma-sprayed hydroxyapatite coatings: A review,” *J. Biomed. Mater. Res.*, vol. 58, no. 5, pp. 570–592, 2001, doi: 10.1002/JBM.1056.

[119] R. Famery, N. Richard, and P. Boch, “Preparation of α- and β-tricalcium phosphate ceramics, with and without magnesium addition,” *Ceram. Int.*, vol. 20, no. 5, pp. 327–336, Jan. 1994, doi: 10.1016/0272-8842(94)90050-7.

[120] P. Habibovic, T. M. Sees, M. A. Van Den Doel, C. A. Van Blitterswijk, and K. De Groot, “Osteoinduction by biomaterials—Physicochemical and structural influences,” *J. Biomed. Mater. Res. A*, vol. 77A, no. 4, pp. 747–762, Jun. 2006, doi: 10.1002/JBM.A.30712.

[121] A. Sola, D. Bellucci, M. G. Raucci, S. Zeppetelli, L. Ambrosio, and V. Cannillo, “Heat treatment of Na_2O-CaO-P_2O_5-SiO_2 bioactive glasses: Densification processes and postsintering bioactivity,” *J. Biomed. Mater. Res. A*, vol. 100A, no. 2, pp. 305–322, Feb. 2012, doi: 10.1002/JBM.A.33276.

[122] E. B. Nery, R. Z. LeGeros, K. L. Lynch, and K. Lee, “Tissue Response to Biphasic Calcium Phosphate Ceramic With Different Ratios of HA/βTCP in Periodontal Osseous Defects,” *J. Periodontol.*, vol. 63, no. 9, pp. 729–735, Sep. 1992, doi: 10.1902/JOP.1992.63.9.729.

[123] I. D. Thompson and L. L. Hench, “Mechanical properties of bioactive glasses, glass-ceramics and composites,” 1998.

[124] L. J. Jha, J. D. Santos, and J. C. Knowles3, “Characterization of apatite layer formation on P_2O_5-CaO, P_2O_5-CaO-Na_2O, and P_2O_5=CaO-Na_20-$A1_2O_3$ glass hydroxyapatite composites”, doi: 10.1002/(SICI)1097-4636(199608)31:4.

[125] J. C. Knowles and W. Bonfield, “Development of a glass reinforced hydroxyapatite with enhanced mechanical properties. The effect of glass composition on mechanical properties and its relationship to phase changes,” *J. Biomed. Mater. Res.*, vol. 27, no. 12, pp. 1591–1598, Dec. 1993, doi: 10.1002/JBM.820271217.

[126] J. C. Knowles, S. Talal, and J. D. Santos, “Sintering effects in a glass reinforced hydroxyapatite,” *Biomaterials*, vol. 17, no. 14, pp. 1437–1442, Jul. 1996, doi: 10.1016/0142-9612(96)87287-5.

[127] F. Baino, S. Caddeo, and C. Vitale-Brovarone, “Sintering effects of bioactive glass incorporation in tricalcium phosphate scaffolds,” *Mater. Lett.*, vol. 274, p. 128010, Sep. 2020, doi: 10.1016/J.MATLET.2020.128010.

[128] I. Cacciotti, “Multisubstituted hydroxyapatite powders and coatings: The influence of the codoping on the hydroxyapatite performances,” *Int. J. Appl. Ceram. Technol.*, vol. 16, no. 5, pp. 1864–1884, Sep. 2019, doi: 10.1111/IJAC.13229.

[129] D. Bellucci, A. Sola, and V. Cannillo, “Hydroxyapatite and tricalcium phosphate composites with bioactive glass as second phase: State of the art and current applications,” *J. Biomed. Mater. Res. A*, vol. 104, no. 4, pp. 1030–1056, Apr. 2016, doi: 10.1002/JBM.A.35619.

[130] A. T. Contreras Jaimes *et al.*, “Deepening our understanding of bioactive glass crystallization using TEM and 3D nano-CT,” *J. Eur. Ceram. Soc.*, vol. 41, no. 9, pp. 4958–4969, Aug. 2021, doi: 10.1016/J.JEURCERAMSOC.2021.02.051.

[131] O. Peitl, E. Dutra Zanotto, and L. L. Hench, “Highly bioactive P_2O_5–Na_2O–CaO–SiO_2 glass-ceramics,” *J. Non. Cryst. Solids*, vol. 292, no. 1–3, pp. 115–126, Nov. 2001, doi: 10.1016/S0022-3093(01)00822-5.

[132] M. U. Hashmi, S. A. Shah, and A. S. Elkady, “Effect of sintering time on crystallization, densification and in-vitro characteristics of bioactive glass ceramics,” *Certified International Journal of Engineering Science and Innovative Technology (IJESIT)*, vol. 9001, no. 1, pp. 2319–5967, 2008.

[133] F. Döhler, D. Groh, S. Chiba, J. Bierlich, J. Kobelke, and D. S. Brauer, “Bioactive glasses with improved processing. Part 2. Viscosity and fibre drawing,” *J. Non. Cryst. Solids*, vol. 432, pp. 130–136, Jan. 2016, doi: 10.1016/J.JNONCRYSOL.2015.03.009.

[134] H. Arstila, E. Vedel, L. Hupa, and M. Hupa, “Factors affecting crystallization of bioactive glasses,” *J. Eur. Ceram. Soc.*, vol. 27, no. 2–3, pp. 1543–1546, Jan. 2007, doi: 10.1016/J.JEURCERAMSOC.2006.04.017.

[135] H. Arstila, L. Hupa, K. H. Karlsson, and M. Hupa, “Influence of heat treatment on crystallization of bioactive glasses,” *J. Non. Cryst. Solids*, vol. 354, no. 2–9, pp. 722–728, Jan. 2008, doi: 10.1016/J.JNONCRYSOL.2007.06.092.

[136] J. Massera, S. Fagerlund, L. Hupa, and M. Hupa, “Crystallization Mechanism of the Bioactive Glasses, 45S5 and S53P4,” *Journal of the American Ceramic Society*, vol. 95, no. 2, pp. 607–613, Feb. 2012, doi: 10.1111/J.1551-2916.2011.05012.X.

[137] L. Lefebvre *et al.*, “Structural transformations of bioactive glass 45S5 with thermal treatments,” *Acta Mater.*, vol. 55, no. 10, pp. 3305–3313, Jun. 2007, doi: 10.1016/J.ACTAMAT.2007.01.029.

[138] D. C. Clupper and L. L. Hench, “Crystallization kinetics of tape cast bioactive glass 45S5,” *J. Non. Cryst. Solids*, vol. 318, no. 1–2, pp. 43–48, Apr. 2003, doi: 10.1016/S0022-3093(02)01857-4.

[139] C.-C. Lin, L.-C. Huang, and P. Shen, “$Na_2CaSi_2O_6$-P_2O_5 based bioactive glasses. Part 1: Elasticity and structure”, doi: 10.1016/j.jnoncrysol.2005.08.020.

[140] D. Bellucci, V. Cannillo, and A. Sola, “An overview of the effects of thermal processing on bioactive glasses,” *Science of Sintering*, vol. 42, no. 3, pp. 307–320, 2010, doi: 10.2298/SOS1003307B.

[141] F. Thiimmler and W. Thomma, “The sintering process,” *Metallurgical Reviews*, vol. 12, no. 1, pp. 69–108, 1967.

[142] O. Bretcanu, X. Chatzistavrou, K. Paraskevopoulos, R. Conradt, I. Thompson, and A. R. Boccaccini, “Sintering and crystallisation of 45S5 Bioglass® powder,” *J. Eur. Ceram. Soc.*, vol. 29, no. 16, pp. 3299–3306, Dec. 2009, doi: 10.1016/J.JEURCERAMSOC.2009.06.035.

[143] X. X. Li, C. Yang, T. Chen, L. C. Zhang, M. D. Hayat, and P. Cao, “Influence of powder shape on atomic diffusivity and resultant densification mechanisms during spark plasma sintering,” *J. Alloys Compd.*, vol. 802, pp. 600–608, Sep. 2019, doi: 10.1016/j.jallcom.2019.06.176.

[144] Q. Z. Chen, A. R. Boccaccini, H. B. Zhang, D. Z. Wang, and M. J. Edirisinghe, “Improved Mechanical Reliability of Bone Tissue Engineering (Zirconia) Scaffolds by Electrospraying,” *Journal of the American Ceramic Society*, vol. 89, no. 5, pp. 1534–1539, May 2006, doi: 10.1111/J.1551-2916.2006.00935.X.

[145] I. Cacciotti, M. Lombardi, A. Bianco, A. Ravaglioli, and L. Montanaro, “Sol-gel derived 45S5 bioglass: synthesis, microstructural evolution and thermal behaviour,” *J. Mater. Sci. Mater. Med.*, vol. 23, no. 8, pp. 1849–1866, Aug. 2012, doi: 10.1007/S10856-012-4667-6.

[146] M. Lombardi *et al.*, “A Comparative Study between Melt-Derived and Sol-Gel Synthesized 45S5 Bioactive Glasses,” *Key Eng. Mater.*, vol. 541, pp. 15–30, Feb. 2013, doi: 10.4028/WWW.SCIENTIFIC.NET/KEM.541.15.

[147] Q. Nawaz *et al.*, "New insights into the crystallization process of sol-gel–derived 45S5 bioactive glass," *Journal of the American Ceramic Society*, vol. 103, no. 8, pp. 4234–4247, Aug. 2020, doi: 10.1111/JACE.17124.

[148] L. L. Hench, G. P. LaTorre, and Ö. H. Andersson, "The Kinetics of Bioactive Ceramics Part III: Surface Reactions for Bioactive Glasses compared with an Inactive Glass," *Bioceramics*, pp. 155–162, Jan. 1991, doi: 10.1016/B978-0-7506-0269-3.50025-6.

[149] S. Fagerlund, J. Massera, N. Moritz, L. Hupa, and M. Hupa, "Phase composition and in vitro bioactivity of porous implants made of bioactive glass S53P4," *Acta Biomater.*, vol. 8, no. 6, pp. 2331–2339, Jul. 2012, doi: 10.1016/J.ACTBIO.2012.03.011.

[150] X. Liu, M. N. Rahaman, G. E. Hilmas, and B. S. Bal, "Mechanical properties of bioactive glass (13-93) scaffolds fabricated by robotic deposition for structural bone repair," *Acta Biomater.*, vol. 9, no. 6, pp. 7025–7034, Jun. 2013, doi: 10.1016/J.ACTBIO.2013.02.026.

[151] H. Niiranen and P. Törmälä, "Bioabsorbable polymer plates coated with bioactive glass spheres," *J. Mater. Sci. Mater. Med.*, vol. 10, no. 12, pp. 707–710, 1999, doi: 10.1023/A:1008966820264.

[152] Q. Fu, M. N. Rahaman, B. S. Bal, W. Huang, and D. E. Day, "Preparation and bioactive characteristics of a porous 13–93 glass, and fabrication into the articulating surface of a proximal tibia," *J. Biomed. Mater. Res. A*, vol. 82A, no. 1, pp. 222–229, Jul. 2007, doi: 10.1002/JBM.A.31156.

[153] S. Fagerlund, J. Massera, M. Hupa, and L. Hupa, "T-T-T behaviour of bioactive glasses 1-98 and 13-93," *J. Eur. Ceram. Soc.*, vol. 32, no. 11, pp. 2731–2738, Aug. 2012, doi: 10.1016/J.JEURCERAMSOC.2011.10.040.

[154] D. Angioni, R. Orrù, G. Cao, S. Garroni, D. Bellucci, and V. Cannillo, "Bioactivity enhancement by a ball milling treatment in novel bioactive glass-hydroxyapatite composites produced by spark plasma sintering," *J. Eur. Ceram. Soc.*, vol. 43, no. 3, pp. 1220–1229, Mar. 2023, doi: 10.1016/J.JEURCERAMSOC.2022.10.077.

[155] D. Bellucci, R. Salvatori, A. Anesi, L. Chiarini, and V. Cannillo, "SBF assays, direct and indirect cell culture tests to evaluate the biological performance of bioglasses and bioglass-based composites: Three paradigmatic cases," *Materials Science and Engineering C*, vol. 96, pp. 757–764, Mar. 2019, doi: 10.1016/j.msec.2018.12.006.

[156] D. Bellucci, E. Veronesi, M. Dominici, and V. Cannillo, "On the in Vitro Biocompatibility Testing of Bioactive Glasses," *Materials*, vol. 13, no. 8, p. 1816, Apr. 2020, doi: 10.3390/MA13081816.

[157] F. Westhauser *et al.*, "Bioactive Glass (BG) ICIE16 Shows Promising Osteogenic Properties Compared to Crystallized 45S5-BG," *International Journal of Molecular Sciences 2020*, vol. 21, no. 5, p. 1639, Feb. 2020, doi: 10.3390/IJMS21051639.

[158] Z. Y. Wu, R. G. Hill, S. Yue, D. Nightingale, P. D. Lee, and J. R. Jones, "Melt-derived bioactive glass scaffolds produced by a gel-cast foaming technique," *Acta Biomater.*, vol. 7, no. 4, pp. 1807–1816, Apr. 2011, doi: 10.1016/J.ACTBIO.2010.11.041.

[159] A. Nommeots-Nomm *et al.*, "Highly degradable porous melt-derived bioactive glass foam scaffolds for bone regeneration," *Acta Biomater.*, vol. 57, pp. 449–461, Jul. 2017, doi: 10.1016/J.ACTBIO.2017.04.030.

[160] Y. Onodera *et al.*, "Origin of the mixed alkali effect in silicate glass," *NPG Asia Materials*, vol. 11, no. 1, pp. 1–11, Dec. 2019, doi: 10.1038/s41427-019-0180-4.

[161] M. C. Crovace *et al.*, "Understanding the mixed alkali effect on the sinterability and in vitro performance of bioactive glasses," *J. Eur. Ceram. Soc.*, vol. 41, no. 7, pp. 4391–4405, Jul. 2021, doi: 10.1016/J.JEURCERAMSOC.2020.11.020.

[162] A. Moghanian, S. Firoozi, and M. Tahriri, "Synthesis and in vitro studies of sol-gel derived lithium substituted 58S bioactive glass," *Ceram. Int.*, vol. 43, no. 15, pp. 12835–12843, Oct. 2017, doi: 10.1016/J.CERAMINT.2017.06.174.

[163] A. L. B. Maçon *et al.*, "Lithium-silicate sol–gel bioactive glass and the effect of lithium precursor on structure–property relationships," *J. Solgel Sci. Technol.*, vol. 81, no. 1, pp. 84–94, Jan. 2017, doi: 10.1007/S10971-016-4097-X.

[164] A. Marikani, A. Maheswaran, M. Premanathan, and L. Amalraj, "Synthesis and characterization of calcium phosphate based bioactive quaternary P_2O_5–CaO–Na_2O–K_2O glasses," *J. Non. Cryst. Solids*, vol. 354, no. 33, pp. 3929–3934, Sep. 2008, doi: 10.1016/J.JNONCRYSOL.2008.05.005.

[165] D. Bellucci, V. Cannillo, and A. Sola, "Calcium and potassium addition to facilitate the sintering of bioactive glasses," *Mater. Lett.*, vol. 65, no. 12, pp. 1825–1827, Jun. 2011, doi: 10.1016/J.MATLET.2011.03.060.

[166] J. Massera and L. Hupa, "Influence of SrO substitution for CaO on the properties of bioactive glass S53P4," *J. Mater. Sci. Mater. Med.*, vol. 25, no. 3, pp. 657–668, 2014, doi: 10.1007/S10856-013-5120-1.

[167] D. Bellucci, A. Sola, R. Salvatori, A. Anesi, L. Chiarini, and V. Cannillo, "Role of magnesium oxide and strontium oxide as modifiers in silicate-based bioactive glasses: Effects on thermal behaviour, mechanical properties and in-vitro bioactivity," *Materials Science and Engineering: C*, vol. 72, pp. 566–575, Mar. 2017, doi: 10.1016/J.MSEC.2016.11.110.

[168] M. Diba, F. Tapia, A. R. Boccaccini, and L. A. Strobel, "Magnesium-Containing Bioactive Glasses for Biomedical Applications," *Int. J. Appl. Glass Sci.*, vol. 3, no. 3, pp. 221–253, Sep. 2012, doi: 10.1111/J.2041-1294.2012.00095.X.

[169] E. Jallot and P. Moretto, "Characterisation, by the PIXE Method, of Trace Elements During Physicochemical Reactions at the Periphery of Bioactive Glass Pastilles in Contact with Biological Fluids," *Instrumentation Science & Technology*, vol. 34, no. 4, pp. 405–416, Aug. 2006, doi: 10.1080/10739140600648803.

[170] J. Perez-Pariente, F. Balas, and M. Vallet-Regi, "Surface and chemical study of SiO2·P2O5·CaO·(MgO) bioactive glasses," *Chemistry of Materials*, vol. 12, no. 3, pp. 750–755, 2000, doi: 10.1021/CM9911114.

[171] R. Sergi, D. Bellucci, R. Salvatori, G. Maisetta, G. Batoni, and V. Cannillo, "Zinc containing bioactive glasses with ultra-high crystallization temperature, good biological performance and antibacterial effects," *Materials Science and Engineering: C*, vol. 104, p. 109910, Nov. 2019, doi: 10.1016/J.MSEC.2019.109910.

[172] S. Shruti *et al.*, "Structural and in vitro study of cerium, gallium and zinc containing sol–gel bioactive glasses," *J. Mater. Chem.*, vol. 22, no. 27, pp. 13698–13706, Jun. 2012, doi: 10.1039/C2JM31767B.

[173] R. Wetzel, O. Bartzok, L. Hupa, and D. S. Brauer, "Low Mg or Zn substitution for improved thermal properties of Bioglass 45S5," *Mater. Lett.*, vol. 256, p. 126599, Dec. 2019, doi: 10.1016/J.MATLET.2019.126599.

[174] R. Wetzel, M. Blochberger, F. Scheffler, L. Hupa, and D. S. Brauer, "Mg or Zn for Ca substitution improves the sintering of bioglass 45S5," *Scientific Reports*, vol. 10, no. 1, pp. 1–10, Sep. 2020, doi: 10.1038/s41598-020-72091-7.

[175] S. K. Arepalli *et al.*, "Influence of barium substitution on bioactivity, thermal and physico-mechanical properties of bioactive glass," *Materials Science and Engineering: C*, vol. 49, pp. 549–559, Apr. 2015, doi: 10.1016/J.MSEC.2015.01.049.

[176] M. Khoeini, S. Hesaraki, and A. Kolahi, "Effect of BaO substitution for CaO on the structural and thermal properties of SiO_2–B_2O_3–Al_2O_3–CaO–Na_2O–P_2O_5 bioactive glass system used for implant coating applications," *Ceram. Int.*, vol. 47, no. 22, pp. 31666–31680, Nov. 2021, doi: 10.1016/J.CERAMINT.2021.08.046.

[177] V. K. Vyas, A. Sampath Kumar, S. P. Singh, and R. Pyare, "Effect of Cobalt Oxide Substitution on Mechanical Behaviour and Elastic Properties of Bioactive Glass and Glass-Ceramics," *Transactions of the Indian Ceramic Society*, vol. 75, no. 1, pp. 12–19, Jan. 2016, doi: 10.1080/0371750X.2016.1149098.

[178] S. Kargozar *et al.*, "Synthesis, physico-chemical and biological characterization of strontium and cobalt substituted bioactive glasses for bone tissue engineering," *J. Non. Cryst. Solids*, vol. 449, pp. 133–140, Oct. 2016, doi: 10.1016/J.JNONCRYSOL.2016.07.025.

[179] T. Y. Kang, J. Y. Seo, J. H. Ryu, K. M. Kim, and J. S. Kwon, "Improvement of the mechanical and biological properties of bioactive glasses by the addition of zirconium oxide (ZrO2) as a synthetic bone graft substitute," *J. Biomed. Mater. Res. A*, vol. 109, no. 7, pp. 1196–1208, Jul. 2021, doi: 10.1002/JBM.A.37113.

[180] A. Moghanian, M. Zohourfazeli, and M. H. M. Tajer, "The effect of zirconium content on in vitro bioactivity, biological behavior and antibacterial activity of sol-gel derived 58S bioactive glass," *J. Non. Cryst. Solids*, vol. 546, p. 120262, Oct. 2020, doi: 10.1016/J.JNONCRYSOL.2020.120262.

[181] L. Drago *et al.*, "In vitro antibiofilm activity of bioactive glass S53P4," *Future Microbiol.*, vol. 9, no. 5, pp. 593–601, 2014, doi: 10.2217/FMB.14.20.

[182] M. Bellantone, H. D. Williams, and L. L. Hench, “Broad-spectrum bactericidal activity of Ag2O-doped bioactive glass,” *Antimicrob. Agents Chemother.*, vol. 46, no. 6, pp. 1940–1945, 2002, doi: 10.1128/AAC.46.6.1940-1945.2002.

[183] S. Begum, W. E. Johnson, T. Worthington, and R. A. Martin, “The influence of pH and fluid dynamics on the antibacterial efficacy of 45S5 Bioglass,” *Biomed. Mater.*, vol. 11, no. 1, Feb. 2016, doi: 10.1088/1748-6041/11/1/015006.

[184] P. Zhou, B. L. Garcia, and G. A. Kotsakis, “Comparison of antibacterial and antibiofilm activity of bioactive glass compounds S53P4 and 45S5,” *BMC Microbiol.*, vol. 22, no. 1, pp. 1–12, Dec. 2022, doi: 10.1186/S12866-022-02617-8.

[185] M. Vincent, R. E. Duval, P. Hartemann, and M. Engels-Deutsch, “Contact killing and antimicrobial properties of copper,” *J. Appl. Microbiol.*, vol. 124, no. 5, pp. 1032–1046, May 2018, doi: 10.1111/JAM.13681.

[186] R. M. Slawson, H. Lee, and J. T. Trevors, “Bacterial interactions with silver,” *Biol. Met.*, vol. 3, no. 3–4, pp. 151–154, Sep. 1990, doi: 10.1007/BF01140573.

[187] D. Arcos and M. Vallet-Regí, “Sol–gel silica-based biomaterials and bone tissue regeneration,” *Acta Biomater.*, vol. 6, no. 8, pp. 2874–2888, Aug. 2010, doi: 10.1016/J.ACTBIO.2010.02.012.

[188] S. Kargozar, M. Montazerian, S. Hamzehlou, H. W. Kim, and F. Baino, “Mesoporous bioactive glasses: Promising platforms for antibacterial strategies,” *Acta Biomater.*, vol. 81, pp. 1–19, Nov. 2018, doi: 10.1016/J.ACTBIO.2018.09.052.

[189] V. Mortazavi, M. Mehdikhani Nahrkhalaji, M. H. Fathi, S. B. Mousavi, and B. Nasr Esfahani, “Antibacterial effects of sol-gel-derived bioactive glass nanoparticle on aerobic bacteria,” *J. Biomed. Mater. Res. A*, vol. 94A, no. 1, pp. 160–168, Jul. 2010, doi: 10.1002/JBM.A.32678.

[190] “ISO 22196:2011 - Measurement of antibacterial activity on plastics and other non-porous surfaces.” Accessed: Dec. 22, 2025. [Online]. Available: https://www.iso.org/standard/54431.html

[191] Japan Standards Association (JSA), “JIS Z 2801: Antibacterial products -- Test for antibacterial activity and efficacy: Japan Standards Association (JSA).” Accessed: Dec. 23, 2025. [Online]. Available: https://archive.org/details/jis.z.2801.e.2010

[192] J. Sjollema *et al.*, “In vitro methods for the evaluation of antimicrobial surface designs,” *Acta Biomater.*, vol. 70, pp. 12–24, Apr. 2018, doi: 10.1016/J.ACTBIO.2018.02.001.

[193] Advancing Standards Transforming Markets (ASTM), “ASTM E2149-20 Standard Test Method for Determining the Antimicrobial Activity of Antimicrobial Agents Under Dynamic Contact Conditions,” 2025. Accessed: Dec. 23, 2025. [Online]. Available: https://store.astm.org/e2149-20.html

[194] R. Kaur and S. Liu, “Antibacterial surface design – Contact kill,” *Prog. Surf. Sci.*, vol. 91, no. 3, pp. 136–153, Aug. 2016, doi: 10.1016/J.PROGSURF.2016.09.001.

[195] A. J. Cunliffe *et al.*, “How Do We Determine the Efficacy of an Antibacterial Surface? A Review of Standardised Antibacterial Material Testing Methods,” *Antibiotics 2021, Vol. 10, Page 1069*, vol. 10, no. 9, p. 1069, Sep. 2021, doi: 10.3390/ANTIBIOTICS10091069.

[196] J. Azeredo *et al.*, “Critical review on biofilm methods,” *Crit. Rev. Microbiol.*, vol. 43, no. 3, pp. 313–351, May 2017, doi: 10.1080/1040841X.2016.1208146.

[197] S. Hu, J. Chang, M. Liu, and C. Ning, “Study on antibacterial effect of 45S5 Bioglass®,” *J. Mater. Sci. Mater. Med.*, vol. 20, no. 1, pp. 281–286, Jan. 2009, doi: 10.1007/S10856-008-3564-5.

[198] O. Leppäranta *et al.*, “Antibacterial effect of bioactive glasses on clinically important anaerobic bacteria in vitro,” *J. Mater. Sci. Mater. Med.*, vol. 19, no. 2, pp. 547–551, Feb. 2008, doi: 10.1007/S10856-007-3018-5.

[199] D. C. Coraça-Huber, M. Fille, J. Hausdorfer, D. Putzer, and M. Nogler, “Efficacy of antibacterial bioactive glass S53P4 against S. aureus biofilms grown on titanium discs in vitro,” *Journal of Orthopaedic Research*, vol. 32, no. 1, pp. 175–177, Jan. 2014, doi: 10.1002/JOR.22463.

[200] T. F. Passos, M. T. Souza, E. D. Zanotto, and C. W. O. de Souza, “Bactericidal activity and biofilm inhibition of F18 bioactive glass against Staphylococcus aureus,” *Materials Science and Engineering: C*, vol. 118, p. 111475, Jan. 2021, doi: 10.1016/J.MSEC.2020.111475.

[201] P. R. Gabbai-Armelin *et al.*, “Characterization and biocompatibility of a fibrous glassy scaffold,” *J. Tissue Eng. Regen. Med.*, vol. 11, no. 4, pp. 1141–1151, Apr. 2017, doi: 10.1002/TERM.2017.

[202] B. M. Elmowafy *et al.*, “Effect of copper and zinc oxide doping in 13–93B3 borate glass for enhanced wound healing,” *Ceram. Int.*, vol. 51, no. 21, pp. 34650–34662, Sep. 2025, doi: 10.1016/J.CERAMINT.2025.05.188.

[203] M. S. N. Shahrbabak, F. Sharifianjazi, D. Rahban, and A. Salimi, “A Comparative Investigation on Bioactivity and Antibacterial Properties of Sol-Gel Derived 58S Bioactive Glass Substituted by Ag and Zn,” *Silicon*, vol. 11, no. 6, pp. 2741–2751, Dec. 2019, doi: 10.1007/S12633-018-0063-2/.

[204] Y. Zhong *et al.*, “Effect of a novel bioactive glass-ceramic on dentinal tubule occlusion: an in vitro study,” *Aust. Dent. J.*, vol. 60, no. 1, pp. 96–103, Mar. 2015, doi: 10.1111/ADJ.12241.

[205] K. B. Holt and A. J. Bard, “Interaction of silver(I) ions with the respiratory chain of Escherichia coli: An electrochemical and scanning electrochemical microscopy study of the antimicrobial mechanism of micromolar Ag,” *Biochemistry*, vol. 44, no. 39, pp. 13214–13223, Oct. 2005, doi: 10.1021/BI0508542.

[206] A. D. Russell and W. B. Hugo, “7 Antimicrobial Activity and Action of Silver,” *Prog. Med. Chem.*, vol. 31, no. C, pp. 351–370, Jan. 1994, doi: 10.1016/S0079-6468(08)70024-9.

[207] M. Akram and R. Hussain, “Antibacterial Properties of Bioactive Glasses,” *Clinical Applications of Biomaterials: State-of-the-Art Progress, Trends, and Novel Approaches*, pp. 357–382, Jun. 2017, doi: 10.1007/978-3-319-56059-5_11.

[208] K. Zheng *et al.*, “Ag modified mesoporous bioactive glass nanoparticles for enhanced antibacterial activity in 3D infected skin model,” *Materials Science and Engineering: C*, vol. 103, p. 109764, Oct. 2019, doi: 10.1016/J.MSEC.2019.109764.

[209] S. Y. Liau, D. C. Read, W. J. Pugh, J. R. Furr, and A. D. Russell, “Interaction of silver nitrate with readily identifiable groups: Relationship to the antibacterial action of silver ions,” *Lett. Appl. Microbiol.*, vol. 25, no. 4, pp. 279–283, 1997, doi: 10.1046/J.1472-765X.1997.00219.X.

[210] O. D. Abodunrin, K. El Mabrouk, and M. Bricha, “Exploring the bioactivity and antibacterial properties of silver and cerium co-doped borosilicate bioactive glass,” *J. Mater. Chem. B*, vol. 13, no. 6, pp. 2100–2113, Feb. 2025, doi: 10.1039/D4TB02416H.

[211] A. A. Ahmed, A. A. Ali, D. A. R. Mahmoud, and A. M. El-Fiqi, “Preparation and characterization of antibacterial P2O 5-CaO-Na2O-Ag2O glasses,” *J. Biomed. Mater. Res. A*, vol. 98 A, no. 1, pp. 132–142, Jul. 2011, doi: 10.1002/JBM.A.33101.

[212] J. Pratten, S. N. Nazhat, J. J. Blaker, and A. R. Boccaccini, “In vitro attachment of staphylococcus epidermidis to surgical sutures with and without Ag-containing bioactive glass coating,” *J. Biomater. Appl.*, vol. 19, no. 1, pp. 47–57, Jul. 2004, doi: 10.1177/0885328204043200.

[213] A. Balamurugan *et al.*, “An in vitro biological and anti-bacterial study on a sol–gel derived silver-incorporated bioglass system,” *Dental Materials*, vol. 24, no. 10, pp. 1343–1351, Oct. 2008, doi: 10.1016/J.DENTAL.2008.02.015.

[214] S. S. Shendage, K. Gaikwad, K. Kachare, S. Kashte, J. Y. Chang, and A. V. Ghule, “In situ silver-doped antibacterial bioactive glass for bone regeneration application,” *J. Mater. Sci.*, vol. 59, no. 24, pp. 10744–10762, Jun. 2024, doi: 10.1007/S10853-024-09805-Z/.

[215] S. Gurunathan, K. J. Lee, K. Kalishwaralal, S. Sheikpranbabu, R. Vaidyanathan, and S. H. Eom, “Antiangiogenic properties of silver nanoparticles,” *Biomaterials*, vol. 30, no. 31, pp. 6341–6350, Oct. 2009, doi: 10.1016/J.BIOMATERIALS.2009.08.008.

[216] S. Akhtach, Z. Tabia, M. Bricha, and K. El Mabrouk, “Structural characterization, in vitro bioactivity, and antibacterial evaluation of low silver-doped bioactive glasses,” *Ceram. Int.*, vol. 47, no. 20, pp. 29036–29046, Oct. 2021, doi: 10.1016/J.CERAMINT.2021.07.066.

[217] J. Konieczny and Z. Rdzawski, “Antibacterial properties of copper and its alloys,” *Archives of Materials Science and Engineering*, vol. Vol. 56, no. nr 2, 2012.

[218] J. Inkinen, R. Mäkinen, M. M. Keinänen-Toivola, K. Nordström, and M. Ahonen, “Copper as an antibacterial material in different facilities,” *Lett. Appl. Microbiol.*, vol. 64, no. 1, pp. 19–26, Jan. 2017, doi: 10.1111/LAM.12680.

[219] P. H. Beswick, G. H. Hall, A. J. Hook, K. Little, D. C. H. McBrien, and K. A. K. Lott, "Copper toxicity: Evidence for the conversion of cupric to cuprous copper in vivo under anaerobic conditions," *Chem. Biol. Interact.*, vol. 14, no. 3–4, pp. 347–356, Aug. 1976, doi: 10.1016/0009-2797(76)90113-7.

[220] M. Hans, S. Mathews, F. Mücklich, and M. Solioz, "Physicochemical properties of copper important for its antibacterial activity and development of a unified model," *Biointerphases*, vol. 11, no. 1, Mar. 2016, doi: 10.1116/1.4935853/594734.

[221] J. V. Rau *et al.*, "Cu-Releasing Bioactive Glass Coatings and Their in Vitro Properties," *ACS Appl. Mater. Interfaces*, vol. 11, no. 6, pp. 5812–5820, Feb. 2019, doi: 10.1021/ACSAMI.8B19082/.

[222] S. S. Shendage, K. Gaikwad, K. Kachare, S. Kashte, and A. V. Ghule, "In vitro and in vivo study of copper-doped bioactive glass for bone regeneration application," *Mater. Chem. Phys.*, vol. 313, p. 128789, Feb. 2024, doi: 10.1016/J.MATCHEMPHYS.2023.128789.

[223] N. Gupta *et al.*, "Effects of transition metal ion dopants (Ag, Cu and Fe) on the structural, mechanical and antibacterial properties of bioactive glass," *Colloids Surf. A Physicochem. Eng. Asp.*, vol. 538, pp. 393–403, Feb. 2018, doi: 10.1016/J.COLSURFA.2017.11.023.

[224] A. Anand *et al.*, "Influence of Copper-Strontium Co-Doping on Bioactivity, Cytotoxicity and Antibacterial Activity of Mesoporous Bioactive Glass," *Gels 2022, Vol. 8, Page 743*, vol. 8, no. 11, p. 743, Nov. 2022, doi: 10.3390/GELS8110743.

[225] R. Koohkan, T. Hooshmand, M. Tahriri, and D. Mohebbi-Kalhori, "Synthesis, characterization and in vitro bioactivity of mesoporous copper silicate bioactive glasses," *Ceram. Int.*, vol. 44, no. 2, pp. 2390–2399, Feb. 2018, doi: 10.1016/J.CERAMINT.2017.10.208.

[226] A. Bari *et al.*, "Copper-containing mesoporous bioactive glass nanoparticles as multifunctional agent for bone regeneration," *Acta Biomater.*, vol. 55, pp. 493–504, Jun. 2017, doi: 10.1016/J.ACTBIO.2017.04.012.

[227] B. M. Elmowafy, A. M. Abdelghany, R. M. Ramadan, R. A. Ghazy, and T. M. Meaz, "Synthesis, structural characterization, and antibacterial studies of new borate 13-93B3 bioglasses with low copper dopant," *Egypt. J. Chem.*, vol. 65, no. 9, pp. 1–10, Sep. 2022, doi: 10.21608/EJCHEM.2022.84829.4137.

[228] F. Foroutan *et al.*, "Antibacterial Copper-Doped Calcium Phosphate Glasses for Bone Tissue Regeneration," *ACS Biomater. Sci. Eng.*, vol. 5, no. 11, pp. 6054–6062, Nov. 2019, doi: 10.1021/ACSBIOMATERIALS.9B01291.

[229] M. Miola and E. Verné, "Bioactive and Antibacterial Glass Powders Doped with Copper by Ion-Exchange in Aqueous Solutions," *Materials*, vol. 9, no. 6, p. 405, May 2016, doi: 10.3390/MA9060405.

[230] S. Soltani-Dehnavi, M. Mehdikhani-Nahrkhalaji, M. Rafienia, and A. Doostmohammadi, "Copper-doped and copper-free bioactive glass nanopowders cytotoxicity and antibacterial

activity assessment," *Scientia Iranica*, vol. 24, no. 3, pp. 1706–1716, Jun. 2017, doi: 10.24200/SCI.2017.4146.

[231] M. Lallukka *et al.*, "Cu-doped bioactive glass with enhanced in vitro bioactivity and antibacterial properties," *Ceram. Int.*, vol. 50, no. 3, pp. 5091–5103, Feb. 2024, doi: 10.1016/J.CERAMINT.2023.11.253.

[232] I. Hammami *et al.*, "Antibacterial Biomaterial Based on Bioglass Modified with Copper for Implants Coating," *J. Funct. Biomater.*, vol. 14, no. 7, p. 369, Jul. 2023, doi: 10.3390/JFB14070369.

[233] S. Akhtach, Z. Tabia, K. El Mabrouk, M. Bricha, and R. Belkhou, "A comprehensive study on copper incorporated bio-glass matrix for its potential antimicrobial applications," *Ceram. Int.*, vol. 47, no. 1, pp. 424–433, Jan. 2021, doi: 10.1016/J.CERAMINT.2020.08.149.

[234] D. K. Blencowe and A. P. Morby, "Zn(II) metabolism in prokaryotes," *FEMS Microbiol. Rev.*, vol. 27, no. 2–3, pp. 291–311, Jun. 2003, doi: 10.1016/S0168-6445(03)00041-X.

[235] S. Jafarirad, M. Mehrabi, B. Divband, and M. Kosari-Nasab, "Biofabrication of zinc oxide nanoparticles using fruit extract of Rosa canina and their toxic potential against bacteria: A mechanistic approach," *Materials Science and Engineering: C*, vol. 59, pp. 296–302, Feb. 2016, doi: 10.1016/J.MSEC.2015.09.089.

[236] T. A. Söderberg, B. Sunzel, S. Holm, T. Elmros, G. Hallmans, and S. Sjöberg, "Antibacterial Effect of Zinc Oxide in Vitro," *Scand. J. Plast. Reconstr. Surg. Hand Surg.*, vol. 24, no. 3, pp. 193–197, 1990, doi: 10.3109/02844319009041278.

[237] T. N. Phan, T. Buckner, J. Sheng, J. D. Baldeck, and R. E. Marquis, "Physiologic actions of zinc related to inhibition of acid and alkali production by oral streptococci in suspensions and biofilms," *Oral Microbiol. Immunol.*, vol. 19, no. 1, pp. 31–38, Feb. 2004, doi: 10.1046/J.0902-0055.2003.00109.X.

[238] M. Riaz, R. Zia, F. Saleemi, H. Ikram, and F. Bashir, "In vitro antimicrobial activity of ZnO based glass–ceramics against pathogenic bacteria," *J. Mater. Sci. Mater. Med.*, vol. 26, no. 12, Dec. 2015, doi: 10.1007/s10856-015-5603-3.

[239] S. Sánchez-Salcedo, S. Shruti, A. J. Salinas, G. Malavasi, L. Menabue, and M. Vallet-Regí, "In vitro antibacterial capacity and cytocompatibility of SiO_2-CaO-P_2O_5 meso-macroporous glass scaffolds enriched with ZnO," *J. Mater. Chem. B*, vol. 2, no. 30, pp. 4836–4847, Aug. 2014, doi: 10.1039/C4TB00403E.

[240] S. Fakher and D. Westenberg, "Evaluation of the antibacterial properties of four bioactive biomaterials for chronic wound management," *Future Microbiol.*, vol. 20, no. 3, pp. 247–258, Feb. 2025, doi: 10.1080/17460913.2025.2453334.

[241] Z. Atasayar, A. Akturk, D. N. Dikmetas, F. Karbancioglu-Guler, M. Erol-Taygun, and S. Küçükbayrak, "Fabrication of electrospun scaffolds with copper and zinc doped 58S bioactive glasses for bone tissue engineering applications," *MRS Adv.*, pp. 1–9, Dec. 2024, doi: 10.1557/S43580-024-01055-0.

[242] N. Azizabadi, P. A. Azar, M. S. Tehrani, and P. Derakhshi, “Synthesis and characteristics of gel-derived SiO_2-CaO-P_2O_5-SrO-Ag_2O-ZnO bioactive glass: Bioactivity, biocompatibility, and antibacterial properties,” *J. Non. Cryst. Solids*, vol. 556, p. 120568, Mar. 2021, doi: 10.1016/J.JNONCRYSOL.2020.120568.

[243] P. A. Dash, S. Mohanty, and S. K. Nayak, “Synthesis and characterization of ZnO/MgO doped mesoporous bioactive glass: Enhanced bioactivity and antibacterial properties for bone tissue engineering applications,” *Ceram. Int.*, vol. 51, no. 23, pp. 38129–38140, Sep. 2025, doi: 10.1016/J.CERAMINT.2025.06.049.

[244] M. Prabhu, K. Kavitha, P. Manivasakan, V. Rajendran, and P. Kulandaivelu, “Synthesis, characterization and biological response of magnesium-substituted nanobioactive glass particles for biomedical applications,” *Ceram. Int.*, vol. 39, no. 2, pp. 1683–1694, Mar. 2013, doi: 10.1016/J.CERAMINT.2012.08.011.

[245] C. Wen *et al.*, “Engineering bioactivity and antibacterial properties in mesoporous borosilicate glass nanospheres through magnesium substitution,” *J. Non. Cryst. Solids*, vol. 665, p. 123614, Oct. 2025, doi: 10.1016/J.JNONCRYSOL.2025.123614.

[246] J. M. Sobek and D. E. Talburt, “Effects of the rare earth cerium on Escherichia coli.,” *J. Bacteriol.*, vol. 95, no. 1, pp. 47–51, Jan. 1968, doi: 10.1128/JB.95.1.47-51.1968.

[247] A. Zambon, G. Malavasi, A. Pallini, F. Fraulini, and G. Lusvardi, “Cerium Containing Bioactive Glasses: A Review,” *ACS Biomater. Sci. Eng.*, vol. 7, no. 9, pp. 4388–4401, Sep. 2021, doi: 10.1021/ACSBIOMATERIALS.1C00414.

[248] R. A. Youness, M. A. Taha, A. A. El-Kheshen, N. El-Faramawy, and M. Ibrahim, “In vitro bioactivity evaluation, antimicrobial behavior and mechanical properties of cerium-containing phosphate glasses,” *Mater. Res. Express*, vol. 6, no. 7, p. 075212, Apr. 2019, doi: 10.1088/2053-1591/AB15B5.

[249] Y. F. Goh, A. Z. Alshemary, M. Akram, M. R. Abdul Kadir, and R. Hussain, “In-vitro characterization of antibacterial bioactive glass containing ceria,” *Ceram. Int.*, vol. 40, no. 1, pp. 729–737, Jan. 2014, doi: 10.1016/J.CERAMINT.2013.06.062.

[250] S. Raimondi *et al.*, “Investigation on the antimicrobial properties of cerium-doped bioactive glasses,” *J. Biomed. Mater. Res. A*, vol. 110, no. 2, pp. 504–508, Feb. 2022, doi: 10.1002/JBM.A.37289.

[251] D. S. Morais *et al.*, “Novel cerium doped glass-reinforced hydroxyapatite with antibacterial and osteoconductive properties for bone tissue regeneration,” *Biomedical Materials*, vol. 10, no. 5, p. 055008, Sep. 2015, doi: 10.1088/1748-6041/10/5/055008.

[252] M. M. Farag, Z. M. Al-Rashidy, and M. M. Ahmed, “In vitro drug release behavior of Ce-doped nano-bioactive glass carriers under oxidative stress,” *Journal of Materials Science: Materials in Medicine*, vol. 30, no. 2, pp. 18-, Jan. 2019, doi: 10.1007/S10856-019-6220-3.

[253] M. B. Taye, H. S. Ningsih, and S. J. Shih, “Antibacterial and In Vitro Bioactivity Studies of Silver-Doped, Cerium-Doped, and Silver–Cerium Co-Doped 80S Mesoporous Bioactive

Glass Particles via Spray Pyrolysis," *Applied Science*, vol. 13, no. 23, p. 12637, Nov. 2023, doi: 10.3390/APP132312637.

[254] F. Dabsie, G. Gregoire, M. Sixou, and P. Sharrock, "Does strontium play a role in the cariostatic activity of glass ionomer?: Strontium diffusion and antibacterial activity," *J. Dent.*, vol. 37, no. 7, pp. 554–559, Jul. 2009, doi: 10.1016/J.JDENT.2009.03.013.

[255] K. Subburam and R. Venkatachalam, "Synthesis, Characterization, and Evaluation of Strontium Oxide (SrO) Nanoparticles: Assessing Their Antibacterial and Anti-Biofilm Properties," 2025, doi: 10.2139/SSRN.5675201.

[256] J. Liu, S. C. F. Rawlinson, R. G. Hill, and F. Fortune, "Strontium-substituted bioactive glasses in vitro osteogenic and antibacterial effects," *Dental Materials*, vol. 32, no. 3, pp. 412–422, Mar. 2016, doi: 10.1016/J.DENTAL.2015.12.013.

[257] A. Mishra *et al.*, "Thermal, structural and in vitro dissolution of antimicrobial copper-doped and slow resorbable iron-doped phosphate glasses," *Journal of Materials Science*, vol. 52, no. 15, pp. 8957–8972, Jan. 2017, doi: 10.1007/S10853-017-0805-3.

[258] N. Alharbi, P. Sk, A.-S. Prof, R. Hill, and M. Chaudhary, "Bactericidal Zinc and Strontium Containing Glasses for Root Canal Sealers," 2025, Accessed: Nov. 11, 2025. [Online]. Available: https://qmro.qmul.ac.uk/xmlui/handle/123456789/111831

[259] J. Rao *et al.*, "Enhancing early enamel lesion management: Effects of silver-strontium co-doped mesoporous bioactive glass on remineralization and antibacterial activity," 2025, doi: 10.2139/SSRN.5580388.

[260] R. Zhao *et al.*, "Evaluation of bioactive glass scaffolds incorporating SrO or ZnO for bone repair: In vitro bioactivity and antibacterial activity," *J. Appl. Biomater. Funct. Mater.*, vol. 19, 2021, doi: 10.1177/22808000211040910.

[261] Q. Ye *et al.*, "Iron and zinc ions, potent weapons against multidrug-resistant bacteria," *Appl. Microbiol. Biotechnol.*, vol. 104, no. 12, pp. 5213–5227, Jun. 2020, doi: 10.1007/S00253-020-10600-4.

[262] K. N. Shoudho, S. Uddin, M. M. H. Rumon, and M. S. Shakil, "Influence of Physicochemical Properties of Iron Oxide Nanoparticles on Their Antibacterial Activity," *ACS Omega*, vol. 9, no. 31, pp. 33303–33334, Aug. 2024, doi: 10.1021/ACSOMEGA.4C02822.

[263] I. Hammami, S. R. Gavinho, A. S. Pádua, M. P. F. Graça, and J. C. Silva, "Synthesis and Characterization of Iron Containing Bioactive Glass for Implants," *2022 10th E-Health and Bioengineering Conference, EHB 2022*, 2022, doi: 10.1109/EHB55594.2022.9991451.

[264] M. V. Predoi *et al.*, "The Effect of Iron Oxide Insertion on the In Vitro Bioactivity, and Antibacterial Properties of the 45S5 Bioactive Glass," *Biomimetics 2024*, vol. 9, no. 6, p. 325, May 2024, doi: 10.3390/BIOMIMETICS9060325.

[265] L. R. Bernstein, "Mechanisms of Therapeutic Activity for Gallium," *Pharmacol. Rev.*, vol. 50, no. 4, pp. 665–682, Dec. 1998, doi: 10.1016/S0031-6997(24)01383-8.

[266] A. J. Salinas and M. Vallet-Regí, “Glasses in bone regeneration: A multiscale issue,” *J. Non. Cryst. Solids*, vol. 432, pp. 9–14, Jan. 2016, doi: 10.1016/J.JNONCRYSOL.2015.03.025.

[267] S. Kaya, M. Cresswell, and A. R. Boccaccini, “Mesoporous silica-based bioactive glasses for antibiotic-free antibacterial applications,” *Materials Science and Engineering: C*, vol. 83, pp. 99–107, Feb. 2018, doi: 10.1016/J.MSEC.2017.11.003.

[268] S.-S. Sandra, S. Antonio, V.-R. Maria, M. Gianluca, L. Gigliola, and M. Ledi, “Development of mesoporous bioactive glasses able to release antibacterial Ga^{3+} ions,” in *Frontiers in Bioengineering and Biotechnology*, Frontiers Media SA, 2016. doi: 10.3389/CONF.FBIOE.2016.01.01476.

[269] A. Rahimnejad Yazdi, L. Torkan, W. Stone, and M. R. Towler, “The impact of gallium content on degradation, bioactivity, and antibacterial potency of zinc borate bioactive glass,” *J. Biomed. Mater. Res. B Appl. Biomater.*, vol. 106, no. 1, pp. 367–376, Jan. 2018, doi: 10.1002/JBM.B.33856.

[270] M. Zinkevich and F. Aldinger, “Thermodynamic assessment of the gallium-oxygen system,” *Journal of the American Ceramic Society*, vol. 87, no. 4, pp. 683–691, Apr. 2004, doi: 10.1111/J.1551-2916.2004.00683.X.

[271] F. Kurtuldu *et al.*, “Cerium and gallium containing mesoporous bioactive glass nanoparticles for bone regeneration: Bioactivity, biocompatibility and antibacterial activity,” *Materials Science and Engineering: C*, vol. 124, p. 112050, May 2021, doi: 10.1016/J.MSEC.2021.112050.

[272] R. D. Houlsby, M. Ghajar, and G. O. Chavez, “Antimicrobial activity of borate-buffered solutions,” *Antimicrob. Agents Chemother.*, vol. 29, no. 5, p. 803, 1986, doi: 10.1128/AAC.29.5.803.

[273] S. Prasad S. *et al.*, “Effect of boron oxide addition on structural, thermal, in vitro bioactivity and antibacterial properties of bioactive glasses in the base S53P4 composition,” *J. Non. Cryst. Solids*, vol. 498, pp. 204–215, Oct. 2018, doi: 10.1016/J.JNONCRYSOL.2018.06.027.

[274] F. Niazvand *et al.*, “Sol-gel derived bioactive glasses containing boron and strontium: Bioactivity, biocompatibility, and antibacterial properties,” *J. Non. Cryst. Solids*, vol. 631, p. 122909, May 2024, doi: 10.1016/J.JNONCRYSOL.2024.122909.

[275] L. Sopchenski, S. Cogo, M. F. Dias-Ntipanyj, S. Elifio-Espósito, K. C. Popat, and P. Soares, “Bioactive and antibacterial boron doped TiO2 coating obtained by PEO,” *Appl. Surf. Sci.*, vol. 458, pp. 49–58, Nov. 2018, doi: 10.1016/J.APSUSC.2018.07.049.

[276] Shweta *et al.*, “h-BN Reinforced Bioactive Glasses for Bone Tissue Engineering: Enhanced Strength and Antibacterial Properties,” *ACS Applied Engineering Materials*, vol. 3, no. 5, pp. 1399–1415, May 2025, doi: 10.1021/ACSAENM.5C00145.

[277] P. Balasubramanian *et al.*, “Ion Release, Hydroxyapatite Conversion, and Cytotoxicity of Boron-Containing Bioactive Glass Scaffolds,” *Int. J. Appl. Glass Sci.*, vol. 7, no. 2, pp. 206–215, Jun. 2016, doi: 10.1111/IJAG.12206.

[278] S. Silver, “Bacterial resistances to toxic metal ions - a review,” *Gene*, vol. 179, no. 1, pp. 9–19, Jan. 1996, doi: 10.1016/S0378-1119(96)00323-X.

[279] J. L. Hobman and L. C. Crossman, “Bacterial antimicrobial metal ion resistance,” *J. Med. Microbiol.*, vol. 64, no. 5, pp. 471–497, May 2015, doi: 10.1099/JMM.0.023036-0.

[280] R. Choudhury and S. Srivastava, “Zinc resistance mechanisms in bacteria,” *Curr. Sci.*, vol. 81, no. 7, p. 768, 2001, Accessed: Jan. 29, 2026. [Online]. Available: http://www.jstor.org/stable/24106396

[281] H. Saito and H. Kobayashi, “Bacterial responses to alkaline stress.,” *Sci. Prog.*, vol. 86, no. Pt 4, pp. 271–282, 2003, doi: 10.3184/003685003783238635.

[282] S. R. Gavinho *et al.*, “Biocompatibility, Bioactivity, and Antibacterial Behaviour of Cerium-Containing Bioglass®,” *Nanomaterials*, vol. 12, no. 24, p. 4479, Dec. 2022, doi: 10.3390/NANO12244479.

[283] S. S. Sharaf, A. M. El-Shafei, R. Refaie, A. A. Gibriel, and R. Abdel-Sattar, “Antibacterial and wound healing properties of cellulose acetate electrospun nanofibers loaded with bioactive glass nanoparticles; in-vivo study,” *Cellulose*, vol. 29, no. 8, pp. 4565–4577, Apr. 2022, doi: 10.1007/S10570-022-04570-1.

[284] A. Munir *et al.*, “Using Copper-Doped Mesoporous Bioactive Glass Nanospheres to Impart Anti-Bacterial Properties to Dental Composites,” *Pharmaceutics 2022, Vol. 14, Page 2241*, vol. 14, no. 10, p. 2241, Oct. 2022, doi: 10.3390/PHARMACEUTICS14102241.

[285] P. Nooeaid *et al.*, “Development of bioactive glass-based scaffolds for controlled antibiotic release in bone tissue engineering via biodegradable polymer layered coating,” *Biointerphases*, vol. 9, no. 4, p. 041001, Dec. 2014, doi: 10.1116/1.4897217/133796.

[286] M. T. Cunha, M. A. Murça, S. Nigro, G. B. Klautau, and M. J. C. Salles, “In vitro antibacterial activity of bioactive glass S53P4 on multiresistant pathogens causing osteomyelitis and prosthetic joint infection,” *BMC Infectious Diseases 2018 18:1*, vol. 18, no. 1, pp. 157-, Apr. 2018, doi: 10.1186/S12879-018-3069-X.

[287] I. Gergely, A. Zazgyva, A. Man, S. Zuh, and T. Pop, “The in vitro antibacterial effect of S53P4 bioactive glass and gentamicin impregnated polymethylmethacrylate beads,” *Acta Microbiol. Immunol. Hung.*, vol. 61, no. 2, pp. 145–160, Jun. 2014, doi: 10.1556/AMICR.61.2014.2.5.

[288] B. L. Correia, A. T. P. C. Gomes, R. Noites, J. M. F. Ferreira, and A. S. Duarte, “New and Efficient Bioactive Glass Compositions for Controlling Endodontic Pathogens,” *Nanomaterials,* vol. 12, no. 9, May 2022, doi: 10.3390/NANO12091577.

[289] M. Kucuk, G. Quevedo, M. Ratakonda, and H. Aksel, “Antibacterial and biocompatibility properties of bioactive glass and double antibiotic-loaded hydrogels in regenerative endodontic treatment,” *Scientific Reports*, vol. 15, no. 1, pp. 23581-, Jul. 2025, doi: 10.1038/s41598-025-09057-0.

[290] M. Cannio, D. Bellucci, J. A. Roether, D. N. Boccaccini, and V. Cannillo, “Bioactive Glass Applications: A Literature Review of Human Clinical Trials,” *Materials, Vol. 14,* vol. 14, no. 18, Sep. 2021, doi: 10.3390/ma14185440.

[291] E. M. Santos, S. Radin, and P. Ducheyne, “Sol–gel derived carrier for the controlled release of proteins,” *Biomaterials*, vol. 20, no. 18, pp. 1695–1700, Sep. 1999, doi: 10.1016/S0142-9612(99)00066-6.

[292] W. Xia and J. Chang, “Well-ordered mesoporous bioactive glasses (MBG): A promising bioactive drug delivery system,” *Journal of Controlled Release*, vol. 110, no. 3, pp. 522–530, Feb. 2006, doi: 10.1016/j.jconrel.2005.11.002.

[293] A. M. El-Kady, N. A. Kamel, M. M. Elnashar, and M. M. Farag, “Production of bioactive glass/chitosan scaffolds by freeze-gelation for optimized vancomycin delivery: Effectiveness of glass presence on controlling the drug release kinetics,” *J. Drug Deliv. Sci. Technol.*, vol. 66, p. 102779, Dec. 2021, doi: 10.1016/j.jddst.2021.102779.

[294] R. K. Wassif, M. Elkayal, R. N. Shamma, and S. A. Elkheshen, “Recent advances in the local antibiotics delivery systems for management of osteomyelitis,” *Drug Deliv.*, vol. 28, no. 1, pp. 2392–2414, 2021, doi: 10.1080/10717544.2021.1998246.

[295] S. K. Nandi, P. Mukherjee, S. Roy, B. Kundu, D. K. De, and D. Basu, “Local antibiotic delivery systems for the treatment of osteomyelitis – A review,” *Materials Science and Engineering: C*, vol. 29, no. 8, pp. 2478–2485, Oct. 2009, doi: 10.1016/j.msec.2009.07.014.

[296] D. Almasri and Y. Dahman, “Bioactive Glass Preloaded with Antibiotics for Delivery of Long-Term Localized Drug Release Exhibiting Inherent Antimicrobial Activity,” *Applied Sciences 2025, Vol. 15,* vol. 15, no. 10, May 2025, doi: 10.3390/app15105363.

[297] S. M. Huang *et al.*, “Synergistic effect of drug/antibiotic-impregnated micro/nanohybrid mesoporous bioactive glass/calcium phosphate composite bone cement on antibacterial and osteoconductive activities,” *Biomaterials Advances*, vol. 152, no. 8, p. 213524, Sep. 2023, doi: 10.1016/j.bioadv.2023.213524.

[298] S. Sánchez-Salcedo, A. García, A. González-Jiménez, and M. Vallet-Regí, “Antibacterial effect of 3D printed mesoporous bioactive glass scaffolds doped with metallic silver nanoparticles,” *Acta Biomater.*, vol. 155, pp. 654–666, Jan. 2023, doi: 10.1016/J.ACTBIO.2022.10.045.

[299] M. Lallukka, M. Miola, E. Verné, and F. Baino, “Silver-doped glass-ceramic scaffolds with antibacterial and bioactive properties for bone substitution,” *Ceram. Int.*, vol. 50, no. 17, pp. 30997–31005, Sep. 2024, doi: 10.1016/J.CERAMINT.2024.05.404.

[300] C. Wu *et al.*, “Copper-containing mesoporous bioactive glass scaffolds with multifunctional properties of angiogenesis capacity, osteostimulation and antibacterial activity,” *Biomaterials*, vol. 34, no. 2, pp. 422–433, 2013, doi: 10.1016/j.biomaterials.2012.09.066.

[301] Y. Yang *et al.*, “Copper-doped mesoporous bioactive glass endows magnesium-based scaffold with antibacterial activity and corrosion resistance,” *Mater. Chem. Front.*, vol. 5, no. 19, pp. 7228–7240, Sep. 2021, doi: 10.1039/D1QM01028J.

[302] C. E. Mariotti, L. Ramos-Rivera, B. Conti, and A. R. Boccaccini, “Zein-Based Electrospun Fibers Containing Bioactive Glass with Antibacterial Capabilities,” *Macromol. Biosci.*, vol. 20, no. 7, p. 2000059, Jul. 2020, doi: 10.1002/MABI.202000059.

[303] N. Pajares-Chamorro *et al.*, “Silver-doped bioactive glass particles for in vivo bone tissue regeneration and enhanced methicillin-resistant staphilococcus aureus (*MRSA*) inhibition,” *Mater. Sci. Eng. C Mater. Biol. Appl.*, vol. 120, p. 111693, Jan. 2020, doi: 10.1016/J.MSEC.2020.111693.

[304] P. Stoor, E. Soderling, and J. I. Salonen, “Antibacterial effects of a bioactive glass paste on oral microorganisms,” *Acta Odontol. Scand.*, vol. 56, no. 3, pp. 161–165, 1998, doi: 10.1080/000163598422901.

[305] G. Koller, J. Roether, K. Bruce, and S. Deb, “Antimicrobial Potential of Bioactive Bone Cements ,” *J. Appl. Biomater. Funct. Mater.*, vol. 6, no. 1, pp. 16–22, 2018, doi: /10.1177/228080000800600103.

[306] J. M. de Araújo Lopes *et al.*, “Biocompatibility, induction of mineralization and antimicrobial activity of experimental intracanal pastes based on glass and glass-ceramic materials,” *Int. Endod. J.*, vol. 53, no. 11, pp. 1494–1505, Nov. 2020, doi: 10.1111/IEJ.13382.

[307] A. N. Saud, E. Koç, O. Özdemir, Y. Cetin, and Y. Yildizhan, “Development and Evaluation of Bioactive Glass Ceramic-Based Endodontic Cement: A Comprehensive Study on Bioactivity, Biocompatibility, Mechanical Properties, Radiopacity, and Antimicrobial Activity,” *Journal of Materials Engineering and Performance*, vol. 34, no. 13, pp. 12750–12767, Sep. 2024, doi: 10.1007/S11665-024-10098-1.

[308] L. L. Dai, M. L. Mei, C. H. Chu, and E. C. M. Lo, “Antibacterial effect of a new bioactive glass on cariogenic bacteria,” *Arch. Oral Biol.*, vol. 117, p. 104833, Sep. 2020, doi: 10.1016/J.ARCHORALBIO.2020.104833.

[309] A. L. Godoy-Santos, L. A. Rosemberg, C. De Cesar-Netto, and D. G. Armstrong, “The use of bioactive glass S53P4 in the treatment of an infected Charcot foot: a case report,” *J. Wound Care*, vol. 28, no. Sup1, pp. S14–S17, Jan. 2019, doi: 10.12968/JOWC.2019.28.SUP1.S14.

[310] M. Bigoni *et al.*, “Clinical applications of Bioactive glass S53P4 in bone infections: a systematic review,” *Eur. Rev. Med. Pharmacol. Sci.*, vol. 23, no. 2 Suppl, pp. 240–251, 2019, doi: 10.26355/EURREV_201904_17498.

[311] J. Ye, J. He, C. Wang, K. Yao, and Z. Gou, “Copper-containing mesoporous bioactive glass coatings on orbital implants for improving drug delivery capacity and antibacterial activity,” *Biotechnology Letters*, vol. 36, no. 5, pp. 961–968, Feb. 2014, doi: 10.1007/S10529-014-1465-X.

[312] Y. Yang *et al.*, “Cu-releasing bioactive glass/polycaprolactone coating on Mg with antibacterial and anticorrosive properties for bone tissue engineering,” *Biomedical Materials*, vol. 13, no. 1, p. 015001, Oct. 2017, doi: 10.1088/1748-605X/AA87F2.

[313] L. R. Rivera *et al.*, “Antibacterial, pro-angiogenic and pro-osteointegrative zein-bioactive glass/copper based coatings for implantable stainless steel aimed at bone healing,” *Bioact. Mater.*, vol. 6, no. 5, pp. 1479–1490, May 2021, doi: 10.1016/J.BIOACTMAT.2020.11.001.

[314] D. M. Marques, V. de C. Oliveira, M. T. Souza, E. D. Zanotto, J. P. M. Issa, and E. Watanabe, “Biomaterials for orthopedics: anti-biofilm activity of a new bioactive glass coating on titanium implants,” *Biofouling*, vol. 36, no. 2, pp. 234–244, Feb. 2020, doi: 10.1080/08927014.2020.1755842.

[315] C. Y. K. Lung, M. M. Abdalla, C. H. Chu, I. Yin, S. R. Got, and J. P. Matinlinna, “A Multi-Element-Doped Porous Bioactive Glass Coating for Implant Applications,” *Materials*, vol. 14, no. 4, p. 961, Feb. 2021, doi: 10.3390/MA14040961.

[316] O. Rodriguez *et al.*, “Titanium addition influences antibacterial activity of bioactive glass coatings on metallic implants,” *Heliyon*, vol. 3, no. 10, p. e00420, Oct. 2017, doi: 10.1016/j.heliyon.2017.e00420.

[317] F. Boschetto *et al.*, “Antibacterial and Osteoconductive Effects of Chitosan/Polyethylene Oxide (PEO)/Bioactive Glass Nanofibers for Orthopedic Applications,” *Applied Sciences 2020, Vol. 10, Page 2360*, vol. 10, no. 7, p. 2360, Mar. 2020, doi: 10.3390/APP10072360.

[318] D. A. Canales *et al.*, “Electrospun fibers of poly (lactic acid) containing bioactive glass and magnesium oxide nanoparticles for bone tissue regeneration,” *Int. J. Biol. Macromol.*, vol. 210, pp. 324–336, Jun. 2022, doi: 10.1016/j.ijbiomac.2022.05.047.

[319] H. N. Wilkinson, S. Iveson, P. Catherall, and M. J. Hardman, “A novel silver bioactive glass elicits antimicrobial efficacy against Pseudomonas aeruginosa and Staphylococcus aureus in an ex vivo skin wound biofilm model,” *Front. Microbiol.*, vol. 9, p. 1450, Jul. 2018, doi: 10.3389/FMICB.2018.01450.

[320] E. Sharifi *et al.*, “Cell loaded hydrogel containing Ag-doped bioactive glass–ceramic nanoparticles as skin substitute: Antibacterial properties, immune response, and scarless cutaneous wound regeneration,” *Bioeng. Transl. Med.*, vol. 7, no. 3, p. e10386, Sep. 2022, doi: 10.1002/BTM2.10386.

[321] P. Roy *et al.*, “Facile synthesis of electrospun antibacterial bioactive glass based micronanofibre (ABGmnf) for exalted wound healing: In vitro and in vivo studies,” *Mater. Chem. Phys.*, vol. 305, p. 127874, Sep. 2023, doi: 10.1016/J.MATCHEMPHYS.2023.127874.

[322] M. E. Galarraga-Vinueza, J. Mesquita-Guimarães, R. S. Magini, J. C. M. Souza, M. C. Fredel, and A. R. Boccaccini, “Anti-biofilm properties of bioactive glasses embedding organic active compounds,” *J. Biomed. Mater. Res. A*, vol. 105, no. 2, pp. 672–679, Feb. 2017, doi: 10.1002/jbm.a.35934.

[323] N. Esfahanizadeh, M. R. Nourani, A. Bahador, N. Akhondi, and M. Montazeri, “The Anti-biofilm Activity of Nanometric Zinc doped Bioactive Glass against Putative Periodontal Pathogens: An in vitro Study,” *Biomedical Glasses*, vol. 4, no. 1, pp. 95–107, Nov. 2020, doi: 10.1515/BGLASS-2018-0009.

[324] E. Verné *et al.*, “Early stage reactivity and in vitro behavior of silica-based bioactive glasses and glass-ceramics,” *Journal of Materials Science: Materials in Medicine 2008 20:1*, vol. 20, no. 1, pp. 75–87, Aug. 2008, doi: 10.1007/s10856-008-3537-8.

[325] Á. J. Leite, A. I. Gonçalves, M. T. Rodrigues, M. E. Gomes, and J. F. Mano, “Strontium-Doped Bioactive Glass Nanoparticles in Osteogenic Commitment,” *ACS Appl. Mater. Interfaces*, vol. 10, no. 27, pp. 23311–23320, Jul. 2018, doi: 10.1021/ACSAMI.8B06154.

[326] J. F. Stebbins, “Structure and dynamics of magnesium in silicate melts: A high-temperature 25Mg NMR study,” *American Mineralogist*, vol. 83, no. 9–10, pp. 1022–1029, Sep. 1998, doi: 10.2138/AM-1998-9-1010.

[327] K. Shimoda, Y. Tobu, M. Hatakeyama, T. Nemoto, and K. Saito, “Structural investigation of Mg local environments in silicate glasses by ultra-high field 25Mg 3QMAS NMR spectroscopy,” *American Mineralogist*, vol. 92, no. 4, pp. 695–698, Apr. 2007, doi: 10.2138/AM.2007.2535.

[328] M. Magallanes-Perdomo, A. H. De Aza, I. Sobrados, J. Sanz, and P. Pena, “Structure and properties of bioactive eutectic glasses based on the $Ca_3(PO_4)_2$–$CaSiO_3$–$CaMg(SiO_3)_2$ system,” *Acta Biomater.*, vol. 8, no. 2, pp. 820–829, Feb. 2012, doi: 10.1016/J.ACTBIO.2011.10.017.

[329] P. Jha and K. Singh, “Effect of MgO on bioactivity, hardness, structural and optical properties of SiO_2-K_2O-CaO-MgO glasses,” *Ceram. Int.*, vol. 42, pp. 436–444, 2016, doi: 10.1016/j.ceramint.2015.08.128.

[330] A. Pedone, G. Malavasi, and M. C. Menziani, “Computational insight into the effect of CaO/MgO substitution on the structural properties of phospho-silicate bioactive glasses,” *Journal of Physical Chemistry C*, vol. 113, no. 35, pp. 15723–15730, Sep. 2009, doi: 10.1021/JP904131T.

[331] S. I. Schmitz *et al.*, “Superior biocompatibility and comparable osteoinductive properties: Sodium-reduced fluoride-containing bioactive glass belonging to the CaO–MgO–SiO2 system as a promising alternative to 45S5 bioactive glass,” *Bioact. Mater.*, vol. 5, no. 1, pp. 55–65, Mar. 2020, doi: 10.1016/J.BIOACTMAT.2019.12.005.

[332] A. Moghanian, A. Sedghi, A. Ghorbanoghli, and E. Salari, “The effect of magnesium content on in vitro bioactivity, biological behavior and antibacterial activity of sol–gel derived 58S bioactive glass,” *Ceram. Int.*, vol. 44, no. 8, pp. 9422–9432, Jun. 2018, doi: 10.1016/J.CERAMINT.2018.02.159.

[333] N. Kanzaki, K. Onuma, G. Treboux, S. Tsutsumi, and A. Ito, “Inhibitory Effect of Magnesium and Zinc on Crystallization Kinetics of Hydroxyapatite,” *Journal of Physical Chemistry B*, vol. 104, no. 17, pp. 4189–4194, May 2000, doi: 10.1021/JP9939726.

[334] M. D. O’Donnell and R. G. Hill, “Influence of strontium and the importance of glass chemistry and structure when designing bioactive glasses for bone regeneration,” *Acta Biomater.*, vol. 6, no. 7, pp. 2382–2385, Jul. 2010, doi: 10.1016/J.ACTBIO.2010.01.006.

[335] J. Isaac, J. Nohra, J. Lao, and E. Jallot, “Effects of Strontium-Doped Bioactive Glass on the Differentiation of Cultured Osteogenic Cells,” 2014, doi: 10.22203/eCM.v021a11.

[336] M. D. O’Donnell, P. L. Candarlioglu, C. A. Miller, E. Gentleman, and M. M. Stevens, “Materials characterisation and cytotoxic assessment of strontium-substituted bioactive glasses for bone regeneration,” *J. Mater. Chem.*, vol. 20, no. 40, pp. 8934–8941, Oct. 2010, doi: 10.1039/C0JM01139H.

[337] S. Kargozar, M. Montazerian, E. Fiume, and F. Baino, “Multiple and promising applications of strontium (Sr)-containing bioactive glasses in bone tissue engineering,” *Front. Bioeng. Biotechnol.*, vol. 7, no. JUL, p. 453733, Jul. 2019, doi: 10.3389/FBIOE.2019.00161.

[338] L. L. Hench, R. J. Splinter, W. C. Allen, and T. K. Greenlee, “Bonding mechanisms at the interface of ceramic prosthetic materials,” *J. Biomed. Mater. Res.*, vol. 5, no. 6, pp. 117–141, 1971, doi: 10.1002/jbm.820050611.

[339] J. M. Tainio *et al.*, “Structure and in vitro dissolution of Mg and Sr containing borosilicate bioactive glasses for bone tissue engineering,” *J. Non. Cryst. Solids*, vol. 533, p. 119893, Apr. 2020, doi: 10.1016/J.JNONCRYSOL.2020.119893.

[340] W. C. Oliver and G. M. Pharr, “An improved technique for determining hardness and elastic modulus using load and displacement sensing indentation experiments,” *J. Mater. Res.*, vol. 7, no. 6, pp. 1564–1583, Jun. 1992, doi: 10.1557/JMR.1992.1564.

[341] C. Ohtsuki, H. Kushitani, T. Kokubo, S. Kotani, and T. Yamamuro, “Apatite formation on the surface of ceravital-type glass-ceramic in the body,” *J. Biomed. Mater. Res.*, vol. 25, no. 11, pp. 1363–1370, Nov. 1991, doi: 10.1002/JBM.820251105.

[342] International Standard Organization, “ISO 10993-12:2021 - Biological evaluation of medical devices — Part 12: Sample preparation and reference materials.” Accessed: May 03, 2024. [Online]. Available: https://www.iso.org/standard/75769.html

[343] F. Boraldi, A. Bartolomeo, C. Di Bari, A. Cocconi, and D. Quaglino, “Donor’s age and replicative senescence favour the in-vitro mineralization potential of human fibroblasts,” *Exp. Gerontol.*, vol. 72, pp. 218–226, Dec. 2015, doi: 10.1016/J.EXGER.2015.10.009.

[344] M. Feoktistova, P. Geserick, and M. Leverkus, “Crystal Violet Assay for Determining Viability of Cultured Cells,” *Cold Spring Harb. Protoc.*, vol. 2016, no. 4, pp. 343–346, Apr. 2016, doi: 10.1101/PDB.PROT087379.

[345] G. Strömberg *et al.*, “Development and Characterization of Non-coated and PLGA-Coated S53P4 and S59 Bioactive Glass Scaffolds for Treatment of Load-Bearing Defects,” *Biomedical Materials & Devices*, 2023, doi: 10.1007/s44174-023-00099-4.

[346] A. R. Boccaccini, Q. Chen, L. Lefebvre, L. Gremillard, and J. Chevalier, “Sintering, crystallisation and biodegradation behaviour of Bioglass®-derived glass-ceramics,” *Faraday Discuss.*, vol. 136, 2007, doi: 10.1039/b616539g.

[347] M. Fabert *et al.*, “Crystallization and sintering of borosilicate bioactive glasses for application in tissue engineering,” *J. Mater. Chem. B*, vol. 5, no. 23, 2017, doi: 10.1039/c7tb00106a.

[348] Q. Z. Chen, I. D. Thompson, and A. R. Boccaccini, “45S5 Bioglass®-derived glass-ceramic scaffolds for bone tissue engineering,” *Biomaterials*, vol. 27, no. 11, pp. 2414–2425, 2006, doi: 10.1016/j.biomaterials.2005.11.025.

[349] R. Björkenheim *et al.*, “Sintered S53P4 bioactive glass scaffolds have anti-inflammatory properties and stimulate osteogenesis in vitro,” *Eur. Cell. Mater.*, vol. 41, 2021, doi: 10.22203/eCM.v041a02.

[350] N. Lotfibakhshaiesh, D. S. Brauer, and R. G. Hill, “Bioactive glass engineered coatings for Ti_6Al_4V alloys: Influence of strontium substitution for calcium on sintering behaviour,” in *Journal of Non-Crystalline Solids*, 2010. doi: 10.1016/j.jnoncrysol.2010.05.017.

[351] C. Volzone and F. M. Stábile, “Structural Changes by Thermal Treatment up to Glass Obtention of P2O5-Na2O-CaO-SiO2 Compounds with Bioglass Composition Types,” *New Journal of Glass and Ceramics*, vol. 3, no. January, 2013.

[352] C. Berbecaru, H. V. Alexandru, G. E. Stan, D. A. Marcov, I. Pasuk, and A. Ianculescu, “First stages of bioactivity of glass-ceramics thin films prepared by magnetron sputtering technique,” *Materials Science and Engineering: B*, vol. 169, no. 1–3, 2010, doi: 10.1016/j.mseb.2010.01.007.

[353] A. Stiller, M. Engblom, E. Vainio, and L. Hupa, “Understanding the crystallization behavior of bioactive glass S53P4 powder compacts under various heating conditions,” *J. Non. Cryst. Solids*, vol. 644, Nov. 2024, doi: 10.1016/j.jnoncrysol.2024.123178.

[354] C. Yang, J. Bai, G. Wang, H. Wang, and S. Ma, “Effect of Na_2O content on wettability, crystallization and performances of sealing glass,” *Journal of Materials Research and Technology*, vol. 23, pp. 4117–4134, Mar. 2023, doi: 10.1016/J.JMRT.2023.02.073.

[355] L. L. Hench, “Bioceramics,” *Journal of the American Ceramic Society*, vol. 81, no. 7, pp. 1705–1728, 1998.

[356] G. El Damrawi, R. M. Ramadan, and M. El Baiomy, “Effect of SrO on the Structure of Apatite and Wollastonite Phases of Na_2O-CaO-SiO_2-P_2O_5 Glass System,” *New Journal of Glass and Ceramics*, vol. 11, no. 02, pp. 45–56, 2021, doi: 10.4236/njgc.2021.112003.

[357] F. Sharifianjazi *et al.*, “Effects of Sr and Mg dopants on biological and mechanical properties of SiO2–CaO–P2O5 bioactive glass,” *Ceram. Int.*, vol. 46, no. 14, 2020, doi: 10.1016/j.ceramint.2020.06.030.

[358] Y. C. Fredholm, N. Karpukhina, R. V Law, and R. G. Hill, “Strontium containing bioactive glasses: Glass structure and physical properties,” 2010, doi: 10.1016/j.jnoncrysol.2010.06.078.

[359] V. Cannillo, L. Esposito, E. Rambaldi, A. Sola, and A. Tucci, “Effect of porosity on the elastic properties of porcelainized stoneware tiles by a multi-layered model,” *Ceram. Int.*, vol. 35, no. 1, 2009, doi: 10.1016/j.ceramint.2007.10.015.

[360] V. Cannillo *et al.*, “Microscale computational simulation and experimental measurement of thermal residual stresses in glass–alumina functionally graded materials,” *J. Eur. Ceram. Soc.*, vol. 26, no. 8, pp. 1411–1419, Jan. 2006, doi: 10.1016/J.JEURCERAMSOC.2005.02.012.

[361] V. Cannillo, C. Leonelli, and A. R. Boccaccini, “Numerical models for thermal residual stresses in Al2O3 platelets/borosilicate glass matrix composites,” *Materials Science and Engineering: A*, vol. 323, no. 1–2, pp. 246–250, Jan. 2002, doi: 10.1016/S0921-5093(01)01345-4.

[362] M. Zarur, A. Seijo-Rabina, A. Goyanes, A. Concheiro, and C. Alvarez-Lorenzo, “pH-responsive scaffolds for tissue regeneration: In vivo performance,” *Acta Biomater.*, vol. 168, no. 13, pp. 22–41, Sep. 2023, doi: 10.1016/j.actbio.2023.07.025.

[363] W. K. Ramp, L. G. Lenz, and K. K. Kaysinger, “Medium pH modulates matrix, mineral, and energy metabolism in cultured chick bones and osteoblast-like cells,” *Bone Miner.*, vol. 24, no. 1, pp. 59–73, Jan. 1994, doi: 10.1016/S0169-6009(08)80131-6.

[364] A. El-Ghannam, P. Ducheyne, and I. M. Shapiro, “Formation of surface reaction products on bioactive glass and their effects on the expression of the osteoblastic phenotype and the deposition of mineralized extracellular matrix,” *Biomaterials*, vol. 18, no. 4, pp. 295–303, Feb. 1997, doi: 10.1016/S0142-9612(96)00059-2.

[365] S. M. Rabiee, N. Nazparvar, M. Azizian, D. Vashaee, and L. Tayebi, “Effect of ion substitution on properties of bioactive glasses: A review,” *Ceram. Int.*, vol. 41, no. 6, pp. 7241–7251, Jul. 2015, doi: 10.1016/J.CERAMINT.2015.02.140.

[366] A. Brandao-Burch, J. C. Utting, I. R. Orriss, and T. R. Arnett, “Acidosis inhibits bone formation by osteoblasts in vitro by preventing mineralization,” *Calcif. Tissue Int.*, vol. 77, no. 3, pp. 167–174, Aug. 2005, doi: 10.1007/S00223-004-0285-8.

[367] A. Antonakos, E. Liarokapis, and T. Leventouri, “Micro-Raman and FTIR studies of synthetic and natural apatites,” *Biomaterials*, vol. 28, no. 19, pp. 3043–3054, Jul. 2007, doi: 10.1016/J.BIOMATERIALS.2007.02.028.

[368] G. Penel, G. Leroy, C. Rey, and E. Bres, “MicroRaman spectral study of the PO4 and CO3 vibrational modes in synthetic and biological apatites,” *Calcif. Tissue Int.*, vol. 63, no. 6, pp. 475–481, Dec. 1998, doi: 10.1007/S002239900561.

[369] A. Awonusi, M. D. Morris, and M. M. J. Tecklenburg, “Carbonate assignment and calibration in the Raman spectrum of apatite,” *Calcif. Tissue Int.*, vol. 81, no. 1, pp. 46–52, Jul. 2007, doi: 10.1007/S00223-007-9034-0.

[370] E. C. Ziemath and M. A. Aegerter, “Raman and Infrared Investigations of Glass and Glass-Ceramics with Composition 2Na2O. 1CaO. 3SiO2,” *J. Mater. Res.*, vol. 9, no. 1, pp. 216–225, 1994, doi: 10.1557/JMR.1994.0216.

[371] D. Bellucci, A. Sola, and V. Cannillo, “Low Temperature Sintering of Innovative Bioactive Glasses,” *Journal of the American Ceramic Society*, vol. 95, no. 4, pp. 1313–1319, Apr. 2012, doi: 10.1111/J.1551-2916.2012.05100.X.

[372] L. L. Hench, “Bioceramics: From Concept to Clinic,” *Journal of the American Ceramic Society*, vol. 74, no. 7, pp. 1487–1510, Jul. 1991, doi: 10.1111/J.1151-2916.1991.TB07132.X.

[373] H. Liu, H. Yazici, C. Ergun, T. J. Webster, and H. Bermek, “An in vitro evaluation of the Ca/P ratio for the cytocompatibility of nano-to-micron particulate calcium phosphates for bone regeneration,” *Acta Biomater.*, vol. 4, no. 5, pp. 1472–1479, Sep. 2008, doi: 10.1016/J.ACTBIO.2008.02.025.

[374] S. Padilla, J. Román, S. Sánchez-Salcedo, and M. Vallet-Regí, “Hydroxyapatite/SiO2-CaO-P2O5 glass materials: In vitro bioactivity and biocompatibility,” *Acta Biomater.*, vol. 2, no. 3, pp. 331–342, 2006, doi: 10.1016/J.ACTBIO.2006.01.006.

[375] X. Liu *et al.*, “A comparison of in vitro cytotoxicity assays in medical device regulatory studies,” *Regulatory Toxicology and Pharmacology*, vol. 97, pp. 24–32, Aug. 2018, doi: 10.1016/J.YRTPH.2018.06.003.

[376] G. Ciapetti, E. Cenni, L. Pratelli, and A. Pizzoferrato, “In vitro evaluation of cell/biomaterial interaction by MTT assay,” *Biomaterials*, vol. 14, no. 5, pp. 359–364, Apr. 1993, doi: 10.1016/0142-9612(93)90055-7.

[377] D. Arcos Navarrete and M. Vallet-Regí, “Bioactive glasses: properties, composition and recent applications”.

[378] A. J. Salinas, M. Vallet-Regi, and J. Heikkilä, “Use of bioactive glasses as bone substitutes in orthopedics and traumatology,” *Bioactive Glasses: Materials, Properties and Applications, Second Edition*, pp. 337–364, Jan. 2018, doi: 10.1016/B978-0-08-100936-9.00014-9.

[379] Y. Liu *et al.*, “3D bioprinting bioglass to construct vascularized full-thickness skin substitutes for wound healing,” *Mater. Today Bio*, vol. 24, Feb. 2023, doi: 10.1016/J.MTBIO.2023.100899.

[380] C. Viennet and P. Muret, “Fibroblast Evaluation: Extracellular Matrix Synthesis,” *Measuring the Skin*, pp. 1–5, 2015, doi: 10.1007/978-3-319-26594-0_124-1.

[381] F. Boraldi, F. D. Lofaro, S. Bonacorsi, A. Mazzilli, M. Garcia-Fernandez, and D. Quaglino, “The Role of Fibroblasts in Skin Homeostasis and Repair,” *Biomedicines 2024, Vol. 12, Page 1586*, vol. 12, no. 7, p. 1586, Jul. 2024, doi: 10.3390/BIOMEDICINES12071586.

[382] A. Anesi *et al.*, “In-vivo evaluations of bone regenerative potential of two novel bioactive glasses,” *J. Biomed. Mater. Res. A*, vol. 111, no. 8, pp. 1264–1278, Aug. 2023, doi: 10.1002/JBM.A.37526.

[383] C. Rodrigues *et al.*, “Bioglass 45S5: Structural characterization of short range order and analysis of biocompatibility with adipose-derived mesenchymal stromal cells in vitro and in

vivo," *Materials Science and Engineering: C*, vol. 103, p. 109781, Oct. 2019, doi: 10.1016/J.MSEC.2019.109781.

[384] A. S. Bakry, H. Takahashi, M. Otsuki, and J. Tagami, "Evaluation of new treatment for incipient enamel demineralization using 45S5 bioglass," *Dent. Mater.*, vol. 30, no. 3, pp. 314–320, Mar. 2014, doi: 10.1016/J.DENTAL.2013.12.002.

[385] A. S. Bakry, Y. Tamura, M. Otsuki, S. Kasugai, K. Ohya, and J. Tagami, "Cytotoxicity of 45S5 bioglass paste used for dentine hypersensitivity treatment," *J. Dent.*, vol. 39, no. 9, pp. 599–603, Sep. 2011, doi: 10.1016/J.JDENT.2011.06.003.

[386] M. Handel, T. R. Hammer, P. Nooeaid, A. R. Boccaccini, and D. Hoefer, "45S5-Bioglass®-Based 3D-Scaffolds Seeded with Human Adipose Tissue-Derived Stem Cells Induce In Vivo Vascularization in the CAM Angiogenesis Assay," *Tissue Eng Part A*, vol. 19, no. 23–24, pp. 2703–2712, Aug. 2013, doi: 10.1089/TEN.TEA.2012.0707.

[387] H. Yu, J. Peng, Y. Xu, J. Chang, and H. Li, "Bioglass Activated Skin Tissue Engineering Constructs for Wound Healing," *ACS Appl. Mater. Interfaces*, vol. 8, no. 1, pp. 703–715, Jan. 2016, doi: 10.1021/ACSAMI.5B09853.

[388] S. Naseri, W. C. Lepry, and S. N. Nazhat, "Bioactive glasses in wound healing: hope or hype?," *J. Mater. Chem. B*, vol. 5, no. 31, pp. 6167–6174, Aug. 2017, doi: 10.1039/C7TB01221G.

[389] I. A. Silver, J. Deas, and M. Erecińska, "Interactions of bioactive glasses with osteoblasts in vitro: effects of 45S5 Bioglass®, and 58S and 77S bioactive glasses on metabolism, intracellular ion concentrations and cell viability," *Biomaterials*, vol. 22, no. 2, pp. 175–185, Jan. 2001, doi: 10.1016/S0142-9612(00)00173-3.

[390] R. M. Day *et al.*, "Assessment of polyglycolic acid mesh and bioactive glass for soft-tissue engineering scaffolds," *Biomaterials*, vol. 25, no. 27, pp. 5857–5866, Dec. 2004, doi: 10.1016/J.BIOMATERIALS.2004.01.043.

[391] R. Detsch *et al.*, "Osteogenic differentiation of umbilical cord and adipose derived stem cells onto highly porous 45S5 Bioglass®-based scaffolds," *J. Biomed. Mater. Res. A*, vol. 103, no. 3, pp. 1029–1037, Mar. 2015, doi: 10.1002/JBM.A.35238.

[392] M. Cerruti, D. Greenspan, and K. Powers, "Effect of pH and ionic strength on the reactivity of Bioglass® 45S5," *Biomaterials*, vol. 26, no. 14, pp. 1665–1674, May 2005, doi: 10.1016/J.BIOMATERIALS.2004.07.009.

[393] M. Rabe, D. Verdes, and S. Seeger, "Understanding protein adsorption phenomena at solid surfaces," *Adv. Colloid Interface Sci.*, vol. 162, no. 1–2, pp. 87–106, Feb. 2011, doi: 10.1016/J.CIS.2010.12.007.

[394] I. D. Xynos, M. V. J. Hukkanen, J. J. Batten, L. D. Buttery, L. L. Hench, and J. M. Polak, "Bioglass® 45S5 stimulates osteoblast turnover and enhances bone formation in vitro: Implications and applications for bone tissue engineering," *Calcif. Tissue Int.*, vol. 67, no. 4, pp. 321–329, Feb. 2000, doi: 10.1007/S002230001134.

[395] L. de Araujo Bastos Santana, P. H. Oliveira Junior, C. Damia, D. dos Santos Tavares, and E. A. dos Santos, "Bioactivity in SBF versus trace element effects: The isolated role of Mg2+ and Zn^{2+} in osteoblast behavior," *Mater. Sci. Eng. C Mater. Biol. Appl.*, vol. 118, Jan. 2021, doi: 10.1016/J.MSEC.2020.111320.

[396] D. D. Schlaepfer, S. K. Hanks, T. Hunter, and P. Van Der Geer, "Integrin-mediated signal transduction linked to Ras pathway by GRB2 binding to focal adhesion kinase," *Nature*, vol. 372, no. 6508, pp. 786–791, 1994, doi: 10.1038/372786a0.

[397] R. Amberg *et al.*, "Design of a migration assay for human gingival fibroblasts on biodegradable magnesium surfaces," *Acta Biomater.*, vol. 79, pp. 158–167, Oct. 2018, doi: 10.1016/J.ACTBIO.2018.08.034.

[398] P. A. Dash, S. Mohanty, and S. K. Nayak, "A review on bioactive glass, its modifications and applications in healthcare sectors," *J. Non. Cryst. Solids*, vol. 614, p. 122404, Aug. 2023, doi: 10.1016/J.JNONCRYSOL.2023.122404.

[399] J. McAndrew, C. Efrimescu, E. Sheehan, and D. Niall, "Through the looking glass; Bioactive glass S53P4 (BonAlive®) in the treatment of chronic osteomyelitis," *Ir. J. Med. Sci.*, vol. 182, no. 3, pp. 509–511, Sep. 2013, doi: 10.1007/S11845-012-0895-5.

[400] N. C. Lindfors, "Clinical Experience on Bioactive Glass S53P4 in Reconstructive Surgery in the Upper Extremity Showing Bone Remodelling, Vascularization, Cartilage Repair and Antibacterial Properties of S53P4," *J. Biotechnol. Biomater.*, vol. 01, no. 05, 2011, doi: 10.4172/2155-952X.1000111.

[401] G. J. Todaro and H. Green, "Quantitative studies of the growth of mouse embryo cells in culture and their development into established lines," *Journal of Cell Biology*, vol. 17, no. 2, pp. 299–313, May 1963, doi: 10.1083/JCB.17.2.299.

[402] R. Pérez-Tanoira *et al.*, "Effects of S53P4 bioactive glass on osteoblastic cell and biomaterial surface interaction," *J. Mater. Sci. Mater. Med.*, vol. 26, no. 10, pp. 1–11, Oct. 2015, doi: 10.1007/S10856-015-5568-2.

[403] N. A. P. van Gestel *et al.*, "The Implantation of Bioactive Glass Granules Can Contribute the Load-Bearing Capacity of Bones Weakened by Large Cortical Defects," *Materials, Vol. 12, Page 3481*, vol. 12, no. 21, p. 3481, Oct. 2019, doi: 10.3390/MA12213481.

[404] N. Bhardwaj and S. C. Kundu, "Electrospinning: A fascinating fiber fabrication technique," *Biotechnol. Adv.*, vol. 28, no. 3, pp. 325–347, May 2010, doi: 10.1016/J.BIOTECHADV.2010.01.004.

[405] F. Ghorbani, T. Reiter, L. Liverani, D. W. Schubert, A. R. Boccaccini, and J. A. Roether, "Progress on Electrospun Composite Fibers Incorporating Bioactive Glass: An Overview," *Adv. Eng. Mater.*, vol. 25, no. 6, p. 2201103, Mar. 2023, doi: 10.1002/adem.202201103.

[406] C. Meng *et al.*, "3D Poly (L-lactic acid) fibrous sponge with interconnected porous structure for bone tissue scaffold," *Int. J. Biol. Macromol.*, vol. 268, p. 131688, May 2024, doi: 10.1016/J.IJBIOMAC.2024.131688.

[407] R. Sergi, V. Cannillo, A. R. Boccaccini, and L. Liverani, “Incorporation of bioactive glasses containing Mg, Sr, and Zn in electrospun PCL fibers by using benign solvents,” *Applied Sciences (Switzerland)*, vol. 10, no. 16, Aug. 2020, doi: 10.3390/app10165530.

[408] C. Y. Wang *et al.*, “The synergistic effects of strontium/magnesium-doped calcium silicate cement accelerates early angiogenesis and bone regeneration through double bioactive ion stimulation,” *Ceram. Int.*, vol. 50, no. 4, pp. 7121–7131, Feb. 2024, doi: 10.1016/J.CERAMINT.2023.12.077.

[409] A. Azari, A. Golchin, M. M. Maymand, F. Mansouri, and A. Ardeshirylajimi, “Electrospun Polycaprolactone Nanofibers: Current Research and Applications in Biomedical Application,” *Adv. Pharm. Bull.*, vol. 12, no. 4, p. 658, 2021, doi: 10.34172/APB.2022.070.

[410] E. Malikmammadov, T. E. Tanir, A. Kiziltay, V. Hasirci, and N. Hasirci, “PCL and PCL-based materials in biomedical applications,” *J. Biomater. Sci. Polym. Ed.*, vol. 29, no. 7–9, pp. 863–893, Jun. 2018, doi: 10.1080/09205063.2017.1394711.

[411] P. Ma and G. Wei, “Polymer/Ceramic Composite Scaffolds for Bone Tissue Engineering,” *Scaffolding In Tissue Engineering*, pp. 241–251, Aug. 2005, doi: 10.1201/9781420027563.pt3.

[412] Y. C. Chiu, Y. H. Lin, Y. W. Chen, T. Y. Kuo, and M. Y. Shie, “Additive manufacturing of barium-doped calcium silicate/poly-ε-caprolactone scaffolds to activate CaSR and AKT signalling and osteogenic differentiation of mesenchymal stem cells,” *J. Mater. Chem. B*, vol. 11, no. 21, pp. 4666–4676, May 2023, doi: 10.1039/d3tb00208j.

[413] Y. Lei, B. Rai, K. H. Ho, and S. H. Teoh, “In vitro degradation of novel bioactive polycaprolactone—20% tricalcium phosphate composite scaffolds for bone engineering,” *Materials Science and Engineering: C*, vol. 27, no. 2, pp. 293–298, Mar. 2007, doi: 10.1016/J.MSEC.2006.05.006.

[414] P. Taddei, M. Di Foggia, F. Causa, L. Ambrosio, and C. Fagnano, “In vitro Bioactivity of Poly(∈-Caprolactone)-Apatite (PCL-AP) Scaffolds for Bone Tissue Engineering: The Influence of the PCL/AP Ratio,” *The International Journal of Artificial Organs*, vol. 29, no. 7, pp. 719–725, Jul. 2006, doi: 10.1177/039139880602900712.

[415] B. Yedekçi, A. Tezcaner, B. Yılmaz, T. Demir, and Z. Evis, “3D porous PCL-PEG-PCL/strontium, magnesium and boron multi-doped hydroxyapatite composite scaffolds for bone tissue engineering,” *J. Mech. Behav. Biomed. Mater.*, vol. 125, p. 104941, Jan. 2022, doi: 10.1016/J.JMBBM.2021.104941.

[416] L. Du, H. Xu, Y. Zhang, and F. Zou, “Electrospinning of polycaprolatone nanofibers with DMF additive: The effect of solution proprieties on jet perturbation and fiber morphologies,” *Fibers and Polymers*, vol. 17, no. 5, pp. 751–759, May 2016, doi: 10.1007/S12221-016-6045-3.

[417] A. Doustgani, “Effect of electrospinning process parameters of polycaprolactone and nanohydroxyapatite nanocomposite nanofibers,” *Textile Research Journal*, vol. 85, no. 14, pp. 1445–1454, 2015, doi: 10.1177/0040517514566109.

[418] P. Wutticharoenmongkol, P. Pavasant, and P. Supaphol, “Osteoblastic phenotype expression of MC3T3-E1 cultured on electrospun polycaprolactone fiber mats filled with hydroxyapatite nanoparticles,” *Biomacromolecules*, vol. 8, no. 8, pp. 2602–2610, 2007, doi: 10.1021/BM700451P.

[419] International Standard Organization (ISO), “Biological evaluation of medical devices — Part 5: Tests for in vitro cytotoxicity,” 2009 [Online]. Available: https://www.iso.org/standard/36406.html

[420] J. Ajita, S. Saravanan, and N. Selvamurugan, “Effect of size of bioactive glass nanoparticles on mesenchymal stem cell proliferation for dental and orthopedic applications,” *Materials Science and Engineering: C*, vol. 53, pp. 142–149, Aug. 2015, doi: 10.1016/J.MSEC.2015.04.041.

[421] F. Valenzuela, C. Covarrubias, C. Martínez, P. Smith, M. Díaz-Dosque, and M. Yazdani-Pedram, “Preparation and bioactive properties of novel bone-repair bionanocomposites based on hydroxyapatite and bioactive glass nanoparticles,” *J. Biomed. Mater. Res. B Appl. Biomater.*, vol. 100B, no. 6, pp. 1672–1682, Aug. 2012, doi: 10.1002/JBM.B.32736.

[422] K. Schickle *et al.*, “Preparation of spherical calcium phosphate granulates suitable for the biofunctionalization of active brazed titanium alloy coatings,” *Biomedizinische Technik*, vol. 60, no. 2, pp. 105–114, Apr. 2015, doi: 10.1515/BMT-2014-0017/MACHINEREADABLECITATION/RIS.

[423] A. García García, “Multiscale analysis of multi-layered tissues constructs : interfaces in the musculo-skeletal system based on tissue engineered osteotendinous junctions.” Accessed: Mar. 11, 2025. [Online]. Available: https://theses.hal.science/tel-02533666v1

[424] H. Fong, I. Chun, and D. H. Reneker, “Beaded nanofibers formed during electrospinning,” *Polymer*, vol. 40, no. 16, pp. 4585–4592, Jul. 1999, doi: 10.1016/S0032-3861(99)00068-3.

[425] B. Cramariuc, R. Cramariuc, R. Scarlet, L. R. Manea, I. G. Lupu, and O. Cramariuc, “Fiber diameter in electrospinning process,” *J. Electrostat.*, vol. 71, no. 3, pp. 189–198, Jun. 2013, doi: 10.1016/J.ELSTAT.2012.12.018.

[426] S. V. Fridrikh, J. H. Yu, M. P. Brenner, and G. C. Rutledge, “Controlling the Fiber Diameter during Electrospinning,” *Phys. Rev. Lett.*, vol. 90, no. 14, p. 4, Apr. 2003, doi: 10.1103/PHYSREVLETT.90.144502.

[427] L. A. Can-Herrera, A. I. Oliva, M. A. A. Dzul-Cervantes, O. F. Pacheco-Salazar, and J. M. Cervantes-Uc, “Morphological and Mechanical Properties of Electrospun Polycaprolactone Scaffolds: Effect of Applied Voltage,” *Polymers 2021*, vol. 13, no. 4, p. 662, Feb. 2021, doi: 10.3390/POLYM13040662.

[428] A. Larrañaga and J. R. Sarasua, “Effect of bioactive glass particles on the thermal degradation behaviour of medical polyesters,” *Polym. Degrad. Stab.*, vol. 98, no. 3, pp. 751–758, 2013, doi: 10.1016/J.POLYMDEGRADSTAB.2012.12.015.

[429] V. R. dos Santos *et al.*, “PHBV Wound Dressing Containing 45B5 Borate Bioactive Glass: Effect of the Particle Incorporation Method on the Cytocompatibility and Antibacterial

Activity," *Materials Research*, vol. 27, p. e20240121, Dec. 2024, doi: 10.1590/1980-5373-MR-2024-0121.

[430] J. R. de Souza *et al.*, "Biodegradable Electrospun PLCL/PEG/Bioactive Glass Composite Scaffold for Bone Tissue Engineering," *J. Biomed. Mater. Res. B Appl. Biomater.*, vol. 112, no. 5, p. e35406, May 2024, doi: 10.1002/JBM.B.35406.

[431] S. C. Wong, A. Baji, and S. Leng, "Effect of fiber diameter on tensile properties of electrospun poly(ε-caprolactone)," *Polymer (Guildf).*, vol. 49, no. 21, pp. 4713–4722, Oct. 2008, doi: 10.1016/J.POLYMER.2008.08.022.

[432] F. Croisier *et al.*, "Mechanical testing of electrospun PCL fibers," *Acta Biomater.*, vol. 8, no. 1, pp. 218–224, Jan. 2012, doi: 10.1016/J.ACTBIO.2011.08.015.

[433] Y. Gou, C. Liu, T. Lei, and F. Yang, "Nanofiber alignment during electrospinning: Effects of collector structures and governing parameters," *2014 International Conference on Manipulation, Manufacturing and Measurement on the Nanoscale, 3M-NANO 2014 - Conference Proceedings*, pp. 62–65, Mar. 2014, doi: 10.1109/3M-NANO.2014.7057341.

[434] T. Courtney, M. S. Sacks, J. Stankus, J. Guan, and W. R. Wagner, "Design and analysis of tissue engineering scaffolds that mimic soft tissue mechanical anisotropy," *Biomaterials*, vol. 27, no. 19, pp. 3631–3638, Jul. 2006, doi: 10.1016/J.BIOMATERIALS.2006.02.024.

[435] A. J. Robinson, A. Pérez-Nava, S. C. Ali, J. B. González-Campos, J. L. Holloway, and E. M. Cosgriff-Hernandez, "Comparative analysis of fiber alignment methods in electrospinning," *Matter*, vol. 4, no. 3, pp. 821–844, Mar. 2021, doi: 10.1016/J.MATT.2020.12.022.

[436] S. Metwally *et al.*, "Single-Step Approach to Tailor Surface Chemistry and Potential on Electrospun PCL Fibers for Tissue Engineering Application," *Adv. Mater. Interfaces*, vol. 6, no. 2, p. 1801211, Jan. 2019, doi: 10.1002/ADMI.201801211.

[437] M. Fadaie, E. Mirzaei, B. Geramizadeh, and Z. Asvar, "Incorporation of nanofibrillated chitosan into electrospun PCL nanofibers makes scaffolds with enhanced mechanical and biological properties," *Carbohydr. Polym.*, vol. 199, pp. 628–640, Nov. 2018, doi: 10.1016/J.CARBPOL.2018.07.061.

[438] A. Oyane, M. Uchida, Y. Yokoyama, C. Choong, J. Triffitt, and A. Ito, "Simple surface modification of poly(ϵ-caprolactone) to induce its apatite-forming ability," *J. Biomed. Mater. Res. A*, vol. 75A, no. 1, pp. 138–145, Oct. 2005, doi: 10.1002/JBM.A.30397.

[439] L. Ji, W. Wang, D. Jin, S. Zhou, and X. Song, "In vitro bioactivity and mechanical properties of bioactive glass nanoparticles/polycaprolactone composites," *Materials Science and Engineering: C*, vol. 46, pp. 1–9, Jan. 2015, doi: 10.1016/J.MSEC.2014.09.041.

[440] Y. B. Kim, J. Y. Lim, G. H. Yang, J. H. Seo, H. S. Ryu, and G. H. Kim, "3D-printed PCL/bioglass (BGS-7) composite scaffolds with high toughness and cell-responses for bone tissue regeneration," *Journal of Industrial and Engineering Chemistry*, vol. 79, pp. 163–171, Nov. 2019, doi: 10.1016/J.JIEC.2019.06.027.

[441] J. M. Lee *et al.*, “The effect of biomechanical stimulation on osteoblast differentiation of human jaw periosteum-derived stem cells,” *Maxillofac. Plast. Reconstr. Surg.*, vol. 39, no. 1, pp. 1–9, Dec. 2017, doi: 10.1186/S40902-017-0104-6.

[442] S. S. Lee, X. Du, I. Kim, and S. J. Ferguson, “Scaffolds for bone-tissue engineering,” *Matter*, vol. 5, no. 9, pp. 2722–2759, Sep. 2022, doi: 10.1016/J.MATT.2022.06.003.

[443] A. J. Engler, S. Sen, H. L. Sweeney, and D. E. Discher, “Matrix Elasticity Directs Stem Cell Lineage Specification,” *Cell*, vol. 126, no. 4, pp. 677–689, Aug. 2006, doi: 10.1016/J.CELL.2006.06.044.

[444] Y. Deng *et al.*, “Bioinspired and osteopromotive polydopamine nanoparticle-incorporated fibrous membranes for robust bone regeneration,” *NPG Asia Materials*, vol. 11, no. 1, pp. 1–13, Jul. 2019, doi: 10.1038/s41427-019-0139-5.

[445] S. S. Banerjee, S. Tarafder, N. M. Davies, A. Bandyopadhyay, and S. Bose, “Understanding the influence of MgO and SrO binary doping on the mechanical and biological properties of β-TCP ceramics,” *Acta Biomater.*, vol. 6, no. 10, pp. 4167–4174, 2010, doi: 10.1016/j.actbio.2010.05.012.

[446] A. M. Dias, I. do Nascimento Canhas, C. G. O. Bruziquesi, M. G. Speziali, R. D. Sinisterra, and M. E. Cortés, “Magnesium (Mg2 +), Strontium (Sr2 +), and Zinc (Zn2 +) Co-substituted Bone Cements Based on Nano-hydroxyapatite/Monetite for Bone Regeneration,” *Biol. Trace Elem. Res.*, vol. 201, no. 6, pp. 2963–2981, Jun. 2023, doi: 10.1007/S12011-022-03382-5.

[447] Y. H. Lin, A. K. X. Lee, C. C. Ho, M. J. Fang, T. Y. Kuo, and M. Y. Shie, “The effects of a 3D-printed magnesium-/strontium-doped calcium silicate scaffold on regulation of bone regeneration via dual-stimulation of the AKT and WNT signaling pathways,” *Biomaterials Advances*, vol. 133, Feb. 2022, doi: 10.1016/j.msec.2022.112660.

[448] L. A. Martini, “Magnesium Supplementation and Bone Turnover,” *Nutr. Rev.*, vol. 57, no. 7, pp. 227–229, Jul. 1999, doi: 10.1111/j.1753-4887.1999.tb06948.x.

[449] E. Gentleman *et al.*, “The effects of strontium-substituted bioactive glasses on osteoblasts and osteoclasts in vitro,” *Biomaterials*, vol. 31, no. 14, pp. 3949–3956, May 2010, doi: 10.1016/j.biomaterials.2010.01.121.

[450] N. Esfahanizadeh, M. Montazeri, M. R. Nourani, and M. Harandi, “Use of bioactive glass doped with magnesium or strontium for bone regeneration: A rabbit critical-size calvarial defects study,” 2022. [Online]. Available: www.ncbi.nlm.nih.gov/pmc/journals/1480

[451] W. Xue, K. Dahlquist, A. Banerjee, A. Bandyopadhyay, and S. Bose, “Synthesis and characterization of tricalcium phosphate with Zn and Mg based dopants,” in *Journal of Materials Science: Materials in Medicine*, Jul. 2008, pp. 2669–2677. doi: 10.1007/s10856-008-3395-4.

[452] G. Şimşek Gündüz, “Gonca Şimşek Gündüz 22 Investigation of the Effect of Needle Diameter and the Solution Flow Rate on Fiber Morphology in the Electrospinning Method,”

Fibres & Textiles in Eastern Europe, vol. 31, no. 4, pp. 22–29, 2023, doi: 10.2478/ftee-2023-0032.

[453] K. A. G. Katsogiannis, G. T. Vladisavljević, and S. Georgiadou, "Porous electrospun polycaprolactone (PCL) fibres by phase separation," *Eur. Polym. J.*, vol. 69, no. 1, pp. 284–295, Aug. 2015, doi: 10.1016/j.eurpolymj.2015.01.028.

[454] H. H. Kim, M. J. Kim, S. J. Ryu, C. S. Ki, and Y. H. Park, "Effect of fiber diameter on surface morphology, mechanical property, and cell behavior of electrospun poly(ε-caprolactone) mat," *Fibers and Polymer*, vol. 17, no. 7, pp. 1033–1042, Jul. 2016, doi: 10.1007/S12221-016-6350-X.

[455] L. A. Bosworth, W. Hu, Y. Shi, and S. H. Cartmell, "Enhancing Biocompatibility without Compromising Material Properties: An Optimised NaOH Treatment for Electrospun Polycaprolactone Fibres," *J. Nanomater.*, vol. 2019, no. 1, p. 4605092, Jan. 2019, doi: 10.1155/2019/4605092.

[456] L. Liverani *et al.*, "Incorporation of bioactive glass nanoparticles in electrospun PCL/chitosan fibers by using benign solvents," *Bioact. Mater.*, vol. 3, no. 1, pp. 55–63, Mar. 2018, doi: 10.1016/J.BIOACTMAT.2017.05.003.

[457] R. Konyalı and A. M. Deliormanlı, "Preparation and mineralization of 13-93 bioactive glass-containing electrospun poly-epsilon-caprolactone composite nanofibrous mats," *Journal of Thermoplastic Composite Materials*, vol. 32, no. 5, pp. 690–709, May 2019, doi: 10.1177/0892705718772889.

[458] M. Kouhi, M. Morshed, J. Varshosaz, and M. H. Fathi, "Poly (ε-caprolactone) incorporated bioactive glass nanoparticles and simvastatin nanocomposite nanofibers: Preparation, characterization and in vitro drug release for bone regeneration applications," *Chemical Engineering Journal*, vol. 228, pp. 1057–1065, Jul. 2013, doi: 10.1016/j.cej.2013.05.091.

[459] X. Hong, M. Edirisinghe, and S. Mahalingam, "Beads, beaded-fibres and fibres: Tailoring the morphology of poly(caprolactone) using pressurised gyration," *Materials Science and Engineering: C*, vol. 69, pp. 1373–1382, Dec. 2016, doi: 10.1016/J.MSEC.2016.07.071.

[460] L. Liverani *et al.*, "Nanocomposite electrospun fibers of poly(ε-caprolactone)/bioactive glass with shape memory properties," *Bioact. Mater.*, vol. 11, p. 230, May 2021, doi: 10.1016/J.BIOACTMAT.2021.09.020.

[461] H. Elkhouly, W. Mamdouh, and D. I. El-Korashy, "Electrospun nano-fibrous bilayer scaffold prepared from polycaprolactone/gelatin and bioactive glass for bone tissue engineering," *J. Mater. Sci. Mater. Med.*, vol. 32, no. 9, p. 111, Sep. 2021, doi: 10.1007/s10856-021-06588-6.

[462] R. Yaseri, M. Fadaie, E. Mirzaei, H. Samadian, and A. Ebrahiminezhad, "Surface modification of polycaprolactone nanofibers through hydrolysis and aminolysis: a comparative study on structural characteristics, mechanical properties, and cellular performance," *Scientific Reports*, vol. 13, no. 1, pp. 9434-, Jun. 2023, doi: 10.1038/s41598-023-36563-w.

[463] J. Meng, G. Yang, L. Liu, Y. Song, L. Jiang, and S. Wang, “Cell adhesive spectra along surface wettability gradient from superhydrophilicity to superhydrophobicity,” *Science China Chemistry*, vol. 60, no. 5, pp. 614–620, Apr. 2017, doi: 10.1007/s11426-016-9031-8.

[464] I. Kansal *et al.*, “Structure, biodegradation behavior and cytotoxicity of alkali-containing alkaline-earth phosphosilicate glasses,” *Materials Science and Engineering: C*, vol. 44, no. 1, pp. 159–165, Nov. 2014, doi: 10.1016/j.msec.2014.08.016.